Ministry of Education and Science of the Russian Federation
Saint Petersburg National Research University of Information Technologies, Mechanics, and Optics

NANOSYSTEMS:

PHYSICS, CHEMISTRY, MATHEMATICS

2015, volume 6(2)

Special Issue

INTERNATIONAL CONFERENCE "WAVE DYNAMICS IN LOW-DIMENSIONAL BRANCHED STRUCTURES "

Наносистемы: физика, химия, математика
2015, том 6, № 2

NANOSYSTEMS:

PHYSICS, CHEMISTRY, MATHEMATICS

Address: University ITMO, Kronverkskiy pr., 49, St. Petersburg 197101, Russia.
Phone: +7(812)232-67-65, **Journal site:** http://nanojournal.ifmo.ru/,
E-mail: popov1955@gmail.com

AIM AND SCOPE

The scope of the journal includes all areas of nano-sciences. Papers devoted to basic problems of physics, chemistry, material science and mathematics inspired by nanosystems investigations are welcomed. Both theoretical and experimental works concerning the properties and behavior of nanosystems, problems of its creation and application, mathematical methods of nanosystem studies are considered.

The journal publishes scientific reviews (up to 30 journal pages), research papers (up to 15 pages) and letters (up to 5 pages). All manuscripts are peer-reviewed. Authors are informed about the referee opinion and the Editorial decision.

Content

FROM THE EDITORIAL BOARD

In memory of Vadim Petrovich Romanov

Vadim Petrovich Romanov, a wonderful person and an outstanding scientist, Doctor of Physics and Mathematics, Professor of Statistical Physics, St. Petersburg State University, Honored Scientist of Russian Federation, member of Editorial Board of the Journal "Nanosystems: Physics, Chemistry, Mathematics" passed away on February 1, 2015, at 78 years of age.

Vadim Petrovich was born on January 8, 1938 in Leningrad. In 1961, he graduated from the Physical Faculty of the Leningrad State University. In that same year, he started to work at the Physical Faculty as a junior researcher. Since 1962, he has worked as an Assistant Professor and from 1971 as an Associate Professor in the Department of General Physics. In 1975, he was elected Associate Professor at the newly created Department of Statistical Physics. From 1983 until his death, he has worked as a professor in this Department. In 1967, V.P. Romanov defended his PhD thesis, and in 1980 his habilitation thesis. In 1983 he was awarded the title of professor in the Department of Statistical Physics.

Professor V.P. Romanov was a renowned expert on the statistical physics of liquid crystals, the theory of electromagnetic and acoustic wave propagation and scattering in strongly inhomogeneous media. He developed the theory of sound propagation in non-ideal liquid solutions, which explained numerous experimental data for the acoustic properties of binary mixtures, and gave new means to investigate the spatial structure of such solutions. Together with the experimentalists, he proposed and successfully implemented a method for extracting high order contributions in light scattering spectra, which provides detailed information about opalescent systems in the vicinity of second order phase transition. These works open new opportunities for finding the equations of state for liquid mixtures. Vadim Petrovich developed a theory of interference and correlation effects in strongly inhomogeneous media, which found application in the study of biological objects by optical methods. He published a series of papers on the propagation of light in liquid crystals with a smoothly

varying characteristics. These studies are important for the creation of next generation liquid crystal displays.

V. P. Romanov published more than 150 scientific papers in the leading Russian and foreign journals. Among them, 5 reviews in the journals “Physics-Uspekhi” and “Physics Reports” on modern problems of physics, book “Exercises in Statistical Physics”, published by “Nauka” publishing house.

Vadim Petrovich has been repeatedly awarded by the title of “Soros Professor”. His research was supported by grants of Russian Foundation of Basic Research, the Government of St. Petersburg, Saint Petersburg State University programs. In the framework of international cooperation, V.P. Romanov organized joint research with Cranfield University in the UK, supported by grants of the Royal Society of Great Britain. In 1996, he received a prize of Saint Petersburg State University for the pedagogical skills, and in 2010 he won the University Award for scientific works. He also was awarded the title “Honored Worker of Higher Professional Education of the Russian Federation”. For a long time professor, Romanov was a member of the Academic Council of the SPbSU Faculty of Physics and a member of the scientific committee of this Faculty, and in 2013, he became a chairman of the Dissertation Council for doctoral and PhD theses at SPbSU.

V.P. Romanov gave much time and effort to teaching, work with students and graduate students. Over the years, he read the general course “Statistical physics and thermodynamics” for students of the Faculty of Physics of SPbSU, a number of special courses for students of Statistical Physics Department. Professor Romanov was the supervisor for 17 PhD theses and scientific advisor of 4 Doctor of Science dissertations. For his students, he always was a real mentor displaying a rare care and kindness.

The bright memory of Vadim Romanov will remain forever in our hearts.

L.Ts. Adzhemyan, E.V. Aksenova, A.P. Kovshik, A.E. Kuchma, V.L. Kuzmin, M.Yu. Nalimov, E.I. Rjumtsev, A.K. Shchekin, A.Yu. Val'kov, P.N. Vorontsov- Velyaminov, S.V. Ulyanov, V.M. Uzdin.

International conference
"Wave dynamics in low-dimensional branched structures"

This issue contains papers presented at the “Wave dynamics in low-dimensional branched structures” workshop held in September 24-25, 2014 in Tashkent. The talks presented at this conference were mainly focused on different aspects of linear and nonlinear evolution equations on networks and confined domains.

Particle and wave transport in branched structures is of importance for different topics of contemporary physics, chemistry and biology. Due to recent progress made in nanoscale and mesoscopic physics, heat, charge, spin and information transport in branched and discrete systems has attracted much attention during the last decade. Remarkably, such processes can be modeled by linear and nonlinear evolution equations on graphs, billiards and chains. This makes the problem of partial differential equations on graphs and confined domains attractive in the contexts of mathematics, physics and chemistry.

The main objective of the Workshop was the bringing together of various ideas, problems and expertise on applications of nonlinear evolution equations and quantum mechanical wave equations to a wide spectrum of systems from condensed matter physics, cold atoms, optics and nanoscale physics. Talks presented at the Workshop covered such topics as linear and nonlinear evolution equations on graphs, spin transport in networks, Dirac and Majorana fermions in branched structures, inverse problems for quantum graphs, BEC and solitons in low-dimensional traps.

A total of 28 talks were presented at the meeting, with 18 invited and 10 short plenary talks.

Panel discussions attracted broad auditorium experts and young researchers working on different topics of physics, mathematics and chemistry.

We would like to thank the members of the organizing Committee, Workshop Secretary, Dr. Olga Karpova and main sponsor of the meeting, Volkswagen Foundation.

Davron Matrasulov
Zarif Sobirov.

NANOSYSTEMS: PHYSICS, CHEMISTRY, MATHEMATICS, 2015, 6 (2), P. 162–172

A solution of nonlinear Schrödinger equation on metric graphs

K. K. Sabirov[1], A. R. Khalmukhamedov[2]

[1]National University of Uzbekistan, 4 University St., 100074, Tashkent, Uzbekistan
[2]Tashkent branch of Moscow State University named after L. V. Lomonosov, 22 Amir Temur St., 100060, Tashkent, Uzbekistan

karimjonsabirov@yahoo.com

PACS 02.30.Jr,02.30.Ik **DOI 10.17586/2220-8054-2015-6-2-162-172**

We treat the Nonlinear Schrödinger equation (NLSE) on Metric graph. An approach developed earlier for NLSE on interval [14], is extended for star graph. Dirichlet boundary conditions are imposed at the ends of bonds are imposed, while continuity conditions are chosen at the vertex of graph.

Keywords: metric graphs, nonlinear Schrödinger equation, solitons.

Received: 2 February 2015

1. Introduction

Wave transport in the nonlinear regime, described by nonlinear evolution equations, such as the nonlinear Schrödinger, Korteweg de Vries and sine Gordon equations, has attracted much attention in different areas of physics over the past five decades (see, e.g. books [1] – [5]).

Recently, one can observe a growing interest in particle and wave transport in branched, network type structures [6] – [13]. Such problem is of importance for different topics in physics, such as hydrodynamics, acoustics, optics, cold atom physics and condensed matter physics. Soliton solutions and connection formulae were derived for simplest graphs in the Ref. [6]. The problem of fast solitons on star graphs was treated in the Ref. [7], where the estimates for the transmission and reflection coefficients were obtained in the limit of very high velocities. The problem of soliton transmission and reflection was studied in [9] by numerically solving the stationary NLSE on graphs. The dispersion relations for linear and nonlinear Schrödinger equations on graphs were discussed in [10]. Ref. [11] treated the stationary NLSE in the context of scattering from nonlinear networks. The stationary NLSE with power focusing nonlinearity on star graphs was studied in recent papers [7, 8], where the existence of nonlinear stationary states were shown for $\delta-$type boundary conditions. In [13], the exact analytical solutions of the stationary NLSE for simplest graphs were obtained.

In this work, we treat time dependent NLSE on metric graphs by considering the simplest topology, a star graph. Unlike the case of the NLSE on an interval, in the case of the graph, the NLSE becomes a multicomponent equation, with the components related to each other through the boundary conditions given at the graph vertex.

Our aim is to solve the (cubic) nonlinear Schrödinger equation on metric graphs. The latter are systems consisting of bonds which are connected at the vertices [16] to a

rule which is called the topology of a graph. The topology of a graph can be relayed in terms of a so-called adjacency matrix, which can be written as [17]:

$$C_{ij} = C_{ji} = \begin{cases} 1, & \text{if } i \text{ and } j \text{ are connected;} \\ 0, & \text{otherwise,} \end{cases} \qquad i, j = 1, 2, \ldots, V.$$

In the following, we consider the so-called primary star graph, consisting of three bonds connected at single vertex. However, our results can be extended to any arbitrary topology. Our approach is based on extending the method proposed by Fokas and its solution for the NLSE on a finite interval [14]. In Refs. [14, 15], an effective method allowing one to obtain a general solution for the NLSE on a finite interval [14] and on a half-line [15] was developed. As it will be shown below, this method can be adapted to the case of the NLSE on a metric graph. Thus, the problem we are going to solve is the nonlinear Schrödinger equation on a graph with bonds $b_j \sim (0, L_j)$, $j = 1, 2, 3$, which can be written as:

$$i\frac{\partial}{\partial t}q_j + \frac{\partial^2}{\partial x_j^2}q_j - 2\lambda|q_j|^2 q_j = 0, \tag{1}$$

$$\lambda = \pm 1, \quad j = 1, 2, 3, \quad L_1 < x_1 < 0, 0 < x_{2,3} < L_{2,3}, \quad 0 < t < T.$$

The initial conditions are given as:

$$q_j(x_j, 0) = q_{0j}(x_j), \quad j = 1, 2, 3, \quad L_1 < x_1 < 0, \quad 0 < x_{2,3} < L_{2,3}, \tag{2}$$

The following boundary conditions provide matching of the bonds at the vertex:

$$q_1(0, t) = q_2(0, t) = q_3(0, t) = g_0(t), \quad 0 < t < T \tag{3}$$

$$q_j(L_j, t) = f_{0j}(t), \quad 0 < t < T, \quad j = 1, 2, 3, \tag{4}$$

$$\frac{\partial}{\partial x_1}q_1(0, t) = \frac{\partial}{\partial x_2}q_2(0, t) + \frac{\partial}{\partial x_3}q_3(0, t), \quad 0 < t < T \tag{5}$$

Furthermore, we define the following functions:

$$g_{1j}(t) = \frac{\partial}{\partial x_j}q_j(0, t), \qquad g_{1j}(t) = \frac{\partial}{\partial x_j}q_j(L_j, t).$$

These functions are considered to be unknown and will be found subsequently.

The difference between Eq. (1) and with that treated in Ref. [14] is caused by bond indices, j. In other words, Eq. (1) is a multicomponent equation in which each component is related to others through the boundary conditions (3) – (5). As we will see below, this makes it possible to rewrite most of the results derived in [14] for the case of metric graphs.

2. Description of the approach

The method we are going to utilize includes three steps [14]. The first step consists of Riemann-Hilbert (RH) problem formulation under the assumption of existence. Following Ref. [14], we assume that there exists a smooth solution $q(x, t) = \{q_1(x_1, t), q_2(x_2, t), q_3(x_3, t)\}$.

Applying the spectral analysis to the Lax pair, we write $q(x, t) = \{q_1(x_1, t), q_2(x_2, t), q_3(x_3, t)\}$ in terms of the solution of a 2×2-matrix RH problem defined in the complex k-plane [14]. Such a problem is uniquely defined in terms of the spectral functions which are given as:

$$\{a_j(k), b_j(k)\}, \quad \{A_j(k), B_j(k)\}, \quad \{\mathbf{A}_j(k), \mathbf{B}_j(k)\}. \tag{6}$$

These functions are defined in terms of the functions:

$$q_{0j}(x_j), \quad \{g_0(t), g_{1j}(t)\}, \quad \{f_{0j}(t), f_{1j}(t)\}, \tag{7}$$

respectively. Here, the functions $g_0(t,\ g_{1j}(t)$ and $f_{1j}(t)$ denote the unknown boundary values for the solution to the NLSE and its derivatives (see Eqs. (3)).

Following Ref. [14], one can show that the spectral functions (6) are not independent, but they satisfy the global relation:

$$(a_j\mathbf{A}_j + \lambda\bar{b}_j e^{2ikL_j}\mathbf{B}_j)B_j - (b_j\mathbf{A}_j + \bar{a}_j e^{2ikL_j}\mathbf{B}_j)A_j = e^{4ik^2T}c_j^+(k), \quad k \in \mathbf{C}_j, \tag{8}$$

where $c_j^+(k)$ has the same meaning as in [14].

The second step implies proof of the existence of the solution to the NLSE, assuming that the above spectral functions satisfy the global relation. The spectral functions given in (6) can be written in terms of the (smooth) functions (7). We also define $q(x,t) = \{q_1(x_1,t), q_2(x_2,t), q_3(x_3,t)\}$ in terms of the solution of the RH problem formulated in Step 1. Assuming that smooth functions $g_{1j}(t)$ and $f_{1j}(t)$ exist such that the spectral functions (6) satisfy the global relation (8), one can prove that:
(i) $q(x,t) = \{q_1(x_1,t), q_2(x_2,t), q_3(x_3,t)\}$ is defined globally for all $L_1 < x_1 < 0$, $0 < x_{2,3} < L_{2,3}$, $0 < t < T$.
(ii) $q(x,t) = \{q_1(x_1,t), q_2(x_2,t), q_3(x_3,t)\}$ solves the NLSE.
(iii) $q(x,t) = \{q_1(x_1,t), q_2(x_2,t), q_3(x_3,t)\}$ satisfies the given initial and boundary conditions:

$$q_j(x_j,0) = q_{0j}(x), \quad q_j(0,t) = g_0(t), \quad q_j(L_j,t) = f_{0j}(t).$$

A byproduct of this proof is that:

$$\frac{\partial}{\partial x_j}q_j(0,t) = g_{1j}(t) \quad \text{and} \quad \frac{\partial}{\partial x_j}q_j(L_j,t) = f_{1j}(t).$$

Finally, the third step presents an analysis of the global relation treated in the second step. Namely, for given q_{0j}, g_0, f_{0j}, one can show that the global relation (8) characterizes g_{1j} and f_{1j} through the solution of a system of nonlinear Volterra integral equations.

Furthermore, following the Ref. [14], we introduce the eigenfunctions, $\left\{\mu_j^{(n)}(x,t,k)\right\}_{n=1}^4$, such that:

$$\mu_j^{(1)}(0,T,k) = I, \quad \mu_j^{(2)}(0,0,k) = I,$$
$$\mu_j^{(3)}(L_j,0,k) = I, \quad \mu_j^{(4)}(L_j,T,k) = I, \quad j = 1,2,3, \tag{9}$$

with $\mu_j^{(n)}$ being the 2×2 matrices, $I = \mathrm{diag}(1,1)$. One can show that these eigenfunctions can be written in terms of the matrices s_j, S_j, S_j^L as:

$$s_j(k) = \mu_j^{(3)}(0,0,k), \quad S_j(k) = \left(e^{2ik^2T\sigma_3}\mu_j^{(2)}(0,T,k)e^{-2ik^2T\sigma_3}\right)^{-1},$$
$$S_j^L(k) = \left(e^{2ik^2T\sigma_3}\mu_j^{(3)}(L_j,T,k)e^{-2ik^2T\sigma_3}\right)^{-1}, \tag{10}$$

where $\sigma_3 = \mathrm{diag}(1,-1)$.

3. Lax pair and its solutions

The Lax pair for our problem can be written as [20]:

$$\frac{\partial}{\partial x}\mu_j + ik\hat{\sigma}_{3,j}\mu_j = Q_j\mu_j, \qquad \frac{\partial}{\partial t}\mu_j + 2ik^2\hat{\sigma}_{3,j}\mu_j = \tilde{Q}_j\mu_j, \tag{11}$$

where $\mu_j(x,t,k)$ is a 2×2 matrix-valued function, $\hat{\sigma}_{3,j}$ is defined by:

$$\hat{\sigma}_{3,j}\cdot = [\sigma_{3,j},\cdot] \qquad \sigma_{3,j} = \mathrm{diag}(1,-1), \tag{12}$$

and the 2×2 matrices Q_j, $\tilde{Q}_j$ are given as:

$$Q_j(x_j,t) = \begin{pmatrix} 0 & q_j(x_j,t) \\ \lambda\bar{q}_j(x_j,t) & 0 \end{pmatrix},$$
$$\tilde{Q}_j(x_j,t,k) = 2kQ_j - i\frac{\partial}{\partial x}Q_j\sigma_{3,j} - i\lambda|q_j|^2\sigma_{3,j}, \quad \lambda = \pm 1. \tag{13}$$

Furthermore, we assume that there exists a sufficiently smooth solution $q_j(x_j,t)$, $j=1,2,3$, $x_1\in[L_1,0]$, $x_{2,3}\in[0,L_{2,3}]$, $t\in[0,T]$, of NLSE.

A solution of equation (11) is given by [14]:

$$\mu_j^{(*)}(x_j,t,k) = I + \int\limits_{(x_{j*},t_*)}^{(x_j,t)} e^{-i(kx_j+2k^2t)\hat{\sigma}_{3,j}}W_j(y,\tau,k), \tag{14}$$

where the closed 1-form W_j is defined by:

$$W_j = e^{i(kx+2k^2t)\hat{\sigma}_{3,j}}(Q_j\mu_j dx + \tilde{Q}_j\mu_j dt), \tag{15}$$

(x_{j*},t_*) is an arbitrary point in the domain $x_1\in[L_1,0]$, $x_{2,3}\in[0,L_{2,3}]$, $t\in[0,T]$, and the integral denotes a line integral connecting smoothly the points indicated.

Following Ref. [14], it can be shown that the functions $\mu_j^{(n)}$ are related by these equations:

$$\mu_j^{(3)}(x_j,t,k) = \mu_j^{(2)}(x_j,t,k)e^{-i(kx_j+2k^2t)\hat{\sigma}_{3,j}}s_j(k), \tag{16}$$

$$\mu_j^{(1)}(x_j,t,k) = \mu_j^{(2)}(x_j,t,k)e^{-i(kx_j+2k^2t)\hat{\sigma}_{3,j}}S_j(k), \tag{17}$$

$$\mu_j^{(4)}(x_j,t,k) = \mu_j^{(3)}(x_j,t,k)e^{-i(kx_j+2k^2t)\hat{\sigma}_{3,j}}S_j^L(k), \tag{18}$$

and one can find from Eq. (16) at $x_j=t=0$, $s(k)=\mu_j^{(3)}(0,0,k)$. Finally, from Eqs. (17) and (18) at $x_j=L_j$, $t=T$ we have:

$$S_j^L(k) = \left(e^{2ik^2T\hat{\sigma}_{3,j}}\mu_j^{(3)}(L_j,T,k)\right)^{-1}$$

and

$$\mu_j^{(4)}(x_j,t,k) = \mu_j^{(2)}(x_j,t,k)e^{-i(kx_j+2k^2t)\hat{\sigma}_{3,j}}\left(s(k)e^{ikL_j\hat{\sigma}_{3,j}}S_j^L(k)\right). \tag{19}$$

4. The global relation

As was mentioned before, the spectral functions $a_j(k)$, $b_j(k)$, $A_j(k)$, $B_j(k)$, $\mathbf{A}_j(k)$, $\mathbf{B}_j(k)$ are not independent, but they satisfy the global relation (8), where $c_j^+(k)$ denotes the element of $-\int_0^{L_j}[\exp(iky\hat{\sigma}_{3,j})](Q_j\mu_j^{(4)})(y,T,k)dy$, and $\mu_j^{(4)}$ is defined by an equation similar to $\mu_j^{(3)}$ with $\int_0^t$ replaced by $-\int_0^T$. The proof is the same as in the case of the NLSE for the finite interval treated in [14]. We now introduce $M_j(x_j,t,k)$, defined by:

$$
\begin{aligned}
M_j^{(+)} &= \left(\frac{\mu_j^{(2)(1)}}{\alpha_j(k)}, \mu_j^{(4)(1)}\right), \quad \arg k \in \left[0, \frac{\pi}{2}\right], \\
M_j^{(-)} &= \left(\frac{\mu_j^{(1)(2)}}{d_j(k)}, \mu_j^{(3)(2)}\right), \quad \arg k \in \left[\frac{\pi}{2}, \pi\right], \\
M_j^{(+)} &= \left(\mu_j^{(3)(3)}, \frac{\mu_j^{(1)(3)}}{\overline{d_j(\bar{k})}}\right), \quad \arg k \in \left[\pi, \frac{3\pi}{2}\right], \\
M_j^{(-)} &= \left(\mu_j^{(4)(4)}, \frac{\mu_j^{(2)(4)}}{\overline{\alpha_j(\bar{k})}}\right), \quad \arg k \in \left[\frac{3\pi}{2}, 2\pi\right],
\end{aligned} \tag{20}
$$

where the scalars $d_j(k)$ and $\alpha_j(k)$ are defined below. These definitions imply:

$$
\det M_j(x_j,t,k) = 1 \tag{21}
$$

and

$$
M_j(x_j,t,k) = I + O\left(\frac{1}{k}\right), \quad k \to \infty. \tag{22}
$$

As in the case of the NLSE on a finite graph studied in [14], it can be shown that M_j satisfies the jump condition:

$$
M_j^{(-)}(x_j,t,k) = M_j^{(+)}(x_j,t,k)J_j(x_j,t,k), \quad k \in \mathbf{R} \cup i\mathbf{R}, \tag{23}
$$

where the 2×2 matrix J_j is defined by:

$$
J_j = \begin{cases}
J_j^{(2)}, & \arg k = 0; \\
J_j(1), & \arg k = \dfrac{\pi}{2}; \\
J_j^{(4)} \equiv J_j^{(3)}(J_j^{(2)})^{-1}J_j^{(1)}, & \arg k = \pi; \\
J_j^{(3)}, & \arg k = \dfrac{3\pi}{2}
\end{cases} \tag{24}
$$

and

$$J_j^{(1)} = \begin{pmatrix} \dfrac{\delta_j(k)}{d_j(k)} & -\mathbf{B}_j(k)e^{2ikL_j}e^{-2i\theta_j} \\ \dfrac{\overline{\lambda B_j(\bar{k})}}{d_j(k)\alpha_j(k)}e^{2i\theta_j} & \dfrac{a_j(k)}{\alpha_j(k)} \end{pmatrix},$$

$$J_j^{(3)} = \begin{pmatrix} \dfrac{\overline{\delta_j(\bar{k})}}{\overline{d(\bar{k})}} & \dfrac{-B_j(k)}{\overline{d_j(\bar{k})\alpha_j(\bar{k})}}e^{-2i\theta_j} \\ \lambda\overline{\mathbf{B}_j(\bar{k})}e^{-2ikL_j}e^{2i\theta_j} & \dfrac{\overline{a(\bar{k})}}{\overline{\alpha_j(\bar{k})}} \end{pmatrix},$$

$$J_j^{(2)} = \begin{pmatrix} 1 & -\dfrac{\beta_j(k)}{\overline{\alpha_j(k)}}e^{-2i\theta_j} \\ \lambda\dfrac{\overline{\beta_j(k)}}{\alpha_j(k)}e^{2i\theta_j} & \dfrac{1}{|\alpha_j(k)|^2} \end{pmatrix},$$

$$\theta_j(x_j,t,k) = kx_j + 2k^2t, \tag{25}$$

$$\alpha_j(k) = a_j(k)\mathbf{A}_j(k) + \lambda\overline{b_j(\bar{k})}e^{2ikL_j}\mathbf{B}_j(k),$$

$$\beta_j(k) = b_j(k)\mathbf{A}_j(k) + \lambda\overline{a_j(\bar{k})}e^{2ikL_j}\mathbf{B}_j(k) \tag{26}$$

$$d_j(k) = a_j(k)\overline{\mathbf{A}_j(\bar{k})} - \lambda b_j(k)e^{2ikL_j}\overline{\mathbf{B}_j(\bar{k})},$$

$$\delta_j(k) = \alpha_j(k)\overline{\mathbf{A}_j(\bar{k})} - \lambda\beta_j(k)e^{2ikL_j}\overline{\mathbf{B}_j(\bar{k})}. \tag{27}$$

The above expressions are the same as those for the NLSE on a finite interval, except for the bond index, j.

Following Ref. [14], one can prove

Theorem. Let $q_{0j}(x)$ be a smooth function. We assume that that the set of functions $g_0(t)$, $g_{1j}(t)$, $f_{0j}(t)$, $f_{1j}(t)$, is admissible with respect to $q_{0j}(x)$ and define the spectral functions $a_j(k)$, $b_j(k)$, $A_j(k)$, $B_j(k)$, $\mathbf{A}_j(k)$, $\mathbf{B}_j(k)$ in terms of $q_{0j}(x)$, $g_0(t)$, $g_{1j}(t)$, $f_{0j}(t)$, $f_{1j}(t)$. We assume that

- $a_j(k)$ has at most simple zeros, $\{k_j^{(n)}\}$, for $\Im k_j^{(n)} > 0$ and has no zeros for $\Im k = 0$.
- $A_j(k)$ has at most simple zeros, $\{K_j^{(n)}\}$, for $\arg K_j^{(n)} \in \left(0, \dfrac{\pi}{2}\right) \cup \left(\pi, \dfrac{3\pi}{2}\right)$ and has no zeros for $\arg k = 0, \dfrac{\pi}{2}, \pi, \dfrac{3\pi}{2}$.
- $\mathbf{A}_j(k)$ has at most simple zeros, $\{\mathbf{K}_j^{(n)}\}$, for $\arg \mathbf{K}_j^{(n)} \in \left(0, \dfrac{\pi}{2}\right) \cup \left(\pi, \dfrac{3\pi}{2}\right)$ and has no zeros for $\arg k = 0, \dfrac{\pi}{2}, \pi, \dfrac{3\pi}{2}$.
- The function
$$d_j(k) = a_j(k)\overline{A_j(\bar{k})} - \lambda b_j(k)\overline{B_j(\bar{k})} \tag{28}$$
has at most simple zeros, $\{\lambda_j^{(n)}\}$, for $\arg \lambda_j^{(n)} \in \left(\dfrac{\pi}{2}, \pi\right)$ and has no zeros for $\arg k = \dfrac{\pi}{2}$ and $\arg k = \pi$.
- The function
$$\alpha_j(k) = a_j(k)\mathbf{A}_j(k) + \lambda\overline{b(\bar{k})}e^{2ikL_j}\mathbf{B}_j(k) \tag{29}$$

has at most simple zeros, $\{v_j^{(n)}\}$, for $\arg v_j^{(n)} \in \left(0, \frac{\pi}{2}\right)$ and has no zeros for $\arg k = 0$, $\arg k = \frac{\pi}{2}$.

- None of the zeros of $a_j(k)$ for $\arg k \in \left(\frac{\pi}{2}, \pi\right)$ coincides with a zero of $d_j(k)$.
- None of the zeros of $a_j(k)$ for $\arg k \in \left(0, \frac{\pi}{2}\right)$ coincides with a zero of $\alpha_j(k)$.
- None of the zeros of $\alpha_j(k)$ for $\arg k \in \left(0, \frac{\pi}{2}\right)$ coincides with a zero of $A_j(k)$ or a zero of $\mathbf{A}_j(k)$.
- None of the zeros of $d_j(k)$ for $\arg k \in \left(\frac{\pi}{2}, \pi\right)$ coincides with a zero of $\overline{A_j(\overline{k})}$ or a zero of $\overline{\mathbf{A}_j(\overline{k})}$.

We define $M_j(x_j, t, k)$ as the solution of the following 2×2 matrix RH problem:

- M_j is sectionally meromorphic in $\mathbf{C}/\{\mathbf{R} \cup \mathrm{i}\mathbf{R}\}$, and has unit determinant.
- $$M_j^{(-)}(x_j, t, k) = M_j^{(+)}(x_j, t, k) J_j(x_j, t, k), \quad k \in \mathbf{R} \cup \mathrm{i}\mathbf{R}, \tag{30}$$
  where M_j is $M_j^{(-)}$ for $\arg k \in \left[\frac{\pi}{2}, \pi\right] \cup \left[\frac{3\pi}{2}, 2\pi\right]$, M_j is $M_j^{(+)}$ for $\arg k \in \left[0, \frac{\pi}{2}\right] \cup \left[\pi, \frac{3\pi}{2}\right]$, and J_j is defined in terms of a_j, b_j, A_j, B_j, $\mathbf{A}_j$, $\mathbf{B}_j$, by equations (24) and (25).
- $$M_j(x_j, t, k) = I + O\left(\frac{1}{k}\right), \quad k \to \infty. \tag{31}$$
- Let $[M_j]_1$ and $[M_j]_2$ denote the first and the second column of the matrix M_j. Then residue conditions:
$$\operatorname*{Res}_{k=v_j^{(n)}} [M_j(x_j, t, k)]_1 = c_j^{(n)(1)} e^{4i(v_j^{(n)})^2 t + 2i v_j^{(n)} x_j} [M_j(x_j, t, v_j^{(n)})]_2, \tag{32}$$
$$\operatorname*{Res}_{k=\overline{v_j^{(n)}}} [M_j(x_j, t, k)]_2 = \lambda \overline{c_j^{(n)(1)}} e^{-4i(v_j^{(n)})^2 t - 2i v_j^{(n)} x_j} [M_j(x_j, t, \overline{v}_j^{(n)})]_1, \tag{33}$$
$$\operatorname*{Res}_{k=\lambda_j^{(n)}} [M_j(x_j, t, k)]_1 = c_j^{(n)(2)} e^{4i(v_j^{(n)})^2 t + 2i v_j^{(n)} x_j} [M_j(x_j, t, \lambda_j^{(n)})]_2, \tag{34}$$
$$\operatorname*{Res}_{k=\overline{\lambda_j^{(n)}}} [M_j(x_j, t, k)]_2 = \lambda \overline{c_j^{(n)(2)}} e^{-4i(v_j^{(n)})^2 t - 2i v_j^{(n)} x_j} [M_j(x_j, t, \overline{\lambda}_j^{(n)})]_1, \tag{35}$$
  where:
$$c_j^{(n)(1)} = \frac{a_j(v_j^{(n)})}{e^{2iv_j^{(n)} L_j} \mathbf{B}_j(v_j^{(n)}) \dot{\alpha}_j(v_j^{(n)})}, \qquad c_j^{(n)(2)} = \frac{\lambda \overline{B_j(\overline{\lambda}_j^{(n)})}}{a_j(\lambda_j^{(n)}) \dot{d}_j(\lambda_j^{(n)})}. \tag{36}$$

Then, $M_j(x_j, t, k)$ exists and is unique. We define $q_j(x_j, t)$ in terms of $M_j(x_j, t, k)$ by

$$q_j(x, t) = 2\mathrm{i} \cdot \lim_{k \to \infty} k (M_j(x, t, k))_{12}. \tag{37}$$

Then, $q_j(x, t)$, together with the following functions:

$$q_j(x,0) = q_{0j}(x), \quad q_j(0,t) = g_0(t), \quad \frac{\partial}{\partial x} q_j(0,t) = g_{1j}(t),$$

$$q_j(L_j,t) = f_{0j}(t), \quad \frac{\partial}{\partial x} q_j(L_j,t) = f_{1j}(t) \tag{38}$$

present the solution for the nonlinear Schrödinger equation (1) with initial and boundary conditions given by Eqs.(2) – (5), respectively. The proof of the theorem is similar to that of the NLSE for a finite interval treated in [14]).

Furthermore, repeating the same steps as in [14] (for $a_j(k) \equiv 1$,$b_j(k) \equiv 0$), we get the following expressions for f_{1j}, g_{1j}:

$$\frac{i\pi}{4} f_{1j} = \int\limits_{\partial D_1^0} \frac{2k^2}{\Delta_j(k)} \left[\hat{M}_j^{(1)}(t,k) - \frac{g_0(t)}{2ik^2} \right] dk - \int\limits_{\partial D_1^0} k^2 \frac{\Sigma_j(k)}{\Delta_j(k)} \left[\hat{\mathbf{M}}_j^{(1)}(t,k) - \frac{f_{0j}(t)}{2ik^2} \right] dk + \\ + \int\limits_{\partial D_1^0} \frac{k}{\Delta_j(k)} \left[F_j(t,k) - F_j(t,-k) \right] dk, \tag{39}$$

$$-\frac{i\pi}{4} g_{1j} = \int\limits_{\partial D_1^0} \frac{2k^2}{\Delta_j(k)} \left[\hat{\mathbf{M}}_j^{(1)}(t,k) - \frac{f_{0j}(t)}{2ik^2} \right] dk - \int\limits_{\partial D_1^0} k^2 \frac{\Sigma_j(k)}{\Delta_j(k)} \left[\hat{M}_j^{(1)}(t,k) - \frac{g_0(t)}{2ik^2} \right] dk - \\ - \int\limits_{\partial D_1^0} \frac{k}{\Delta_j(k)} \left[e^{-2ikL_j} F_j(t,k) - e^{2ikL_j} F_j(t,-k) \right] dk, \tag{40}$$

where:

$$\Sigma_j(k) = e^{2ikL_j} + e^{-2ikL_j}, \tag{41}$$

$$\begin{aligned} F_j(t,k) = \quad & \frac{if_{0j}(t)}{2} e^{2ikL_j} \hat{\mathbf{M}}_j^{(2)} - \frac{ig_0(t)}{2} \hat{M}_j^{(2)} + \\ & + \left[\overline{\hat{\mathbf{L}}_j^{(2)}} - i\lambda \frac{f_{0j}(t)}{2} \overline{\hat{\mathbf{M}}_j^{(1)}} + k \overline{\hat{\mathbf{M}}_j^{(2)}} \right] \cdot \left[\hat{L}_j^{(1)} - i \frac{g_0(t)}{2} \hat{M}_j^{(2)} + k \hat{M}_j^{(1)} \right] - \\ & - e^{2ikL_j} \left[\overline{\hat{L}_j^{(2)}} - i\lambda \frac{g_0(t)}{2} \overline{\hat{M}_j^{(1)}} + k \overline{\hat{M}_j^{(2)}} \right] \cdot \left[\hat{\mathbf{L}}_j^{(1)} - i \frac{f_{0j}(t)}{2} \hat{\mathbf{M}}_j^{(2)} + k \hat{\mathbf{M}}_j^{(1)} \right]. \end{aligned} \tag{42}$$

Finally, from Eqs. (40) and (5) we obtain:

$$g_0(t) = \frac{\int\limits_{\partial D_1^0} k^2 \frac{\Sigma_1(k)}{\Delta_1(k)} \hat{M}_1^{(1)} dk - \int\limits_{\partial D_1^0} \frac{2k^2}{\Delta_1(k)} \left[\hat{\mathbf{M}}_1^{(1)} - \frac{f_{01}(t)}{2ik^2}\right] dk}{\frac{1}{2i}\int\limits_{\partial D_1^0} \frac{\Sigma_1(k)}{\Delta_1(k)} dk - \frac{1}{2i}\sum\limits_{j=2}^{3} \int\limits_{\partial D_1^0} \frac{\Sigma_j(k)}{\Delta_j(k)} dk} -$$

$$- \frac{\sum\limits_{j=2}^{3} \left\{ \int\limits_{\partial D_1^0} k^2 \frac{\Sigma_j(k)}{\Delta_j(k)} \hat{M}_j^{(1)} dk - \int\limits_{\partial D_1^0} \frac{2k^2}{\Delta_j(k)} \left[\hat{\mathbf{M}}_j^{(1)} - \frac{f_{0j}(t)}{2ik^2}\right] dk \right\}}{\frac{1}{2i}\int\limits_{\partial D_1^0} \frac{\Sigma_1(k)}{\Delta_1(k)} dk - \frac{1}{2i}\sum\limits_{j=2}^{3} \int\limits_{\partial D_1^0} \frac{\Sigma_j(k)}{\Delta_j(k)} dk} +$$

$$+ \frac{\int\limits_{\partial D_1^0} \frac{k}{\Delta_1(k)} \left[e^{-2ikL_1} F_1(t,k) - e^{2ikL_1} F_1(t,-k)\right] dk}{\frac{1}{2i}\int\limits_{\partial D_1^0} \frac{\Sigma_1(k)}{\Delta_1(k)} dk - \frac{1}{2i}\sum\limits_{j=2}^{3} \int\limits_{\partial D_1^0} \frac{\Sigma_j(k)}{\Delta_j(k)} dk} -$$

$$- \frac{\sum\limits_{j=2}^{3} \int\limits_{\partial D_1^0} \frac{k}{\Delta_j(k)} \left[e^{-2ikL_j} F_j(t,k) - e^{2ikL_j} F_j(t,-k)\right] dk}{\frac{1}{2i}\int\limits_{\partial D_1^0} \frac{\Sigma_1(k)}{\Delta_1(k)} dk - \frac{1}{2i}\sum\limits_{j=2}^{3} \int\limits_{\partial D_1^0} \frac{\Sigma_j(k)}{\Delta_j(k)} dk}. \tag{43}$$

We note that $\mu_j^{(1)}(0,t,k)$ and $\mu_j^{(2)}(0,t,k)$ are solutions of:

$$\frac{\partial}{\partial t}\mu_j + 2ik^2 \hat{\sigma}_{3,j}\mu_j = \tilde{Q}_j(0,t,k)\mu_j, \tag{44}$$

where:

$$\tilde{Q}_j(0,t,k) = \begin{pmatrix} -i\lambda|q_j(0,t)|^2 & 2kq_j(0,t) + i\frac{\partial}{\partial x_j} q_j(0,t) \\ 2k\bar{q}_j(0,t) - i\frac{\partial}{\partial x_j}\bar{q}_j(0,t) & i\lambda|q_j(0,t)|^2 \end{pmatrix}. \tag{45}$$

Therefore, it satisfies:

$$\tilde{Q}_j(0,t,k) = \sigma_{3,j}\Sigma\overline{\tilde{Q}_j(0,t,\bar{k})}\Sigma\sigma_{3,j}, \tag{46}$$

where $\overline{\tilde{Q}_j(0,t,\bar{k})} = \begin{pmatrix} i\lambda|q_j(0,t)|^2 & 2k\bar{q}_j(0,t) + i\frac{\partial}{\partial x_j}\bar{q}_j(0,t) \\ 2kq_j(0,t) - i\frac{\partial}{\partial x_j} q_j(0,t) & -i\lambda|q_j(0,t)|^2 \end{pmatrix}$, $\Sigma = \begin{pmatrix} \lambda & 0 \\ 0 & \lambda \end{pmatrix}$.

This implies the following symmetry for boundary scattering matrix:

$$S_j(k) = \sigma_{3,j}\Sigma\overline{S_j(\bar{k})}\Sigma\sigma_{3,j}, \tag{47}$$

where $\overline{S_j(\bar{k})} = \begin{pmatrix} A_j(k) & \overline{B_j(\bar{k})} \\ \lambda B_j(k) & \overline{A_j(\bar{k})} \end{pmatrix}$.

5. Conclusions

In this paper, we treated the nonlinear Schrödinger equation with cubic nonlinearity on a metric graph. The boundary conditions were imposed to provide continiuty and current conservation at the graph vertex. Our approach is based an extension applied earlier by Fokas [14] for the solution to the NLSE on a finite interval with Dirichlet boundary conditions. Unlike the case of the NLSE on the interval in [14], in the case of our graph, we have:
i) Multicomponent NLSE, whose components are related to each other through the vertex boundary conditions.
ii) Additional, Neumann type boundary conditions at the graph vertex.
iii)Additional unknown functions, g_0, g_1, f_0, f_1 in the initial and boundary conditions. However, this doesn't lead to serious complication for adopting method of [14] for the case of graphs, although results obtained are completely different from those of NLSE for finite interval. We note that the above treatment of NLSE on star graph can be extended to other graph topologies as well.

References

[1] Y.S. Kivshar and G.P. Agarwal. *Optical Solitons: From Fibers to Photonic Crystals*. Academic, San Diego (2003).
[2] M.J. Ablowitz and P.A. Clarkson. *Solitons, Nonlinear Evolution Equations and Inverse Scattering*. Cambridge: Cambridge University Press (1999).
[3] C.J. Pethick and H. Smith. *Bose-Einstein Condensation in Dilute Gases*. Cambridge University Press, Cambridge, England (2002).
[4] L. Pitaevskii and S. Stringari. *Bose-Einstein Condensation*. Oxford University Press, Oxford, England (2003).
[5] T. Dauxois and M. Peyrard. *Physics of Solitons*. Cambridge University Press, Cambridge, England (2006).
[6] Z. Sobirov, D. Matrasulov, K. Sabirov, et al. Integrable nonlinear Schrodinger equation on simple networks: Connection formula at vertices. *Phys. Rev. E*, **81**, P. 066602 (2010).
[7] R. Adami, C. Cacciapuoti, D. Finco, D. Noja. Fast solitons on star graphs. *Reviews in Mathematical Physics*, **23** (04), P. 409–451 (2011).
[8] R. Adami, C. Cacciapuoti, D. Finco, D. Noja. On the structure of critical energy levels for the cubic focusing NLS on star graphs. *Journal of Physics A: Mathematical and Theoretical*, **45** (19), P. 192001 (2012).
[9] R.C. Cascaval and C.T. Hunter. Linear and nonlinear Schrodinger equations on simple networks. *Libertas Mathematica*, **30**, P. 85–98 (2010).
[10] V. Banica and L.I. Ignat. Dispersion for the Schrödinger equation on networks *Journal of Mathematical Physics*; **52** (8), P. 083703–083703-14 (2011).
[11] S. Gnutzmann, U. Smilansky, and S. Derevyanko. Stationary scattering from a nonlinear network. *Phys. Rev. A*, **83**, P. 033831 (2011).
[12] R. Adami, D. Noja, C. Ortoleva. Orbital and asymptotic stability for standing waves of a nonlinear Schrödinger equation with concentrated nonlinearity in dimension three. *Journal of Mathematical Physics*, **54**, P. 013501–013533 (2013).
[13] K.K. Sabirov, Z.A. Sobirov, D. Babajanov and D.U. Matrasulov. Stationary Nonlinear Schrödinger Equation on Simplest Graphs. *Phys.Lett. A*, **377**, P. 860–865 (2013).
[14] A.S. Fokas and A.R. Its. The nonlinear Schrödinger equation on the interval. *J. Phys. A: Math. Gen*, **37** P. 6091 (2004).
[15] A.S. Fokas, A.R. Its and L.-Y. Sung. The nonlinear Schrödinger equation on the half-line. *Nonlinearity*, **18**, P. 1771 (2005).

[16] F. Harary. *Graph Theory*. Addison-Wesley, Reading (1969), 274 p.
[17] T. Kottos and U. Smilansky. Periodic Orbit Theory and Spectral Statistics for Quantum Graphs. *Ann.Phys.*, **274** (1) P. 76–124 (1999).
[18] A. Boutet de Monvel and V.Kotlyarov. Scattering problem for the Zakharov-Shabat equations on the semi-axis. *Inverse Problems*, **16**, P. 1813 (2000).
[19] P.D. Lax. Integrals of nonlinear equations of evolution and solitary waves. *Commun. Pure Appl. Math.*, **21**, P. 467–490 (1968).
[20] V.E. Zakharov and A. Shabat. Exact theory of two-dimensional self-focusing and one-dimentional self-modulation of waves in nonlinear media. *Sov. Phys. JETP*, **34** (1), P. 62–69 (1972).

NANOSYSTEMS: PHYSICS, CHEMISTRY, MATHEMATICS, 2015, 6 (2), P. 173–181

Time-dependent quantum graph

[1,2]D. U. Matrasulov, [1]J. R. Yusupov, [2]K. K. Sabirov, [2,3]Z. A. Sobirov

[1] Turin Polytechnic University in Tashkent, 17. Niyazov Str., 100095, Tashkent, Uzbekistan
[2] National University of Uzbekistan, 100174, Tashkent, Uzbekistan
[3] Tashkent Financial Institute, 60A, Amir Temur Str., 100000, Tashkent, Uzbekistan

dmatrasulov@gmail.com

PACS 03.65.Aa, 03.65.Ge **DOI 10.17586/2220-8054-2015-6-2-173-181**

In this paper, we study quantum star graphs with time-dependent bond lengths. Quantum dynamics are treated by solving Schrodinger equation with time-dependent boundary conditions given on graphs. The time-dependence of the average kinetic energy is analyzed. The space-time evolution of a Gaussian wave packet is treated for an harmonically breathing star graph.

Keywords: quantum graph,time-dependent boundary conditions,wave packet dynamics.

Received: 2 February 2015

1. Introduction

Quantum particle dynamics in nanoscale networks and discrete structures is of fundamental and practical importance. Usually, such systems are modeled by so-called quantum graphs. These systems have attracted much attention in physics [1–3] and mathematics [5–7] over the past two decades.

In physics, quantum graphs were introduced as a toy model for studies of quantum chaos by Kottos and Smilansky [1]. However, the concept of studying a system confined to a graph dates back to Pauling [4], who suggested the use of such systems for modeling free electron motion in organic molecules. Over the last two decades, quantum graphs have found numerous applications in modeling different discrete structures and networks in nanoscale and mesoscopic physics (e.g., see reviews [1–3] and references therein).

Mathematical properties of the Schrödinger operators on graphs [5–7] and inverse problems for quantum graphs [8,9], were also the subject of extensive research recently. Also, an experimental realization of quantum graphs is discussed in Ref. [5, 10, 11]. Despite the certain progress made in the study of quantum graphs, some important aspects still remain relatively unexplored. This is especially true for problems of driven graphs, i.e. graphs perturbed by time-dependent external forces. An important example of such a driving force is that caused by driven (moving) boundaries. Treatment of such system requires solving the Schrödinger equation with time-dependent boundary conditions. Earlier, the problem of time-dependent boundary conditions in the Schrödinger equation has attracted much attention in the context of quantum Fermi acceleration [12–14], although different aspects of the problem were treated by many authors [16–27]. Detailed study of the problem can be found in a series of papers by Makowski and co-authors [21–23]. It was pointed out in the above Refs. that the problem of 1D box with a moving wall can be mapped onto that of an harmonic oscillator with time-dependent frequency confined inside the static box [21].

In this paper, we treat a similar problem for quantum star graph, i.e. we study the problem of quantum graphs with time-dependent bonds. In particular, we consider

harmonically breathing quantum star graphs, cases of monotonically contracting and expanding graphs. The latter can be solved exactly analytically. Motivation for the study of time-dependent graphs comes from such practically important problems as quantum Fermi acceleration in nanoscale network structures, tunable particle transport in quantum wire networks, molecular wires, different lattices and discrete structures. In particular, sites, vertices, nodes of such discrete structures can fluctuate, which makes them time-dependent. We will study the time-dependence of the average kinetic energy and wave packet dynamics in harmonically breathing graphs.

Graphs are systems consisting of bonds which are connected at the vertices. The bonds are connected according to a rule which is called the topology of a graph. The topology of a graph is given in terms of adjacency matrix [1, 2]:

$$C_{ij} = C_{ji} = \begin{cases} 1, & \text{if } i \text{ and } j \text{ are connected;} \\ 0, & \text{otherwise.} \end{cases} \quad i, j = 1, 2, ..., V. \tag{1}$$

Quantum dynamics of a particle on a graph is described by a one-dimensional Schrödinger equation [1, 2] (in the units $\hbar = 2m = 1$):

$$-i\frac{d^2}{dx^2}\Psi_b(x) = k^2\Psi_b(x), \quad b = (i, j), \tag{2}$$

where b denotes a bond connecting ith and $j$the vertices, and for each bond b, the component Ψ_b of the total wavefunction Ψ_b is a solution of Eq.(2).

The wavefunction, Ψ_b, satisfies boundary conditions at the vertices, which ensures continuity and current conservation [1]. The general scheme for finding eigenfunctions and eigenvalues for such boundary conditions can be found in Ref. [1]. Different types of boundary conditions for the Schrodinger equation on graphs are discussed in the Refs. [5–7]. In the following, we restrict our consideration to the simplest graph, the so-called star graph. The star graph consists of three or more bonds connected at a single vertex which is called the branching point. Other points are called edge vertices. The eigenvalue problem for a star graph with N bonds is given by the following Schrödinger equation:

$$-\frac{d^2}{dx^2}\phi_j(y) = k^2\phi_j(y), \quad 0 \leqslant y \leqslant l_j, \ j = 1, ..., N. \tag{3}$$

Here we consider the following boundary conditions [11]:

$$\begin{cases} \phi_1|_{y=0} = \phi_2|_{y=0} = ... = \phi_N|_{y=0}, \\ \phi_1|_{y=l_1} = \phi_2|_{y=l_2} = ... = \phi_N|_{y=l_N} = 0, \\ \sum\limits_{j=1}^{N} \frac{\partial}{\partial y}\phi_j|_{y=0} = 0. \end{cases} \tag{4}$$

The eigenvalues can be found by solving the following equation [11]:

$$\sum_{j=1}^{N} \tan^{-1}(k_n l_j) = 0, \tag{5}$$

where the corresponding eigenfunctions are given as [11]:

$$\phi_j^{(n)} = \frac{B_n}{sin(k_n l_j)} sin(k_n(l_j - y)), \tag{6}$$

where normalization coefficients are given as:

$$B_n = \left[\sum_j \left(L_j + \sin\left(2k_nL_j\right)\right)\sin^{-2}\left(k_nL_j\right)/2\right]^{-1/2}. \tag{7}$$

2. Time-dependent graph

A time-dependent graph implies that the lengths of the bonds of a graph are time-varying, i.e., when L_j is a function of time. In this case, the particle dynamics in graph are described by the following time-dependent Schrödinger equation:

$$i\frac{\partial}{\partial t}\Psi_j(x,t) = -\frac{\partial^2}{\partial x^2}\Psi_j(x,t), \quad 0 < x < L_j(t), \ j = 1, ..., N, \tag{8}$$

with N being the number of bonds.

In the following, we will consider the boundary conditions given by:

$$\begin{cases} \Psi_1|_{x=0} = \Psi_2|_{x=0} = ... = \Psi_N|_{x=0}, \\ \Psi_1|_{x=L_1(t)} = \Psi_2|_{x=L_2(t)} = ... = \Psi_N|_{x=L_N(t)} = 0, \\ \sum\limits_{j=1}^{N} \frac{\partial}{\partial x}\Psi_j|_{x=+0} = 0. \end{cases} \tag{9}$$

These boundary conditions imply that only edge vertices of the graph are moving while the center (branching point) is fixed. Furthermore, we assume that $L_j(t)$ is given as $L_j(t) = l_jL(t)$, where $L(t)$ is a continuous function and l_j are positive constants. Then, using the coordinate transformation:

$$y = \frac{x}{L(t)}, \tag{10}$$

Eq.(8) can be rewritten as:

$$i\frac{\partial}{\partial t}\Psi_j(y,t) = -\frac{1}{L^2}\frac{\partial^2}{\partial y^2}\Psi_j(y,t) + i\frac{\dot{L}}{L}y\frac{\partial}{\partial y}\Psi_j(y,t), \quad 0 < y < l_j, \ j = 1, ..., N. \tag{11}$$

It is clear that the Schrödinger operator in the right hand side of Eq.(11) is not Hermitian due to the presence of a second term. Therefore, using the transformation:

$$\Psi_j(y,t) = \frac{1}{\sqrt{L}}e^{i\frac{L\dot{L}}{4}y^2}\varphi_j(y,t), \tag{12}$$

we can make it Hermitian as:

$$i\frac{\partial}{\partial t}\varphi_j(y,t) = -\frac{1}{L^2}\frac{\partial^2}{\partial y^2}\varphi_j(y,t) + \frac{L\ddot{L}}{4}y^2\varphi_j(y,t), \quad 0 < y < l_j, \ j = 1, ..., N. \tag{13}$$

We note that the functions $\varphi_j(y,t)$ satisfy the boundary conditions (9) with $y = l_j$ instead of $x = L_j(t)$.

Time and coordinate variables in Eq.(13) can be separated only in the case when $L(t)$ obeys the equation:

$$\frac{L^3\ddot{L}}{4} = -C^2 = const, \tag{14}$$

In this case, using the substitution $\varphi_j(y,t) = \phi_j(y)\exp\left(-ik^2\int\limits_0^t L^{-2}(s)ds\right)$, we get:

$$\frac{d^2}{dy^2}\phi_j + (k^2 - C^2y^2)\phi_j = 0, \quad y \in (0, l_j). \tag{15}$$

For $C \neq 0$ from Eq.(14), we have:

$$L(t) = \sqrt{\alpha t^2 + \beta t + \gamma}, \quad C^2 = \frac{1}{16}(\beta^2 - 4\alpha\gamma), \tag{16}$$

and

$$L(t) = \sqrt{\beta t + \gamma}, \quad C^2 = \frac{1}{16}\beta^2. \tag{17}$$

In both cases, exact solutions of Eq.(13) can be obtained in terms of confluent hypergeometric functions. In particular, for the case when the time-dependence of $L(t)$ is given by Eq.(17), fundamental solutions of Eq.(13) can be written as:

$$\phi_{j,1} = y \exp\left(\frac{C}{2}y\right) M\left(\frac{3}{4} - \frac{k}{4C}, \frac{3}{2}, -Cy^2\right),$$

and

$$\phi_{j,2} = \exp\left(\frac{C}{2}y\right) M\left(\frac{1}{4} - \frac{k}{4C}, \frac{1}{2}, -Cy^2\right).$$

Therefore, the general solution of Eq.(13) is given as:

$$\phi_j(y) = D_j\phi_{j,1} + G_j\phi_{j,2}, \quad D_j, G_j = const. \tag{18}$$

From the boundary conditions given by Eq.(4), we have:

$$G_j = A, \quad D_j = A \cdot \alpha_j(k), \quad j = 1, 2, 3, ..., N,$$

where A is an arbitrary constant and:

$$\alpha_j(k) = -\frac{M\left(\frac{1}{4} - \frac{k}{4C}, \frac{1}{2}, -Cl_j^2\right)}{l_j M\left(\frac{3}{4} - \frac{k}{4C}, \frac{3}{2}, -Cl_j^2\right)}, \quad j = 1, 2, ..., N.$$

Taking into account the relations:

$$\left.\frac{d\phi_{j,1}(y)}{dy}\right|_{y=0} = 1, \ \left.\frac{d\phi_{j,2}(y)}{dy}\right|_{y=0} = \frac{C}{2},$$

from Eq.(4), we obtain the following spectral equation for finding the eigenvalues, k_n of Eq.(13):

$$\sum_{j=1}^{N} \frac{1}{l_j} \frac{M\left(\frac{1}{4} - \frac{k}{4C}, \frac{1}{2}, -Cl_j^2\right)}{M\left(\frac{3}{4} - \frac{k}{4C}, \frac{3}{2}, -Cl_j^2\right)} = \frac{CN}{2}. \tag{19}$$

Thus, the eigenfunctions of Eq.(13) can be written as:

$$\phi_j(y, k_n) = A\left[\alpha_j(k_n)\phi_{j,1}(y) + \phi_{j,2}(y)\right], \quad j = 1, 2, ..., N. \tag{20}$$

Furthermore, we provide the solution for Eq.(13) for the simplest case $L(t) = at + b$, which corresponds to $C = 0$ in Eq.(14). In this case, the eigenvalues for Eq.(13), which can be written in terms of the time-dependence of the wall are given as:

$$\phi_j(y, k_n) = \frac{A}{sin(k_n l_j)} sin(k_n(l_j - y)), \quad j = 1, 2, ..., N, \tag{21}$$

where k_n is the nth positive root of the equation:

$$\sum_{j=1}^{N} \tan^{-1}(l_j k) = 0. \tag{22}$$

and $L(t) > 0$, A is the normalization constant.

Now, let us consider the harmonically breathing graph, i.e. the case when the time-dependence of $L(t)$ is given as:

$$L(t) = b + a\cos\omega t,$$

with $\omega = 2\pi T^{-1}$ being oscillation frequency and T is the oscillation period. It is clear that in this case, the time and coordinate variables in Eq.(13) cannot be separated. Expanding $\varphi(y,t)$ in Eq.(13) in terms of the complete set of static graphs solutions gives the wave functions as:

$$\varphi_j(y,t) = \sum_n C_n(t)\phi_j^{(n)}(y), \tag{23}$$

and inserting this expansion into Eq.(13) we have:

$$\dot{C}_m(t) = \sum_n M_{mn}C_n(t),$$

where

$$M_{mn} = -i\frac{k_m^2}{L^2(t)} - i\frac{L\ddot{L}}{4}\sum_j \int_0^{l_j} y^2\phi_j^{(n)}\phi_j^{(m)}dy.$$

3. Wave packet evolution in harmonically breathing graph

The quantity we are interested in computing is the average kinetic energy, which is defined as:

$$E(t) = \langle\psi|H|\psi\rangle = \sum_{j=1}^{N}\int_0^{L_j(t)}\left|\frac{\partial\psi_j(x,t)}{\partial x}\right|^2 dx. \tag{24}$$

In Figure 1, the time dependence of the average kinetic energy of the harmonically breathing star graph is presented for different breathing frequency and amplitude values. As can be seen from these plots, $\langle E(t)\rangle$ is almost periodic for $\omega = 0.5$ and $a = 1$, while for $\omega = 10$ and $a = 1$, such periodicity is completely broken and energy increases with time. For $\omega = 10$ and $a = 20$, $\langle E(t)\rangle$ demonstrates "quasiperiodic behavior". The appearance of periodic behavior in $\langle E(t)\rangle$ can be explained by synchronization of the particle motion with the frequency. Over time, the lack of such synchronization causes break in the periodicity of the average energy.

Additionally, we consider wave packet evolution in an harmonically breathing star graph by taking the wave function at $t = 0$ (for the first bond) as the following Gaussian wave packet:

$$\Psi_1(x,0) = \Phi(x) = (2\pi\sigma^2)^{-1/2}\exp\left(-(x-\mu)^2/2\sigma\right), \tag{25}$$

with σ being the width of the packet. For other bonds, the initial wave function is assumed to be zero, i.e. $\Psi_2(x,0) = \Psi_3(x,0) = 0$. Then, for the initial values of the functions $\varphi^{(j)}(y,t)$ in Eq.(23) we have:

$$\varphi_j(y,0) = L(0)e^{-i\frac{L(0)\dot{L}(0)}{4}y^2}\Phi(y).$$

Correspondingly, the expansion coefficients at $t = 0$ can be written as:

$$C_n(0) = \sum_j \int_0^{l_j} \varphi_j(y,0)\phi_j^{(n)^*}(y).$$

In calculating the wave packet evolution, we choose the initial condition as the Gaussian wave packet being on the first bond only, while for the other two bonds, the wave functions at $t = 0$ are taken as zero. In Figure 2, the time evolution of the wave packet is plotted for

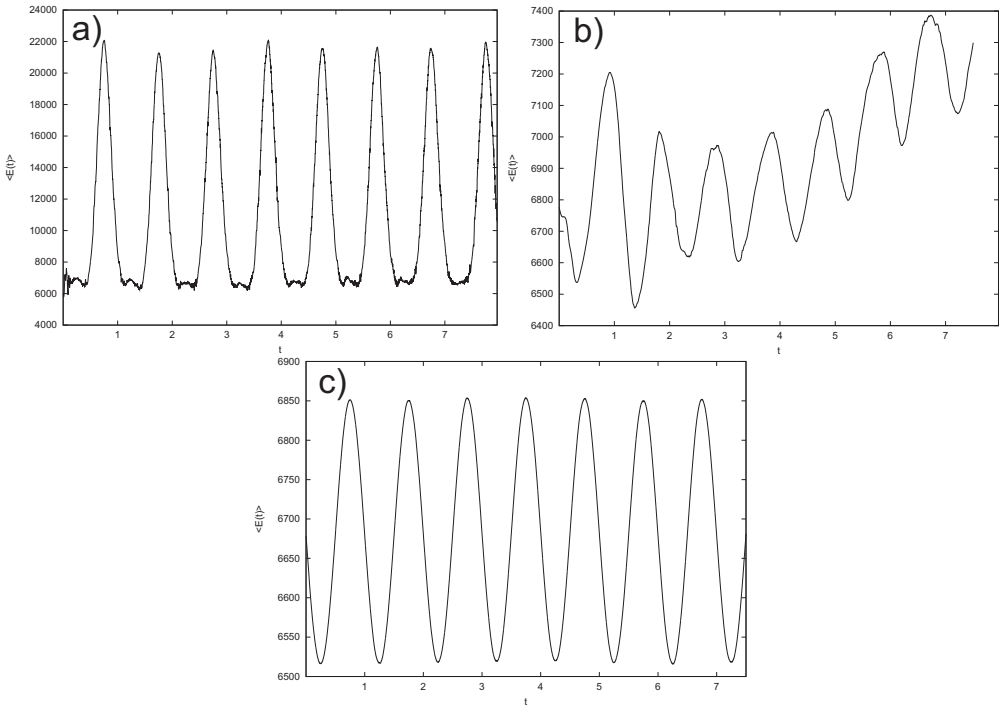

FIG. 1. Time-dependence of the average kinetic energy for an harmonically oscillating primary star graph. Time is presented in the units of the oscillation period $T = 2\pi/\omega$

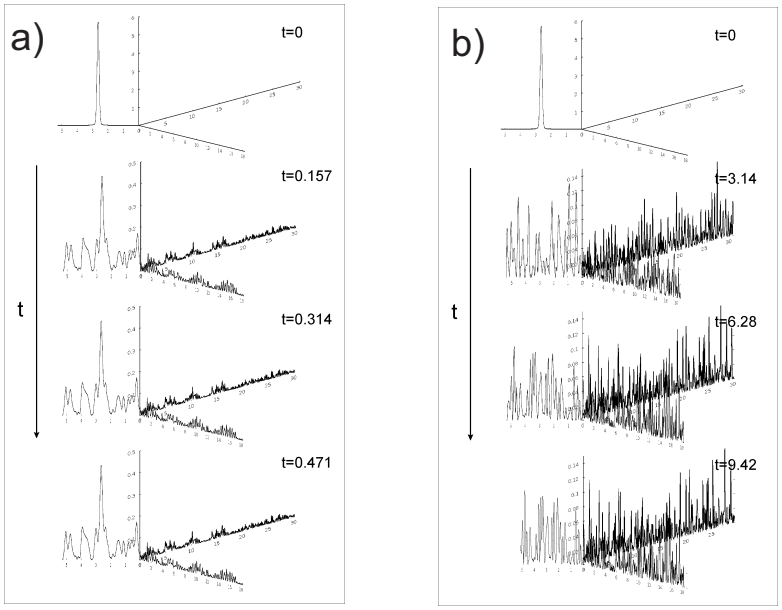

FIG. 2. Time evolution of the Gaussian wave packet given by Eq.(25) for the parameters: a) Wave packet evolution in static star graph b) $\omega = 0.5,\ a = 1$;.

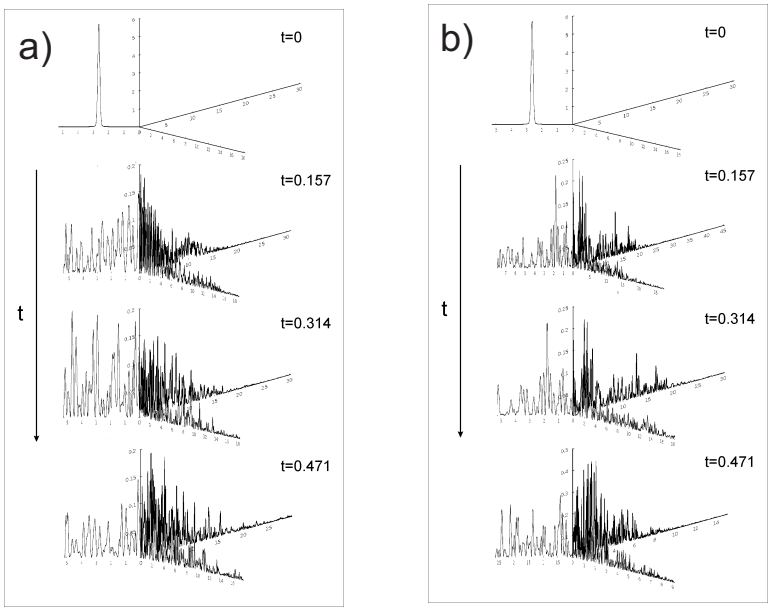

FIG. 3. Time evolution of the Gaussian wave packet given by Eq.(25) for the parameters: a) $\omega = 10,\ a = 20$; b) $\omega = 10,\ a = 1$;.

an harmonically breathing primary star graph whose bonds oscillate according to the law $L(t) = 40 + a\cos\omega t$. The oscillation parameters (frequency and amplitude) are chosen as follows: a) $\omega = 10,\ a = 20$; b) $\omega = 10,\ a = 1$; c) $\omega = 0.5,\ a = 1$. Figure 2a presents wave packet evolution in a static(time-independent) star graph. At $t = 0$, a Gaussian packet of width σ and velocity v_0 is assumed being in the first bond. As can be seen from these plots, for higher frequencies, dispersion of the packet and its transition to other bonds occurs more quickly compared to that of smaller frequencies. Again, an important role is played here by the possible synchronization between the bond edge and wave packet motions. The existence or absence of such synchronization defines how the collision of the packet with the bond edges will occur and how extensively it gains or loses its energy. Therefore, a more detailed treatment of the wave packet dynamics in harmonically breathing graphs should be based on the analysis of the role of synchronization and its criteria. Figure 4 presents time evolution of the probability densities corresponding to plots in Figure 2 and Figure 3. The parameters of the wave packet and oscillation parameters are the same as those in Figure 2 and Figure 3.

4. Conclusions

In this paper, we have treated a time-dependent quantum network by considering monotonically expanding and harmonically breathing quantum star graphs. Edge boundaries were considered to be time-dependent, while the branching point was assumed to be fixed. The time-dependence of the average kinetic energy and space-time evolution of the Gaussian wave packet were studied by solving the Schrodinger equation with time-dependent boundary conditions. It was found that for certain frequencies, energy is a periodic function of time, while for others, it can be a non-monotonically growing function of time. Such a feature can be caused by possible synchronization of the particles' motion and the motions of the moving edges of graph bonds. A similar feature can also be seen in the analysis of wave packet evolution. The above study can be useful for the treatment of particle transport

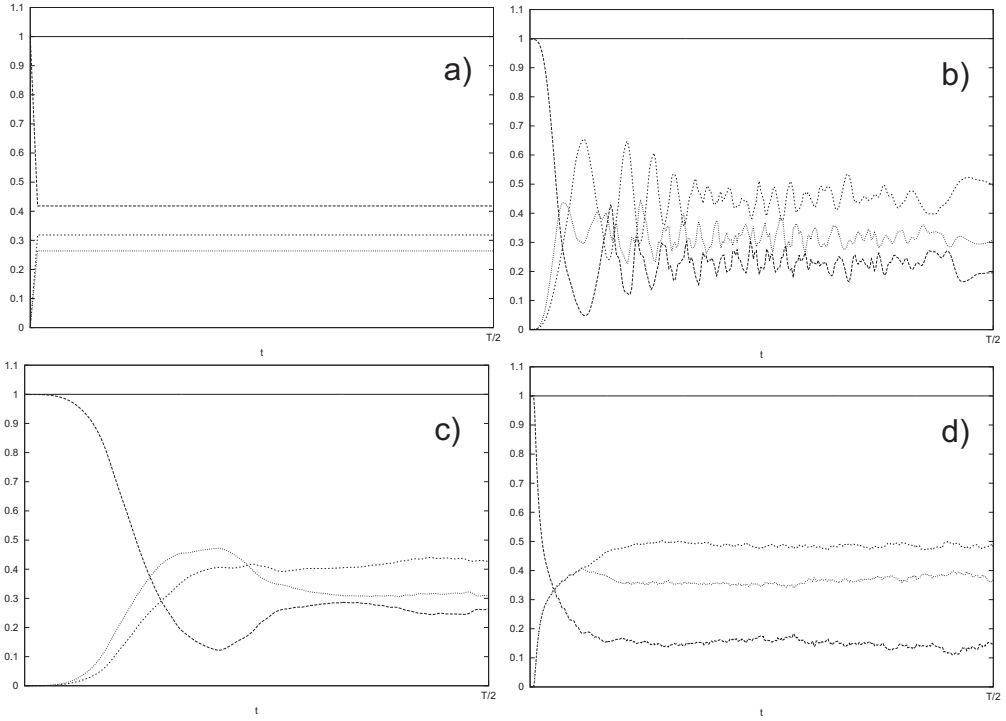

FIG. 4. Time evolution of the probability density: a) for static graph; b) time-dependent graph with $\omega = 10$ and $a = 20$; c) time-dependent graph with $\omega = 10$, and $a = 1$; d) time-dependent graph with $\omega = 0.5$, and $a = 1$.

in different discrete structures, such as molecular and quantum wire networks, networks of carbon nanotubes, crystal lattices, and others nanoscale systems that can be modeled by quantum graphs.

Acknowledgements

This work was supported in part by a research grant of Third World Academy of Sciences (Ref. 12-144RG/PHYS/AS_G).

References

[1] Kottos T. and Smilansky U. Periodic Orbit Theory and Spectral Statistics for Quantum Graphs. *Ann.Phys.*, **274**(1), P.76–124 (1999).

[2] Gnutzmann S. and Smilansky U. Quantum graphs: Applications to quantum chaos and universal spectral statistics. *Adv.Phys.*, **55**(5-6) P.527–625 (2006).

[3] Gnutzmann S., Keating J.P. and Piotet F. Eigenfunction statistics on quantum graphs. *Ann.Phys.*, **325**(12) P.2595–2640 (2010).

[4] Pauling L. The Diamagnetic Anisotropy of Aromatic Molecules. *J. Chem. Phys.*, **4** P.673 (1936).

[5] Exner P., Seba P. and Stovicek P. Quantum interference on graphs controlled by an external electric field. *J. Phys. A: Math. Gen.*, **21** P.4009–4019 (1988).

[6] Exner P. and Seba P. Free quantum motion on a branching graph. *Rep. Math. Phys.*, **28**(1) P.7–26 (1989).

[7] Exner P. A duality between Schrödinger operators on graphs and certain Jacobi matrices. *Ann. Inst. H. Poincare: Phys. Theor.*, **66**(4) P.359–371 (1997).

[8] Boman J. and Kurasov P. Symmetries of quantum graphs and the inverse scattering problem. *Adv. Appl. Math.*, **35**(1), P.58–70 (2005).

[9] Cheon T., Exner P. and Turek O. Approximation of a general singular vertex coupling in quantum graphs. *Ann.Phys.*, **325**(3) P.548–578 (2010).

[10] Hul O., Bauch S., Pakonski P., Savytskyy N., Zyczkowski K. and Sirko L. Experimental simulation of quantum graphs by microwave networks. *Phys. Rev. E*, **69**, P.056205 (2004).
[11] Keating J.P. Fluctuation statistics for quantum star graphs. Quantum graphs and their applications. *Contemp. Math.*, **415**, P.191–200 (2006).
[12] Jose J.V. and Gordery R. Study of a quantum fermi-acceleration model. *Phys. Rev. Lett.*, **56**, P.290 (1986).
[13] Karner G. On the quantum Fermi accelerator and its relevance to 'quantum chaos'. *Lett. Math. Phys.*, **17**, P.329–339 (1989).
[14] Seba P. Quantum chaos in the Fermi-accelerator model. *Phys. Rev. A*, **41**, P.2306 (1990).
[15] Doescher S.W. and Rice M.H. Infinite Square-Well Potential with a Moving Wall. *Am. J. Phys.*, **37**, P.1246 (1969).
[16] Munier A., Burgan J.R., Feix M. and Fijalkow E. Schrödinger equation with time-dependent boundary conditions. *J. Math. Phys.*, **22**, P.1219 (1981).
[17] Pinder D.N. The contracting square quantum well. *Am. J. Phys.*, **58**, P.54 (1990).
[18] Razavy M. Time-dependent harmonic oscillator confined in a box. *Phys. Rev. A*, **44**, P.2384 (1991).
[19] Pereshogin P. and Pronin P. Effective Hamiltonian and Berry phase in a quantum mechanical system with time dependent boundary conditions. *Phys. Lett. A*, **156**(1-2), P.12–16 (1991).
[20] Scheininger C. and Kleber M. Quantum to classical correspondence for the Fermi-acceleration model. *Physica D*, **50**(3), P.391–404 (1991).
[21] Makowski A.J. and Dembinski S.T. Exactly solvable models with time-dependent boundary conditions. *Phys. Lett. A*, **154**(5-6), P.217–220 (1991).
[22] Makowski A.J. and Peplowski P. On the behaviour of quantum systems with time-dependent boundary conditions. *Phys. Lett. A*, **163**(3), P.143–151 (1992).
[23] Makowski A.J. Two classes of exactly solvable quantum models with moving boundaries. *J. Phys. A: Math. Gen.*, **25**, P.3419 (1992).
[24] Willemsen J.E. Exact solution of the wave dynamics of a particle bouncing chaotically on a periodically oscillating wall. *Phys. Rev. E*, **50**, P.3116 (1994).
[25] Moralez D.A., Parra Z. and Almeida R. On the solution of the Schrödinger equation with time dependent boundary conditions. *Phys. Lett. A*, **185**(3), P.273–276 (1994).
[26] Yuce C. Singular potentials and moving boundaries in 3D. *Phys. Lett. A*, **321**(5-6), P.291–294 (2004).
[27] Glasser M.L., Mateo J., Negro J. and Nieto L.M. Quantum infinite square well with an oscillating wall. *Chaos, Solitons and Fractals*, **41**(4), P.2067–2074 (2009).
[28] Kostrykin R. and Schrader R. Kirchhoff's rule for quantum wires. *J. Phys. A: Math. Gen.*, **32**, P.595 (1999).

NANOSYSTEMS: PHYSICS, CHEMISTRY, MATHEMATICS, 2015, 6 (2), P. 182–191

An introduction to the spectral asymptotics of a damped wave equation on metric graphs

[1]J. Lipovský

[1] Department of Physics, Faculty of Science, University of Hradec Králové, Rokitanského 62, 500 03 Hradec Králové, Czechia

jiri.lipovsky@uhk.cz

PACS 03.65.Db, 03.65.Ge **DOI 10.17586/2220-8054-2015-6-2-182-191**

This paper summarizes the main results of [1] for the spectral asymptotics of the damped wave equation. We define the notion of a high frequency abscissa, a sequence of eigenvalues with imaginary parts going to plus or minus infinity and real parts going to some real number. We give theorems on the number of such high frequency abscissas for particular conditions on the graph. We illustrate this behavior in two particular examples.

Keywords: damped wave equation, spectrum, metric graphs.

Received: 2 February 2015

1. Introduction

The current text is a brief introduction to the spectral asymptotics of the damped wave equation on metric graphs. Our paper summarizes the main results of the paper [1] and gives ideas of their proofs. If the reader wants a detailed study of this problem or proofs of certain theorems, we refer to this paper. Its main results were obtained in collaboration with prof. Pedro Freitas during my stay in Lisbon.

Our aim is to study the damped wave equation

$$\partial_{tt}u(t,x) + 2a(x)\partial_t u(t,x) = \partial_{xx}u(t,x) + b(x)u(t,x) \tag{1}$$

on a metric graph. The problem of damped wave equation was studied in detail for a segment with Dirichlet conditions on both ends [2]. Paper [1], to the author's knowledge, is the first attempt to treat the problem for the graph. In the case of a segment, there exists a sequence of eigenvalues with imaginary parts going to plus and minus infinity and real part approaching the negative average of the damping function on the segment. In paper [2], an asymptotic expansion of the eigenvalues was obtained.

We show that in the case of a metric graph, there are several sequences of eigenvalues which we call *high frequency abscissas*. Our main results are three theorems on the number of these high frequency abscissas. This paper is structured as follows: in the second section we describe the model, next we give theorems on the asymptotics of eigenvalues and eigenfunctions and locations of eigenvalues and high frequency abscissas; next, we introduce the method of pseudo orbit expansion; in section 5, we give three main theorems on the number of high frequency abscissas; and finally, we show two particular examples to illustrate their behavior.

2. Description of the model

Let us consider a metric graph Γ with $N < \infty$ finite edges $\{e_j\}_{j=1}^N$ of lengths $\{l_j\}_{j=1}^N$. On each edge we consider a damped wave equation:

$$\partial_{tt} w_j(t,x) + 2a_j(x)\partial_t w_j(t,x) = \partial_{xx} w_j(t,x) + b(x) w_j(t,x), \tag{2}$$

with damping functions $a_j(x)$ and potentials $b_j(x)$ real and bounded. The functions at the j-th vertex are connected by coupling conditions similar to the case of quantum graphs

$$(U_j - I)\Psi_j + i(U_j + I)\Psi_j' = 0\,,$$

where U_j is a unitary square matrix, I is a unit matrix, Ψ_j is the vector of limits of functional values in the vertex from all neighboring edges and, similarly, Ψ_j' is the vector of outgoing derivatives. The coupling on the whole graph can be described by a large $2N \times 2N$ unitary matrix U (for more details see [3, 4]), which describes not only the coupling, but also the topology of the graph. Then, the coupling conditions are:

$$(U - I)\Psi + i(U + I)\Psi' = 0\,. \tag{3}$$

The ansatz $w_j(t,x) = \mathrm{e}^{\lambda t} u_j(x)$ leads to the differential equation:

$$\partial_{xx} u_j(x) - (\lambda^2 + 2\lambda a_j(x) - b_j(x)) u_j(x) = 0\,. \tag{4}$$

Our aim is to solve this equation and find complex numbers λ. Its real parts give the time decay for the solutions to the damped wave equation.

There exists a second approach to the problem, which is equivalent to the previous approach. One finds the eigenvalues of a non-self-adjoint operator:

$$H = \begin{pmatrix} 0 & I \\ I\frac{\mathrm{d}^2}{\mathrm{d}x^2} + B & -2A \end{pmatrix},$$

where A and B are $N \times N$ diagonal matrices with $a_j(x)$ and $b_j(x)$ on the diagonal. The domain of this operator consists of functions $(\psi_1(x), \psi_2(x))^{\mathrm{T}}$ with components of both ψ_1 and ψ_2 in $W^{2,2}(e_j)$ for the corresponding edge and satisfying coupling conditions (3) at the vertices.

In the following text, we will sometimes use the term *standard conditions*. These conditions (sometimes referred to in the literature as Kirchhoff, Neumann or free coupling) imply that the function is continuous at the vertex and the sum of outgoing derivatives is equal to zero. The corresponding vertex coupling matrix is $U = 2/dJ - I$, where d is the degree of a given vertex and J has all entries equal to one.

3. Eigenfunction and eigenvalue asymptotic properties and the locations of high frequency abscissas

First, we present a theorem from [2] on the asymptotic behavior of eigenfunctions on a segment.

Theorem 3.1. *Let $a \in \mathcal{C}^{m+1}[0,1]$ and $b \in \mathcal{C}^m[0,1]$. Then there exist two linearly independent solutions $u_\pm(x,\lambda)$ of equation (4) satisfying the initial condition $u_\pm(0,\lambda) = 1$ having the asymptotics:*

$$u_\pm(x,\lambda) = \mathrm{e}^{\pm\lambda x \pm \int_0^x \phi_\pm(t,\lambda)\,\mathrm{d}t}, \tag{5}$$

in the $C^2[0,1]$ *norm as* $\operatorname{Im}\lambda \to \infty$ *with:*

$$\phi_\pm(x,\lambda) = \sum_{i=0}^{m} \frac{\phi_i^\pm(x)}{\lambda^i} + \mathcal{O}(\lambda^{-m-1}), \tag{6}$$

and

$$\phi_0^{(\pm)}(x) = a(x)\,, \quad \phi_1^{(\pm)}(x) = -\frac{1}{2}(\pm a'(x) + a^2(x) + b(x))\,,$$
$$\phi_i^{(\pm)}(x) = -\frac{1}{2}\left(\pm\phi'^{(\pm)}_{i-1} + \sum_{s=0}^{i-1}\phi_s^{(\pm)}\phi_{i-s-1}^{(\pm)}\right).$$

Now, we can formulate the theorem on the asymptotics of eigenvalues for a graph with all the edges of lengths equal to one.

Theorem 3.2. *Let us assume a graph with* N *finite edges of lengths 1 with the coupling between vertices given by matrix* U*. Let on each edge be damping* $a_j \in \mathcal{C}^{N+1}([0,1])$ *and potential* $b_j \in \mathcal{C}^N([0,1])$*. Then, there exists such a* $K_0 \in \mathbb{R}_+$ *that for* $K > K_0$*, if* $\lambda = r + iK$ *is an eigenvalue, then* $\lambda + 2\pi i + \mathcal{O}(1/K)$ *is also an eigenvalue. Similarly, if* $\lambda = r - iK$ *is an eigenvalue, then* $\lambda - 2\pi i + \mathcal{O}(1/K)$ *is also an eigenvalue. This means that there exist sequences of eigenvalues with the asymptotics* $\lambda_{ns} = 2\pi i n + c_0^s + \mathcal{O}(1/n)$*.*

Idea of the proof: Since two linearly independent solutions exist, according to the previous theorem, one can write the general solution as their linear combination. Substituting for the coupling conditions, one finds the secular equation in the form:

$$P_0 \mathrm{e}^{\lambda+\langle a_1\rangle+\lambda+\langle a_2\rangle+\cdots+\lambda+\langle a_N\rangle+\mathcal{O}(1/\lambda)} + P_{11}\mathrm{e}^{-\lambda-\langle a_1\rangle+\lambda+\langle a_2\rangle+\cdots+\lambda+\langle a_N\rangle+\mathcal{O}(1/\lambda)} +$$
$$P_{12}\mathrm{e}^{\lambda+\langle a_1\rangle-\lambda-\langle a_2\rangle+\cdots+\lambda+\langle a_N\rangle+\mathcal{O}(1/\lambda)} + \cdots + P_{21}\mathrm{e}^{-\lambda-\langle a_1\rangle-\lambda-\langle a_2\rangle+\cdots+\lambda+\langle a_N\rangle+\mathcal{O}(1/\lambda)} +$$
$$\cdots + P_{N1}\mathrm{e}^{-\lambda-\langle a_1\rangle-\lambda-\langle a_2\rangle-\cdots-\lambda-\langle a_N\rangle+\mathcal{O}(1/\lambda)} = 0\,,$$

where P_{mn} is a polynomial in λ of degree $2N$ with m minuses before λ; n only distinguishes different polynomials. Since $1/\lambda = \mathcal{O}(1/K)$, one finds that the first term of the asymptotics is equal to zero for $\lambda_0 + 2\pi i$ if λ_0 is an eigenvalue. Hence, such $\lambda = \lambda_0 + 2\pi i + \mathcal{O}(1/\lambda_0)$ exists for which the secular equation is equal to zero. □

Now, we define the notion of a high frequency abscissa, which will be very important in subsequent sections.

Definition 3.3. We say that c_0 is a *high frequency abscissa* of the operator H if there exists a sequence of eigenvalues of H, say $\{\lambda_n\}_{n=1}^\infty$, such that:

$$\lim_{n\to\infty} \operatorname{Im}\lambda_n = \pm\infty \text{ and } \lim_{n\to\infty} \operatorname{Re}\lambda_n = c_0.$$

The next theorem says that only the average of the damping function on each edge is important for the location of high frequency abscissas.

Theorem 3.4. *Let* Γ *be a graph with* N *commensurate edges of lengths* $l_j = m_j l_0$*,* $m_j \in \mathbb{N}$*,* $j = 1,\ldots,N$*, with the coupling conditions (3). Let the damping functions* $a_j(x)$ *and* $b_j(x)$ *be bounded and continuous on each edge. Let* λ_n *be eigenvalues of the corresponding problem (4) and* μ_n *eigenvalues for* a_j *and* b_j *replaced by their averages. Then, the constant terms* c_0 *in the asymptotic expansion of* λ_n *coincide with the corresponding constant terms in the asymptotic expansion of* μ_n*.*

Now, we write a theorem on the location of nonreal eigenvalues, which has a nice corollary. It shows that the high frequency abscissas are located between the negative maximum of the averages of the damping functions on each edge and the negative minimum of these damping functions.

Theorem 3.5. *Let us consider a damped wave equation on a graph with N edges of lengths l_j, bounded damping coefficients $a_j(x)$ and potentials $b_j(x)$, and the coupling conditions given by (3). If λ is an eigenvalue of H with nontrivial imaginary part $\Im(\lambda) \neq 0$, then its real part satisfies:*

$$\Re(\lambda) = -\frac{\sum_{j=1}^{N} \int_0^{l_j} a_j(x)|u_j(x)|^2 \,\mathrm{d}x}{\sum_{j=1}^{N} \|u_j(x)\|_2^2},$$

where $u_j(x)$ denotes the corresponding wavefunction components.

Idea of the proof: The main idea of the proof is to take the equation (4), multiply it on the left by $\bar{u_j}(x)$, integrate over each edge and sum over all the edges. The imaginary part of the result is:

$$0 = 2\mathrm{i}\,\Im(\lambda) \sum_{j=1}^{N} \int_{e_j} \left(a_j(x) + \Re(\lambda)\right) |u_j(x)|^2 \,\mathrm{d}x,$$

from which the conclusion follows. □

Corollary 3.6. *Let us consider a damped wave equation on graph Γ with damping functions on the edges $a_j(x)$ and potentials $b_j(x)$. We denote the average of the damping function on each edge by $\bar{a}_j$. Then, the real part of nonreal eigenvalues of H (and therefore also all high frequency abscissas) lie in the interval $[-\max_j \bar{a}_j, -\min_j \bar{a}_j]$.*

4. Pseudo orbit expansion

There is a different approach to the secular equation than the one shown in the previous sections. The secular equation can be constructed by the method of pseudo orbit expansion, which has been developed for quantum graphs [5–7]. This theory was adapted for the damped wave equation in [1], and now, we summarize its main ideas.

First, the metric graph Γ is replaced by a directed graph Γ_2, each edge is replaced by two edges e_j and $\hat{e}_j$ in both directions. The functional values on both corresponding directed edges must be the same, hence if we use the ansatz:

$$f_{e_j}(x) = \alpha_{e_j}^{\mathrm{in}} \mathrm{e}^{\tilde{\lambda}_j x} + \alpha_{e_j}^{\mathrm{out}} \mathrm{e}^{-\tilde{\lambda}_j x}\,,$$
$$f_{\hat{e_j}}(x) = \alpha_{\hat{e}_j}^{\mathrm{in}} \mathrm{e}^{\tilde{\lambda}_j x} + \alpha_{\hat{e}_j}^{\mathrm{out}} \mathrm{e}^{-\tilde{\lambda}_j x}\,,$$

we have from $f_{e_j}(x) = f_{\hat{e}_j}(l_j - x)$ the relation between the coefficients of this ansatz:

$$\alpha_{\hat{e}_j}^{\mathrm{out}} = \mathrm{e}^{\tilde{\lambda}_j l_j} \alpha_{e_j}^{\mathrm{in}}\,, \qquad \alpha_{e_j}^{\mathrm{out}} = \mathrm{e}^{\tilde{\lambda}_j l_j} \alpha_{\hat{e}_j}^{\mathrm{in}}\,, \tag{7}$$

where $\tilde{\lambda}_j = \sqrt{\lambda^2 + 2\lambda a_j - b_j}$. Furthermore, we will now define several variables. The vertex scattering matrix maps the vector $\vec{\alpha}_v^{\mathrm{in}}$ into $\vec{\alpha}_v^{\mathrm{out}}$ by the relation $\vec{\alpha}_v^{\mathrm{out}} = \sigma_v(\lambda)\vec{\alpha}_v^{\mathrm{in}}$. Here, $\vec{\alpha}_v^{\mathrm{in,out}} = (\alpha_{e_{v1}}^{\mathrm{in,out}}, \ldots, \alpha_{e_{vd}}^{\mathrm{in,out}})^{\mathrm{T}}$ and v denotes the vertex. The matrix $\Sigma(\lambda)$ is block-diagonalizable and it is written in the basis corresponding to:

$$\vec{\alpha} = (\alpha_{e_1}, \ldots, \alpha_{e_N}, \alpha_{\hat{e}_1}, \ldots, \alpha_{\hat{e}_N})^{\mathrm{T}}\,.$$

This is block diagonal with blocks $\sigma_v(\lambda)$ if written in the following basis:

$$(\alpha_{e_{v_1 1}}^{\mathrm{in}}, \ldots, \alpha_{e_{v_1 d_1}}^{\mathrm{in}}, \alpha_{e_{v_2 1}}^{\mathrm{in}}, \ldots, \alpha_{e_{v_2 d_2}}^{\mathrm{in}}, \ldots,)^{\mathrm{T}}.$$

Furthermore, we define

$$J = \begin{pmatrix} 0 & I \\ I & 0 \end{pmatrix} \quad \text{and} \quad L = \exp\left(\operatorname{diag}\left(-\tilde{\lambda}_1 l_1, \ldots, -\tilde{\lambda}_N l_N, -\tilde{\lambda}_1 l_1, \ldots, -\tilde{\lambda}_N l_N\right)\right),$$

which then allows us to write:

$$\begin{pmatrix} \vec{\alpha}_e^{\text{in}} \\ \vec{\alpha}_{\hat{e}}^{\text{in}} \end{pmatrix} = L \begin{pmatrix} \vec{\alpha}_{\hat{e}}^{\text{out}} \\ \vec{\alpha}_e^{\text{out}} \end{pmatrix} = LJ \begin{pmatrix} \vec{\alpha}_e^{\text{out}} \\ \vec{\alpha}_{\hat{e}}^{\text{out}} \end{pmatrix} = LJ\Sigma(\lambda) \begin{pmatrix} \vec{\alpha}_e^{\text{in}} \\ \vec{\alpha}_{\hat{e}}^{\text{in}} \end{pmatrix},$$

where we have used the definition of the matrix L and relations (7), then the definition of the matrix J and finally the definition of the matrix Σ. Since the vectors on the left and the right side are the same, we obtain the secular equation:

$$\det\left(LJ\Sigma(\lambda) - I_{2N\times 2N}\right) = 0\,. \tag{8}$$

Next, following the terminology of [7], we define the following notions.

Definition 4.1. *A* periodic orbit *is a closed trajectory on the graph* Γ_2. *An* irreducible pseudo orbit $\bar{\gamma}$ *is a collection of periodic orbits where none of the directed bonds is contained more than once. Let* $m_{\bar{\gamma}}$ *denote the number of periodic orbits in* $\bar{\gamma}$, $L_{\bar{\gamma}} = \sum_{e\in\bar{\gamma}} \tilde{\lambda}_e l_e$ *where the sum is over all directed bonds in* $\bar{\gamma}$ *and* $\tilde{\lambda}_e = \sqrt{\lambda^2 + 2a_e\lambda - b_e}$. *The coefficients* $A_{\bar{\gamma}} = \Pi_{\gamma_j\in\bar{\gamma}} A_{\gamma_j}$ *with* A_{γ_j} *given as multiplication of entries of* $S(\lambda) = J\Sigma(\lambda)$ *along the trajectory* γ_j.

We give without the proof a theorem which gives the secular equation (8) in the terms of pseudo orbit expansion.

Theorem 4.2. *The secular equation for the damped wave equation on a metric graph is given by:*

$$\sum_{\bar{\gamma}} (-1)^{m_{\bar{\gamma}}} A_{\bar{\gamma}}(\lambda) \exp(-L_{\bar{\gamma}}(\lambda)) = 0$$

with $L_{\bar{\gamma}}$ *being the sum of the lengths of all directed edges along a particular irreducible pseudo orbit* $\bar{\gamma}$.

5. Number of distinct high frequency abscissas

In this section, we state the three main theorems of this paper. These theorems give upper and lower bounds on the number of distinct high frequency abscissas for a graph which has all edges of lengths 1. The first theorem gives an upper bound for a graph with general coupling conditions.

Theorem 5.1. *Let* Γ *be an equilateral graph with* N *edges of the length* 1. *Let us assume a damped wave equation on* Γ *with damping and constant potential functions constant on each edge* $a_j(x) \equiv a_j$, $b_j(x) \equiv b_j$ *and with general coupling given by (3) for a given unitary matrix* U. *Then there are at most* $2N$ *high frequency abscissas.*

Idea of the proof: We perform an expansion according to the theorem 3.2. In the first term of the n-asymptotics of the secular equation (written by the pseudo orbit expansion) is a polynomial equation in $y = \mathrm{e}^{c_0}$ of order $2N$. This polynomial equation has $2N$ complex solutions, therefore, there are at most $2N$ different numbers c_0 and $2N$ distinct high frequency abscissas. □

For a special type of graphs, the bound can be improved. In the second theorem, we consider a bipartite graph, the graph which can be colored by only two colors, with the neighboring vertices having different colors. Another definition is that there is not a loop of edges of odd length. In this case, there are at most N distinct high frequency abscissas.

Theorem 5.2. *Let Γ be a graph with N edges all of which have lengths equal to 1, (general) Robin coupling at the boundary and standard coupling otherwise. Let us suppose that the graph is bipartite. Then, for any damping functions bounded and $\mathcal{C}^2$ at each edge, there are at most N high frequency abscissas.*

Idea of the proof: Similarly to the previous theorem, we can construct the leading term of the n asymptotics of the secular equation. In the pseudo orbit expansion, we obtain only pseudo orbits, which have even length. Due to this fact there are only terms with e^{2c_0} in the secular equation. The first term of the n-expansion is a polynomial equation in e^{2c_0} of order N. Hence, there are at most N high frequency abscissas. □

The third theorem gives a lower bound on the number of high frequency abscissas. A tree graph with vertices of odd degree is considered.

Theorem 5.3. *Let Γ be a tree graph with N edges all with unit length, Robin coupling at the boundary and standard coupling otherwise. Let us suppose that all vertices have odd degree. Then, there always exists such a damping, for which the number of high frequency abscissas is greater than or equal to N.*

Idea of the proof: The main idea is that the contribution of the pseudo orbits to the coefficient in the secular equation cancels if and only if there is a vertex of Γ with a degree $2v$ and the pseudo orbit contains exactly v edges which emanate from this vertex. This can be proven using rather technical lemma 6.3 from the paper [1]. Hence, if a tree graph has all vertices of odd degree, then there is no cancellation and all the coefficients in the secular equation are nonzero. Now, we construct the damping function. We choose constant damping on each edge with $0 \ll a_N \ll a_{N-1} \ll \cdots \ll a_1$. Now we can rewrite the first term of the secular equation as:

$$C_N \mathrm{e}^{2a_1+2a_2+\cdots+2a_N} y^N + C_{N-1}\mathrm{e}^{2a_1+2a_2+\cdots+2a_{N-1}} \left[1+\mathcal{O}\left(\mathrm{e}^{-2(a_{N-1}-a_N)}\right)\right] y^{N-1} + \\ + \cdots + C_2 \mathrm{e}^{2a_1+2a_2} \left[1+\mathcal{O}\left(\mathrm{e}^{-2(a_2-a_3)}\right)\right] y^2 + C_1 \mathrm{e}^{2a_1} \left[1+\mathcal{O}\left(\mathrm{e}^{-2(a_1-a_2)}\right)\right] y + C_0 = 0\,,$$

with $y = \mathrm{e}^{2c_0}$. We recall that none of the coefficients C_i are equal to zero. Now, if y is close to e^{-2a_1}, the last two terms are dominant, for y close to e^{-2a_2} the terms with C_2 and C_1 are dominant, etc. Hence we have

$$y_j = -\frac{C_{j-1}}{C_j}\,\mathrm{e}^{-2a_j}\left[1+\mathcal{O}\left(\mathrm{e}^{-2(a_j-a_{j+1})}\right)\right]\,.$$

We obtain N distinct numbers y_j and hence N distinct numbers c_0 and N distinct high frequency abscissas. □

6. Examples

Now, we present two particular examples, which illustrate the behavior of the eigenvalues.

6.1. Two loops with different damping coefficients

The first example of a graph consists of two loops, each loop having three edges of lengths 1 (see figure 1). Let us assume that there is constant damping a_1 on the first loop and a_2 on the second loop. Therefore, one can use the ansatz $f_j(x) = \alpha_j \sinh\left(\tilde{\lambda}_j(\lambda)x\right) +$

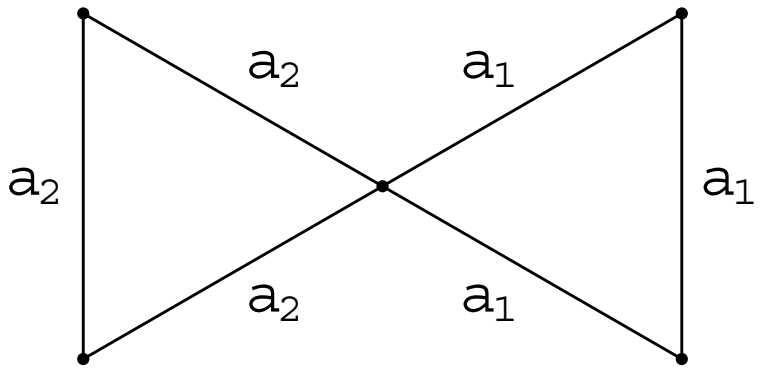

FIG. 1. Graph with two loops

$\beta_j \cosh\left(\tilde{\lambda}_j(\lambda)x\right)$, where j distinguishes the loop. We choose $x = 0$ at the middle of each loop. From the continuity at the central vertex, we have:

$$\alpha_j \sinh\left(\frac{3}{2}\tilde{\lambda}_j(\lambda)\right) + \beta_j \cosh\left(\frac{3}{2}\tilde{\lambda}_j(\lambda)\right) = -\alpha_j \sinh\left(\frac{3}{2}\tilde{\lambda}_j(\lambda)\right) + \beta_j \cosh\left(\frac{3}{2}\tilde{\lambda}_j(\lambda)\right).$$

Therefore, we either have $\alpha_1 = \alpha_2 = 0$ or $\sinh\left(\frac{3}{2}\tilde{\lambda}_1(\lambda)\right) = 0$ or $\sinh\left(\frac{3}{2}\tilde{\lambda}_2(\lambda)\right) = 0$.

First, we will assume $\alpha_1 = \alpha_2 = 0$. From the standard conditions at the central vertex we have:

$$\beta_1 \cosh\frac{3\tilde{\lambda}_1(\lambda)}{2} = \beta_2 \cosh\frac{3\tilde{\lambda}_2(\lambda)}{2},$$
$$\beta_1\tilde{\lambda}_1(\lambda) \sinh\frac{3\tilde{\lambda}_1(\lambda)}{2} + \beta_2\tilde{\lambda}_2(\lambda) \sinh\frac{3\tilde{\lambda}_2(\lambda)}{2} = 0.$$

where

$$\tilde{\lambda}_j \equiv \tilde{\lambda}_j(\lambda) = \sqrt{\lambda^2 + 2a_j\lambda - b_j}.$$

This set of equations is solvable under the condition:

$$\tilde{\lambda}_2 \sinh\frac{3\tilde{\lambda}_2}{2} \cosh\frac{3\tilde{\lambda}_1}{2} + \tilde{\lambda}_1 \sinh\frac{3\tilde{\lambda}_1}{2} \cosh\frac{3\tilde{\lambda}_2}{2} = 0.$$

or, equivalently by:

$$(\tilde{\lambda}_1 + \tilde{\lambda}_2) \sinh\frac{3(\tilde{\lambda}_1 + \tilde{\lambda}_2)}{2} + (\tilde{\lambda}_1 - \tilde{\lambda}_2) \sinh\frac{3(\tilde{\lambda}_1 - \tilde{\lambda}_2)}{2} = 0.$$

Using the asymptotic expansion $\lambda_n = 2\pi i n + c_0 + \mathcal{O}\left(\frac{1}{n}\right)$ one obtains

$$4\pi i n \left(\mathrm{e}^{6\pi i n + \frac{3}{2}(a_1+a_2+2c_0)} - \mathrm{e}^{-6\pi i n - \frac{3}{2}(a_1+a_2+2c_0)}\right) + \mathcal{O}(1) = 0,$$

and therefore:

$$3(a_1 + a_2 + 2c_0) + 2\pi i n = 0, \tag{9}$$
$$c_0^{(s)} = -\frac{a_1 + a_2}{2} + \frac{s\pi i}{6}, \quad s \in \{0, \ldots, 5\}$$

Now, let us return to the condition $\sinh\left(\frac{3}{2}\tilde{\lambda}_j(\lambda_n)\right) = 0$. This leads to:

$$3a_j + 3c_0^{(s)} + \mathcal{O}\left(\frac{1}{n}\right) = 2\pi i s \quad \Rightarrow \quad c_0^s = -a_j + \frac{2\pi i s}{3}, \quad s \in \{0, 1, 2\}$$

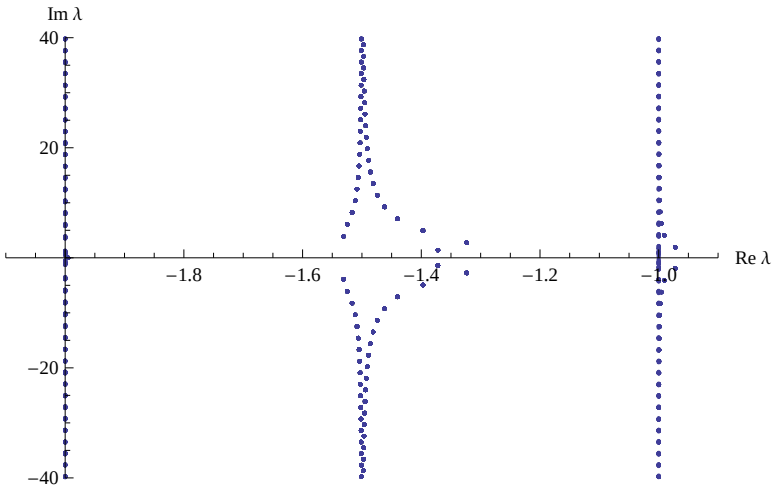

FIG. 2. Spectrum of a graph in figure 1, $a_1 = 2$, $a_2 = 1$, $b_1 = 0$, $b_2 = 0$

Hence, we have three high frequency abscissas at $-a_1$, $-a_2$ and $-\frac{a_1+a_2}{2}$. The eigenfunctions for the first two abscissas are supported on the first loop or the second loop, respectively. The third one has eigenfunction supported on both loops. Eigenvalues for particular choice $a_1 = 2$ and $a_2 = 1$ are shown in figure 2.

6.2. Star graph with different lengths of the edges

The second example illustrates eigenvalue behavior in the case when the lengths of the edges are not equal to one. Let us consider a star graph consisting of three edges of lengths l_1, l_2 and l_3. We assume Dirichlet coupling at the free ends and standard coupling in the central vertex.

If we use the ansatz $f_j(x) = \alpha_j \sinh \tilde{\lambda}_j x$ on each edge with $x = 0$ at the free end, we obtain the secular equation:

$$\sum_{j=1}^{3} \tilde{\lambda}_j \cosh \tilde{\lambda}_j l_j \prod_{\substack{i=1 \\ i\neq j}}^{3} \sinh \tilde{\lambda}_i l_i = 0\,.$$

In figure 3, we show the eigenvalues for particular choice of the damping $a_1 = 3$, $a_2 = 4$, $a_3 = 5$ and the lengths of the edges $l_1 = 1$, $l_2 = 1$, $l_3 = 1.03$. If we wanted to apply the theorems from the previous sections, we would have 303 edges of lengths 0.01, which means that the bound on the number of the high frequency abscissas would be 606. In figures 4 and 5, the behavior is shown for other combinations of edge lengths.

7. Conclusion

We have summarized the main results of a paper [1]. The main results are three theorems in section 5 on graphs with edges of unit lengths. If we have a graph with general coupling, the number of high frequency abscissas is bounded from above by $2N$. For a bipartite graph with standard coupling, the bound can be improved to N. And finally, for a tree graph with vertices of odd degree, one can find such a damping for which there is at least N high frequency abscissas.

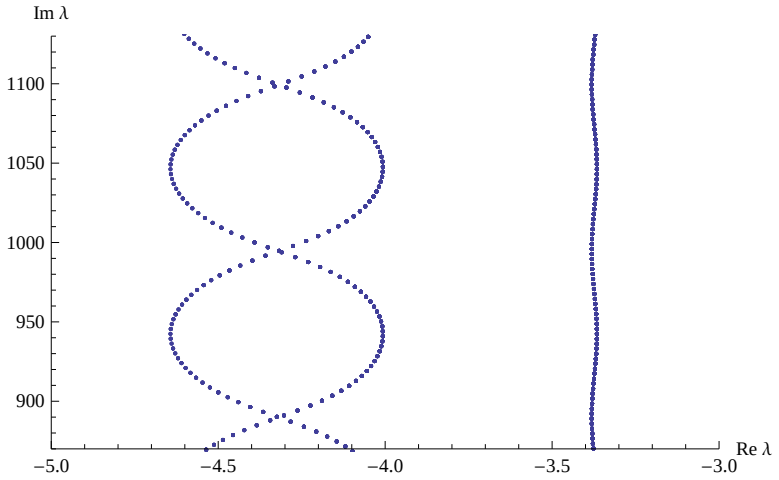

FIG. 3. Spectrum of a star graph with different edges lengths, $l_1 = 1$, $l_2 = 1$, $l_3 = 1.03$

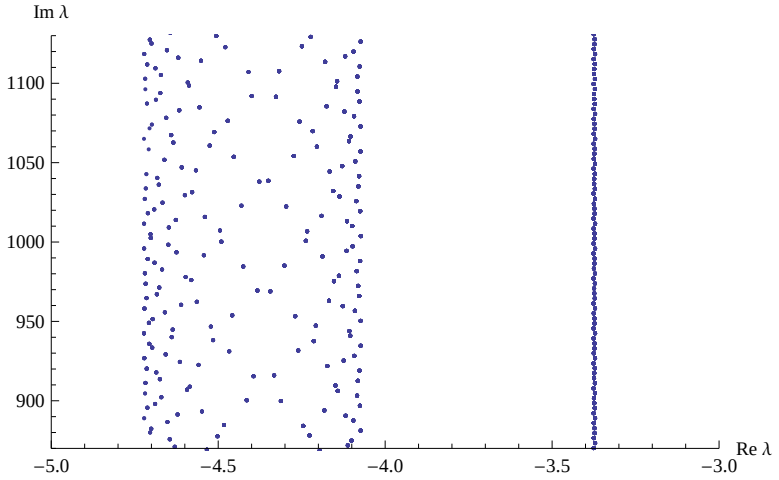

FIG. 4. Spectrum of a star graph with different edges lengths, $l_1 = 1$, $l_2 = 1$, $l_3 = 1.41$

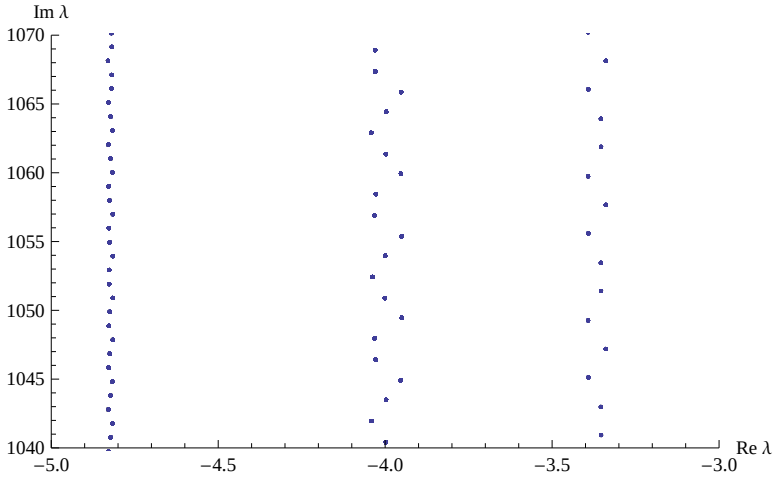

FIG. 5. Spectrum of a star graph with different edges lengths, $l_1 = 1.5$, $l_2 = 2.1$, $l_3 = 3.1$

Acknowledgements

The research was supported by the project Development of postdoc activities at the University of Hradec Králové, CZ.1.07/2.3.00/30.0015.

References

[1] Freitas P., Lipovský J. Eigenvalue asymptotics for the damped wave equation on metric graphs (2013). arXiv : `http://arxiv.org/abs/1307.6377`.

[2] Borisov D., Freitas P. Eigenvalue asymptotics, inverse problems and a trace formula for the linear damped wave equation. *J. Diff. Eq.*, **247**, P. 3028-3039 (2009).

[3] Kuchment P. Quantum graphs: an introduction and a brief survey. Analysis on Graphs and Its Applications. Proc. Symp. Pure. Math. (Providence, RI: American Mathematical Society), P. 291-314 (2008).

[4] Exner P., Lipovský J. Resonances from perturbations of quantum graphs with rationally related edges. *J. Phys. A.: Math. Theor.*, **43**, P. 105301 (2010).

[5] Kottos T., Smilansky U. Quantum chaos on graphs. *Phys. Rev. Lett.*, **79**, P. 4794-4797 (1997).

[6] Akkermans E., Comtet A., Desbois J., Montambaux G., Texier C. Spectral determinant on quantum graphs. *Annals of Physics*, **284**, P. 10-51 (2000).

[7] Band R., Harrison J. M., Joyner C. H. Finite pseudo orbit expansion for spectral quantities of quantum graphs. *J. Phys. A: Math. Theor.*, **45**, P. 325204 (2012).

NANOSYSTEMS: PHYSICS, CHEMISTRY, MATHEMATICS, 2015, 6 (2), P. 192–197

The relativistic inverse scattering problem for quantum graphs

K. K. Sabirov[1], Z. A. Sobirov[1], O. V. Karpova[1,2], A. A. Saidov[2]

[1]National University of Uzbekistan, 4 University St., 100074, Tashkent, Uzbekistan

[2]Turin Polytechnic University in Tashkent, 17 Niyazov St., 100095, Tashkent, Uzbekistan

karimjonsabirov@yahoo.com

PACS 02.30.Zz, 03.65.Pm **DOI 10.17586/2220-8054-2015-6-2-192-197**

In this paper, we treat the inverse scattering problem for the Dirac equation on metric graphs. Using the known scattering data, we recover the potential in the Dirac equation. The Gel'fand-Levitan-Marchenko integral equation is derived and potential is explicitly obtained for the case of a primary star graph.

Keywords: quantum graph, inverse scattering problem, Dirac equation.

Received: 2 February 2015

1. Introduction

The study of particle and wave transport in branched structures and networks is of fundamental and practical importance in different topics of contemporary physics. In particular, transport in such nanoscale systems as quantum networks, molecular chains, networks of carbon nanotubes or quantum wires and the problem of charge transport in a DNA double helix can be successfully modeled by quantum mechanical wave equations on metric graphs. Initially, the concept of quantum graphs was introduced by Pauling more than half a century ago to describe electron transport in complex molecular chains of organic molecules. The difference between the usual graph and the quantum graph (both from the mathematical term) is that the dynamics of particles in such systems are described with quantum-mechanical wave equations. Quantum graphs can be considered as a class of confined quantum systems where the dynamics strongly depends on the topology of a graph. The topology of the graph can be given in terms of adjacency matrix:

$$C_{i,j} = C_{j,i} = \begin{cases} 1, & \text{if } i,j \text{ are connected,} \\ 0, & \text{otherwise.} \end{cases}$$

Direct spectral and scattering problems on quantum graphs have been studied earlier in the context of quantum chaos theory (see reviews [1,2] and references therein). The inverse problem for quantum graphs can be divided into two types: the problem of the recovering the potential in the wave equation and the problem of finding the topology of a graph using the given spectral data. The latter is a more difficult problem because of possible isospectrality of graphs for different topologies [3]. In this paper, we solve the inverse scattering problem for the massless Dirac equation, given on the graph of the simplest topology, the so-called star graph. The importance of this problem is a result of its application for modeling charge, information and spin transport in branched nanostrctures (e.g., networks of graphene nanoribbons, carbon nanotubes (CNT) and quantum wires). The dynamics of quasi-particles in such systems are described by the massless Dirac equation. In this paper, we propose an

algorithm for reconstructing the potential of the Dirac equation using the available elements of the scattering matrix.

2. Formulation of the problem

Consider a star graph consisting of three semi-infinite edges connected at one point (see. Fig. 1). On each edge, we b_j determine the coordinates $x_j \in [0, \infty)$ where $x_j = 0$ corresponds to the vertex of the graph. The Dirac equation on the each edge b_j is given as:

$$\begin{pmatrix} -1 & 0 \\ 0 & 1 \end{pmatrix} \frac{d}{dx} f_j(x_j) + \begin{pmatrix} 0 & q_j(x_j) \\ -p_j(x_j) & 0 \end{pmatrix} f_j(x_j) = i\zeta f_j(x_j), \tag{1}$$

where $f_j(x_j) = \begin{pmatrix} f_{j,1}(x_j) \\ f_{j,2}(x_j) \end{pmatrix}$, $j = 1, 2, 3$. The following boundary conditions are imposed at the branching point:

$$\begin{aligned} &f_{1,1}(0) = f_{2,1}(0) = f_{3,1}(0), \\ &f_{1,2}(0) + f_{2,2}(0) + f_{3,2}(0) = 0. \end{aligned} \tag{2}$$

Let us define scattering matrices on each bond as:

$$S_j(\zeta_j) = \begin{pmatrix} a_j(\zeta) & b_j(\zeta) \\ \bar{b}_j(\zeta) & -\bar{a}_j(\zeta) \end{pmatrix}, j = 1, 2, 3. \tag{3}$$

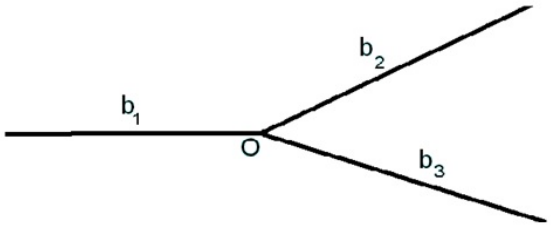

FIG. 1. Star graph

3. The direct scattering problem

We find three solutions $f^{(m)}(x, \zeta) = \left\{ f_1^{(m)}(x_1, \zeta), f_2^{(m)}(x_2, \zeta), f_3^{(m)}(x_3, \zeta) \right\}$, $m = 1, 2, 3$ for the problem given by Eqs. (1)–(3). Furthermore, we define the functions $\psi_j(x_j, \zeta)$, $\bar{\psi}_j(x_j, \zeta)$ as solutions of the following integral equations:

$$\begin{aligned} &\psi_{j,1}(x_j, \zeta) = \int_{x_j}^{+\infty} q_j(t) e^{-i\zeta(x_j - t)} \psi_{j,2}(t, \zeta) dt, \\ &\psi_{j,2}(x_j, \zeta) = e^{i\zeta x_j} + \int_{x_j}^{+\infty} \int_{t}^{+\infty} p_j(t) q_j(z) e^{-i\zeta(2t - x_j - z)} \psi_{j,2}(z, \zeta) dz dt, \end{aligned} \tag{4}$$

$$\begin{aligned} &\bar{\psi}_{j,1}(x_j, \zeta) = e^{-i\zeta x_j} + \int_{x_j}^{+\infty} \int_{t}^{+\infty} q_j(t) p_j(z) e^{i\zeta(2t - x_j - z)} \bar{\psi}_{j,1}(z, \zeta) dz dt, \\ &\bar{\psi}_{j,2}(x_j, \zeta) = \int_{x_j}^{+\infty} p_j(t) e^{i\zeta(x_j - t)} \bar{\psi}_{j,1}(t, \zeta) dt. \end{aligned} \tag{5}$$

Also, we introduce the solutions $\varphi_j(x_j, \zeta)$, $\bar{\varphi}_j(x_j, \zeta)$ obeying the following integral equations:

$$\begin{aligned} &\varphi_{j,1}(x_j, \zeta) = e^{-i\zeta x_j} + \int_0^{x_j} \int_0^{t} q_j(t) p_j(z) e^{i\zeta(2t - x_j - z)} \varphi_{j,1}(z, \zeta) dz dt, \\ &\varphi_{j,2}(x_j, \zeta) = \int_0^{x} p_j(t) e^{i\zeta(x_j - t)} \varphi_{j,1}(t, \zeta) dt, \end{aligned} \tag{6}$$

$$\begin{array}{l}\bar{\varphi}_{j,1}(x_j,\zeta)=\int_0^{x_j} q_j(t)e^{-i\zeta(x_j-t)}\bar{\varphi}_{j,2}(t,\zeta)dt,\\ \bar{\varphi}_{j,2}(x_j,\zeta)=-e^{i\zeta x_j}+\int_0^x\int_0^t p_j(t)q_j(z)e^{-i\zeta(2t-x_j-z)}\bar{\varphi}_{j,2}(z,\zeta)dzdt.\end{array} \tag{7}$$

It is easy to see that if $q_j, p_j \in L_1$, then the functions $e^{i\zeta x_j}\varphi_j(x_j,\zeta)$, $e^{-i\zeta x_j}\psi_j(x_j,\zeta)$ are analytic on the upper plane $Im\zeta > 0$, $e^{-i\zeta x_j}\bar{\varphi}_j(x_j,\zeta)$, $e^{i\zeta x_j}\bar{\psi}_j(x_j,\zeta)$ are analytic on the lower plane $Im\zeta < 0$.

Since the functions $\psi_j(x_j,\zeta)$, $\bar{\psi}_j(x_j,\zeta)$ obey the boundary conditions:

$$\left.\begin{array}{l}\psi_j(x_j,\zeta)\sim\begin{pmatrix}0\\1\end{pmatrix}e^{i\zeta x_j}\\ \bar{\psi}_j(x_j,\zeta)\sim\begin{pmatrix}1\\0\end{pmatrix}e^{-i\zeta x_j}\end{array}\right\}\quad \text{at } x_j\to+\infty, \tag{8}$$

the solutions $\psi_j(x_j,\zeta)$, $\bar{\psi}_j(x_j,\zeta)$ are linearly independent. This follows from the condition for the Wronskian: $W(\psi_j,\bar{\psi}_j)=-1$. Therefore we have:

$$\begin{array}{l}\varphi_j=a_j(\zeta)\bar{\psi}_j+b_j(\zeta)\psi_j,\\ \bar{\varphi}_j=-\bar{a}_j(\zeta)\psi_j+\bar{b}_j(\zeta)\bar{\psi}_j.\end{array} \tag{9}$$

It follows from Eqs. (6)–(7) that functions $\varphi_j(x_j,\zeta)$, $\bar{\varphi}_j(x_j,\zeta)$ satisfy conditions:

$$\begin{array}{l}\varphi_j(0,\zeta)=\begin{pmatrix}1\\0\end{pmatrix},\\ \bar{\varphi}_j(0,\zeta)=\begin{pmatrix}0\\-1\end{pmatrix}.\end{array} \tag{10}$$

Furthermore, from $W\left(\varphi_j,\,\bar{\varphi}_j\right)=-1$ we have:

$$a_j\bar{a}_j+b_j\bar{b}_j=1, \tag{11}$$

which implies that:

$$\begin{array}{l}\psi_j(0,\zeta)=\begin{pmatrix}\bar{b}_j\\a_j\end{pmatrix},\\ \bar{\psi}_j(0,\zeta)=\begin{pmatrix}\bar{a}_j\\-b_j\end{pmatrix}.\end{array} \tag{12}$$

The solutions $f^{(m)}(x,\zeta)=\left\{f_1^{(m)}(x_1,\zeta),f_2^{(m)}(x_2,\zeta),f_3^{(m)}(x_3,\zeta)\right\}$, $m=1,2,3$ can be written as:

$$\begin{array}{l}f_j^{(m)}(x_j,\zeta)=t_j^{(m)}(\zeta)\bar{\psi}_j(x_j,\zeta),\ m\neq j,\ j=1,2,3,\\ f_m^{(m)}(x_m,\zeta)=\varphi_m(x_m,\zeta)+r_m^{(m)}(\zeta)\psi_m(x_m,\zeta)e^{-2i\zeta x_m},\ m=1,2,3.\end{array} \tag{13}$$

The coefficients $r_m^{(m)}$, $t_j^{(m)}$ $(m\neq j,\ \ m,j=1,2,3)$ can be found from the boundary conditions for $f^{(m)}(x,\zeta)$. For example, at m=1 we have:

$$\begin{array}{l}\varphi_{1,1}(0,\zeta)+r_1^{(1)}(\zeta)\psi_{1,1}(0,\zeta)=t_2^{(1)}(\zeta)\bar{\psi}_{2,1}(0,\zeta)=t_3^{(1)}(\zeta)\bar{\psi}_{3,1}(0,\zeta),\\ \varphi_{1,2}(0,\zeta)+r_1^{(1)}(\zeta)\psi_{1,2}(0,\zeta)+t_2^{(1)}(\zeta)\bar{\psi}_{2,2}(0,\zeta)+t_3^{(1)}(\zeta)\bar{\psi}_{3,2}(0,\zeta)=0.\end{array} \tag{14}$$

Using Eqs. (11)-(12), one can obtain:

$$\begin{array}{l} r_1^{(1)}(\zeta) = \frac{\bar{a}_2 b_3 + b_2 \bar{a}_3}{a_1 \bar{a}_2 \bar{a}_3 - \bar{b}_1 \bar{a}_2 b_3 - \bar{b}_1 b_2 \bar{a}_3}, \\ t_2^{(1)}(\zeta) = \frac{a_1 \bar{a}_3}{a_1 \bar{a}_2 \bar{a}_3 - \bar{b}_1 \bar{a}_2 b_3 - \bar{b}_1 b_2 \bar{a}_3}, \\ t_3^{(1)}(\zeta) = \frac{a_1 \bar{a}_2}{a_1 \bar{a}_2 \bar{a}_3 - \bar{b}_1 \bar{a}_2 b_3 - \bar{b}_1 b_2 \bar{a}_3}. \end{array} \tag{15}$$

The above analysis is usually called the direct scattering problem. In the following, we will treat the inverse scattering problem.

4. The inverse scattering problem

Using the following integral representations for the functions $\psi_j(x_j, \zeta)$, $\bar{\psi}_j(x_j, \zeta)$:

$$\psi_j(x, \zeta) = \begin{pmatrix} 0 \\ 1 \end{pmatrix} e^{i\zeta x_j} + \int_{x_j}^{+\infty} K_j(x_j, s) e^{i\zeta s} ds, \tag{16}$$

$$\bar{\psi}_j(x, \zeta) = \begin{pmatrix} 1 \\ 0 \end{pmatrix} e^{-i\zeta x_j} + \int_{x_j}^{+\infty} \bar{K}_j(x_j, s) e^{-i\zeta s} ds, \tag{17}$$

where $K_j(x_j, s) = \begin{pmatrix} K_{j,1}(x_j, s) \\ K_{j,2}(x_j, s) \end{pmatrix}$, $\bar{K}_j(x_j, s) = \begin{pmatrix} \bar{K}_{j,1}(x_j, s) \\ \bar{K}_{j,2}(x_j, s) \end{pmatrix}$ are two-component vectors. To obey fy the boundary conditions (8), we assume that $K_j(x_j, s) = 0$ at $x_j > s$. Now, we will prove the existence of representations (16)–(17). To do that, it is enough to insert Eqs. (16)–(17) into (1). Then, from Eq. (16) we obtain:

$$\begin{array}{l} \int_{x_j}^{+\infty} e^{i\zeta s} \left[\left(\partial_{x_j} - \partial_s \right) K_{j,1}(x_j, s) - q_j(x_j) K_{j,2}(x_j, s) \right] ds - \\ - \left[q_j(x_j) + 2K_{j,1}(x_j, x_j) \right] e^{i\zeta x_j} + \lim\limits_{s \to \infty} \left[K_{j,1}(x_j, s) e^{i\zeta s} \right] = 0 \end{array} \tag{18}$$

$$\begin{array}{l} \int_{x_j}^{+\infty} e^{i\zeta s} \left[\left(\partial_{x_j} + \partial_s \right) K_{j,2}(x_j, s) - p_j(x_j) K_{j,1}(x_j, s) \right] ds - \\ - \lim\limits_{s \to \infty} \left[K_{j,2}(x_j, s) e^{i\zeta s} \right] = 0 \end{array} . \tag{19}$$

Thus, for the existence of representations (16)–(17), it is necessary and sufficient that functions $K_j(x_j, s)$ obey the following equations:

$$\begin{array}{l} \left(\partial_{x_j} - \partial_s \right) K_{j,1}(x_j, s) - q_j(x_j) K_{j,2}(x_j, s) = 0, \\ \left(\partial_{x_j} + \partial_s \right) K_{j,2}(x_j, s) - p_j(x_j) K_{j,1}(x_j, s) = 0, \end{array} \tag{20}$$

with the boundary conditions:

$$\begin{array}{l} K_{j,1}(x_j, x_j) = -\frac{1}{2} q_j(x_j), \\ \lim\limits_{s \to +\infty} K_j(x_j, s) = 0. \end{array} \tag{21}$$

Solutions for problems (20)–(21) (the Gursah problem) exist and are unique. The above treatment can be done for the function $\bar{K}_j(x_j, s)$, as well.

Let given C_j contour that begins from $-\infty + i0^+$, rounds above all zeros of $a_j(\zeta)$ and poles of $r_j^{(j)}(\zeta)$, and ends at $+\infty + i0^+$. We introduce the following function:

$$g_1^{(1)}(x_1, \zeta) = \varphi_1(x_1, \zeta) + r_1^{(1)}(\zeta) \psi_1(x_1, \zeta) e^{-2i\zeta x_1} \tag{22}$$

Then, from Eq. (9) we have:

$$\begin{array}{l} g_1^{(1)}(x_1, \zeta) = \varphi_1(x_1, \zeta) + r_1^{(1)}(\zeta) \psi_1(x_1, \zeta) e^{-2i\zeta x_1} = \\ = a_1(\zeta) \bar{\psi}_1(x_1, \zeta) + \left\{ b_1(\zeta) + r_1^{(1)}(\zeta) e^{-2i\zeta x_1} \right\} \psi_1(x_1, \zeta) \end{array} . \tag{23}$$

The last equation can be rewritten as:

$$\begin{aligned}\frac{g_1^{(1)}(x_1,\zeta)}{a_1(\zeta)} &= \bar{\psi}_1(x_1,\zeta) + \left\{\frac{b_1(\zeta)}{a_1(\zeta)} + \frac{r_1^{(1)}(\zeta)}{a_1(\zeta)}e^{-2i\zeta x_1}\right\}\psi_1(x_1,\zeta) = \\ &= \bar{\psi}_1(x_1,\zeta) + R_1^{(1)}(x_1,\zeta)\psi_1(x_1,\zeta).\end{aligned} \tag{24}$$

where $R_1^{(1)}(x_1,\zeta) = \frac{b_1(\zeta)}{a_1(\zeta)} + \frac{r_1^{(1)}(\zeta)}{a_1(\zeta)}e^{-2i\zeta x_1}$. Inserting Eqs. (16) and (17) into (24):

$$\begin{aligned}\frac{g_1^{(1)}(x_1,\zeta)}{a_1(\zeta)} &= \begin{pmatrix}1\\0\end{pmatrix}e^{-i\zeta x_1} + \int_{x_1}^{+\infty}\bar{K}_1(x_1,s)e^{-i\zeta s}ds + \\ &+R_1^{(1)}(x_1,\zeta)\left(\begin{pmatrix}0\\1\end{pmatrix}e^{i\zeta x_1} + \int_{x_1}^{+\infty}K_1(x_1,s)e^{i\zeta s}ds\right),\end{aligned} \tag{25}$$

multiplying Eq. (25) by $\frac{1}{2\pi}e^{i\zeta y}d\zeta$ and integrating along the contour C_1 at $y{>}x_1$, by taking into account the representation $\delta(x) = \frac{1}{2\pi}\int_{C_1}e^{i\zeta x}d\zeta$ the Dirac-δ function we have:

$$\begin{aligned}&\frac{1}{2\pi}\int_{C_1}\frac{g_1^{(1)}(x_1,\zeta)}{a_1(\zeta)}e^{i\zeta y}d\zeta = \begin{pmatrix}1\\0\end{pmatrix}\delta(y-x_1) + \int_{x_1}^{+\infty}\bar{K}_1(x_1,s)\delta(y-s)ds + \\ &+\begin{pmatrix}0\\1\end{pmatrix}\left[\frac{1}{2\pi}\int_{C_1}R_1^{(1)}(x_1,\zeta)e^{i\zeta(x_1+y)}d\zeta\right] + \int_{x_1}^{+\infty}K_1(x_1,s)\left[\frac{1}{2\pi}\int_{C_1}R_1^{(1)}(x_1,\zeta)e^{i\zeta(y+s)}d\zeta\right]ds.\end{aligned} \tag{26}$$

Since the functions $e^{i\zeta x_j}\varphi_j(x_j,\zeta)$, $e^{-i\zeta x_j}\psi_j(x_j,\zeta)$ are analytic on the upper half of the plane $Im\zeta > 0$, $y{>}x_1$ and the contour C_1 round above zeros of $a_1(\zeta)$ and poles of $r_1^{(1)}(\zeta)$, the integral of the left hand side of equality (26) is equal to zero. Therefore we get:

$$\bar{K}_1(x_1,y) + \begin{pmatrix}0\\1\end{pmatrix}F_1(x_1,x_1+y) + \int_{x_1}^{+\infty}K_1(x_1,s)F_1(x_1,y+s)ds = 0, \tag{27}$$

where $F_1(x,y) = \frac{1}{2\pi}\int_{C_1}R_1^{(1)}(x,\zeta)e^{i\zeta y}d\zeta$.

Repeating the same procedure for the function $\bar{f}_1^{(1)}(x,\zeta)$, we obtain:

$$K_1(x_1,y) - \begin{pmatrix}0\\1\end{pmatrix}\bar{F}_1(x_1,x_1+y) - \int_{x_1}^{+\infty}\bar{K}_1(x_1,s)\bar{F}_1(x_1,y+s)ds = 0, \tag{28}$$

where $\bar{F}_1(x,y) = \frac{1}{2\pi}\int_{\bar{C}_1}\bar{R}_1^{(1)}(x,\zeta)e^{-i\zeta y}d\zeta$ and $\bar{C}_1$ is the same contour as C_1, but rounds below the zeros of $\bar{a}_1(\zeta)$ and poles of $\bar{r}_1^{(1)}(\zeta)$.

Similarly, one can obtain the following equations for the functions K_2 and K_3:

$$\begin{aligned}\bar{K}_j(x_j,y) + \begin{pmatrix}0\\1\end{pmatrix}F_j(x_j,x_j+y) + \int_{x_j}^{+\infty}K_j(x_j,s)F_j(x_j,y+s)ds = 0,\\ K_j(x_j,y) - \begin{pmatrix}0\\1\end{pmatrix}\bar{F}_j(x_j,x_j+y) - \int_{x_j}^{+\infty}\bar{K}_j(x_j,s)\bar{F}_j(x_j,y+s)ds = 0,\end{aligned} \tag{29}$$

where

$$F_j(x,y) = \frac{1}{2\pi}\int_{C_j}R_j^{(j)}(x,\zeta)e^{i\zeta y}d\zeta, \bar{F}_j(x,y) = \frac{1}{2\pi}\int_{\bar{C}_j}\bar{R}_j^{(j)}(x,\zeta)e^{-i\zeta y}d\zeta,$$

$$R_j^{(j)}(x,\zeta) = \frac{b_j(\zeta)}{a_j(\zeta)} + \frac{r_j^{(j)}(\zeta)}{a_j(\zeta)}e^{-2i\zeta x_j}, \bar{R}_j^{(j)}(x,\zeta) = \frac{\bar{b}_j(\zeta)}{\bar{a}_j(\zeta)} + \frac{\bar{r}_j^{(j)}(\zeta)}{\bar{a}_j(\zeta)}e^{2i\zeta x_j}, j = 2,3.$$

From Eq. (21), we obtain:

$$q_j(x_j) = -2K_{j,1}(x_j, x_j). \tag{30}$$

Using the same approach used for Eqs. (18) and (19), we get the following formula for the potential $p_j(x_j)$:

$$p_j(x_j) = -2\bar{K}_{j,2}(x_j, x_j). \tag{31}$$

5. Conclusions

In this paper, we developed a procedure for finding the unknown potential in the Dirac equation on metric graphs using a given scattering matrix. In this case, the solutions for the inverse scattering problem were obtained by solving Gelfand-Levitan-Marchenko integral equations. The above results can be used in different practically important problems for emerging nanotechnologies. In addition, they can be useful for solving some nonlinear evolution equations on metric graphs such as nonlinear Schrodinger and KdV equations.

References

[1] Gnutzmann S. and Smilansky U. Quantum graphs: Applications to quantum chaos and universal spectral statistics. *Advances in Physics*, **55**(5-6) July-October, P. 527–625 (2006).

[2] Kottos T., Smilansky U. Periodic Orbit Theory and Spectral Statistics for Quantum Graphs. *Annals of Physics*, **274**, P. 76–124 (1999).

[3] Shapira T., Smilansky U. Quantum graphs which sound the same. *Math., Phys., Chem.*, **213**, P. 17–29 (2006).

[4] Kuchment P. Quantum graphs: I. Some basic structures. *Waves Random Media*, **14**, P. S107-S128 (2004).

[5] Levitan B.M., Sargsyan I.S. *Shturm-Liuville and Dirac operators*. Moscow: Nauka, 432 p. (1988).

[6] Gasymov M.G., Levitan B.M. Definition of the Dirac system on scattering phase. *Dokl. Akad. Nauk USSR*, **167**(6), P. 1219–1222 (1966).

[7] Asymova G.M., Guseynov I.M. Inverse problem of the scattering theory for grid equation of the First order. *Dokl. Acad. Nauk Az SSR*, **39**(11), P. 12–15 (1983).

[8] Khanmamedov Ag. Kh. Inverse scattering problem for the difference Dirac operator on a half-line. *Dokl. Akad. Hauk*, **424**(5), P. 597–598 (2009).

[9] Bolte J., Harrison J. Spectral Statistics for the Dirac Operator on Graphs. arXiv:nlin.CD/0210029, **1**(15) Oct, P. 1-28 (2002).

[10] Gerasimenko N.I., Pavlov B.S. Scatterng problem on noncompact graphs. *Theor. Mathem. Phys.*, **74**(3), P. 345–359 (1988).

[11] Gerasimenko N.I. Inverse scattering problem on the noncompact graph. *Theor. Mathem. Phys.*, **75**(2), P. 187–200 (1988).

[12] Zakharov V.B. and Shabat A.B. Exact theory of two-dimensional self-focusing and one-dimensional self-modulation of waves in nonlinear media. *Sov. Phys. JETP.*, **34**(1), P. 62–69 (1972).

NANOSYSTEMS: PHYSICS, CHEMISTRY, MATHEMATICS, 2015, 6 (2), P. 198–204

Cauchy problem for the linearized KdV equation on general metric star graphs

Z. A. Sobirov[1,2], M. I. Akhmedov[2], H. Uecker[3]

[1]Faculty of Mathematics, National University of Uzbekistan,
Vuzgorodok, 100047 Tashkent, Uzbekistan
[2]Applied Mathematics Department of Tashkent Financial Institute,
100000 Tashkent, Uzbekistan
[3]Institut für Mathematik, Universität Oldenburg, D26111 Oldenburg, Germany

hannes.uecker@uni-oldenburg.de

PACS 02.30.Em, 02.30.Jr **DOI 10.17586/2220-8054-2015-6-2-198-204**

Keywords: KdV, initial value problem, PDE on metric graphs, exact solution, third order differential equation.

Received: 2 February 2015

1. Introduction

The Korteweg-de Vries (KdV) equation has attracted much attention in the literature, both in the context of physics and mathematics. This equation was found to permit soliton solutions and allow the modeling of solitary wave propagation on a water surface, a phenomena first discovered by Scott Russell in 1834. The KdV equation is also used, e.g., to model the unidirectional propagation of small amplitude long waves in nonlinear dispersive systems such as ion-acoustic waves in a collisionless plasma, and magnetosonic waves in a magnetized plasma etc [11]. The linearized KdV provides an asymptotic description of linear, undirectional, weakly dispersive long waves, for example, shallow water waves. Earlier, it was proven that via normal form transforms, the solution of the KdV equation can be reduced to the solution for the linear KdVequation [12]. Belashov and Vladimirov [12] numerically investigated the evolution of a single disturbance $u(0,x) = u_0 \exp(-x^2/l^2)$ and showed that in the limit $l \to 0$, $u_0 l^2 = \text{const}$, the solution of the KdV equation is qualitatively similar to the solution of the linearized KdV equation. Boundary value problems on half lines were considered in [2, 5, 7].

Here, summarizing and extending the results in [13], we investigate the linearized KdV equation on star graphs Γ with $m+k$ semi-infinite bonds connected at one point, called the vertex. The bonds are denoted by B_j, $j = 1, 2, ..., k+m$, the coordinate x_j on B_j is defined from $-\infty$ to 0 for $j = 1, 2, ..., k$, and from 0 to $+\infty$ for $j = k+1, ..., k+m$ such that on each bond, the vertex corresponds to 0. On each bond we consider the linear equation:

$$\left(\frac{\partial}{\partial t} + \frac{\partial^3}{\partial x_j^3}\right) u_j(x_j, t) = f_j(x,t), \quad t > 0, \; x_j \in B_j. \tag{1}$$

Below, we will also use x instead of x_j ($j = 1, 2, ..., k+m$). We investigate an initial value problem, and using the method of potentials, construct solution formulas.

2. Formulation of the problems

To solve linear KdV equation on an interval, one needs to impose three boundary conditions (BC): two on the left end of the x-interval and one on the right end, (see, e.g., [5,6] and references therein). For the star graph with $m+k$ semi-infinite bonds, we need to impose $k+2m$ BCs, which should also provide connection between the bonds. In detail, we require:

$$u_1(0;t) = a_j u_j(0;t), \quad j = \overline{2, k+m}, \tag{2}$$

$$u_x^+(+0;t) = B u_x^-(-0;t), \tag{3}$$

$$\sum_{i=1}^{k} a_i^{-1} u_{ixx}(-0;t) = \sum_{i=k+1}^{k+m} a_i^{-1} u_{ixx}(+0;t), \tag{4}$$

for $t > 0$, where $u^-(x;t) = (u_1(x,t), \ldots, u_k(x,t))^T$, $u^+(x;t) = (u_{k+1}(x,t), \ldots, u_{k+m}(x,t))^T$, subscripts x and double x mean the first and the second order partial derivatives with respect to x, a_k are non-zero constants, B is a $m \times k$ matrix.

Furthermore, we assume that the $f_j(x,t)$ and the initial conditions:

$$u_j(x,0) = u_{0j}(x), \quad x \in \overline{B_j}, \ (j = 1, 2, ..., k+m), \tag{5}$$

are sufficiently smooth enough and bounded, and that $u_{0,j}$ satisfies the vertex conditions (2) – (4).

It should be noted that the above vertex conditions are not the only possible ones. The main motivation for our choice is caused by the fact that they guarantee uniqueness of the solution and, if the solutions decay (to zero) at infinity,the norm (energy) conservation.

Here, we introduce some notation that will be useful in the following. For any vector, $\mathbf{v} = (v_1, v_2, \ldots, v_{k+m})^T$ we put $\tilde{\mathbf{v}} = (v_2, \ldots, v_{k+m})^T$, $\mathbf{v}^- = (v_1, \ldots, v_k)^T$, $\tilde{\mathbf{v}}^- = (v_2, \ldots, v_k)^T$, $\mathbf{v}^+ = (v_{k+1}, \ldots, v_{k+m})^T$.

3. Existence and uniqueness of solutions

Lemma 1. *Let $I_k - B^T B$ be negatively defined matrix. Then the problem has at most one solution in $H^3(\Gamma)$.*

Proof of Lemma 1. Using the equation (1) one can easily get:

$$\frac{\partial}{\partial t} \int_a^b u_j^2(x,t)dx = \left(2u_j u_{jxx} - u_{jx}^2\right) \Big|_{x=a}^{x=b} + 2 \int_a^b f_j(x,t) u_j(x,t) dx$$

for appropriate values of constants a and b. From this equality and vertex conditions (2) – (4) we have:

$$\frac{d}{dt} \|\mathbf{u}(\cdot,t)\|_\Gamma^2 \le \left(\partial \mathbf{u}^-(0,t)\right)^T \left(I_k - B^T B\right) \partial \mathbf{u}^-(0,t) + 2 \|\mathbf{u}(\cdot,t)\|_\Gamma \|\mathbf{f}(\cdot,t)\|_\Gamma .$$

According to condition of Lemma 1, we get:

$$\|\mathbf{u}(\cdot,t)\|_\Gamma \le \|\mathbf{u}(\cdot,0)\|_\Gamma + \int_0^t \|\mathbf{f}(\cdot,\tau)\|_\Gamma \, d\tau. \tag{6}$$

The inequality (6) proves the lemma.

Notice that equality in (6) (i.e. energy conservation) holds iff $B^TB = I_m$.

We shall construct solutions and prove existence theorems for data from the Schwartz class of smooth decreasing functions, and for data in Sobolev classes.

Let $S(B_k)$ be the Schwartz space of rapidly decaying functions on the closure of B_k, $k = 1, 2, 3$. We say $v(x,t) \in C^1([0,T];\, S(B_k))$ ($T > 0$) if v and $\dfrac{\partial v}{\partial t}$ in $C([0,T];\, S(B_k))$.

Theorem 1. *Assume that $I_k - B^TB$ is negatively defined matrix, $u_{0k}(x) \in S(B_k)$, $f_k(x,t) \in C^1([0,T];\, S(B_k))$ for some $T > 0$ and that $u_{0k}^{(p)} \equiv \dfrac{\partial^{3p}}{\partial x^{3p}} u_{0k}(x)$ and $f_k^{(p)} = \dfrac{\partial^{3p}}{\partial x^{3p}} f_k(x,t)$ satisfy vertex conditions (1) – (5) for any nonnegative integer p. Then (1) – (5) has a solution in $C^1([0,T];\, S(B_k))$.*

To treat the case of Sobolev data consider function $\mathbf{v} = (v_1(x_1), v_2(x_2), \ldots, v_{k+m}(x_{k+m}))$ defined on the graph. We suppose that $v_k \in S(B_k)$ and the functions $v_k^{(p)} \equiv \dfrac{\partial^{3p}}{\partial x^{3p}} v_k(x)$ satisfy vertex conditions (2) –(4) for any non-negative integer p. We denote the set of all such functions v by $S^-(\Gamma)$ ($S^+(\Gamma)$), and define $W^-(\Gamma)$ (or $W^+(\Gamma)$) as the closure of the set $S^-(\Gamma)$ (or $S^+(\Gamma)$) with respect to the norm $\|v\|_{3,\Gamma} = \sum_{k=1}^{3} \|v_k\|_{H^3(B_k)}$.

Theorem 2. *Let $I_k - B^TB$ be negatively defined matrix,*
$\mathbf{u}_0 \equiv (u_{01}(x_1), u_{02}(x_2), \ldots, u_{0,k+m}(x_{k+m})) \in W^{\pm}(\Gamma)$. *Then (1) – (5) has a unique solution in $L_\infty(0,T,W^{\pm}(\Gamma))$.*

First, we construct exact solutions, using the results from the theory of potentials for the linearized KdV equation. For that purpose, we give some preliminaries from [1,3,5].

4. Some preliminaries from potentials theory

The following functions are called fundamental solutions of the equation $u_t - u_{xxx} = 0$ (see [1,3,5,12]):

$$U(x,t;\xi,\eta) = \begin{cases} \dfrac{1}{(t-\eta)^{1/3}} f\left(\dfrac{x-\xi}{(t-\eta)^{1/3}}\right), & \text{if } t > \eta; \\ 0, & \text{if } t \le \eta, \end{cases}$$

$$V(x,t;\xi,\eta) = \begin{cases} \dfrac{1}{(t-\eta)^{1/3}} \phi\left(\dfrac{x-\xi}{(t-\eta)^{1/3}}\right), & \text{if } t > \eta; \\ 0, & \text{if } t \le \eta, \end{cases}$$

where $f(x) = \dfrac{\pi}{3^{1/3}} Ai\left(-\dfrac{x}{3^{1/3}}\right)$, $\phi(x) = \dfrac{\pi}{3^{1/3}} Bi\left(-\dfrac{x}{3^{1/3}}\right)$ for $x \ge 0$, $\phi(x) = 0$ for $x < 0$ and $\mathrm{Ai}(x)$ and $\mathrm{Bi}(x)$ are the Airy functions. The functions $f(x)$ and $\phi(x)$ are integrable and $\int_{-\infty}^{0} f(x)dx = \dfrac{\pi}{3}$, $\int_0^{+\infty} f(x)dx = \dfrac{2\pi}{3}$, $\int_0^{+\infty} \phi(x)dx = 0$. We summarize some properties of potentials for (1) from [3,5]. For given ω, f and ϕ let:

$$u(x,t) = \int_a^b U(x,t;\xi,0)\omega(\xi)d\xi, \quad v(x,t) = \int_0^t \int_a^b U(x,t;\xi,\tau) f(\xi,\tau) d\xi d\tau,$$

$$w^{(1)}(x,t) = \int_\eta^t U_{x\xi}(x,\eta;a,t)\phi(\eta)d\eta, \quad w^{(2)}(x,t) = \int_\eta^t V_{x\xi}(x,\eta;a,t)\phi(\eta)d\eta.$$

Lemma 2. *a) Let* $\omega \in BV([a,b])$. *Then* $u(x,t)$ *satisfies* $u_t - u_{xxx} = 0$ *for* $t > 0$ *and:*

$$\lim_{(x,y)\to(x_0,0)} u(x,t) = \begin{cases} \pi\omega(x_0), & \text{if } x_0 \in (a,b); \\ 0, & \text{if } x_0 \notin (a,b). \end{cases}$$

b) Let $f \in L^2((a,b)\times(0,T)$. *Then,* $v(x,t)$ *satisfies* $u_t - u_{xxx} = \pi f(x,t)$ *in* $(a,b)\times(0,T]$, $T > 0$ *and initial condition* $u(x,0) = 0$, $x \in (a,b)$.

c) If $\phi \in H^1(0,T)$, *then :*

$$\lim_{x\to a+0} w^{(1)}(x,t) = \frac{2\pi}{3}\phi(y), \quad \lim_{x\to a-0} w^{(1)}(x,t) = -\frac{\pi}{3}\phi(y), \quad \lim_{x\to a+0} w^{(2)}(x,t) = 0.$$

Now, we are ready to construct exact solutions for the considered problems. We assume that initial data and source terms in each bond are sufficiently smooth and bounded functions.

5. Integral formula for exact solution

We look for solution in the form:

$$\mathbf{u}(x,t) = \int_0^t U(x,t;0,\eta)\boldsymbol{\phi}(\eta)d\eta + \int_0^t V(x,t;0,\eta)\boldsymbol{\psi}(\eta)d\eta + \mathbf{F}(x,t), \tag{7}$$

where

$$F_k(x,t) = \frac{1}{\pi}\int_{B_k} U(x,t;\xi,0)u_k(\xi,0)d\xi + \frac{1}{\pi}\int_0^t\int_{B_k} U(x,t;\xi,\eta)f_k(\xi,\eta)d\xi d\eta.$$

$\boldsymbol{\phi}(t) = (\phi_1(t),\dots,\phi_{k+m}(t))^T$, $\boldsymbol{\psi}(t) = (0,\dots,0,\psi_{k+1}(t),\dots,\psi_{k+m}(t))^T$ are unknown vector functions.

According to vertex conditions (2) – (4), we get:

$$\tilde{\mathbf{C}}\cdot\int_0^t \frac{f(0)}{(t-\tau)^{1/3}}\phi_1(\tau)d\tau = \int_0^t \frac{f(0)}{(t-\tau)^{1/3}}\tilde{\boldsymbol{\phi}}(\tau)d\tau + \int_0^t \frac{\varphi(0)}{(t-\tau)^{1/3}}\tilde{\boldsymbol{\psi}}(\tau)d\tau - \left(\tilde{\mathbf{C}}F_1 - \tilde{\mathbf{F}}\right)\Big|_{x=0}, \tag{8}$$

$$\int_0^t \frac{f'(0)}{(t-\tau)^{2/3}}\boldsymbol{\phi}^+(\tau)d\tau + \int_0^t \frac{\varphi'(0)}{(t-\tau)^{2/3}}\boldsymbol{\psi}^+(\tau)d\tau = \mathbf{B}\int_0^t \frac{f'(0)}{(t-\tau)^{2/3}}\boldsymbol{\phi}^-(\tau)d\tau - \left(\partial\mathbf{F}^+(0,t) - \mathbf{B}\cdot\partial\mathbf{F}^-(0,t)\right), \tag{9}$$

$$2(\mathbf{C}^-)^T f^-(t) + (\mathbf{C}^+)^T f^+(t) = \frac{3}{\pi}\left(-\mathbf{C}^-\middle|\mathbf{C}^+\right)\partial^2\mathbf{F}(0,t), \tag{10}$$

where $\mathbf{C} = \left(1, \frac{1}{a_2}, \frac{1}{a_3}, \dots, \frac{1}{a_{k+m}}\right)$.

Abel's integral equations (8), (9) can be written in terms of fractional integrals [9]:

$$J^{\alpha}_{(0,t)}f(t) := \frac{1}{\Gamma(\alpha)}\int_0^t (t-\tau)^{\alpha-1}f(\tau)d\tau, \quad 0 < \alpha < 1,$$

and solved using the inverse operators, i.e. the Riemann-Liouville fractional derivatives [8, 9] defined by:

$$D^{\alpha}_{(0,t)}f(t) := \frac{1}{\Gamma(1-\alpha)}\frac{d}{dt}\int\limits_0^t (t-\tau)^{-\alpha} f(\tau)d\tau, \quad 0<\alpha<1.$$

Using the relation $D^{\alpha}_{(0,t)}J^{\alpha}_{(0,t)} = I$ from (8) and (9), we obtain the linear algebraic equations:

$$f(0)\left(\tilde{\mathbf{C}}\big| - \mathbf{I}_{m+k-1}\right)\boldsymbol{\phi}(t) - \left(\mathbf{0}_{(m+k-1)\times 1}\big|\mathbf{I}_{m+k-1}\right)\varphi(0)\boldsymbol{\psi}(t) = \\ - \frac{1}{\Gamma(1/3)}\left(\tilde{\mathbf{C}}\big| - \mathbf{I}_{m+k-1}\right) D^{2/3}_{(0,t)}\mathbf{F}(0,t), \quad (11)$$

$$f'(0)\left(\mathbf{B}\big| - \mathbf{I}_m\right)\boldsymbol{\phi}(t) + \varphi'(0)\left(\mathbf{0}_{m\times k}\big| - \mathbf{I}_m\right)\boldsymbol{\psi}(t) = -\frac{1}{\Gamma(2/3)} D^{1/3}_{(0,t)}\left(\mathbf{B}\big| - \mathbf{I}_m\right)\partial\mathbf{F}(0,t). \quad (12)$$

We rewrite the system of equations (10), (11) and (12) in the following matrix form:

$$M\cdot\begin{pmatrix}\boldsymbol{\phi}(t)\\ \boldsymbol{\psi}^{+}(t)\end{pmatrix} = \mathbf{G}(t), \quad \mathbf{G}(t) = \begin{pmatrix} -\frac{1}{\Gamma(1/3)}\left(\tilde{\mathbf{C}}\big| - \mathbf{I}_{m+k-1}\right) D^{2/3}_{(0,t)}\mathbf{F}(0,t)\\ -\frac{1}{\Gamma(2/3)} D^{1/3}_{(0,t)}\left(\mathbf{B}\big| - \mathbf{I}_m\right)\partial\mathbf{F}(0,t)\\ \frac{3}{\pi}(-\mathbf{C}^{-}\big|\mathbf{C}^{+})\partial^2\mathbf{F}(0,t)\end{pmatrix},$$

where

$$M = \left(\begin{array}{c|c|c|c} f(0)\tilde{C}^{-} & -f(0)I_{k-1} & 0_{(k-1)\times m} & 0_{(k-1)\times m}\\ f(0)C^{+} & 0_{m\times(k-1)} & -f(0)I_m & -\phi(0)I_m\\ f'(0)B & & -f'(0)I_m & -\phi'(0)I_m\\ 2C^{-} & & C^{+} & 0_{1\times m}\end{array}\right)$$

Now we must prove that $\det(M)\neq 0$.

Suppose that $\det(M) = 0$. Then, the homogenous equation $M\boldsymbol{\alpha} = 0$ has a non-trivial, time independent solution $\boldsymbol{\alpha} = (\alpha_1, \alpha_2, \ldots, \alpha_{k+m})$ (notice that M is constant matrix). Therefore, putting in (7) $\boldsymbol{\phi}(t) = \boldsymbol{\phi}_0 = (\alpha_1, \ldots, \alpha_{k+m})^T = \text{const}$, $\boldsymbol{\psi}(t) = \boldsymbol{\psi}_0 = (0, \ldots, 0, \alpha_{k+m+1}, \ldots, \alpha_{k+2m}) = \text{const}$, we obtain a solution for the problem with $\mathbf{u}_0(x)\equiv 0$, $\mathbf{f}(x,t)\equiv 0$. According to the uniqueness theorem, we have:

$$\boldsymbol{\phi}_0\int\limits_0^t \frac{1}{(t-\tau)^{1/3}} f\left(\frac{x}{(t-\tau)^{1/3}}\right)d\tau + \boldsymbol{\psi}_0\int\limits_0^t \frac{1}{(t-\tau)^{1/3}}\varphi\left(\frac{x}{(t-\tau)^{1/3}}\right)d\tau = 0,$$

or

$$\boldsymbol{\phi}_0 f\left(\frac{x}{t^{1/3}}\right) + \boldsymbol{\psi}_0\varphi\left(\frac{x}{t^{1/3}}\right) = 0,$$

for any fixed t. The last equality contradicts the condition of linear independence for the Airy functions $\mathrm{Ai}(x)$ and $\mathrm{Bi}(x)$. This proves the statement $\det(M)\neq 0$.

Summarizing the above studies, we obtain:

$$\mathbf{u}(x,t) = \mathbf{F}(x,t) + \int_0^t \mathbf{U}(x,t-\tau)M^{-1}\mathbf{G}(\tau)d\tau$$

with

$$\mathbf{U}(x,t) = \begin{pmatrix} U(x,t;0,0)\mathbf{I}_k & | & \mathbf{0}_{k\times m} & | & \mathbf{0}_{k\times m} \\ \mathbf{0}_{m\times k} & | & U(x,t;0,0)\mathbf{I}_m & | & V(x,t;0,0)\mathbf{I}_m \end{pmatrix}.$$

6. Proof of existence theorems

Proof of Theorem 1. According to the theory of potentials [3, 5], the solutions constructed in the previous sections and their x-derivatives, up to the second order, are continuous functions in the closure of each bondof the graph.

Now, we consider the functions $v_j(x_j,t)$ that are solutions of the considered problem with initial conditions $v_j(x,0) = \dfrac{d^3}{dx^3}u_{0j}(x)$, and with f_j replaced by $\dfrac{\partial^3}{\partial x^3}f_j$. According to the conditions of the theorem, one can easily obtain $\dfrac{\partial^3 u_j}{\partial x^3}(x,t) = v_j(x,t)$. From this, we conclude that the functions $u_j(x,t)$, $j = 1,2,3$ and their x-derivatives of any order are continuous functions in the closure of B_j.

Now, we consider the half lines corresponding to each bond separately. Notice that $u_j(x,t)$ is a solution of the linearized KdV equation on the half line B_j and satisfies compatibility conditions at the point $x = 0$, $t = 0$. Applying Theorem 1.1 from [7], we get that these solutions define a C^1 map from $[0,T]$ into $S(\bar{B}_j)$.

Proof of Theorem 2. Above, we proved the estimate:

$$\|\mathbf{u}(\cdot,t)\|_\Gamma \le \|\mathbf{u}(\cdot,0)\|_\Gamma + \int_0^t \|\mathbf{f}(\cdot,\tau)\|_\Gamma \, d\tau.$$

Note that for the function v, constructed above, the same estimate holds.

Summing up these two estimates, we have:

$$\|\mathbf{u}(\cdot,t)\|_{3,\Gamma} \le \|\mathbf{u}(\cdot,0)\|_{3,\Gamma} + \int_0^t \|\mathbf{f}(\cdot,\tau)\|_{3,\Gamma} \, d\tau. \tag{13}$$

By construction, $S^{\pm}(\Gamma)$ is dense in $W^{\pm}(\Gamma)$. This, together with the *a priori* estimate (13) proves the theorem. Thus, we have shown the existence and uniqueness of the solution for the linearized KdV equation on a metric star graph and derived its explicit solution. The above approach can also be extended to cases of graphs with different topologies.

Acknowledgement

We gratefully thank the Volkswagen Stiftung for financial support.

References

[1] S. Abdinazarov. The general boundary value problem for the third order equation with multiple characteristics (in Russian). *Differential Equations*, **13** (1), P. 3–12 (1981).

[2] J.L. Bona and A.S. Fokas. Initial-boundary-value problems for linear and integrable nonlinear dispersive partial differential equations. *Nonlinearity*, **21**, P. 195–203 (2008).

[3] L. Cattabriga. Unproblema al contorno per unaequazione parabolica di ordine dispari. *Annali della Scuola Normale Superiore di Pisa*, **13** (3), P.163–203 (1959).

[4] J.E. Colliander and C.E. Kenig. The generalized Korteweg-de Vries equation on the half line. *Commun. Partial Differ. Equations*, **27** (11–12), P. 2187–2266 (2002).

[5] T.D. Djuraev. *Boundary value problems for mixed and mixid-composite type equations*, (in russian). Fan, Tashkent, 1979.

[6] A.V. Faminskii and N.A. Larkin. Initial-boundary value problems for quasilinear dispersive equations posed on a bounded interval. *Electron. J. Differ. Equ.*, **1**, P. 1–20 (2010).

[7] A.S. Fokas and L.Y. Sung. Initial boundary value problems for linear dispersive evolution equations on the half line. *Industrial Mathematics Institute Preprint Series*, **11**, P. 1–29 (1999).

[8] M. Rahimy. Applications of fractional differential equations. *Applied Mathematical Sciences*, **4** (50), P. 2453–2461 (2010).

[9] R. Gorenflo and F. Mainard. Fractional calculus: Integral and differential equations of fractional order. `ArXiv:0805.3823v1` (2008).

[10] E. Taflin. Analytic linearization of the Korteweg-De Vries equation. *Pacific Journal Of Mathematics*, **108** (1), P. 203–220 (1983).

[11] V. Belashov and S. Vladimirov. *Solitary waves in dispersive complex media: theory, simulation, application*. Springer, 2005.

[12] G.B. Whitham. *Linear and nonlinear waves*. Pure and Applied Mathematics, Wiley-Interscience, 1974.

[13] Z.A. Sobirov, H. Uecker and M. Akhmedov. Exact solutions of the Cauchy problem for the linearized KdV equation on metric star graphs. *Uz. Math. J.*, to appear. Preprint: `http://www.staff.uni-oldenburg.de/hannes.uecker/pre/049-lkdvgr.pdf`.

NANOSYSTEMS: PHYSICS, CHEMISTRY, MATHEMATICS, 2015, 6 (2), P. 205–212

Uncertainty relation between angle and orbital angular momentum: interference effect in electron vortex beams

Shogo Tanimura

Department of Complex Systems Science, Graduate School of Information Science, Nagoya University, Nagoya 464-8601, Japan

tanimura@is.nagoya-u.ac.jp

PACS 03.65.-w, 03.65.Ta, 07.78.+s, 42.50.-p, 42.50.Tx

DOI 10.17586/2220-8054-2015-6-2-205-212

The uncertainty relation between angle and orbital angular momentum had not been formulated in a similar form as the uncertainty relation between position and linear momentum because the angle variable is not represented by a quantum mechanical self-adjoint operator. Instead of the angle variable operator, we introduce the complex position operator $\hat{Z} = \hat{x} + i\hat{y}$ and interpret the order parameter $\mu = \langle \hat{Z} \rangle / \sqrt{\langle \hat{Z}^\dagger \hat{Z} \rangle}$ as a measure of certainty of the angle distribution. We prove the relation between the uncertainty of angular momentum and the angle order parameter. We also prove its generalizations and discuss experimental methods for testing these relations.

Keywords: uncertainty relation, orbital angular momentum, order parameter, vortex electron beam.

Received: 4 November 2014

1. Introduction

Uncertainty relations elucidate the difference between classical physics and quantum physics. In classical physics, accuracy of measurement is not limited in principle and it is assumed that any observables can be measured simultaneously and precisely. However, in quantum physics, the accuracy of simultaneous measurements of two observables is limited by the uncertainty relation.

Originally, Heisenberg [1] formulated the uncertainty relation between position Q and linear momentum P as:

$$\Delta Q \, \Delta P \gtrsim h, \tag{1}$$

with the Planck constant h. He deduced this relation via a Gedankenexperiment. Later, Weyl, Kennard, and Robertson [2] gave a rigorous proof of this relation. In the context of quantum mechanics, the position is represented by a self-adjoint operator $\hat{Q}$ and the uncertainty of the position is defined as the variance:

$$(\Delta Q)^2 := \left\langle \psi \middle| \left(\hat{Q} - \langle \psi | \hat{Q} | \psi \rangle \right)^2 \middle| \psi \right\rangle = \langle \psi | \hat{Q}^2 | \psi \rangle - \langle \psi | \hat{Q} | \psi \rangle^2, \tag{2}$$

for a normalized state vector $|\psi\rangle$. The uncertainty ΔP of momentum is defined in a similar way.

It is natural to expect a similar relation:

$$\Delta \phi \, \Delta L \gtrsim h, \tag{3}$$

holds for the angle ϕ and the angular momentum L as shown in the textbook [3]. However, in a plane, the coordinate values $\{\phi + 2\pi n\}$ with any integer n represent the same point as ϕ indicates. In other words, the angle variable ϕ is a multivalued function. In quantum

mechanics, the spectrum of a self-adjoint operator should have one-to-one correspondence with the values of an observable. Hence, there is no self-adjoint operator $\hat{\phi}$ corresponding to the multivalued angle variable ϕ. Therefore, the angle uncertainty $\Delta\phi$ cannot be defined as the position uncertainty ΔQ was defined.

The uncertainty relation between angle and orbital angular momentum is a long-standing issue in physics. Many people have proposed other definitions of the angle uncertainty and have formulated several versions of the uncertainty relation between angle and angular momentum [4] – [9]. However, most of these relations treat a particle moving on a one-dimensional circle. They did not consider a particle moving in two- or three-dimensional spaces. Thus, we do not yet have an angle-angular momentum uncertainty relation that is applicable for a realistic situation.

In this paper, we introduce the moment of position distribution in a plane, which is an arbitrary two-dimensional subspace in the configuration space of the particle. We propose to use the moment of position as an indicator of certainty or bias of angle distribution. The main results of this work are inequalities (27), (32), (36), which represent the uncertainty relation between the moments of position and the orbital angular momentum. Our results are applicable for a particle moving in configuration space having more than two dimensions.

2. Robertson inequality

The Robertson inequality [2] is one formulation of general uncertainty relations. The Robertson inequality has a clear meaning and it is applicable to any kind of observable. Hence, it is regarded as the universal formulation of uncertainty relations. Although the Robertson inequality is well known and its proof is rather simple, here, we write its derivation to make a comparison with our uncertainty relation of the angle and angular momentum, which is derived in the next section.

For any vectors $|\alpha\rangle$ and $|\beta\rangle$ of a Hilbert space $\mathscr{H}$, the Schwarz inequality:

$$\langle\alpha|\alpha\rangle\langle\beta|\beta\rangle \geq \Big|\langle\alpha|\beta\rangle\Big|^2, \tag{4}$$

holds. The equality holds if and only if the two vectors $|\alpha\rangle$ and $|\beta\rangle$ are linearly dependent. Let $\psi \in \mathscr{H}$ be an arbitrary normalized vector satisfying $\langle\psi|\psi\rangle = 1$. For self-adjoint operators $\hat{A}$ and $\hat{B}$ on $\mathscr{H}$, we set:

$$\langle\hat{A}\rangle := \langle\psi|\hat{A}|\psi\rangle, \tag{5}$$

$$\Delta\hat{A} := \hat{A} - \langle\hat{A}\rangle\hat{I}, \tag{6}$$

$$|\alpha\rangle := \Delta\hat{A}|\psi\rangle, \tag{7}$$

$$|\beta\rangle := \Delta\hat{B}|\psi\rangle, \tag{8}$$

where $\hat{I}$ is the identity operator on $\mathscr{H}$. Then, the Schwarz inequality (4) becomes:

$$\langle\psi|(\Delta\hat{A})^2|\psi\rangle\langle\psi|(\Delta\hat{B})^2|\psi\rangle \geq \Big|\langle\psi|\Delta\hat{A}\,\Delta\hat{B}|\psi\rangle\Big|^2. \tag{9}$$

The standard deviation of the observable $\hat{A}$ is defined as:

$$\sigma(\hat{A}) := \Big(\langle\psi|(\Delta\hat{A})^2|\psi\rangle\Big)^{\frac{1}{2}}. \tag{10}$$

Then, it is easy to see that:

$$\begin{aligned}\Delta\hat{A}\,\Delta\hat{B} &= \frac{1}{2}\Big(\Delta\hat{A}\,\Delta\hat{B}+\Delta\hat{B}\,\Delta\hat{A}\Big)+\frac{1}{2}\Big(\Delta\hat{A}\,\Delta\hat{B}-\Delta\hat{B}\,\Delta\hat{A}\Big)\\ &= \frac{1}{2}\{\Delta\hat{A},\Delta\hat{B}\}+\frac{1}{2}[\Delta\hat{A},\Delta\hat{B}].\end{aligned} \tag{11}$$

Since $\langle\psi|\{\Delta\hat{A},\Delta\hat{B}\}|\psi\rangle$ is a real number and $\langle\psi|[\Delta\hat{A},\Delta\hat{B}]|\psi\rangle$ is a pure imaginary number, the right-hand side of (9) can be rewritten as:

$$\Big|\langle\psi|\Delta\hat{A}\,\Delta\hat{B}|\psi\rangle\Big|^2=\frac{1}{4}\langle\psi|\{\Delta\hat{A},\Delta\hat{B}\}|\psi\rangle^2+\frac{1}{4}\Big|\langle\psi|[\Delta\hat{A},\Delta\hat{B}]|\psi\rangle\Big|^2. \tag{12}$$

Moreover, we can see that:

$$[\Delta\hat{A},\Delta\hat{B}]=[\hat{A},\hat{B}]. \tag{13}$$

Therefore, (9) implies

$$\begin{aligned}\sigma(\hat{A})^2\sigma(\hat{B})^2 &\geq \Big|\langle\psi|\Delta\hat{A}\,\Delta\hat{B}|\psi\rangle\Big|^2=\frac{1}{4}\langle\psi|\{\Delta\hat{A},\Delta\hat{B}\}|\psi\rangle^2+\frac{1}{4}\Big|\langle\psi|[\Delta\hat{A},\Delta\hat{B}]|\psi\rangle\Big|^2\\ &\geq \frac{1}{4}\Big|\langle\psi|[\hat{A},\hat{B}]|\psi\rangle\Big|^2.\end{aligned} \tag{14}$$

By taking squre roots of the both sides, we obtain the Robertson inequality:

$$\sigma(\hat{A})\cdot\sigma(\hat{B})\geq\frac{1}{2}\Big|\langle\psi|[\hat{A},\hat{B}]|\psi\rangle\Big|, \tag{15}$$

which means that the two observables cannot have precise values simultaneously if $\langle\psi|[\hat{A},\hat{B}]|\psi\rangle\neq 0$. On the other hand, the following quantity:

$$\begin{aligned}C_s(\hat{A},\hat{B}) &:= \frac{1}{2}\langle\psi|\{\Delta\hat{A},\Delta\hat{B}\}|\psi\rangle=\frac{1}{2}\langle\psi|\{\Delta\hat{A},\hat{B}\}|\psi\rangle=\frac{1}{2}\langle\psi|\{\hat{A},\Delta\hat{B}\}|\psi\rangle\\ &= \frac{1}{2}\langle\psi|\{\hat{A},\hat{B}\}|\psi\rangle-\langle\psi|\hat{A}|\psi\rangle\langle\psi|\hat{B}|\psi\rangle,\end{aligned} \tag{16}$$

is called the symmetrized covariance of $\hat{A}$ and $\hat{B}$. Then, (14) can be rewritten as:

$$\sigma(\hat{A})^2\cdot\sigma(\hat{B})^2 \geq \Big|C_s(\hat{A},\hat{B})\Big|^2+\frac{1}{4}\Big|\langle\psi|[\hat{A},\hat{B}]|\psi\rangle\Big|^2. \tag{17}$$

Sometimes this is referred to as the Schrödinger inequality [10].

3. Angular order parameter and orbital angular momentum

In this section, we show our main result. Let us consider a quantum mechanical particle in a configuration space whose dimensionality is equal to or larger than two. The system has four observables $\hat{x},\hat{y},\hat{p}_x,\hat{p}_y$, which satisfy the canonical commutation relations $[\hat{x}_j,\hat{p}_k]=i\hbar\delta_{jk}$. We introduce two operators:

$$\hat{Z}:=\hat{x}+i\hat{y},\qquad \hat{L}:=\hat{x}\hat{p}_y-\hat{y}\hat{p}_x. \tag{18}$$

The operator $\hat{Z}$ is not self-adjoint but it is related to position of the particle. The self-adjoint operator $\hat{L}$ is called the orbital angular momentum (OAM). They satisfy the following:

$$[\hat{L},\hat{Z}]=\hbar\hat{Z}, \tag{19}$$

and:

$$[\hat{L},\hat{Z}^n]=n\hbar\,\hat{Z}^n \tag{20}$$

for any natural number $n = 1, 2, 3, \dots$. With a normalized vector $\psi \in \mathscr{H}$ we define:

$$\langle \hat{L} \rangle := \langle \psi | \hat{L} | \psi \rangle, \qquad \Delta \hat{L} := \hat{L} - \langle \hat{L} \rangle \hat{I}. \tag{21}$$

By substituting:

$$|\alpha\rangle = \Delta \hat{L} |\psi\rangle, \qquad |\beta\rangle = \hat{Z} |\psi\rangle, \tag{22}$$

into the Schwarz inequality (4) and by noting $\langle \alpha | = \langle \psi | \Delta \hat{L}^\dagger = \langle \psi | \Delta \hat{L}$ and $\langle \beta | = \langle \psi | \hat{Z}^\dagger$, we get:

$$\langle \psi | (\Delta \hat{L})^2 | \psi \rangle \langle \psi | \hat{Z}^\dagger \hat{Z} | \psi \rangle \geq \Big| \langle \psi | \Delta \hat{L}\, \hat{Z} | \psi \rangle \Big|^2. \tag{23}$$

Hence:

$$\sqrt{\langle (\Delta \hat{L})^2 \rangle} \sqrt{\langle \hat{Z}^\dagger \hat{Z} \rangle} \geq \Big| \langle \Delta \hat{L}\, \hat{Z} \rangle \Big|. \tag{24}$$

In a similar way, by substituting:

$$|\alpha\rangle = \hat{Z}^\dagger |\psi\rangle, \qquad |\beta\rangle = \Delta \hat{L} |\psi\rangle, \tag{25}$$

into (4), we get:

$$\sqrt{\langle \hat{Z} \hat{Z}^\dagger \rangle} \sqrt{\langle (\Delta \hat{L})^2 \rangle} \geq \Big| \langle \hat{Z} \Delta \hat{L} \rangle \Big|. \tag{26}$$

Note that $\hat{Z}\hat{Z}^\dagger = \hat{Z}^\dagger \hat{Z}$. The triangle inequality $|a| + |b| \geq |a - b|$ holds for any complex number a, b. The commutation relation (19) implies $[\Delta \hat{L}, \hat{Z}] = [\hat{L}, \hat{Z}] = \hbar \hat{Z}$. By adding (24) with (26) and multiplying $1/2$, we obtain:

$$\begin{aligned} \sqrt{\langle (\Delta \hat{L})^2 \rangle} \sqrt{\langle \hat{Z}^\dagger \hat{Z} \rangle} &\geq \frac{1}{2} \Big\{ \big| \langle \Delta \hat{L}\, \hat{Z} \rangle \big| + \big| \langle \hat{Z} \Delta \hat{L} \rangle \big| \Big\} \\ &\geq \frac{1}{2} \Big\{ \big| \langle \Delta \hat{L} \hat{Z} - \hat{Z} \Delta \hat{L} \rangle \big| \Big\} \\ &= \frac{1}{2} \hbar \, \big| \langle \hat{Z} \rangle \big|. \end{aligned} \tag{27}$$

This is one of our main results.

By replacing the operator $\hat{Z}$ with $\hat{Z}^n$, we can derive more general inequalities:

$$\sqrt{\langle (\Delta \hat{L})^2 \rangle} \sqrt{\langle (\hat{Z}^\dagger \hat{Z})^n \rangle} \;\geq\; \frac{1}{2} n \hbar \, \big| \langle \hat{Z}^n \rangle \big| \qquad (n = 1, 2, 3, \dots), \tag{28}$$

via a similar inference. The nonnegative number:

$$\sigma(\hat{L}) := \sqrt{\langle \psi | (\Delta \hat{L})^2 | \psi \rangle} = \langle \psi | \hat{L}^2 | \psi \rangle - \langle \psi | \hat{L} | \psi \rangle^2, \tag{29}$$

is the standard deviation of the orbital angular momentum. The complex number

$$\langle \hat{Z}^n \rangle = \langle \psi | (\hat{x} + i\hat{y})^n | \psi \rangle = \iint_{-\infty}^{\infty} (x + iy)^n \Big| \psi(x, y) \Big|^2 \, dx \, dy \tag{30}$$

is the *n-th moment* of probability density for the wave function $\psi(x, y)$[1]. If the probability density $|\psi(x, y)|^2$ is rotationally invariant, all the moments vanish $\langle \hat{Z}^n \rangle = 0$ $(n = 1, 2, 3, \dots)$. Conversely, if the system exhibits a nonvanishing moment $\langle \hat{Z}^n \rangle \neq 0$ for some n, the probability density, $|\psi(x, y)|^2$, is not rotationally invariant. Hence, the expectation value

[1] If the dimension of the configuration space is larger than two, it is necessary to use a suitable wave function $\psi(x, y, x, \dots)$.

$\langle \hat{Z}^n \rangle$ is interpreted as an order parameter to measure the degree of breaking of the rotational symmetry. The complex number:

$$\mu_n := \frac{\langle \hat{Z}^n \rangle}{\sqrt{\langle (\hat{Z}^\dagger \hat{Z})^n \rangle}} = \frac{\langle (\hat{x} + i\hat{y})^n \rangle}{\sqrt{\langle (\hat{x}^2 + \hat{y}^2)^n \rangle}}, \tag{31}$$

is called the *normalized n-th moment of position distribution* or the *normalized angular order parameter*, which indicates bias or asymmetry of angular distribution of the particle. Then, we have:

$$\sigma(\hat{L}) \geq \frac{1}{2} n\hbar \frac{\left| \langle \hat{Z}^n \rangle \right|}{\langle (\hat{Z}^\dagger \hat{Z})^n \rangle^{1/2}} = \frac{1}{2} n\hbar \left| \mu_n \right| \qquad (n = 1, 2, 3, \dots). \tag{32}$$

This is the main result of our work. This inequality implies that if the uncertainty $\sigma(\hat{L})$ of OAM is small, the normalized moment $|\mu_n|$ must be small. In this case, the angular distribution is not strongly biased and hence the uncertainty of angle must be large.

However, if the uncertainty of angle is small, the angular distribution is strongly biased and hence, the normalized moment $|\mu_n|$ becomes large, then the inequality (32) implies that the uncertainty $\sigma(\hat{L})$ of OAM must become large.

4. Tighter inequality

The necessary and sufficient conditions for the equality in (27) are the two equalities in (24), (26) and the other equality $\langle \Delta\hat{L}\hat{Z} \rangle = -\langle \hat{Z}\Delta\hat{L} \rangle$. Actually, there is no state vector satisfying these three conditions simultaneously, and hence, the equality in (27) is never attained. In this sense, the inequality (27) is not tight.

It is desirable to find a tighter inequality. For this purpose, we introduce self-adjoint operators:

$$\hat{x}_n := \frac{1}{2}\left(\hat{Z}^n + \hat{Z}^{\dagger n} \right) \qquad \hat{y}_n := \frac{1}{2i}\left(\hat{Z}^n - \hat{Z}^{\dagger n} \right), \tag{33}$$

for $n = 1, 2, 3, \dots$. Then, we have:

$$\hat{Z}^n = \left(\hat{x} + i\hat{y} \right)^n = \hat{x}_n + i\hat{y}_n. \tag{34}$$

Using these, it is easy to see that:

$$\begin{aligned} \Delta\hat{L}\,\hat{Z}^n &= \frac{1}{2}\{\Delta\hat{L}, \hat{Z}^n\} + \frac{1}{2}\left[\Delta\hat{L}, \hat{Z}^n\right] \\ &= \frac{1}{2}\{\Delta\hat{L}, (\hat{x}_n + i\hat{y}_n)\} + \frac{1}{2} n\hbar \hat{Z}^n \\ &= \frac{1}{2}\{\Delta\hat{L}, \hat{x}_n\} + i\frac{1}{2}\{\Delta\hat{L}, \hat{y}_n\} + \frac{1}{2} n\hbar (\hat{x}_n + i\hat{y}_n). \end{aligned} \tag{35}$$

Hence, (23) is equivalent to:

$$\begin{aligned} \langle (\Delta\hat{L})^2 \rangle \cdot \langle \hat{Z}^\dagger \hat{Z} \rangle &\geq \left| \frac{1}{2}\langle \{\Delta\hat{L}, \hat{x}_n\} \rangle + \frac{1}{2} n\hbar \langle \hat{x}_n \rangle \right|^2 + \left| \frac{1}{2}\langle \{\Delta\hat{L}, \hat{y}_n\} \rangle + \frac{1}{2} n\hbar \langle \hat{y}_n \rangle \right|^2 \\ &= \left| C_s(\hat{L}, \hat{x}_n) + \frac{1}{2} n\hbar \langle \hat{x}_n \rangle \right|^2 + \left| C_s(\hat{L}, \hat{y}_n) + \frac{1}{2} n\hbar \langle \hat{y}_n \rangle \right|^2. \end{aligned} \tag{36}$$

This is the tightest inequality whose equality can be attained. However, the equality holds if and only if the state is an eigenstate of $\hat{L}$. In this case, both sides of (36) are zero.

5. Experimental realization

We have formulated the uncertainty relations (27), (32), (36). In order to test these relations, we need to have a method for controlling and measuring angular momenta of particles.

In optics, there is a method for controlling and measuring angular momenta of photons. Franke-Arnold and Padgett *et al.* [11, 12] have tested the uncertainty relation of Judge [4] and Berbett, Pegg [7], by using an analyzer of photon angular momentum.

Uchida and Tonomura [13] first made a coherent electron beam carrying nonzero orbital angular momentum. Such electron beam has a wave front whose shape looks like a vortex. Verbeeck *et al.* [14] and McMorran *et al.* [15] developed fork-shaped diffraction gratings, which control orbital angular momenta of electrons. They observed circularly symmetric diffraction patterns for eigenstates of orbital angular momentum. Thus, they verified that the uncertainty in angular distribution was maximum when the uncertainty of angular momentum was minimum.

Recently, Hasegawa and Saitoh *et al.* [16, 17] made a superposition of two coherent electron beams carrying different angular momenta. As a result, they produced a quantum state that has an uncertain orbital angular momentum. They observed an interference pattern that was circularly asymmetric. Thus, they verified that the uncertainty in angular distribution became smaller when the uncertainty of angular momentum became larger. Yet, quantitative analysis of the uncertainty relation was not performed in experiments using electrons.

6. Generalization

The angular momentum $\hat{L}$ is a generator of rotational transformations, which transform the angle variable $(\hat{x}+i\hat{y})/\sqrt{\hat{x}^2+\hat{y}^2}$. A nonzero value of the order parameter $\mu = \langle\hat{x}+i\hat{y}\rangle/\sqrt{\langle\hat{x}^2+\hat{y}^2\rangle}$ indicates breaking of rotational symmetry, or certainty of the angle distribution, which accompanies uncertainty of the angular momentum. The relation between the angle order parameter and the uncertainty of the angular momentum is expressed by the inequality (32).

This kind of relation between a symmetry generator and a symmetry-breaking order parameter can be formulated in a more general form. Suppose that we have a self-adjoint operator $\hat{G}$, which is a generator of symmetry transformations and is called charge. Also, suppose that we have another operator, $\hat{\Phi}$. It is not necessary to assume that $\hat{\Phi}$ is a self-adjoint operator. Then, the inequality:

$$\sigma(\hat{G}) \geq \frac{|\langle[\hat{G},\hat{\Phi}]\rangle|}{\sqrt{\langle\hat{\Phi}^\dagger\hat{\Phi}\rangle}+\sqrt{\langle\hat{\Phi}\hat{\Phi}^\dagger\rangle}}, \tag{37}$$

holds. The expectation value $\langle[\hat{G},\hat{\Phi}]\rangle = \langle\psi|[\hat{G},\hat{\Phi}]|\psi\rangle$ is taken with respect to a state $|\psi\rangle$. This is a generalization of (27) and its proof is straightforward.

On the left-hand side of (37), the standard deviation $\sigma(\hat{G})$ measures uncertainty of the charge, while on the right-hand side of (37), the commutator $[\hat{G},\hat{\Phi}]$ represents transformation of $\hat{\Phi}$ by $\hat{G}$. If the state $|\psi\rangle$ is invariant under the transformation generated by $\hat{G}$, then $\langle\psi|[\hat{G},\hat{\Phi}]|\psi\rangle = 0$. If the order parameter $\langle[\hat{G},\hat{\Phi}]\rangle$ exhibits a nonzero value, then the state is not invariant and the uncertainty of the charge must satisfy inequality (37).

This formulation is applicable to the uncertainty relation between the particle number and the phase. In this case, we take $\hat{G} = \hat{a}^\dagger \hat{a}$ and $\hat{\Phi} = \hat{a}$, with the creation and annihilation operators $\hat{a}^\dagger$ and $\hat{a}$.

This formulation is applicable also to the complementarity relation [18] between the particle and wave natures.

7. Summary

The uncertainty relation between angle and orbital angular momentum does not have a formulation similar to the uncertainty relation between position and linear momentum. The angle variable is not represented by a quantum mechanical self-adjoint operator, although the other observables are represented by self-adjoint operators. We reviewed the general formulation of the uncertainty relation between noncommutative observables, which was proved by Robertson. Instead of the angle variable operator, we introduced the complex position operator $\hat{Z} = \hat{x} + i\hat{y}$ and interpreted the order parameter $\mu = \langle \hat{Z} \rangle / \sqrt{\langle \hat{Z}^\dagger \hat{Z} \rangle}$ as a measure of certainty of angle distribution. Then, we have proven relation (27) between the uncertainty of angular momentum and the certainty of angle. We proved relations (32), which are generalizations to higher moments of angular distribution $\mu_n = \langle \hat{Z}^n \rangle / \sqrt{\langle (\hat{Z}^\dagger \hat{Z})^n \rangle}$. We proved also the tightest inequality (36). A theoretical generalization to the uncertainty relation (37) between a symmetry generator and an order parameter was shown. Methods for controlling angular momenta of photons and electrons were discussed. Quantitative experimental tests of the relations will be discussed in future publications.

In this paper, we considered uncertainties of values of observables that are inherent in quantum states. However, we did not consider measurement process of observables. An actual measurement process involves measurement error and causes disturbance on the state of the measured system. Ozawa [19] formulated a quantitative relation between the measurement error and the disturbance. Branciard [20] established the tightest inequality that the error and the disturbance obey. We do not yet know this kind of error-disturbance relation for the angle and angular momentum.

Hayashi [21] formulated quantum estimation theory for the group action, which can be regarded as a generalization of the problem that was considered in our work. This aspect warrants further investigation.

Acknowledgements

The author thanks Keisuke Watanabe, who discussed with me the tighter version of the uncertainty inequality, Eq. (36). He thanks Prof. Katsuhiro Nakamura and Prof. Davron Matrasulov for their warm hospitality for supporting his stays in Uzbekistan. This manuscript is written as a part of the proceedings of the workshop, Wave dynamics in low-dimensional branched structures, held during September 23–24, 2014 in Tashkent, Uzbekistan. This work is financially supported by the Grant-in-Aid for Scientific Research of Japan Society for the Promotion of Science, Grant No. 26400417.

References

[1] Heisenberg W. Über den anschaulichen Inhalt der quantentheoretischen Kinematik und Mechanik. *Z. Physik*, **43**, P. 172 (1927).
[2] Robertson H.P. The uncertainty principle. *Phys. Rev.*, **34**, P. 163 (1929).
[3] Schiff L.I. *Quantum Mechanics*, 3rd edition, McGraw-Hill (1968).
[4] Judge D. On the uncertainty relation for L_z and φ. *Phys. Lett.*, **5**, P. 189 (1963).

[5] Kraus K. Remark on the uncertainty between angle and angular momentum. *Z. Physik*, **188**, P. 374 (1965).
[6] Carruthers P., Nieto M.M. Phase and angle variables in quantum mechanics. *Rev. Mod. Phys.*, **40**, P. 411 (1968).
[7] Bernett S.M., Pegg D.T. Quantum theory of rotation angles. *Phys. Rev. A*, **41**, P. 3427 (1990).
[8] Ohnuki Y., Kitakado S. Fundamental algebra for quantum mechanics on S^D and gauge potentials. *J. Math. Phys.*, **34**, P. 2827 (1993).
[9] Tanimura S. Gauge field, parity and uncertainty relation of quantum mechanics on S^1. *Prog. Theor. Phys.*, **90**, P. 271 (1993).
[10] Schrödinger E. Zum Heisenbergschen Unschärfeprinzip. *Sitzungsberichte der Preussischen Akademie der Wissenschaften, Physikalisch-mathematische Klasse*, **19**, P. 296 (1930).
[11] Franke-Arnold S., Barnett S.M., et al. Uncertainty principle for angular position and angular momentum. *New J. Phys.*, **6**, P. 103 (2004).
[12] Pegg D.T., Barnett S.M., et al. Minimum uncertainty states of angular momentum and angular position. *New J. Phys.*, **7**, P. 62 (2005).
[13] Uchida M. Tonomura A. Generation of electron beams carrying orbital angular momentum. *Nature*, **464**, P. 737 (2010).
[14] Verbeeck J., Tian H., Schattschneider P. Production and application of electron vortex beams. *Nature*, **467**, P. 301 (2010).
[15] McMorran B.J., Agrawal A., et al. Electron vortex beams with high quanta of orbital angular momentum. *Science*, **331**, P. 192 (2011).
[16] Hasegawa Y., Saitoh K., et al. Young's interference experiment with electron beams carrying orbital angular momentum. *J. Phys. Soc. Jap.*, **82**, P. 033002 (2013).
[17] Hasegawa Y., Saitoh K., Tanaka N., Uchida M. Propagation dynamics of electron vortex pairs. *J. Phys. Soc. Jap.*, **82**, P. 073402 (2013).
[18] Tanimura S. The incompatibility relation between visibility of interference and distinguishability of paths. `ArXiv quant-ph/0703118` (2007).
[19] Ozawa M. Universally valid reformulation of the Heisenberg uncertainty principle on noise and disturbance in measurement. *Phys. Rev. A*, **67**, P. 042105 (2003).
[20] Branciard C. Error-tradeoff and error-disturbance relations for incompatible quantum measurements. *Proceedings of the National Academy of Science of the USA*, **110** (17), P. 6742 (2013).
[21] Hayashi M. Fourier analytic approach to quantum estimation of group action. `ArXiv 1209.3463v2` (2012).

NANOSYSTEMS: PHYSICS, CHEMISTRY, MATHEMATICS, 2015, 6 (2), P. 213–215

Perturbative hydrodynamic Gross–Pitaevskii treatment for Bose–Einstein condensate in infinite length ring with disorder

D. B. Abdullaev[1], B. Abdullaev[1], and M. M. Musakhanov[2]

[1]Institute of Applied Physics, National University of Uzbekistan, Tashkent 100174, Uzbekistan
[2]National University of Uzbekistan, Tashkent 100174, Uzbekistan

abdullaev_davron@mail.ru, bakhodir_abdullaev@yahoo.com, yousufmm@list.ru

PACS 47.37.+q, 67.10.Jn, 67.85.Jk **DOI 10.17586/2220-8054-2015-6-2-213-215**

For the derivation of the dilute Bose–Einstein condensate density and its phase, we have developed the perturbative approach for the solution of the stationary state couple Gross–Pitaevskii hydrodynamic equations. The external disorder potential is considered as a small parameter in this approach. We have derived expressions for the total density, condensate density, condensate density depletion and superfluid velocity of the Bose–Einstein condensate in an infinite length ring with disorder potential having a general form. For the delta correlated disorder, the explicit analytical forms of these quantities (except the superfluid velocity) have been obtained.

Keywords: Bose–Einstein condensate in ring, Gross–Pitaevskii hydrodynamic equations, disorder potential, condensate density, condensate density depletion, delta correlated disorder.

Received: 2 February 2015

The Gross–Pitaevskii equation [1, 2]:

$$i\hbar\frac{\partial\psi\left(\boldsymbol{x},t\right)}{\partial t}=\left(-\frac{\hbar^2}{2m}\nabla^2+U\left(\boldsymbol{x}\right)+g\left|\psi\left(\boldsymbol{x},t\right)\right|^2\right)\psi\left(\boldsymbol{x},t\right). \tag{1}$$

is a powerful approach for the description of the Bose–Einstein condensate of the dilute ultracold atomic Bose gases [3], which have been recently observed in many experiments on cooling of atoms in magnetic traps and laser radiation (see references on experimental papers in [3]). In Eq. (1), the term proportional to g describes the contact interaction between two atoms in the s-scattering approximation.

With the existence of the external potential $U\left(\boldsymbol{x}\right)$ (confining trap or disorder potential) and a fluidity flow, the condensate wave function $\psi\left(\boldsymbol{x},t\right)=\sqrt{n\left(\boldsymbol{x},t\right)}e^{iS(\boldsymbol{x},t)}$ becomes a function not only of the condensate density $n\left(\boldsymbol{x},t\right)$, but also of its phase $S\left(\boldsymbol{x},t\right)$. For that case, it is rather convenient to describe a system by the couple hydrodynamic equations for the condensate density and its phase, originating from the Gross–Pitaevskii equation:

$$\begin{gathered}\frac{\partial n}{\partial t}+\nabla\left(n\boldsymbol{v}_s\right)=0,\\ m\frac{\partial\boldsymbol{v}_s}{\partial t}+\nabla\left(\frac{1}{2}m\boldsymbol{v}_s^2+U\left(\boldsymbol{x}\right)+gn-\frac{\hbar^2}{2m\sqrt{n}}\nabla^2\sqrt{n}\right)=0.\end{gathered} \tag{2}$$

Here, m is the mass of an atom, the superfluid velocity is expressed by formula $\boldsymbol{v}_s=\hbar\nabla S\left(\boldsymbol{x},t\right)/m$ and for simplicity, we have omitted arguments in expressions for $n\left(\boldsymbol{x},t\right)$, $S\left(\boldsymbol{x},t\right)$, $\boldsymbol{v}_s\left(\boldsymbol{x},t\right)$. For the stationary case, when time derivatives of the condensate density and the superfluid velocity are equal to zero, Eq. (2) reduces to:

$$\nabla\left(n\boldsymbol{v}_s\right)=0,$$
$$\nabla\left(\frac{1}{2}m\boldsymbol{v}_s^2+U\left(\boldsymbol{x}\right)+gn-\frac{\hbar^2}{2m\sqrt{n}}\nabla^2\sqrt{n}\right)=0. \tag{3}$$

Here and below, the kinetic energy of a superfluidity and external potential are expressed in gn^0 units and we introduce $y=\left(n/n^0\right)^{1/2}$. Condensate density n^0 is the solution of the second equation of Eqs. (3) obtained at $U\left(\boldsymbol{x}\right)=0$.

We will find the solution of Eqs. (3) using the perturbative approach, substituting in them expansions: $y\left(\boldsymbol{x}\right)=1+\varepsilon_1\left(\boldsymbol{x}\right)+\varepsilon_2\left(\boldsymbol{x}\right)$ and $\boldsymbol{v}_s\left(\boldsymbol{x}\right)=\boldsymbol{v}_{s0}+\boldsymbol{v}_{s1}\left(\boldsymbol{x}\right)+\boldsymbol{v}_{s2}\left(\boldsymbol{x}\right)$, where numerical indexes mean the order of the correction, the superfluid velocity $\boldsymbol{v}_{s0}$ corresponds to case $U\left(\boldsymbol{x}\right)=0$, and using in these expansions the Fourier integral transforms. For weak disorder, we consider $U\left(\boldsymbol{x}\right)$ as the first order correction and also use its Fourier transform.

Our interest is in the calculation of the total density of particles and the condensate density of particles $\dfrac{\left\langle n\left(\boldsymbol{x}\right)\right\rangle}{n^0}=\left\langle y^2\left(\boldsymbol{x}\right)\right\rangle$, $\dfrac{\left\langle n_0\left(\boldsymbol{x}\right)\right\rangle}{n^0}=\left\langle y\left(\boldsymbol{x}\right)\right\rangle^2$, respectively, averaged over the ensemble of the disorder potential. We denote the averaging procedure by $\langle\cdots\rangle$. We point out the property $\left\langle U\left(\boldsymbol{x}\right)\right\rangle=0$ for the disorder potential and existence of its correlator $\left\langle U\left(\boldsymbol{x}\right)U\left(\boldsymbol{x}'\right)\right\rangle=R\left(\left|\boldsymbol{x}-\boldsymbol{x}'\right|\right)$, whose Fourier transform is $\left\langle U\left(\boldsymbol{k}\right)U\left(\boldsymbol{k}'\right)\right\rangle=\left(2\pi\right)^1\delta\left(\boldsymbol{k}+\boldsymbol{k}'\right)R\left(\boldsymbol{k}\right)$.

We obtain expressions for the total density, condensate density, and condensate density depletion, respectively:

$$\frac{\left\langle n\left(\boldsymbol{x}\right)\right\rangle}{n^0}=1+\frac{1}{1-m\boldsymbol{v}_{s0}^2}\int\frac{dk}{2\pi}\frac{R\left(\boldsymbol{k}\right)\left[\frac{\hbar^2\boldsymbol{k}^2}{2mgn^0}-6m\boldsymbol{v}_{s0}^2\right]}{\left[\frac{\hbar^2\boldsymbol{k}^2}{2mgn^0}+2\left(1-m\boldsymbol{v}_{s0}^2\right)\right]^2},$$
$$\frac{\left\langle n_0\left(\boldsymbol{x}\right)\right\rangle}{n^0}=1+\frac{1}{1-m\boldsymbol{v}_{s0}^2}\int\frac{dk}{2\pi}\frac{R\left(\boldsymbol{k}\right)\left[\frac{\hbar^2\boldsymbol{k}^2}{2mgn^0}-1-5m\boldsymbol{v}_{s0}^2\right]}{\left[\frac{\hbar^2\boldsymbol{k}^2}{2mgn^0}+2\left(1-m\boldsymbol{v}_{s0}^2\right)\right]^2}, \tag{4}$$
$$\frac{\left\langle n\left(\boldsymbol{x}\right)-n_0\left(\boldsymbol{x}\right)\right\rangle}{n^0}=\int\frac{dk}{2\pi}\frac{R\left(\boldsymbol{k}\right)}{\left[\frac{\hbar^2\boldsymbol{k}^2}{2mgn^0}+2\left(1-m\boldsymbol{v}_{s0}^2\right)\right]^2}$$

and the expression for the superfluid velocity:

$$\left\langle\boldsymbol{v}_s\left(\boldsymbol{x}\right)\right\rangle=\boldsymbol{v}_{s0}-\frac{\boldsymbol{v}_{s0}}{1-m\boldsymbol{v}_{s0}^2}\int\frac{dk}{2\pi}\frac{R\left(\boldsymbol{k}\right)\left[\frac{\hbar^2\boldsymbol{k}^2}{2mgn^0}-4-2m\boldsymbol{v}_{s0}^2\right]}{\left[\frac{\hbar^2\boldsymbol{k}^2}{2mgn^0}+2\left(1-m\boldsymbol{v}_{s0}^2\right)\right]^2}. \tag{5}$$

We consider the Bose–Einstein condensate in the one dimensional ring trap, whose torus circumference is given by the length L. The trap of this geometry has a periodic boundary condition. Thus, all properties and quantities of the system must appear with periodic length L. For instance, the delta correlated disorder potential correlation function is:

$$R\left(\boldsymbol{x}\right)=r\sum_{j=-\infty}^{j=\infty}\delta\left(\boldsymbol{x}-Lj\right), \tag{6}$$

where $r=U_0^2$ for the average strength U_0 of the disorder potential. According to this, they must be expanded to the Fourier series with discrete values for the wave vectors. However, for a limit of the infinite length $L\to\infty$, these series on discrete wave values can easily be

transformed into the integral expressions on the continuous wave vector for quantities, in which we have interest, by replacing $\sum \to \int Ldk/2\pi$.

For $L \to \infty$, the asymptotic expressions for the ring geometry total density, condensate density, and condensate density depletion, respectively, are:

$$\begin{aligned}
\frac{\langle n(\boldsymbol{x})\rangle}{n^0} &= 1 + \frac{\pi p^{1/2} r\left(1 - 4m\boldsymbol{v}_{s0}^2\right)}{2^{3/2} L \left(gn^0\right)^2 \left(1 - m\boldsymbol{v}_{s0}^2\right)^{5/2}}, \\
\frac{\langle n_0(\boldsymbol{x})\rangle}{n^0} &= 1 + \frac{\pi p^{1/2} r\left(1 - 7m\boldsymbol{v}_{s0}^2\right)}{2^{5/2} L \left(gn^0\right)^2 \left(1 - m\boldsymbol{v}_{s0}^2\right)^{5/2}}, \\
\frac{\langle n(\boldsymbol{x}) - n_0(\boldsymbol{x})\rangle}{n^0} &= \frac{\pi p^{1/2} r}{2^{5/2} L \left(gn^0\right)^2 \left(1 - m\boldsymbol{v}_{s0}^2\right)^{3/2}},
\end{aligned} \tag{7}$$

where $p = 2mL^2 gn^0 / \left((2\pi)^2 \hbar^2\right)$.

In conclusion, we have developed the perturbative approach for the stationary state hydrodynamic Gross–Pitaevskii equations in the external disorder potential and applied it to investigate the one dimensional Bose–Einstein condensate of ring geometry. We have found expressions for the total density, condensate density, condensate density depletion and superfluid velocity of that condensate for the disorder potential, which has a general form, considering this potential perturbatively. For the delta correlated disorder, the explicit analytical forms of these quantities (except the superfluid velocity) have been obtained. It is interesting that for the superfluid velocity $\boldsymbol{v}_{s0} = 0$, i.e. no initial superfluid flow in the condensate, above expressions for the total density, condensate density, and condensate density depletion reproduce the same expressions for the static Bose–Einstein condensate [4].

References

[1] E. M. Lifshitz and L. P. Pitaevskii. *Statistical Physics, Part 2: Theory of Condensed State*, Course of Theoretical Physics, V. 9, Elsevier Ltd., Amsterdam 1980, 387 p.

[2] L. Pitaevskii and S. Stringari, *Bose–Einstein Condensation*, Oxford University Press, Oxford, 2003, 492 p.

[3] L. Dalfovo, S. Giorgini, L. P. Pitaevskii, and S. Stringari. Theory of Bose–Einstein condensation in trapped gases. *Rev. Mod. Phys.*, **71**, P. 463 –512 (1999).

[4] C. Krumnow and A. Pelster. Dipolar Bose–Einstein condensates with weak disorder. *Phys. Rev. A*, **84**, P. 021608(R) (2011).

NANOSYSTEMS: PHYSICS, CHEMISTRY, MATHEMATICS, 2015, 6 (2), P. 216–223

Quantum dynamics in a kicked square billiards

[1]S. Rakhmanov, [2]D. Babajanov, [1,2]O. Karpova*,[3]F. Khoshimova

[1]Faculty of Physics, National University of Uzbekistan, Vuzgorodok, Tashkent 100174,Uzbekistan

[2]Turin Polytechnic University in Tashkent, 17 Niyazov Str., Tashkent 100095, Uzbekistan

[3]Navoi State Mining Institute, 27 Janubiy ko'chasi, Navoiy, Uzbekistan

*ola_july@mail.ru

PACS 73.63.Kv **DOI 10.17586/2220-8054-2015-6-2-216-223**

We study kicked particle dynamics in a rectangular quantum billiard. The kicking potential is chosen as localized at the center of the billiard. The exact solution for the time-dependent Schrödinger equation for a single kicking period is derived. Using this solution, the time-dependence of the average kinetic energy and probability density as a function of spatial coordinates are computed. Different regimes for trapping of the particle in kicking area are analyzed. It is found that depending of the values of kicking parameters, the average kinetic energy can be a periodic or a monotonically growing function of time or can be suppressed. Such behavior is explained in terms of particle trapping regimes. Wave packet dynamics are also studied.

Keywords: quantum dynamics, billiard, Schrödinger equation.

Received: 2 February 2015

1. State of the art and statement of the problem

The study of particle dynamics in driven confined quantum systems is of practical importance for different newly emerging topics of nanoscale physics and nanotechnology. In fact, many nanoscale systems, materials and devices are subject to the influence of different external perturbations and environmental effects. The role of such effects in particle transport is relevant to the problem of tuning electronic, optic and acoustic properties of different nanoelectronic devices. Conversely, in confined quantum systems, particle dynamics also depend also on the geometry of the confinement boundaries. Due to these two facts driven confined systems have become an ideal testing ground for solving the problem of tunable particle transport in low-dimensional functional materials, such as quantum dots, wires networks etc. The most convenient tool for modeling of confined systems are so-called billiard geometries, or simply billiards. These are finite-size spatial domains with hard or soft walls providing confinement.

Earlier, billiards were the subject of extensive study in nonlinear dynamics [1] and quantum chaos theory [10]. In particular, it was found that classical particle dynamics in billiards strongly depended on the geometry of its boundaries. For instance, dynamics can be regular or chaotic depending on the shape of the billiard. In the quantum case, such a feature is on display in the energy spectrum of the system, implying that for billiards whose dynamics are integrable in the classical limit, level spacing distribution is always of the Poisson type, while for classically chaotic billiards, the distribution is Gaussian in nature [4].

Later, quantum billiards have found effective application as models for quantum dots in nanoscale physics [16]. Quantum dots are nanoscale domains in semiconducting structures of molecular systems, in which electronic motion is restricted to a finite domain by providing constant electric fields. It was found that by changing the shape and size of the

dot to be modeled by the quantum billiard, one can manipulate electron transport in the dot. Despite the fact that both quantum dots and billiards have been extensively studied, most of the works on this topic are restricted by considering isolated systems, i.e. in the absence of external forces. However, driven quantum systems are more attractive from the viewpoint of environmental effects and external perturbation effects on particle transport. We note that classical and quantum dynamics of periodically driven systems were also the subject of extensive research in the past. It was found that for a periodically driven classical system, the average kinetic energy increased linearly with time, while for the corresponding quantum system, such growth is suppressed [1]. The latter is called a quantum localization phenomenon, which is, to some extent, an analog of the well-known Anderson localization in solid state physics.

In this paper, we study the quantum dynamics of a periodically driven particle confined in a square-shaped billiard. We derive an exact analytical solution for the time-dependent Schrödinger equation which describes the dynamics of such a system. Using the obtained solution, we compute the average kinetic energy as function of time. Also, we analyze wave packet evolution in our system.

2. Kicked square billiard

Before starting the treatment of driven billiard, let us briefly recall the corresponding unperturbed system. The motion of a quantum particle in a square billiard is described by the following stationary Schrödinger equation:

$$H_0\psi_{nm} = \epsilon_{nm}\psi_{nm}, \tag{1}$$

where

$$H_0 = -\frac{1}{2}\left(\frac{\partial^2}{\partial x^2} + \frac{\partial^2}{\partial y^2}\right), \tag{2}$$

$$\psi_{nm} = \frac{2}{a}\sin\frac{n\pi x}{a}\sin\frac{m\pi y}{a}, \tag{3}$$

a is the side of square,

$$\epsilon_{nm} = \frac{\pi^2}{a^2}(n^2 + m^2) \tag{4}$$

are the eigenfunctions and eigenvalues, respectively.

The external potential is chosen in the form of delta kicks as:

$$V(x, y, t) = \varepsilon(\cos x + \cos y)\sum_{l=0}^{\infty}\delta(t - lT). \tag{5}$$

This potential is a two dimensional generalization of the well-known delta-kicks studied earlier in the Ref. [1]. Schematically, the kicked billiard we are going to study can be represented as in Fig.1.

Particle dynamics in such a billiard are described by the following time-dependent Schrödinger equation:

$$i\frac{\partial\Psi}{\partial t} = [H_0 + V(x, y, t)]\Psi, \tag{6}$$

where

$$\Psi = \Psi(x, y, t)$$

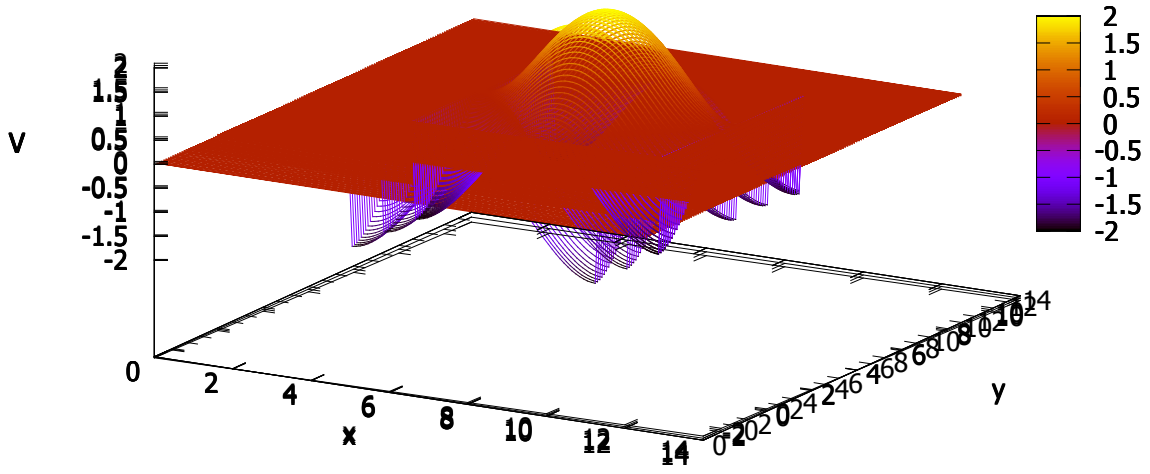

FIG. 1. Profile of the external kicking potential

The wave function of the system, i.e. the solution of Eq.(6) can be expanded in terms of unperturbed billiard wave functions given by Eq.(3) as:

$$\Psi(x,y,t) = \sum A_{nm}(t)\psi_{nm}(x,y), \tag{7}$$

This allows us to find expansion coefficients explicitly and exactly:

$$A_{nm}(t+T) = \sum_{n',m'} A_{n'm'}(t)V_{nmn'm'}e^{-i\epsilon_{n'm'}T}, \tag{8}$$

where

$$V_{nmn'm'} = \int\int \psi^*_{nm}(x,y)e^{i\varepsilon(\cos x+\cos y)}\psi_{n'm'}(x,y)dxdy. \tag{9}$$

In the derivation of this expression, we used the relation:

$$e^{i\varepsilon cosx} = \sum_l i^l J_l(\varepsilon)e^{ilx}, \tag{10}$$

We note that the expansion coefficients obey the normalization condition:

$$\sum_{n,m} |A_{nm}(0)|^2 = 1. \tag{11}$$

One important characteristic of the dynamics in driven systems is the average kinetic energy of a driven particle. For our system, it can be defined as:

$$E(t) = \int \Psi^*(x,y,t)H_0\Psi(x,y,t)dxdy = \sum_{n,m} |A_{nm}(t)|^2\epsilon_{nm}. \tag{12}$$

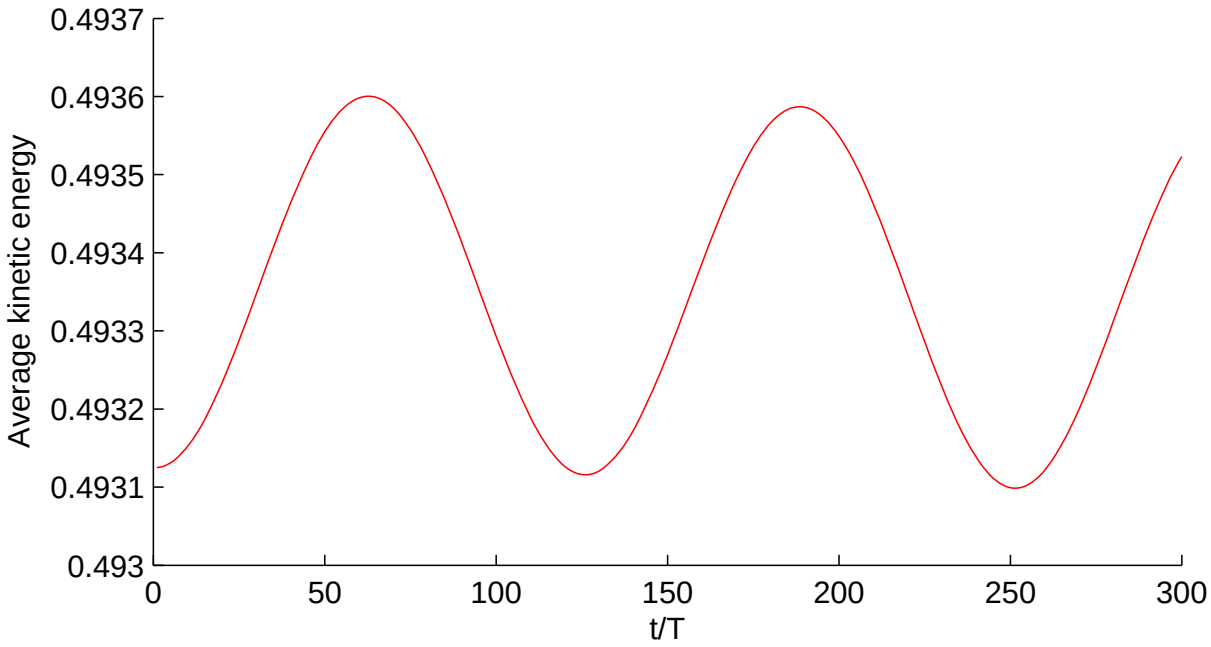

FIG. 2. Time dependence of the average kinetic energy ($\varepsilon = 0.001, T = 0.1$)

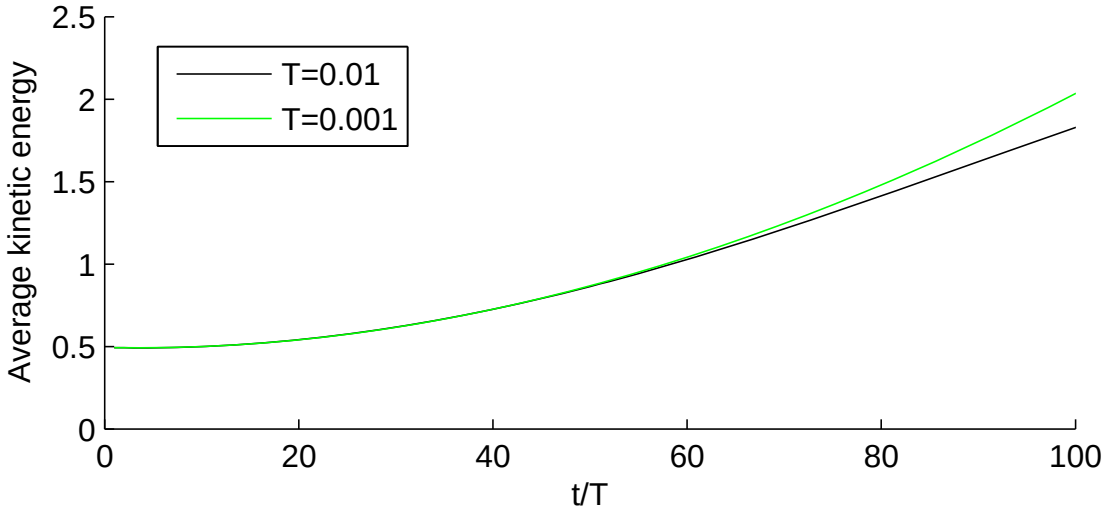

FIG. 3. Time dependence of the average kinetic energy for fixed ε at different values of the kicking period ($\varepsilon = 0.001, T_1 = 0.01, T_2 = 0.001$)

3. Particle dynamics in a kicked square billiard

We are interested in analyzing this quantity as a function of time. In calculating the average kinetic energy, we take a few non-zero initial values of the expansion coefficients which obey the above normalization conditions given by (11). In Fig.2, $E(t)$ is plotted.

As is seen from these plots, $E(t)$ is periodic in time with a period much higher than that of the kicking force. Figs. 3 and 4 present the average kinetic energy as a function of time for fixed T at fixed kicking strength, ε.

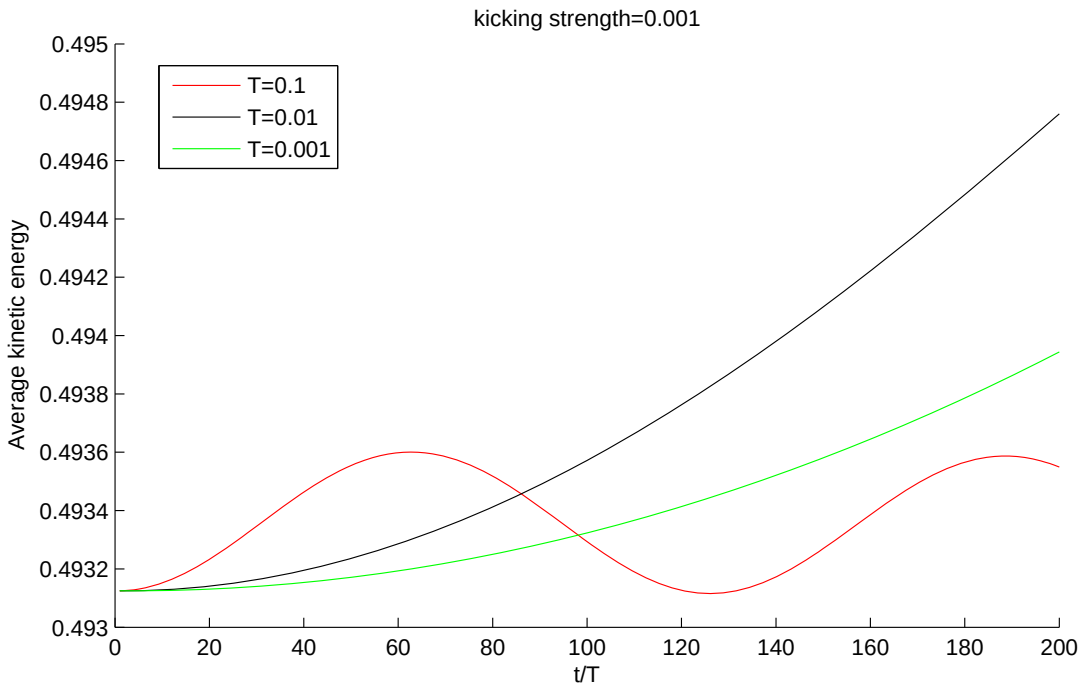

FIG. 4. Time dependence of the average kinetic energy for fixed ε at different kicking period values ($\varepsilon = 0.001, T_1 = 0.1, T_2 = 0.01, T_3 = 0.001$)

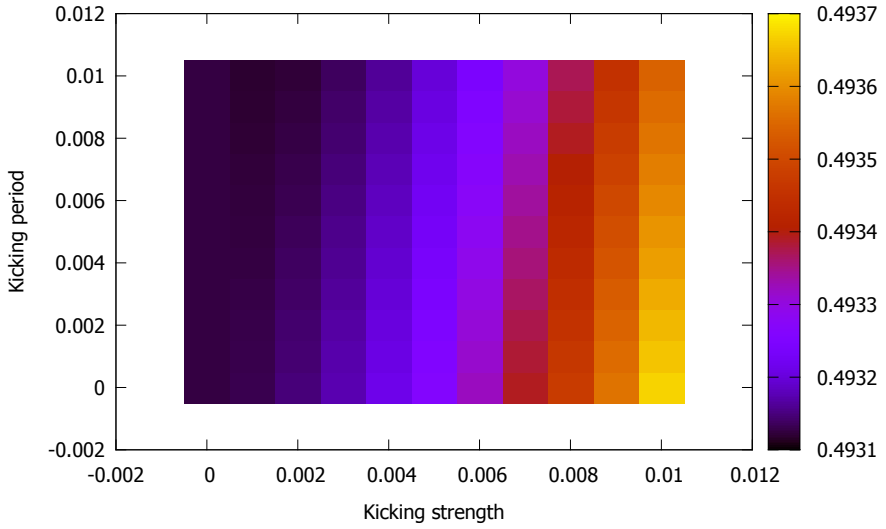

FIG. 5. Average kinetic energy as a function of kicking strength and period (at $t = 20T$)

One can observe from these plots that the profile of $E(t)$ depends on the kicking period. The dependence of the average kinetic energy upon the kicking parameters can clearly be seen from the plot in Fig. 5, where it is plotted as a function of T and ε. This plot shows that the growth of $E(t)$ is as intense as higher ε and as shorter T. To explain the above behavior of $E(t)$, we analyzed the spatio-temporal evolution of the probability density for our system, $|\Psi(x, y, t)|^2$. Figs. 6 and 7 present comparison of $|\Psi(x, y, t)|^2$ at different moments of time with the profile of the kicking potential. It is clear from these plots that the localization

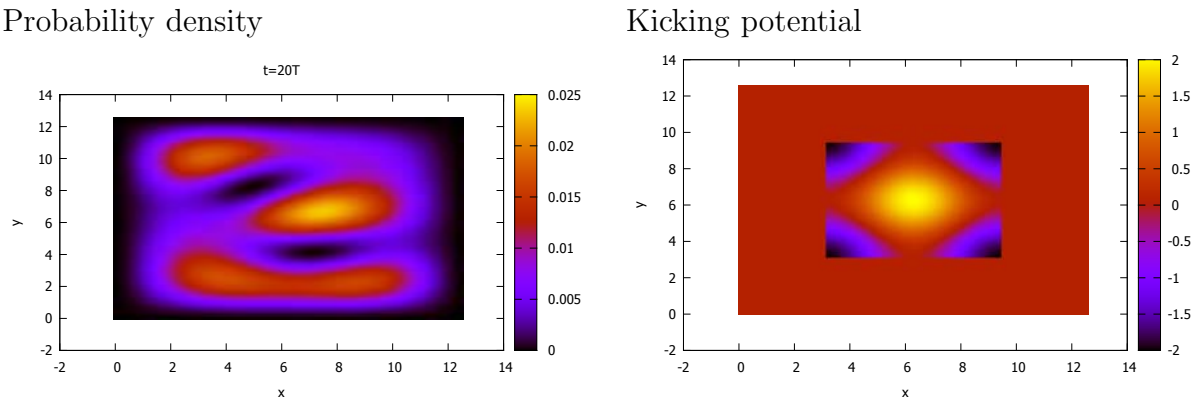

FIG. 6. Probability density versus coordinates ($t = 20T, \varepsilon = 0.001, T = 1.26$)

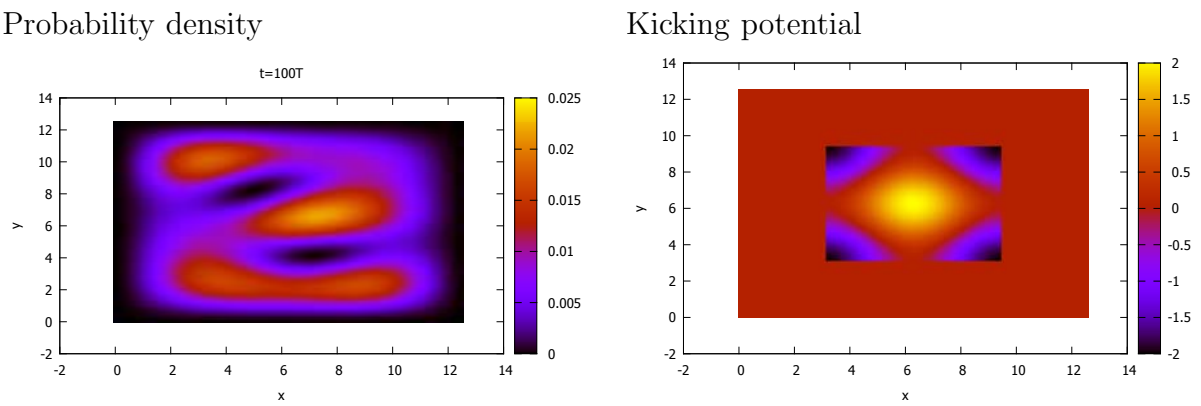

FIG. 7. Probability density versus coordinates. ($t = 100T, \varepsilon = 0.001, T = 1.26$)

of the probability density is periodic in time, i.e. probability density is periodically localized on the areas of billiard where the kicking potential is negative and positive. If the particle motion is localized on the area where the kicking potential is repulsive (positive), it gains the energy, while on the area where the potential is negative, it looses energy. In other words, particle is periodically trapped on the areas where it gains and loses energy. This is the reason for the time-periodic behavior of the average kinetic energy.

4. Wave packet evolution

Another characteristic of particle transport in driven systems is the wave packet dynamics, i.e. the evolution of the packet profile in space and time. In this work, we consider evolution of Gaussian wave packets, i.e. we assume that at $t = 0$ the wave packet has a Gaussian profile as:

$$\Psi(x, y, 0) = \Phi(x, y) = \frac{1}{\pi\sqrt{\pi}} \exp\left(-\frac{x^2 + y^2}{2d^2}\right) \sum_{n,m} \sin\frac{\pi n x}{a} \sin\frac{\pi m y}{a}. \tag{13}$$

Then, the expansion coefficients at $t = 0$ can be expressed via the wave packet as:

$$A_{mn}(0) = \frac{1}{\pi\sqrt{\pi}} \exp\left(-\frac{x^2 + y^2}{2d^2}\right), \tag{14}$$

where d is the width of packet.

$(t = 0, \varepsilon = 0.001, T = 100)$ $(t = 3T, \varepsilon = 0.001, T = 100)$

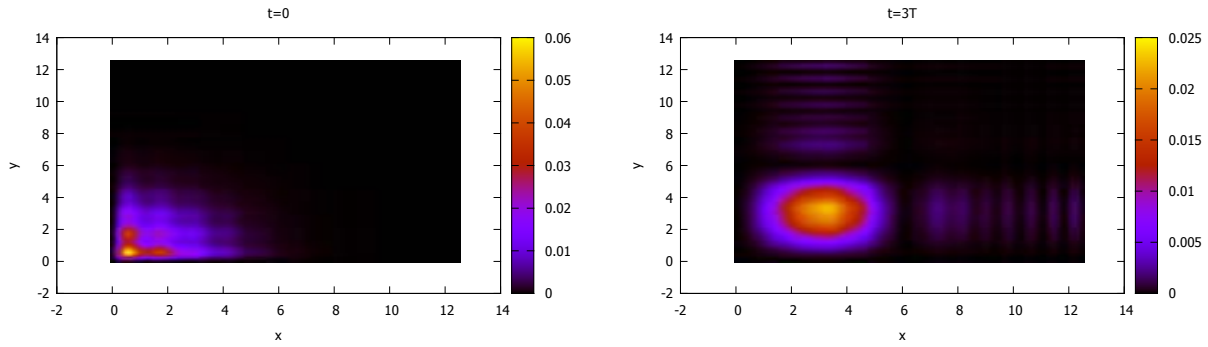

$(t = 31T, \varepsilon = 0.001, T = 100)$ $(t = 46T, \varepsilon = 0.001, T = 100)$

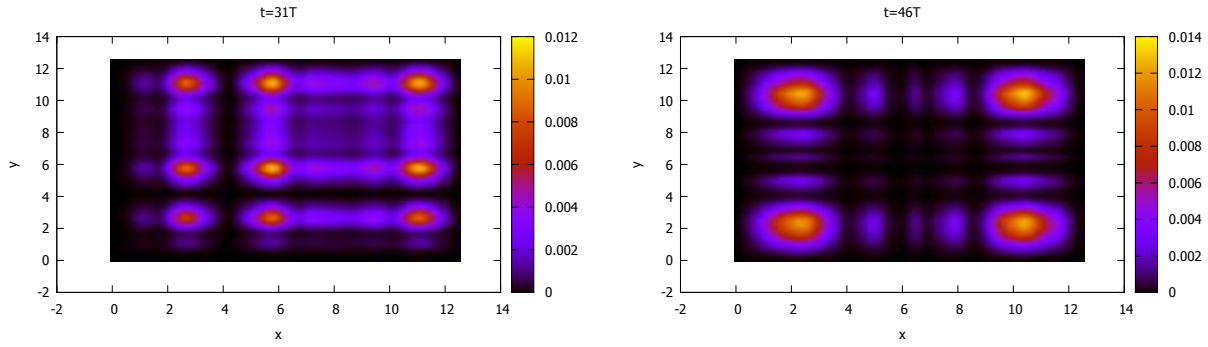

FIG. 8. Wave packet evolution

In upper left panel of Fig. 8, the time evolution of the wave packet is presented for the moment $t = 0$ for the values of the kicking parameters $\varepsilon = 0.001, T = 100$. Other panels of Fig. 8 depict the time evolution of the wave packet for the following time points $t_1 = 3T, t_2 = 31T, t_3 = 46T$ for the values of the kicking parameters $\varepsilon = 0.001, T = 100$. As is seen from these plots, the dispersion of the packet occurs after certain number of kicks.

5. Conclusions

Summarizing, in this work, we have studied the quantum dynamics of a particle confined in a square billiard and interacting with an external time-periodic force having the form of delta-kicks. The system is described by the time-dependent Schrödinger equation. An exact solution for this time-dependent Schrödinger equation is found during single kicking period. Using the obtained solution, characteristics of the particle dynamics, such as the average kinetic energy, solution of the single state energy, probability density and wave packet transport can be computed. The average kinetic energy was found to be periodic in time. This periodicity was shown to be a result of particle interaction, which is periodically located in areas where the kicking force is attractive or repulsive. When particle is confined to a negative force area, it continuously loses its energy, and conversely, when trapped on a positive force area, it gains energy. Similar behavior was found for single state energy. Analysis of the wave packet profile in time and space showed that after a certain number of kicks and collisions with the billiard wall, dispersion of the Gaussian wave packet occurs. The results obtained in this work can be useful for the problem of tunable Fermi acceleration

in quantum systems, and tunable electronic transport in nanoscale devices, e.g. quantum dots, wires, wells etc.

References

[1] G. Casati, B.V. Chirikov, J. Ford, F.M. Izrailev, in: G. Casati, J.Ford (Eds.), *Lecture Notes in Physics*, vol. 93, Springer-Verlag, Berlin, p. 334 (1979).

[2] Lichtenberg A.J., Lieberman M.A. *Regular and stochastic motion*. N.Y.-Heidelberg-Berlin, Springer-Verlag, 499 pp. (1983).

[3] R.Z. Sagdeev, D.A. Usikov, G.M. Zaslavsky, *Nonlinear Physics: From Pendulum to Turbulence and Chaos*. Academic Publisher, New York (1988).

[4] M.C. Gutzwiller, *Chaos in classical and quantum systems*, New York, Springer Verlag (1990).

[5] Bagrov V.G. and Gitman D.M. *Exact Solutions of Relativistic Wave Equations*, Dordrecht, Kluwer (1990).

[6] A.J. Lichtenberg, M.A. Lieberman, *Regular and Chaotic Dy-namics*. Springer-Verlag, New York (1992).

[7] Thaller B. *The Dirac Equation*. Berlin, Springer (1992).

[8] M.F. Shlesinger, G.M. Zaslavsky, U. Frish (Eds.), *Lvy Flights and Related Topics in Physics*. Springer-Verlag (1995).

[9] G. Casati and B.V. Chirikov(eds.) *Quantum chaos between order and disorder a selection of papers*. Cambridge University Press, New York (1995).

[10] Hans-Jürgen Stöckmann. *Quantum Chaos: An Introduction*. Cambridge University Press (1995).

[11] De Vincenzo S. *Thesis Magister scientiarum in science, physics mention*. Universidad Central de Venezuela, Caracas (1996). (in Spanish)

[12] K. Nakamura *Quantum Versus Chaos. Questions Emerging from Mesoscopic Cosmos*. Kluwer Academic Dordrecht (1997).

[13] Yoseph Imry. *Introduction to Mesoscopic Physics*. Oxford University Press (1997).

[14] H.-J. Stöckmann, *Quantum Chaos: An Introduction*. Cambridge University Press, Cambridge, UK (1999).

[15] K. Richter, *Semiclassical Theory of Mesoscopic Quantum Systems*. Springer, Berlin (2000).

[16] K. Nakamura and T. Harayama. *Quantum Chaos and Quantum Dots*. Oxford University Press (2004).

NANOSYSTEMS: PHYSICS, CHEMISTRY, MATHEMATICS, 2015, 6 (2), P. 224–243

Time-dependent quantum circular billiard

[1,2]D. B. Babajanov,[1,2]D. U. Matrasulov, [1,3]Z. A. Sobirov, [4]S. K. Avazbaev,[1,2]O. V. Karpova

[1] National University of Uzbekistan, Tashkent, Uzbekistan
[2] Turin Polytechnic University in Tashkent, 17. Niyazov Str., 100095, Tashkent, Uzbekistan
[3] Tashkent Financial Institute, 60A, Amir Temur Str., 100000 Tashkent, Uzbekistan
[4] ARC Centre for Antimatter-Matter Studies, Department of Applied Physics, Curtin University, G.P.O. Box U1987, Perth 6845, Australia

*d_babajanov@yahoo.com

PACS 03.65.Ge **DOI 10.17586/2220-8054-2015-6-2-224-243**

The motion of a quantum particle in a time-dependent circular billiard is studied on the basis of the Schrödinger equation with time-dependent boundary conditions. The cases of monotonically expanding (contracting), non-harmonically, harmonically breathing circles the case when billiard wall suddenly disappears are explored in detail. The exact analytical solutions for monotonically expanding and contracting circles are obtained. For all cases, the time-dependence of the quantum average energy is calculated. It is found that for an harmonically breathing circle, the average energy is time-periodic in the adiabatic regime with the same period as that of the oscillation. For intermediate frequencies which are comparable with the initial frequency of the particle in unperturbed billiard, such periodicity is broken. However, for very high frequencies, the average energy once again becomes periodic. A qualitative analysis of the border between adiabatic and non-adiabatic regimes is provided.

Keywords: quantum billiards, Schrödinger equation.

Received: 2 February 2015

1. Introduction

Billiards are convenient models for the study of classical and quantum dynamics of non-integrable systems. They have been extensively studied in both experimental [1] and theoretical contexts [2,3]. A remarkable feature of particle motion in billiards is the dependence of the dynamics on the geometry of the billiard boundaries. Depending on the geometry, the dynamics can be regular, mixed or chaotic in the classical case. The corresponding quantum dynamics exhibit certain features in the statistical properties of the energy spectrum. For those systems, whose classical dynamics are chaotic, the nearest-neighbor energy level spacing distribution function of the corresponding quantum system is of Wigner type, while for regular systems this distribution is Poissonian [2,3]. Most of the studies on billiards deal with static billiards. However, in recent years there is a growing interest in the classical dynamics of time-dependent billiards [4]- [8]. One of the key questions that has been investigated is whether there will be Fermi acceleration in such two-dimensionally confined geometries. Studies of time-dependent billiards with a regular static counterpart, such as the breathing circle, show that there is no unbounded growth of the velocity, while for some non-integrable geometries, like the stadium [4,5] and the (eccentric) annular billiard [6], Fermi acceleration is possible. Recently, the classical dynamics of particles in time-dependent elliptic billiard have been studied and tunable Fermi acceleration has been shown to exist in such a system, even though the static counterpart is integrable [7,8]. Despite certain progress made in the study of the classical dynamics of time-dependent billiards, the quantum dynamics of such systems are still an open problem. At the present time , no detailed treatment of the problem

on the basis of two-dimensional time-dependent Schrödinger equation has yet been done. In the quantum case, the problem of time-dependence is reduced to solving the two-dimensional Schrödinger equation with time-dependent boundary conditions. The one-dimensional counterpart of this problem has been extensively studied [10] - [28]. These studies showed that even for the one-dimensional case, the Schrödinger equation with time-dependent boundary conditions cannot be solved exactly for an arbitrary time-dependence of the boundary conditions. In the case of the 1D box, the time-dependent boundary conditions can be reduced to static ones, leading to a Schrödinger equation which can be interpreted as a time-dependent confined harmonic oscillator [13, 16–18]. Makowsky et al. solved this problem for special cases of the time-dependence of the boundaries [16]. In particular, they classified the types of time-dependent boundary conditions for which an exact analytical solution of the problem can be obtained.

In the case of periodic (harmonic) time-dependence of the boundaries, the problem can be solved numerically by an expansion of the wave function in terms of Gaussian wave packets [17]. Scheininger and Kleber treated the case of a special type of periodically time-dependent boundaries by solving the problem in terms of the full-circle propagator [15]. Seba studied the case of time-periodic boundary conditions in terms of Floquet operators [24]. In a very recent work, Ref. [28], the quantum infinite square well with an oscillating wall was studied. It was shown that three types of regimes are possible in such a system, which can be classified as adiabatic (for low oscillation frequencies), chaotic (for intermediate frequencies) and periodic (for high oscillation frequencies). In particular, the average energy was found to be time-periodic for the adiabatic and periodic regimes, while for the chaotic regime, periodicity was broken.

In this work, we address the two-dimensional extension of the problem considered by Makowski et al. [16]. We solve the Schrödinger equation for the circular billiard with a time-dependent radius. In particular, we consider the following cases:
i) monotonically expanding (contracting) circle;
ii) non-harmonically breathing circle;
iii) harmonically breathing circle.

The classical counterpart of this system has been studied earlier Ref. [30], where it was shown that unbounded velocity gain is not possible. In Ref. [31] dynamics, statistical properties of quasi-energy levels and wave functions for the quantum system have been studied for harmonically oscillating circle. The "scars" in the quantum quasi-energy eigenfunctions corresponding to classical unstable periodic orbits were found in [31].

This paper is organized as follows: in the next section we briefly recall the case of the circular billiard with fixed boundaries. Section 3 presents the analytical solution when time and coordinate variables can be separated. In section 4, we study the case when billiard wall disappears suddenly. Non-harmonically breathing circle is studied in section 5. Section 6 provides detailed study of the circle with harmonically oscillating boundaries, by solving the time-dependent Schrödinger equation numerically. Finally, section 7 presents the discussion of the obtained results and some concluding remarks.

2. Static circular billiard

The circular billiard is defined by the potential:

$$V(r,\theta) = V(r) = \begin{cases} 0 & \text{for } r < r_0, \\ \infty & \text{for } r \geqslant r_0, \end{cases} \tag{1}$$

where r_0 is the radius of circle. The corresponding quantum mechanical eigenvalue problem is given by:

$$-\frac{\hbar^2}{2\mu}\left(\frac{\partial^2}{\partial r^2}+\frac{1}{r}\frac{\partial}{\partial r}+\frac{1}{r^2}\frac{\partial^2}{\partial\theta^2}\right)\psi(r,\theta)=E\psi(r,\theta), \tag{2}$$

with μ being the mass of the particle. Angular and radial variables in this equation can be separated with $\psi(r,\theta)=R(r)\Theta(\theta)$ (the system of units $\mu=\hbar=1$ is used throughout the paper)

$$-\frac{1}{2}\left(\frac{d^2R}{dr^2}+\frac{1}{r}\frac{dR}{dr}\right)+\frac{m^2}{2r^2}R=ER, \tag{3}$$

$$\frac{d^2\Theta_{(m)}(\theta)}{d\theta^2}=-m^2\Theta_{(m)}(\theta), \tag{4}$$

where $R(r)$ and $\Theta(\theta)$ are the radial and angular solutions, respectively, and m is the angular quantum number. The boundary conditions for Eqs. 3 and 4 are given by:

$$R(r_0)=0,$$

$$\Theta_{(m)}(\theta+2\pi)=\Theta_{(m)}(\theta).$$

We note that using the substitution $R(r)=u(r)/\sqrt{r}$, Eq.(3) can be reduced into a form which does not contain the first derivative of the radial wave function:

$$-\frac{1}{2}\frac{d^2u}{dr^2}+\frac{m^2-1/4}{2r^2}u=Eu. \tag{5}$$

The solution for the radial equation satisfying the above boundary condition can be written in terms of the regular Bessel functions [29, 33–35]:

$$R_{mn}(r)=N_{mn}J_m(\lambda_{mn}r), \tag{6}$$

where n is the radial quantum number and the eigenvalues are defined by:

$$E_{mn}=\frac{\lambda_{mn}^2}{2r_0^2}, \tag{7}$$

λ_{mn} is the n-th zero of the m-th Bessel function $J_m(r)$ and N_{mn} is the normalization constant given by:

$$N_{mn}^2\int_0^{r_0}\mid J_m(\lambda_{mn}r)\mid^2 rdr=1. \tag{8}$$

The angular equation has normalized solutions of the form:

$$\Theta_{(m)}(\theta)=\frac{1}{\sqrt{2\pi}}e^{im\theta}. \tag{9}$$

Eqs. (6) -(9) completely define the solution of the time-independent quantum mechanical circular billiard problem.

3. Monotonically expanding circle

Now, we proceed to a time-dependent circle. The central symmetry of the circular billiard allows us to solve the problem within the radial Schrödinger equation. We restrict ourselves to the case when just the radius of the circle is time-dependent so that central symmetry is remained. First, we consider a monotonically expanding (contracting) circle. For circular billiards with time-dependent radius, the radial Schrödinger equation can be written as:

$$i\frac{\partial R}{\partial t} = -\frac{1}{2}\frac{\partial^2 R}{\partial r^2} - \frac{1}{2r}\frac{\partial R}{\partial r} + \frac{m^2}{2r^2}R, \tag{10}$$

and the boundary conditions are given by:

$$R(r(t),t) = 0 \quad \text{for} \;\; r = r_0(t).$$

As shown earlier for example in Refs. [11]- [18], to solve Eq.(10) we need to make the boundary conditions time-independent. This is can done by using the coordinate transformation:

$$y = \frac{r}{r_0(t)}. \tag{11}$$

Thus, Eq.(10) reduces to:

$$i\frac{\partial R(y,t)}{\partial t} = -\frac{1}{2r_0^2}\frac{\partial^2 R}{\partial y^2} - \left(\frac{1}{2r_0^2 y} - i\frac{\dot{r}_0}{r_0}y\right)\frac{\partial R}{\partial y} + \frac{m^2}{2r_0^2 y^2}R. \tag{12}$$

Inserting the substitution:

$$R(y,t) = \frac{1}{r_0(t)\sqrt{y}}\exp\left(\frac{i}{2}\dot{r}_0(t)r_0(t)y^2\right)\phi(y,t), \tag{13}$$

into Eq.(12), we get:

$$ir_0^2\frac{\partial \phi}{\partial t} = -\frac{1}{2}\frac{\partial^2 \phi}{\partial y^2} + \left(\frac{1}{2}r_0^3\ddot{r}_0 y^2 + \frac{m^2 - 1/4}{2y^2}\right)\phi. \tag{14}$$

Eq.(14) can be interpreted as the Schrödinger equation for a time-dependent harmonic oscillator confined to a unit circle. Time and coordinate variables in Eq.(14) can be separated, provided that the following condition is fulfilled:

$$r_0^3\ddot{r}_0 = const = -C, \;\; C > 0. \tag{15}$$

Separating variables by:

$$\phi(y,t) = \varphi(y)T(t),$$

we get:

$$-\frac{1}{2}\frac{d^2\varphi}{dy^2} + \left(-\frac{1}{2}Cy^2 + \frac{m^2 - 1/4}{2y^2}\right)\varphi = k^2\varphi, \tag{16}$$

and

$$ir_0^2\frac{dT}{dt} = k^2 T(t), \tag{17}$$

where k is the separation constant. The general solution for Eq.(15) can be written as:

$$r_0(t) = \sqrt{at^2 + bt + c}, \tag{18}$$

where

$$C = \frac{b^2 - 4ac}{4}.$$

For $C = \frac{b^2}{4}$ we have a circle expanding with non-constant velocity:

$$r_0(t) = \sqrt{at + b}. \tag{19}$$

For $C = 0$ this solution corresponds to a linearly expanding (contracting) circle:

$$r_0(t) = at + b.$$

For the linearly expanding (contracting) circle, Eq. (16) is formally the same as Eq. (5), the one for the static circular billiard. However, because of the relation (13), the solution of the original time-dependent radial equation (10) is different from that of the static circular billiard. For the time-dependent radial wave function, we have:

$$R_{mn}(r,t) = \frac{1}{r_0(t) J_{m+1}(\lambda_{mn})} \exp\left(\frac{i}{2}\frac{\dot{r}_0(t)}{r_0(t)} r^2\right) J_m\left(\frac{\lambda_{mn} r}{r_0(t)}\right) \exp\left(-i \int_0^t \frac{\lambda_{mn}^2 d\tau}{r_0^2(\tau)}\right). \tag{20}$$

For $a = 0$, the solution coincides with the one of the static billiard given by Eq.(6). For $C \neq 0$, the solution of Eq. (16) is expressed in terms of the confluent hypergeometric functions [35]:

$$\varphi(y) = y^{m+1/2} e^{-0.5i\sqrt{C}y^2} M(d, m+1, i\sqrt{C}y^2), \tag{21}$$

where:

$$d = \frac{m+1}{2} + \frac{k^2}{2\sqrt{C}} i.$$

The eigenvalues k are defined by the condition $\varphi(1) = 0$, or:

$$M(d, m+1, i\sqrt{C}) = 0, \tag{22}$$

where only d depends on k. Thus the solution of Eq.(10) can be written as:

$$R_{mn}(r,t) = N_{mn} \frac{r^m}{r_0^{m+1}(t)} \exp\left(\frac{ir^2}{2}\left(\frac{\dot{r}_0(t)}{r_0(t)} - \frac{\sqrt{C}}{r_0^2(t)}\right)\right) \times$$

$$\times M\left(\frac{m+1}{2} + \frac{k_{mn}^2}{2\sqrt{C}} i, m+1, i\sqrt{C}\frac{r^2}{r_0^2(t)}\right) \exp\left(-ik_{mn}^2 \int_0^t \frac{d\tau}{r_0^2(\tau)}\right), \tag{23}$$

where N_{mn} is the normalization constant given by

$$\int |R_{mn}|^2 r dr = 1.$$

A quantity which is of interest from the viewpoint of Fermi acceleration in time-dependent billiards, is the average kinetic energy, which is defined as:

$$\langle E_m(t) \rangle = \langle \psi(r,t) | H | \psi(r,t) \rangle,$$

where:

$$H = -\frac{1}{2}\frac{\partial^2}{\partial r^2} - \frac{1}{2r}\frac{\partial}{\partial r} + \frac{m^2}{2r^2}. \tag{24}$$

The asymptotic behavior of the average energy for the linearly expanding (contracting) circle in the limits $t \to \infty$ and $r_0(t) \to \infty$ can easily be estimated. Indeed, since radial and angular variables are separated and H does not depend on the angular variables, the average energy can be written in terms of the time-dependent radial wave functions as:

$$\langle E_{mn}(t) \rangle = \int_0^{r_0(t)} R_{mn}^*(r,t) H R_{mn}(r,t) r dr = \frac{1}{2}\int_0^{r_0(t)} \left| \frac{\partial R_{mn}}{\partial r} \right|^2 r dr + \frac{m^2}{2}\int_0^{r_0(t)} \frac{|R_{mn}|^2}{r} dr.$$

Taking into account the relation:

$$\mid \frac{\partial R_{mn}}{\partial r} \mid^2 = \frac{1}{r_0^2(t) J_{m+1}^2(\lambda_{mn})} \left[\left(\frac{\dot{r_0}}{r_0} \right)^2 J_m^2 \left(\frac{\lambda_{mn} r}{r_0} \right) r^2 + \left(\frac{\partial}{\partial r} J_m \left(\frac{\lambda_{mn} r}{r_0} \right) \right)^2 \right], \tag{25}$$

we get:

$$\langle E_{mn}(t) \rangle = C_1 + C_2 \frac{1}{(at+b)^2}, \tag{26}$$

where the constants C_1 and C_2 are given by:

$$C_1 = \frac{a^2}{J_{m+1}^2(\lambda_{mn})} \int_0^1 y^3 J_m^3(\lambda_{mn} y) dy, \tag{27}$$

$$C_2 = \frac{1}{J_{m+1}^2(\lambda_{mn})} \int_0^1 \left(\frac{\partial}{\partial y} J_m(\lambda_{mn} y) \right)^2 y dy + \frac{m^2}{J_{m+1}^2(\lambda_{mn})} \int_0^1 \frac{1}{y} J_m^2(\lambda_{mn} y) dy. \tag{28}$$

From Eq.(26), the average energy of the particle in a linearly expanding ($a > 0$) circle goes to $E_{mn}(t) \to C_1$ for $t \to \infty$, while for the linearly contracting ($a < 0, b > 0$) circle we get asymptotically $E_{mn}(t) \to +\infty$ for $t \to -\frac{b}{a}$. Such asymptotic behavior is confirmed by Fig. 1, where $\langle E_{mn}(t) \rangle$ is shown for the linearly expanding and contracting circles for different values of the expanding (contracting) velocities a. It is clear that the difference between adiabatic ($a << 1$) and non-adiabatic ($a >> 1$) regimes is exhibited in the decay rate of the curve. Furthermore, the curves are symmetric for the expanding and contracting circles (for the same expanding/contracting velocities). We note that the above described asymptotic behavior is true not only for linearly expanding (contracting) circles but also for other types of monotonically expanding circles, as long as the radius is given by either Eqs. (18) or (19).

4. Suddenly removed billiard walls

In the time-dependent billiard problem, it is important to explore differences between adiabatic and non-adiabatic regimes of the wall's motion. In this section, we consider the case when the billiard wall is removed (disappears) suddenly. To some extent, this situation is equivalent to when the billiard expands with infinite velocity, so that it can be considered a highly non-adiabatic regime. A similar problem for the one-dimensional infinite well has been previously considered [27] in the context of diffraction in time. Our purpose is to explore the time-evolution of the wavefunction, mean position, and its time derivative for such regime of wall's motion. We assume that at $t = 0$ the initial state wavefunction of the system is the eigenstate of the circular billiard given by:

$$\varphi_{mn}(r, \theta) = \frac{\sqrt{2}}{r_0 J_{m+1}(\lambda_{mn})} J_m \left(\frac{\lambda_{mn} r}{r_0} \right) e^{im\theta}. \tag{29}$$

Time evolution of the wavefunction can be calculated using the Green's function, $G(\mathbf{r}, t; \mathbf{r}', 0)$ [27]

$$\psi(\mathbf{r}, t) = \int d\mathbf{r}' G(\mathbf{r}, t; \mathbf{r}', 0) \psi(\mathbf{r}', 0). \tag{30}$$

For the case of circular billiard the time evolution is given by [polyanin]

$$\psi(r, \theta, t) = \frac{1}{2\pi i t} \int_0^{2\pi} \int_0^{r_0} r' \exp \left[i \frac{r^2 + r'^2 - 2rr' \cos(\theta - \theta')}{2t} \right] \varphi(r', \theta') dr' d\theta', \tag{31}$$

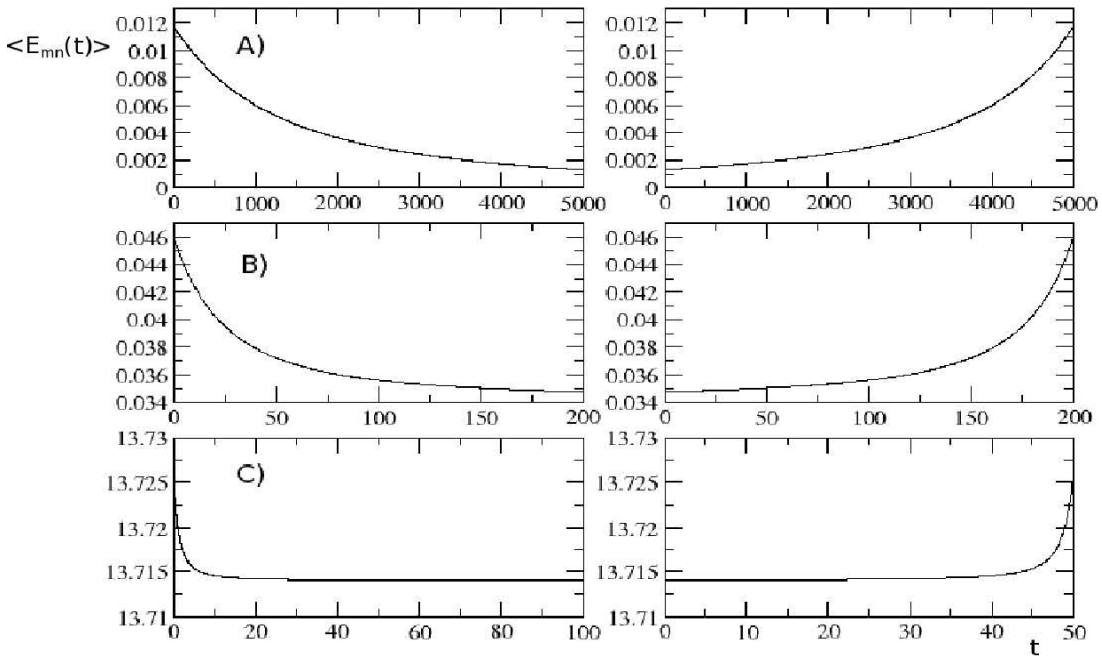

FIG. 1. The time-dependence of the quantum average energy for linearly expanding $r_0(t) = b_1 + at$ (left panel) and (with the same velocity as that of the expanding circle) contracting $r_0(t) = b_2 - at$ (right panel) circles. The initial state is taken to be an eigenstate of (16) with $m = 1, n = 1$. The parameters are: A) $a = 0.01, b_1 = 25, b_2 = 75$, B) $a = 0.5, b_1 = 25, b_2 = 125$, C) $a = 10.0, b_1 = 25, b_2 = 525$

and for $m = 0$:

$$\psi(r,t) = \frac{1}{it}\int_0^{r_0} r' \exp\left[i\frac{r^2 + r'^2}{2t}\right] I_0\left(-\frac{irr'}{t}\right)\varphi(r')dr', \tag{32}$$

where $I_0(r')$ is the modified Bessel function. The wavefunction is normalized as:

$$N(t) = \int_0^{\infty} |\psi|^2 r dr = 1. \tag{33}$$

The mean position can be calculated as:

$$\langle r(t)\rangle = \int_0^{\infty} |\psi|^2 r^2 dr. \tag{34}$$

In Fig. 2, we show the r-dependence of the $m = 0, n = 3$ circular billiard wavefunction (with initial radius $r_0 = 40$) at different moments of time ($t = 100, t = 300, t = 500$). It is clear that the wavefunction decays with increasing r and completely disappears at upper r-limit. The decay distance is longer as t is longer. In addition, we explored the time evolution of the wavefunction, mean position and its time derivative after removing the wall. As an initial state, we chose the static billiard wavefunction for $m = 0, 1, 2$, $n = 1, 2, 3$. The results are shown in Fig. 3. As we can see in Fig 3, where the mean position (left panel) and its time derivative (right panel), after some initial period the states will expand with constant velocity. As can be seen from Fig. 3, $\langle r(t)\rangle$ grows monotonically in time. This implies that the motion of the particle is not localized after the wall's removal and can go to infinity; as large as the initial state energy and as high as the growth rate of $\langle r\rangle$. Completely different

behavior can be observed for $\frac{d\langle r(t)\rangle}{dt}$; unlike the mean position, $\frac{d\langle r(t)\rangle}{dt}$ grows during some initial time period, after which it becomes constant. Again, the growth rate is proportional to the initial state energy. The accuracy of wavefunction evolution has been checked by monitoring norm conservation.

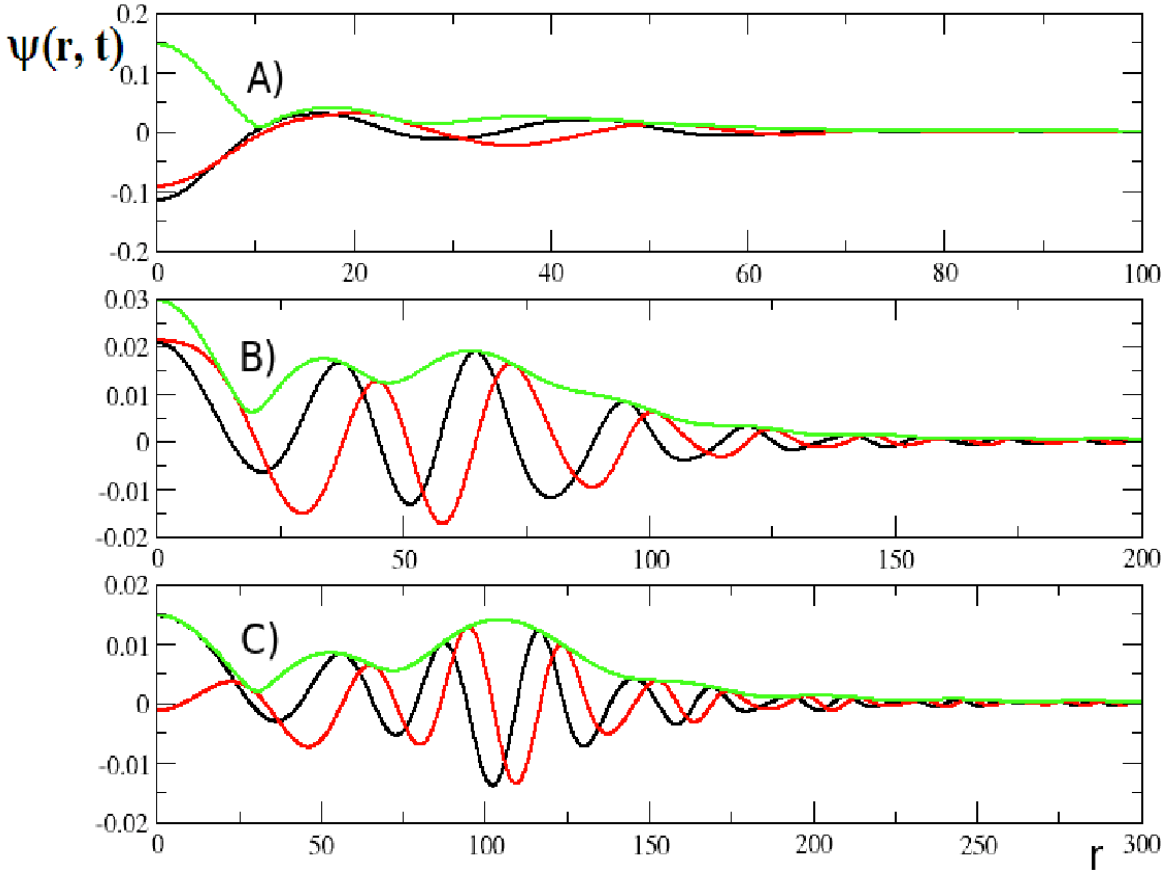

FIG. 2. The wavefunction of $m = 0, n = 3$ state as a function of r (the real part (black), the imaginary part (red), the absolute value of the wavefunction (green)): A) $t = 100$, B) $t = 300$, C) $t = 500$

5. Non-harmonically breathing circle

In this section, we consider the following type of time- dependence:

$$r_0(t) = \begin{cases} \rho_0 + vt, & 0 < t < \frac{1}{2}T, \\ \rho_0 + v(T-t), & \frac{1}{2}T < t < T. \end{cases} \tag{35}$$

This means that the time-law of the radius is periodic but not harmonic and it is still possible to find an exact solution of Eq.(14). For a fixed value of T, it is clear that the oscillation amplitude depends on the velocity, v: the higher the velocity the larger the amplitude will be. The oscillation frequency is defined as $\omega = 2\pi/T$. We have to solve Eq.(14) with the boundary conditions $\phi(0,t) = \phi(1,t) = 0$. The boundary condition at $y = 0$ follows from the substitution (13). It is clear that the motion of the boundary can be considered as the (subsequent) combination of linearly expanding and contracting circles.

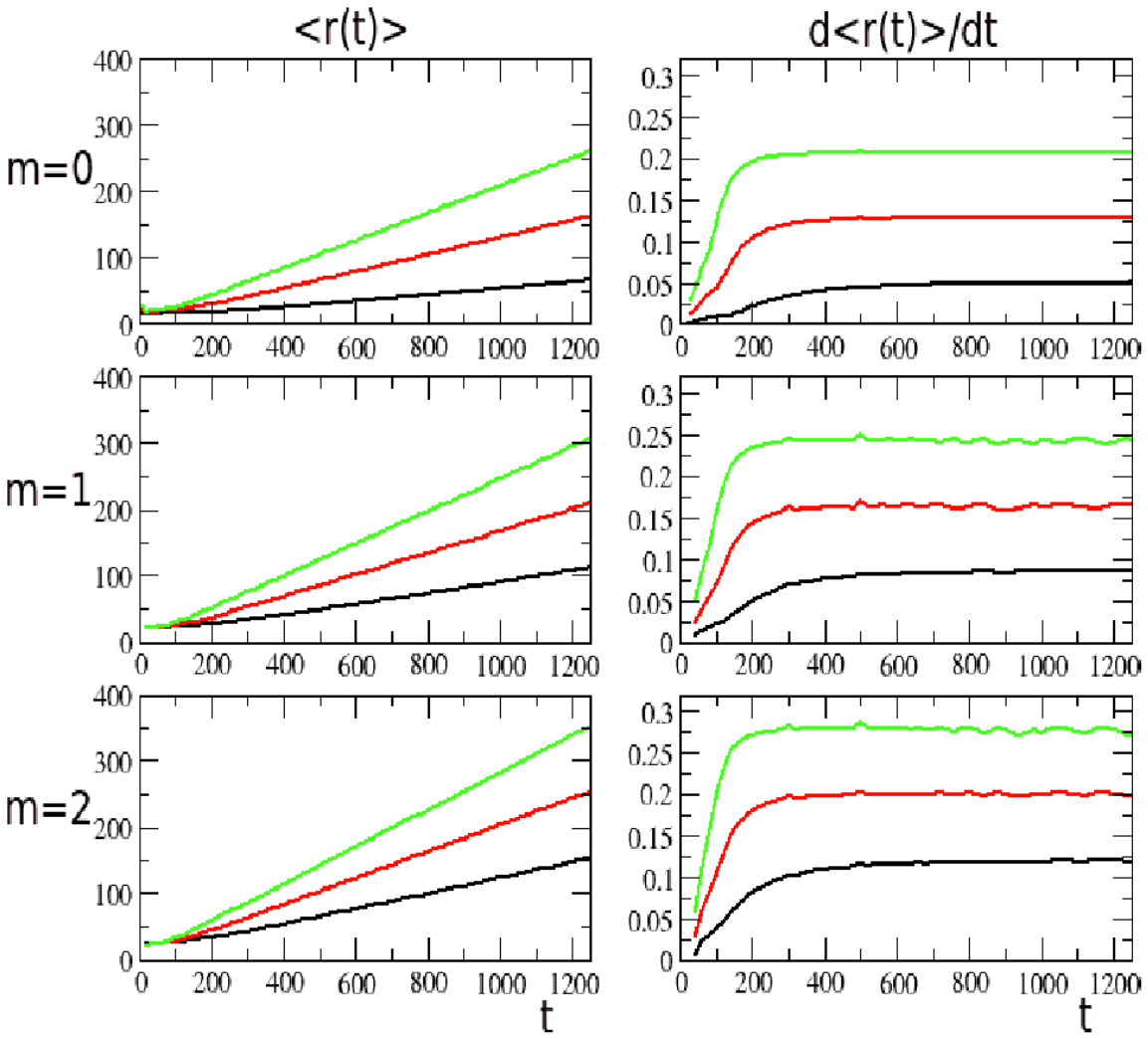

FIG. 3. Mean position and its time-derivative (expansion rate). $n = 1$ (black), $n = 2$ (red), $n = 3$ (green)

The one-dimensional Schrödinger equation with such a boundary condition is solved in Ref. [15] in terms of the full-cycle propagator. Here, we use the same prescription as in Ref. [15] to obtain the solution for Eq.(14). The solution for Eq.(14) can be found in each time interval, $0 < t < \frac{1}{2}T$ and $T < t < T$, from which, general solutions can be constructed. First, we note that for $r_0^3\ddot{r}_0 = 0$, time and coordinate variables in Eq.(14) can be separated and the solution can be written as:

$$\phi_{mn}(y,t) = \frac{\sqrt{2}}{J_{m+1}(\lambda_{mn})}\sqrt{y}J_m\left(\lambda_{mn}y\right)\exp\left(-2i\lambda_{mn}^2\int_0^t\frac{d\tau}{r_0^2(\tau)}\right), \tag{36}$$

where $0 < \lambda_{m1}, < \lambda_{m2}, < ...$ are zeros of the Bessel function given by $J_m(\lambda_{mn}) = 0$. In the following, the angular quantum number m will be considered as fixed, and consequently, we will omit the subscript m in the following. The solution of Eq.(14) in the time interval

$0 < t < \frac{1}{2}T$ can be written in terms of the functions (36) as:

$$\phi(y,t) = \sum_{n=1}^{\infty} A_n \phi_n(y,t).$$

The expansion coefficients can be found as Fourier coefficients using the initial value of ϕ i.e. from the relation:

$$\phi(y,+0) = \sum_{n=1}^{N} A_n Y_n(y), \tag{37}$$

that gives:

$$A_n = \int_0^1 Y_n(y) \cdot \phi(y,+0)\, dy,$$

where:

$$Y_n(y) = \frac{\sqrt{2}}{J_{m+1}(\lambda_{mn} y)} \sqrt{y} J_m\left(\lambda_{mn} y\right).$$

To find the solution in the general case, we note that:

$$r_0 \ddot{r}_0 y^2 = -2vy^2 \left[\rho_1 \delta\left(t - \frac{1}{2}T\right) - \rho_0 \delta(t-T) + ...\right], \tag{38}$$

where $\rho_1 = \rho_0 + \frac{1}{2}vT$. The solution of Eq.(14) jumps at $t = \frac{1}{2}T$:

$$\phi\left(y, \frac{1}{2}T + 0\right) = \exp\left(ivy^2\rho_1\right) \phi\left(y, \frac{1}{2}T - 0\right). \tag{39}$$

The solution of Eq.(14) in the interval $\frac{1}{2}T < t < T$ can be written as:

$$\phi(y,t) = \sum_{n=1}^{\infty} \tilde{A}_n Y_n(y) \exp\left(-2i\lambda_{mn}^2 \int_{T/2}^{t} \frac{d\tau}{r_0^2(\tau)}\right), \tag{40}$$

where Fourier coefficients can be found as:

$$\tilde{A}_n = \int_0^1 Y_n(y) \phi\left(y, \frac{1}{2}T + 0\right) dy = \int_0^1 Y_n(y) e^{ivy^2\rho_1} \phi\left(y, \frac{1}{2}T - 0\right) dy =$$

$$= \sum_l A_l \exp\left(-2i\lambda_{ml}^2 \int_0^{T/2} \frac{d\tau}{r_0^2(\tau)}\right) \int_0^1 Y_n(y) e^{ivy^2\rho_1} Y_l(y) dy.$$

At $t = T$ the solution has a jump:

$$\phi(y, T+0) = e^{-ivy^2\rho_0} \phi(y, T-0).$$

Expanding $\phi(y, T+0)$ in terms of $\phi_n(y, T+0)$, we get:

$$\phi(y, T+0) = \sum_n \bar{A}_n \phi(y,+0) = \sum_n \bar{A}_n Y_n(y),$$

we can find expansion coefficients as:

$$\bar{A}_n = \int_0^1 Y_n(y) \phi(y, T+0) dy = \int_0^1 Y_n(y) e^{-iv\rho_0} \phi(y, T-0) dy =$$

$$= \sum_j \tilde{A}_j \exp\left(-2i\lambda_{mj}^2 \int_{T/2}^{T} \frac{d\tau}{r_0^2(\tau)}\right) \int_0^1 Y_n(y) e^{ivy^2\rho_1} Y_j(y) dy = \sum_l A_l U_{nl}.$$

The full-cycle propagator is given by:

$$U_{nl} = \sum_j C_{jl}(\rho_1) \exp\left(-i\frac{T}{\rho_0\rho_1}\lambda_{ml}^2\right) C_{nj}^*(\rho_0) \exp\left(-i\frac{T}{\rho_0\rho_1}\lambda_{mj}^2\right),$$

with

$$C_{nj}(\rho) = \int_0^1 Y_n(y) e^{ivy^2\rho} Y_j(y) dy.$$

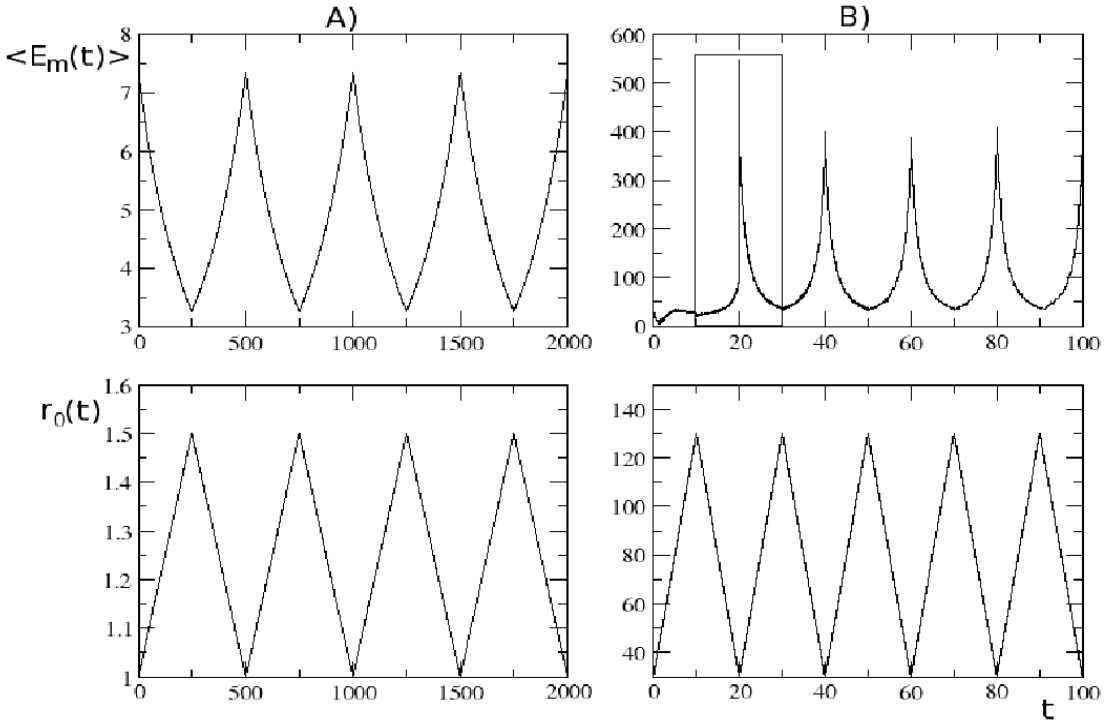

FIG. 4. Time-dependence of the quantum mechanical average energy for the circular billiard with non-harmonically oscillating radius for different oscillation parameters, $m = 1$, $l = 1$, A) $T = 500$, $v = 0.002$, $\rho_0 = 1.0$, B) $T = 20$, $v = 10$, $\rho_0 = 30$

Thus, we have derived the full-cycle propagator for the non-harmonically breathing circle. Eq.(38) implies that the frequency of the harmonic oscillator in Eq.(14) has a periodic delta-kicking form. This reduces our problem to solving the Schrödinger equation with a delta-kicking potential (where between the kicks circle expands/contracts linearly), whose solution can be obtained in terms of the full-cycle propagator describing the (exact) evolution of the wave function within one period. Having obtained the full-cycle propagator, we can find solutions for the full time-period $0 < t < T$, from which one can construct the solutions for any number of periods.

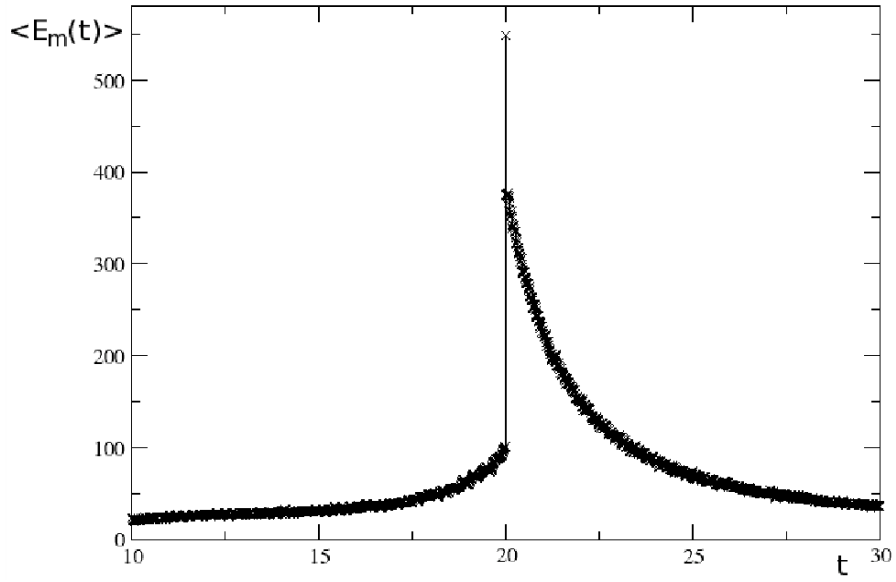

FIG. 5. Magnification of the selected part in Fig.2(B)

In Fig. 4, the time-dependence of the average energy is plotted for different values of v, T and ρ_0. The expansion coefficients for the initial state (in Eq. (37)) are chosen as:

$$A_n(0) = \int_0^1 \varphi_n(y)\varphi_l(y) \exp\left(-\frac{i}{2}\dot{r}_0(t)r_0(0)y^2\right) dy, \tag{41}$$

so that $\langle E(0)\rangle = \frac{\lambda_{ml}^2}{2r_0^2}$.

It is clear that in the adiabatic regime (for high oscillation periods), the time-dependence of $\langle E(t)\rangle$ is periodic and for each period it can be separated into symmetric parts, which correspond to linearly expanding and contracting circle average energies (Fig. 4(A)). However, this symmetry is broken in the non-adiabatic regime, corresponding to small oscillation periods. This can be seen from Fig. 4(B), where $\langle E(t)\rangle$ is plotted for $T = 20$, $v = 10$ and $\rho_0 = 30$. Such a behavior can be explained by the fact that in the adiabatic regime, the particle follows the wall's motion, while for higher frequencies, it cannot follow the wall's motion. This leads to a breaking of the symmetry, i.e. parts of $\langle E(t)\rangle$ (within one period) corresponding to contracting and expanding circles are not symmetric. This can be clearly seen from Fig. 5, which presents the magnification of a part of the $\langle E(t)\rangle-$curve (Fig. 4(B)) for the time interval from 10 to 30. It is clear that the maximum value of the left hand part (corresponding to contracting circle) is much smaller than that of the right hand part corresponding to the expanding circle. Such an asymmetry is caused by the presence of a delta-function in the Schrödinger equation. As follows from Eq. (38), the potential in the Schrödinger equation has a jump at $t = T/2$. This jump is as high as the value of v in Eq. (38). Therefore for smaller velocities the jump is quite small, while for higher values of v it is much larger and can be clearly seen in Fig. 5.

6. Harmonically breathing circle

As we have seen in the previous sections, an analytical solution of the Schrödinger equation of the circular billiard with a time-dependent radius and corresponding boundary conditions is possible in a few cases of the time-dependence only. In particular, no analytical

solution can be obtained in the case of a harmonic time-dependence, since time and coordinate variables cannot be separated in the Schrödinger equation. In this section, we consider the case of a harmonically oscillating radius which is given by:

$$r_0(t) = a + b\cos(\omega t), \tag{42}$$

where ω is the oscillation frequency. The classical dynamics of circular billiards with oscillating boundaries have been investigated in the context of Fermi acceleration [29] and particle motion inside collectively excited nuclei [32]. In Fig. 6, the time-dependence of the energy averaged over an ensemble of 1000 trajectories is plotted for $\omega = 2$ and $\omega = 5$ for the classical system. The growth of the energy is strongly suppressed for both values of the frequency. It is clear that the character of suppression is the same for both frequencies, although the critical value at which suppression starts is higher for higher frequency values. This is in good accordance with previous studies of the breathing circle, see, e.g., Refs. [29, 30].

To numerically solve Eq. (14) with the boundary conditions given by Eq. (42), we expand the function $\phi(y,t)$ in terms of the eigenfunctions of Eq.(14) at $C = 0$:

$$\phi(y,t) = \sum_n c_n(t)\varphi_n(y), \tag{43}$$

where:

$$\varphi_n(y) = \frac{\sqrt{2y}J_m(\lambda_{mn}y)}{J_{m+1}(\lambda_{mn})}. \tag{44}$$

Inserting the expansion (43) into Eq.(14) we have:

$$ir_0^2\sum_n \dot{c}_n\varphi_n = \sum_n c_n\left(\frac{\lambda_{mn}^2}{2} + \frac{1}{2}r_0^3\ddot{r}_0y^2\right)\varphi_n. \tag{45}$$

By multiplying with φ_k^* and integrating over y from 0 to 1, we get a system of differential equations for the expansion coefficients $c_n(t)$:

$$\dot{c}_n(t) = -\frac{i}{2r_0^2}\lambda_{mn}^2c_n - \frac{i}{2}\ddot{r}_0r_0\sum_k M_{kn}c_k, \tag{46}$$

where:

$$M_{kn} = \int_0^1 \varphi_n(y)\varphi_k(y)y^2dy.$$

The system of differential equations (46) is solved using ZVODE package [26], which uses variable-coefficient methods. The number of basis functions for the results presented in Figs. (7-10) was taken as 200, while for those in the Fig. 9 we used 3000 basis functions. The convergence of the calculations are checked by increasing the number of basis functions.

Solving Eqs.(46) numerically, we obtain $\phi(y,t)$ and thus the radial wave functions $R(y,t)$. The average energy can be calculated as:

$$\langle E_m(t)\rangle = \int_0^1 R^*(y,t)HR(y,t)ydy =$$

$$= \frac{1}{2r_0^2}\left(\sum_n |c_n|^2\lambda_{mn}^2 + r_0^2\dot{r}_0^2\int_0^1 y^2|\phi|^2dy + 2r_0\dot{r}_0Im\int_0^1 y\phi^*\frac{\partial\phi}{\partial y}dy\right). \tag{47}$$

Using Eq. (47), we numerically compute the average energy as a function of time for different oscillation frequencies. The initial values of the expansion coefficients can be chosen using Eq. (41). Then, for harmonically oscillating boundary (Eq. (42)) the expansion coefficients of the initial state become $c_n(0) = \delta_{nl}$, because $\dot{r}_0(0) = 0$ in Eq. (41).

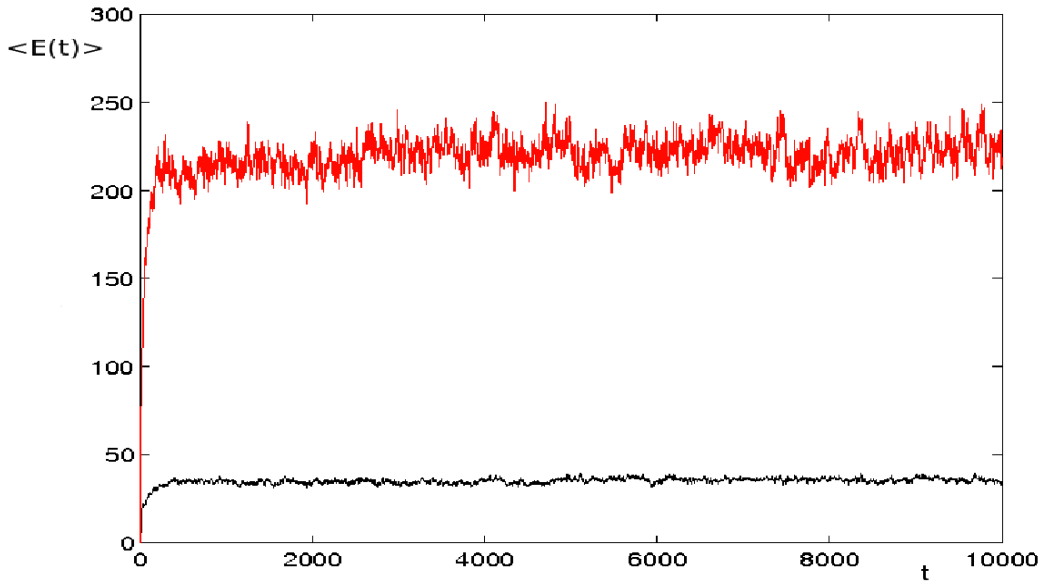

FIG. 6. Time-dependence of the classical average energy for circular billiard with harmonically oscillating radius; black - $r_0(t) = 20 + \cos(2t)$, red - $r_0(t) = 20 + \cos(5t)$

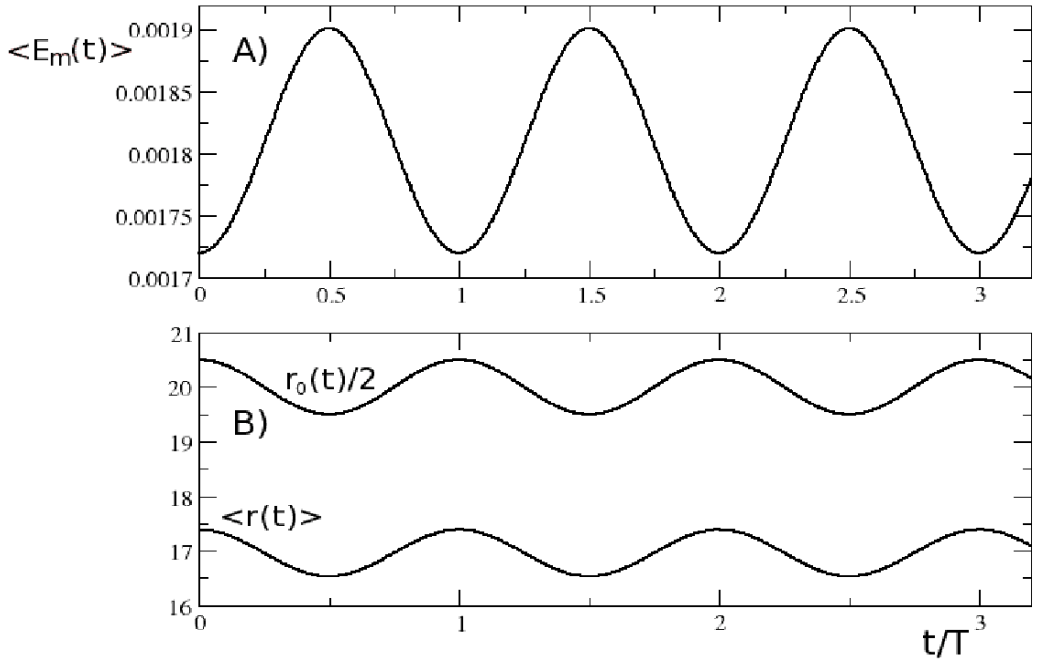

FIG. 7. Time-dependence of the quantum average energy (A) and mean position (B) for the circular billiard with harmonically oscillating radius; $m = 0$, $l = 1$, $r_0(t) = 40 + \cos(0.0005t)$

Furthermore, we compare $\langle E_m(t) \rangle$ for different regimes of the wall's motion: a) slowly oscillating (adiabatic) wall,

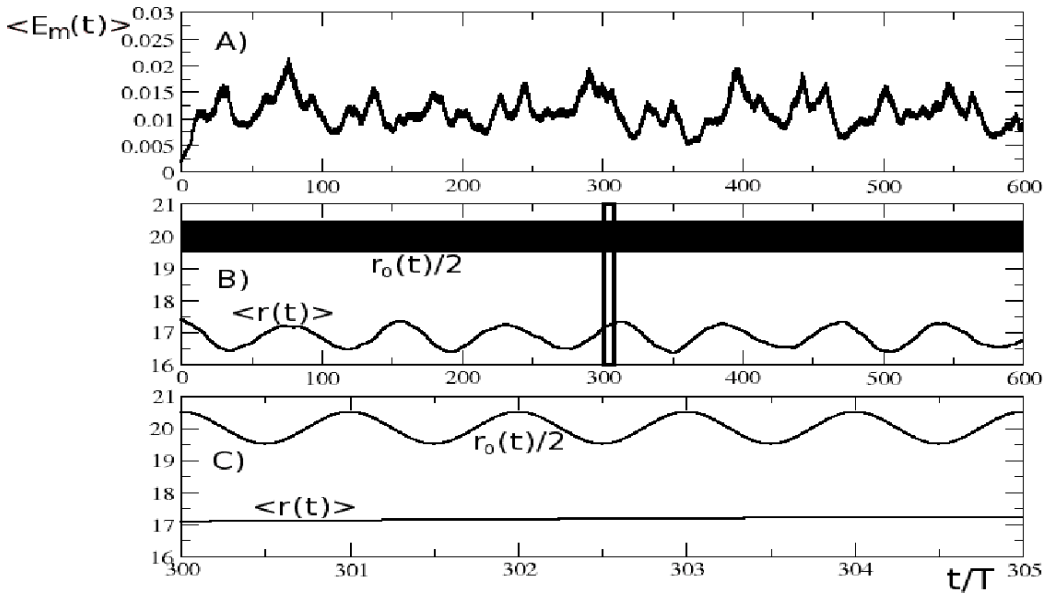

FIG. 8. Time-dependence of the quantum average energy (A) and mean position (B) for the circular billiard with harmonically oscillating radius; $m = 0$, $l = 1$, $r_0(t) = 40 + \cos(0.6t)$. (C) is the magnification of the selected part in (B)

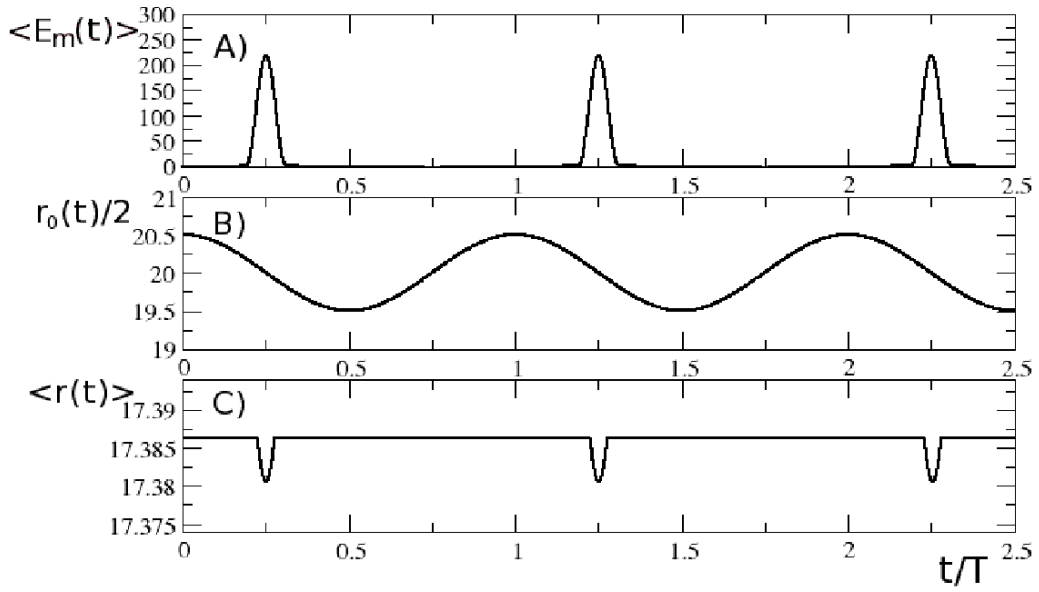

FIG. 9. Time-dependence of the quantum average energy (A), $r_0(t)/2$ (B) and mean position (C) for the circular billiard with harmonically oscillating radius; $m = 0$, $l = 1$, $r_0(t) = 40 + \cos(250t)$

b) high oscillation frequency,
c) intermediate wall oscillation frequencies.

In Fig. 7(A), the time-dependence of the average energy, $\langle E_m(t)\rangle$ is plotted for the adiabatic regime ($\omega = 5 \times 10^{-4}$). As can be seen from this figure, $\langle E_m(t)\rangle$ is periodic in time

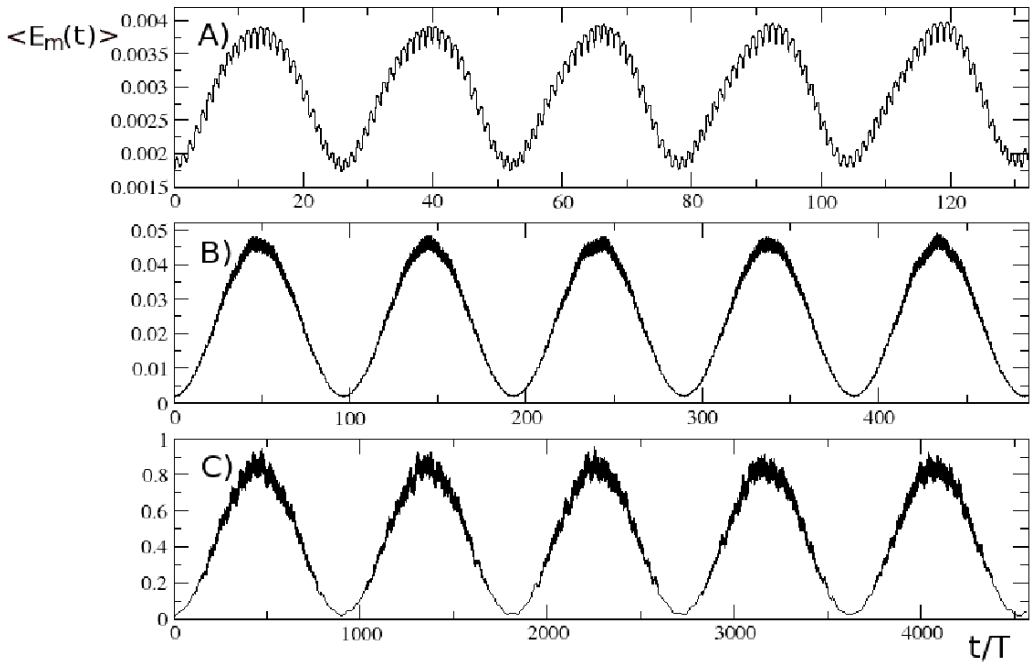

FIG. 10. Time-dependence of the quantum average energy for the circular billiard with harmonically oscillating radius; $m = 0$, $l = 1$, $r_0(t) = 40+\cos(\omega t)$, A) $\omega = 0.02$, B) $\omega = 0.1$, C) $\omega = 1.7$

and the period is the same as the period of the applied driving law. This can be explained by the fact that in the adiabatic regime, the particle follows the wall's motion. This is clearly seen from Fig. 7(B), where $r_0(t)/2$ is compared with the expectation value of the position of the particle in billiard, $\langle r(t)\rangle$.

Fig. 8(A) presents $\langle E_m(t)\rangle$ for higher values of the wall's oscillation frequency, ($\omega = 0.6$). It is clear that the periodicity of $\langle E_m(t)\rangle$ is broken and this can be explained by Fig. 8(B), where $r_0(t)/2$ and the mean position are compared for this regime. For this value of the frequency, the motion of the billiard particle is no longer adiabatic and it doesn't follow the wall's motion.

In Fig. 9(A), the time-dependence of the average energy is plotted for a very high frequency value, $\omega = 250$. It is clear from this plot that the periodicity of $\langle E_m(t)\rangle$ is recovered in this highly oscillating regime. Comparison of $\langle r(t)\rangle$ and $r_0(t)/2$ in Fig. 9(B) shows that the particle doesn't "feel" the wall's motion in this regime.

Finally, a remarkable feature of the harmonically breathing circle can be observed in the intermediate regime. Namely, for some values of the frequency $\langle E_m(t)\rangle$ can be time-periodic with the period which is much larger than that of wall's oscillation. Fig. 10 presents the plots of the average energy for ($\omega = 0.02$, $\omega = 0.1$, $\omega = 1.7$) which exhibit such a periodicity. The appearance of such periodicity for intermediate oscillation frequencies may be caused by the existence of a special resonance-like regime of motion where the periodic motion is possible for certain frequencies only.

To qualitatively determine the border between the adiabatic and non-adiabatic regimes, we study the behavior of the expansion coefficients, c_n for different oscillation frequencies. It is clear that billiard wall's position changes very slowly, the wavefunction of the billiard particle should be slightly different than that of the static billiard. Therefore, in the wave-function of the adiabatically expanding (contracting) billiard, which is given by Eq.(43) only

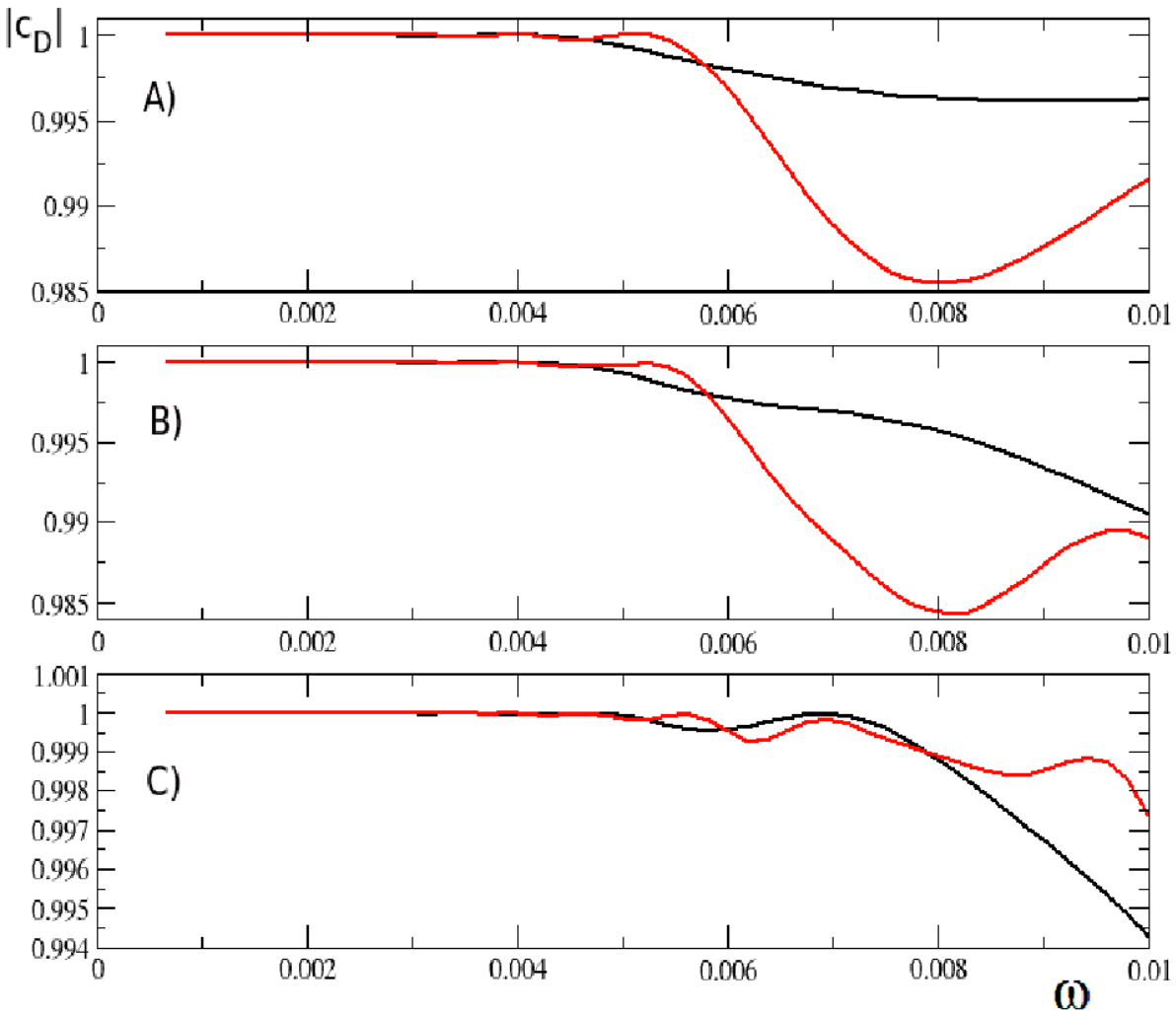

FIG. 11. The absolute value of the dominating expansion coefficient ($|c_D|$) as a function of ω, measured after one period (black curves), and after two periods (red curves). Initial states are A) $m = 0, n = 1$, B) $m = 0, n = 2$, C) $m = 0, n = 3$

one expansion coefficient, c_D (which corresponds to the initial state) is dominating. Thus, the dependence of this coefficient on the expansion (contraction) rate can be considered as an indicator for the fact whether wall's motion adiabatic or not. In application to the harmonically breathing billiard, this implies that the breaking of the dominance of the coefficient c_D coefficient when the oscillation frequency reaches some threshold value can be considered as a breaking of the adiabatic regime. Fig. 11 represents $|c_D|$ as a function of the wall's oscillation frequency, ω. Up to a certain value of ω, $|c_D|$ is approximately equal to 1. After exceeding some (critical) value of ω, $|c_D|$ starts to become less than 1, which implies breaking of the adiabatic regime.

Thus, we can conclude that for the harmonically breathing circle the behavior of the average energy as a function of time is mostly similar to that of harmonically oscillating $1D$-box, studied in the Ref. [28]. However, unlike to that system, in the breathing circle, $\langle E_m(t) \rangle$

can be time-periodic even for certain frequency values, which belong to the intermediate frequency range.

7. Conclusions

We have studied the quantum dynamics of a circular billiard with different driving laws for the radius. An exact analytical solution was obtained for cases of monotonically expanding and contracting circles. Non-harmonically time-periodic boundary conditions (sawtooth-like motion) were considered in terms of the analytically-derived full-cycle propagator. Using this propagator, the time-dependence of the average energy was calculated. It was found that in the adiabatic regime, when the wall moves slowly, the time-dependence of the average energy was periodic and for each period, $\langle E(t)\rangle$ can be constructed from corresponding $\langle E(t)\rangle$s of linearly expanding and contracting circles. In other words, the part of the curve for the average energy corresponding to one period consisted of two symmetric parts, describing linearly expanding and contracting circles. However, for smaller oscillation periods when adiabaticity was broken, such symmetry was broken, though $\langle E(t)\rangle$ was still periodic. To explore more deeply the difference between adiabatic and highly adiabatic regimes, we considered the case when billiard wall suddenly disappears. It was found for this case that the mean position of the billiard particle grew monotonically in time, which implies that over a long period, the motion becomes infinite.

The case of the harmonically breathing circle was studied by solving the time-dependent Schrödinger equation numerically by means of a basis set expansion. When the oscillation frequency of the radius was very small (compared to the initial frequency, ω_0), the systems remained in the adiabatic regime and $\langle E(t)\rangle$ was periodic with the same period as that of the applied driving law. Such periodicity broken down by increasing the oscillation frequency. However, for some intermediate range frequencies, $\langle E(t)\rangle$ can become periodic in time with a period much larger than that of the driving law. For very high oscillation frequencies, the average energy became time-periodic again, with the same period as that of the driving law. The border between adiabatic and non-adiabatic regime is roughly defined by the dependence of the dominating expansion coefficient in Eq.(43) on the wall's oscillation frequency. Namely, the situation when the dominance of these coefficients breaks can be considered as a fingerprint for the transition from an adiabatic into a non-adiabatic regime. In our opinion, the explanation of such periodicity requires deeper exploration of the studied system, which will be the subject of forthcoming research. Finally, the importance of the above study is due to its direct relevance to quantum Fermi acceleration in confined geometries and the problem of quantum dynamics in driven systems. The latter is of importance for many mesoscopic and nanoscale systems such as quantum dots, confined cold atoms and molecules. Finally, we note that extension of the above study to the case of open quantum billiards is of importance because of their direct relevance to quantum dots. Currently, such studies are ongoing.

8. Acknowledgement

This work is supported in part by a grant of Volkswagen Foundation (*Nr.* I/82 136).

References

[1] Stöckmann H.-J. *Quantum Chaos: An Introduction*. Cambridge University Press, Cambridge, UK (1999).

[2] Eckhardt B. Quantum mechanics of classically non-integrable systems. *P*hys. Rep., **163**, P. 205–297 (1988).

[3] Gutzwiller M.C. *Chaos in Classical and Quantum Mechanics*. Springer, New York (1990).

[4] Loskutov A.Yu., Ryabov A.B. and Akinshin L.G. Properties of some chaotic billiards with time-dependent boundaries. *J. Phys. A*, **33**, P. 7973 (2000).

[5] Loskutov A.Yu. and Ryabov A.B. Particle Dynamics in Time-Dependent Stadium-Like Billiards. *J. Stat. Phys.*, **108**, P. 995–1014 (2002).

[6] De Carvalho R.E., De Souza F.C. and Leonel E.D. Fermi acceleration on the annular billiard: a simplified version, *J. Phys. A: Math. Gen.*, **39**, P. 3561(2006).

[7] Lenz F., Diakonos F.K. and Schmelcher P. Classical dynamics of the time-dependent elliptical billiard. *Phys. Rev. E*, **76**, P. 066213 (2007).

[8] Lenz F., Diakonos F.K. and Schmelcher P. Tunable Fermi Acceleration in the Driven Elliptical Billiard. *Phys. Rev. Lett.*, **100**, P. 014103 (2008).

[9] Cohen D., Wisniacki D.A. Stadium billiard with moving walls. *Phys. Rev. E*, **67**, P. 026206 (2003).

[10] Doescher S.W. and Rice M.H. Infinite Square-Well Potential with a Moving Wall. *Am. J. Phys.*, **37**, P. 1246 (1969).

[11] Munier A., Burgan J.R., Feix M. and Fijalkow E. Schrödinger equation with time-dependent boundary conditions. *J. Math. Phys.*, **22**, P. 1219 (1981).

[12] Pinder D.N. The contracting square quantum well. *Am. J. Phys.*, **58**, P. 54 (1990).

[13] Razavy M. Time-dependent harmonic oscillator confined in a box. *Phys. Rev. A*, **44**, P. 2384 (1991).

[14] Pereshogin P., Pronin P. Effective Hamiltonian and Berry phase in a quantum mechanical system with time dependent boundary conditions. *Phys. Lett. A*, **156**, P. 12–16 (1991).

[15] Scheininger C. and Kleber M. Quantum to classical correspondence for the Fermi-acceleration model. *Physica D*, **50**, P. 391–404 (1991).

[16] Makowski A.J. and Dembinski S.T. Exactly solvable models with time-dependent boundary conditions. *Phys. Lett. A*, **154**, P. 217–220 (1991).

[17] Makowski A.J. and Peplowski P. On the behaviour of quantum systems with time-dependent boundary conditions. *Phys. Lett. A*, **163**, P. 143–151 (1992).

[18] Makowski A.J. Two classes of exactly solvable quantum models with moving boundaries. *J. Phys. A: Math. Gen.*, **25**, P. 3419 (1992).

[19] Willemsen J.E. Exact solution of the wave dynamics of a particle bouncing chaotically on a periodically oscillating wall. *Phys. Rev. E*, **50**, P. 3116 (1994).

[20] Morales D.A., Parra Z., Almeida R. On the solution of the Schrödinger equation with time dependent boundary conditions. *Phys. Lett. A*, **185**, P. 273–276 (1994).

[21] C. Yuce. Singular potentials and moving boundaries in 3D. *Phys. Lett. A*, **321**, P. 291–294 (2004).

[22] Jose J.V., Gordery R. Study of a quantum fermi-acceleration model. *Phys. Rev. Lett.*, **56**, P. 290 (1986).

[23] Karner G. On the quantum Fermi accelerator and its relevance to 'quantum chaos'. *Lett. Math. Phys. A*, **17**, P. 329–339 (1989).

[24] Seba P. Quantum chaos in the Fermi-accelerator model. *Phys. Rev. A*, **41**, P. 2306 (1990).

[25] Jana T.K., Roy P. A class of exactly solvable Schrödinger equation with moving boundary condition. *Phys. Lett. A*, **372**, P. 2368–2373 (2008).

[26] www.netlib.org

[27] Godoy S. Diffraction in time: Fraunhofer and Fresnel dispersion by a slit. *Phys. Rev. A*, **65**, P. 042111 (2002).

[28] Glasser M.L., Mateo J., Negro J. and Nieto L.M. Quantum infinite square well with an oscillating wall. *Chaos, Solitons and Fractals*, **41**, P. 2067–2074 (2009).

[29] Koiller J., Markarian R., Kamphorst S.O. and De Carvalho S.P. Time-dependent billiards. *Nonlinearity*, **8**, P. 983 (1995).

[30] Kamphorst S.O., De Carvalho S.P. Bounded gain of energy on the breathing circle billiard. *Nonlinearity*, **12**, P. 1363-1371 (1999).

[31] Badrinarayanan R., Jose J.V., Chu G. Quantum manifestations of classical chaos in a Fermi accelerating disk. *Physica D*, **83**, P. 1–29 (1995).

[32] Burgio G.F., Baldo M., Rapisarda A., Schuck P. Chaoticity in vibrating nuclear billiards. *Phys. Rev. C*, **52**, P. 2475 (1995).
[33] Robinett R.W., Heppelmann S. Quantum wave-packet revivals in circular billiards. *Phys. Rev. A*, **65**, P. 062103 (2002).
[34] Robinett R.W. Quantum mechanics of the two-dimensional circular billiard plus baffle system and half-integral angular momentum. *Eur. J. Phys.*, **24**, P. 231 (2003).
[35] Abramowitz M., Stegun I.A. *Handbook of mathematical functions*. M.: Nauka. (1964).

NANOSYSTEMS: PHYSICS, CHEMISTRY, MATHEMATICS, 2015, 6 (2), P. 244–248

Femtosecond pulse shaping via engineered nonlinear photonic crystals

U. K. Sapaev[1], V. E. Eshniyazov[1], B. Kh. Eshchanov[1], D. B. Yusupov[2]

[1]Department of Physics, National University of Uzbekistan, named after M. Ulugbek, 100174 Tashkent, Uzbekistan

[2]Tashkent State Technical University , Universitetskaya ul. 2 Tashkent, 100095 Uzbekistan

usapaev@gmail.com

PACS 42.65.-ky, 42.79.Nv **DOI 10.17586/2220-8054-2015-6-2-244-248**

Non-stationary second harmonic generation by femtosecond pulses, taking into account both group velocity mismatch and dispersion in nonlinear photonic crystals (quasi-phase matched crystals) with domains of arbitrary sizes has been studied numerically. A simulated-annealing algorithm, working on the basis of numerical calculation, is developed to design quasi-phase matching gratings which can yield the desired amplitude and phase profile for second-harmonic pulses in the presence of pump depletion.

Keywords: second harmonic generation, quasi-phase matched crystals, nonlinear photonic crystals, pulse shaping.

Received: 2 February 2015

1. Introduction

Nonlinear Photonic Crystals (NPC) are of great interest because of their utility in practical applications, where it is necessary to control laser radiation. This interest in NPC's is especially warranted because they do not require the phase matching, which is necessary for uniform nonlinear crystals [1]. In such type of crystals, phase matching (or phase synchronism) of the interacting waves is obtained by periodically changing the sign of the second-order susceptibility, effectively widening the spectral range of frequency converters. Quasi-phase matched (QPM) or NPC gratings can also be used to provide dramatic pulse compression [2-3] and improved conversion efficiencies [4-5].

QPM gratings with a non-uniform periodicity can exhibit a longitudinally variable spectral response and entail the realization of advanced parametric processes [6], from highly efficient second harmonic generation (SHG) and parametric amplification in the case of a linear QPM chirp [4-5,7-9], to compression of second harmonic (SH) pulses when employing chirped fundamental-frequency (FF) pulses, [2-3, 10-11].

One of the interesting practical tasks, which can be solved by QPM gratings during SHG is the generation of SH pulses with arbitrarily chosen amplitude and phase profiles under the regime of pump depletion. A few methods have been developed to this end. Among them, the optimal control technique, based on Lagrange multipliers and real amplitudes [12-13], was applied to tailor ultra-short SH pulses by spatially varying the size of the nonlinearity. More recently, a similar approach was employed to design QPM gratings for picosecond SHG from femtosecond (fs) input FF pulses [14-19].

In this work, we discuss arbitrary fs pulse shaping based on SHG in engineered QPM in the regime of strongly depleted FF pump, taking into account both group velocity mismatch (GVM) and dispersion (GVD). To accomplish this, in contrast to previous work on the topic, we employ a simulated annealing algorithm (SAA), using simple fast Fourier

transform and fourth-order Runge–Kutta algorithms. We improved the SAA, which was developed in previous work [18].

2. Coupled-wave equations for SHG in arbitrary QPM gratings; numerical approach

The slowly varying envelope equations describing pulse evolution under collinear frequency doubling in QPM are:

$$\begin{array}{l} \frac{\partial A_1}{\partial z} + \frac{1}{V_1}\frac{\partial A_1}{\partial t} - i\frac{\alpha_1}{2}\frac{\partial^2 A_1}{\partial t^2} = -i\gamma_1\delta(z)(A_1)^* A_2 \exp(-i\Delta k z) \\ \frac{\partial A_2}{\partial z} + \frac{1}{V_2}\frac{\partial A_2}{\partial t} - i\frac{\alpha_2}{2}\frac{\partial^2 A_2}{\partial t^2} = -i\gamma_2\delta(z)(A_1)^2 \exp(i\Delta k z) \end{array}, \tag{1}$$

with boundary conditions:

$$\begin{array}{l} A_1(z,t)|_{z=0} = A_o \exp(-2\ln 2(t/\tau)^2 + i\varphi_1) \\ A_2(z,t)|_{z=0} = 0 \end{array}, \tag{2}$$

where A_1 and A_2 are the complex amplitudes of FF and SH pulses, respectively; A_o the peak amplitude of the FF excitation; V_1 and α_1 (V_2 and α_2) the group velocity and the dispersive GVD spreading at FF (SH), respectively; τ input pulse duration (FWHM in intensity); γ_1 and γ_2 nonlinear coupling coefficients, with $\gamma \approx \gamma_1 \approx \gamma_2 \approx \frac{2\pi}{n(\omega_o)\lambda} d^{eff} \approx \frac{2\pi}{n(2\omega_o)\lambda} d^{eff}$; $n(\omega_o)$ and $n(2\omega_o)$ the refractive indices of FF and SH waves, respectively; d^{eff} the effective nonlinearity $d^{eff} = \chi^{(2)}/2$; $\Delta k = 2k_1(\omega_o) - k_2(2\omega_o)$ the phase-mismatch; φ_1 an initial FF phase and $\delta(z)$ the unitary sign-changing function defining the arbitrarily sized domains of the QPM grating (see Fig. 1).

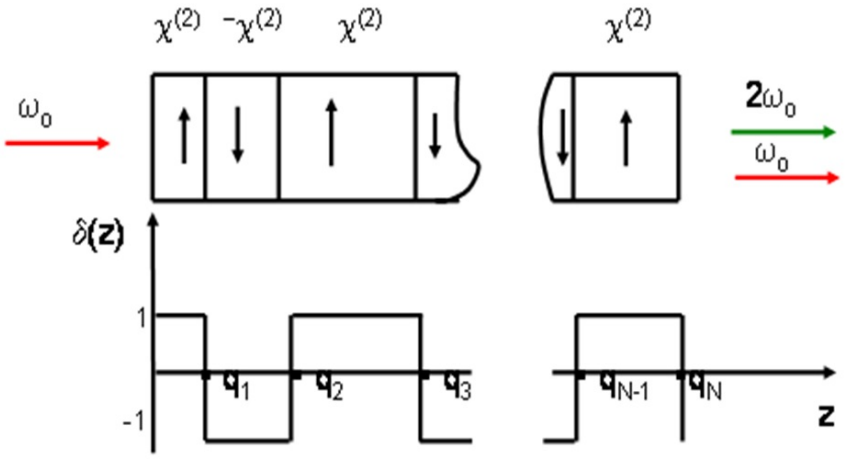

FIG. 1. Scheme of the arbitrary QPM grating, with $\delta(z)$ the dimensionless sign-changing aperiodic function of amplitude $|\delta(z)| = 1$. The grating is comprised of N inverted domains with individual lengths q_m ($1 \leqslant m \leqslant N$)

Set (2) could be numerically integrated by various methods. The fast Fourier transform for the linear portion and the fourth-order Runge–Kutta (RK) method for the nonlinear regime ensure high accuracy and reduced iteration times. However, because of the aperiodic nature of $\delta(\xi)$, we resort to RK with variable integration steps $d\xi(m)$ (m is the domain number) inside each domain (see Fig. 2). GVM and GVD are accounted for by the fast Fourier transform.

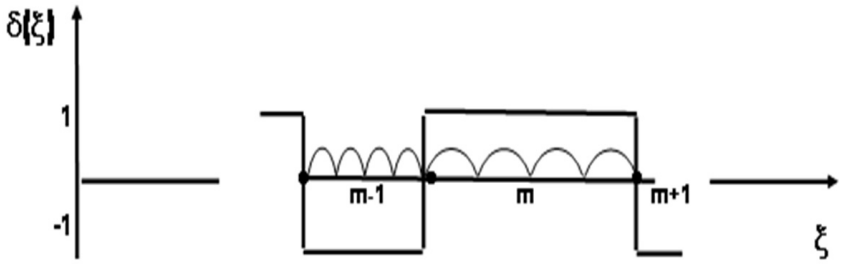

FIG. 2. Integration scheme. Here the number of steps in each domain is j=4

3. Results

We used SAA, which was developed earlier in [18]. This stems from the high accuracy of the PG-FROG traces used in calculating the RMS error [18]. Figure 3 shows the results obtained for a case of FF (1560 nm) for a 100 fs FF to a Gaussian SH pulse with duration of 100 fs with a efficiency conversion of 20 %. Here and below, for all our calculations, we chose a 1 GW/cm^2 peak intensity for FF time profile. However, for the domain size, we adopted a coarse resolution of 100 nm, two orders of magnitude larger than what is achievable with the algorithm; we obtained an excellent convergence to the desired profile and conversion efficiency. Figure 3 (left) plots time profiles of FF (dotted) and desired (dashed) and calculated SH profiles (solid); Figure 3 (center) shows power evolutions of the interaction pulses in arbitrary designed QPM grating; Figure 3 (right) shows change of domain sizes as a function of their numbers.

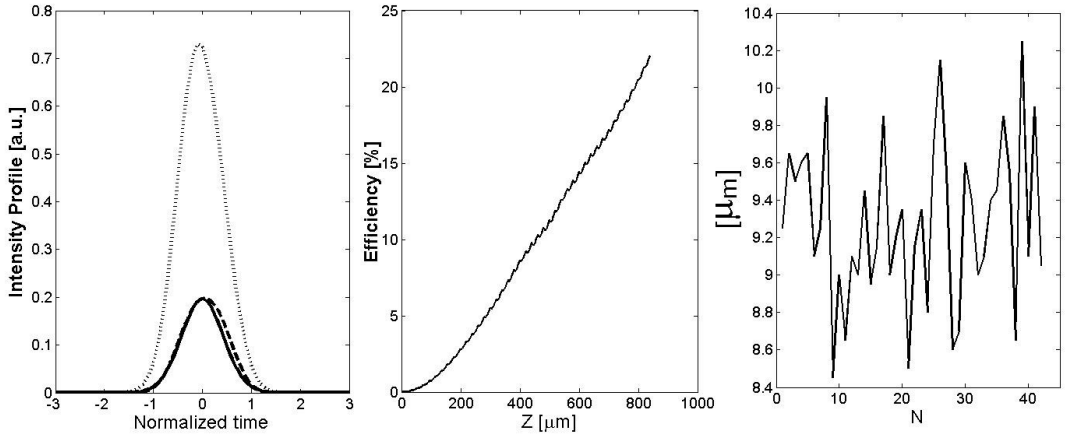

FIG. 3. Results of SAA algorithm for 100 fs SH pulse with a 20 % efficiency (center) for Lithium Niobate crystal at 1550 nm FF wavelength: (left) FF intensity distributions (doted), desired target SH profiles (dashed) and obtained SH profile (solid); (right) change of domain sizes as a function of their numbers

Noticeably, the required grating length increased as compared to a case, when we chose higher efficiency conversion (Fig. 4. shows these results). The grating is even longer than above; the agreement between the target and output pulses is quite satisfactory, despite the small but appreciable discrepancy between their PG-FROG traces. The results above demonstrate the good performance of the algorithm when simple Gaussian SH pulses are desired as the output, owing to the lack of sharp (temporal or spectral) features. Fig. 4.

shows results for higher SH efficiency conversion (∼40%) other parameters with the same condition as Fig. 3. But here, the desired SH profile is chosen to be 150 fs.

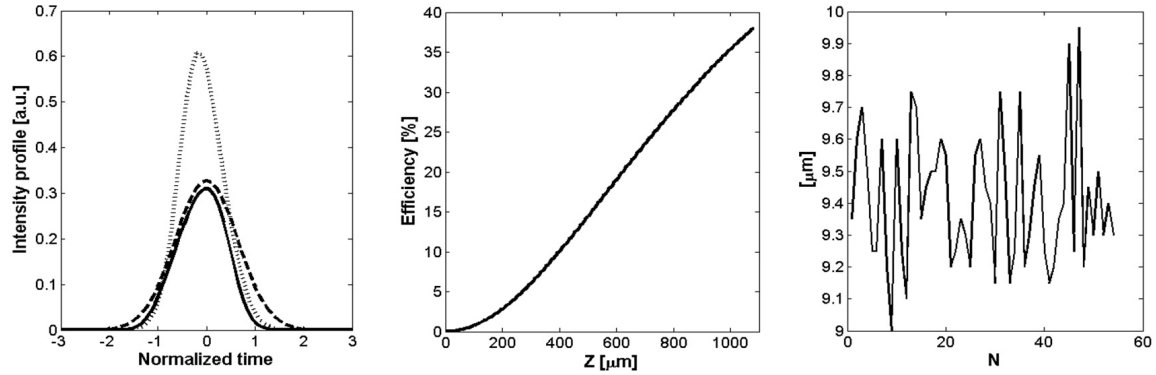

FIG. 4. Results for higher SH efficiency conversion (40%). All curves are determined as Fig. 3. Here desired SH profile is chosen to be 150 fs

We also studied the chosen problem for shorter FF (50 fs) and SH (50 fs) pulses with 10% efficiency conversion. For this case, we could get results faster than previous cases as shown in Fig. 5. This results from the fact that shorter nonlinear QPM crystals generate shorter SH pulses, due to GVM between the interacting harmonics. For this we could initially get excellent results, and secondly, faster run times than in previous cases.

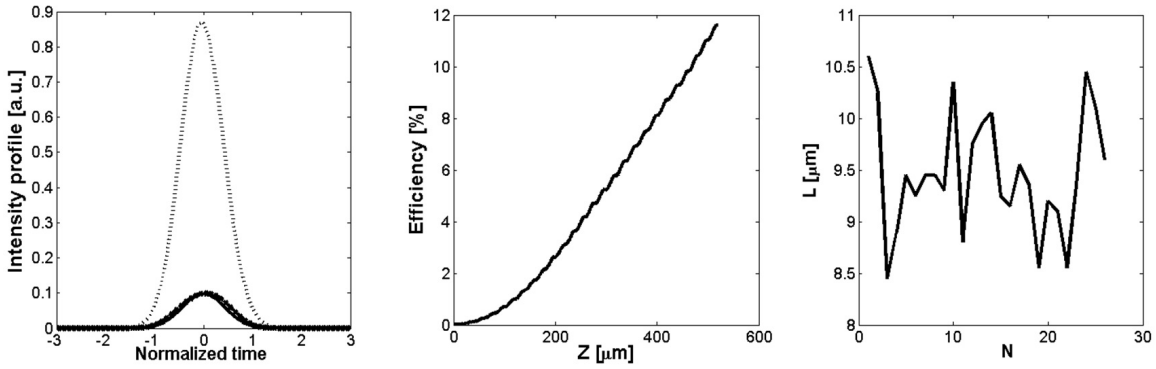

FIG. 5. Results for shorter FF (50 fs) and desired SH (50 fs) pulses with efficiency conversion of 10%. All curves are determined as Fig. 3 and 4

It is necessary to note that for fs FF pulses it is easy to obtain the desired SH pulses of almost the same duration with high efficiency up to 50% (we did not present that result here). This is caused by smaller influence of GVM. But when we concentrate longer desired SH pulses than FF pulse, the codes run for a longer time and give worse results due to large number of domains. We believe this comes from our program interface, which was Matlab without parallel computing. So, if we could use some program interface with parallel computing, we could obtain excellent results more quickly for "heavy" target SH pulses.

4. Conclusions

In conclusion, we were able to design a variety of femtosecond pulse profiles through second-harmonic generation of 100 fs and 50 fs Gaussian inputs at the FF using improved

SAA. PG-FROG spectrograms were used to calculate RMS errors and lead to rapid convergence of the method with high accuracy. The results, outlined for the relevant case of an aperiodically poled Lithium Niobate crystal, demonstrate that proper engineering of a quasi-phase-matched grating is feasible even under severe pump depletion and in the presence of limited fabrication resolution. The presented results can be used for obtaining femtosecond pulses with desired amplitude and phase profiles.

References

[1] Armstrong J. A., Bloembergen N., Ducuing J. and Pershan P. S. Interactions between Light Waves in a Nonlinear Dielectric. *Physical Review*, **127**(5), P. 1918–1939 (1962).

[2] Arbore M. A., Marco O., Fejer M.M., Pulse compression during second-harmonic generation in aperiodic quasi-phase-matching gratings. *Optics Letters*, **22**(12), P. 865–867 (1997).

[3] Arbore M.A., Galvanauskas A., Harter D., Chou M.H. and Fejer M.M. Engineerable compression of ultra-short pulses by use of second-harmonic generation in chirped-period-poled lithium niobate. *Optics Letters*, **22**(17), P. 1341–1343 (1997).

[4] Artigas D., Reid D.T., Fejer M.M. and Torner L. Pulse compression and gain enhancement in a degenerate optical parametric amplifier based on aperiodically poled crystals. *Optics Letters*, **27**(6), P. 442–444 (2002).

[5] Artigas D., Reid D.T. Efficient femtosecond optical parametric oscillators based on aperiodically poled nonlinear crystals. *Optics Letters*, **27**(10), P. 851–853 (2002).

[6] Fejer M.M., Magel G.A., Jundt D. H. and Byer R. L., Quasi-phase-matched second harmonic generation – Tuning and tolerances. *IEEE J. Quantum Electron*, **28**(11), P. 2631–2653 (1992).

[7] Loza-Alvarez P., Reid D.T., Faller P., Ebrahimzadeh M. and Sibbett W., Simultaneous second-harmonic generation and femtosecond-pulse compression in aperiodically poled $KTiOPO_4$ with a $RbTiOAsO_4$-based optical parametric oscillator. *J. Opt. Soc. Am. B*, **16**(9), P. 1553–1560 (1999).

[8] Loza-Alvarez P., Reid D. T., Faller P., Ebrahimzadeh M., Sibbett W., Karlsson H. and Laurell F. Simultaneous femtosecond-pulse compression and second-harmonic generation in aperiodically poled $KTiOPO_4$. *Optics Letters*, **24**(15), P. 1071–1073 (1999).

[9] Beddard T., Ebrahimzadeh M., Reid D.T. and Sibbett W. Five-optical-cycle pulse generation in the mid infrared from an optical parametric oscillator based on aperiodically poled lithium niobate. *Optics Letters*, **25**(14), P. 1052–1054 (2000).

[10] Imeshev G., Arbore M.A., Fejer M.M., Galvanauskas A., Fermann M. and Harter D. Ultrashort-pulse second-harmonic generation with longitudinally nonuniform quasi-phase-matching gratings: pulse compression and shaping. *J. Opt. Soc. Am. B*, **17**(2), P. 304–318 (2000).

[11] Imeshev G., Arbore M.A., Kasriel S. and Fejer M.M., Pulse shaping and compression by second-harmonic generation with quasi-phase-matching gratings in the presence of arbitrary dispersion. *J. Opt. Soc. Am. B*, **17**(8), P. 1420–1437 (2000).

[12] Buffa R. Transient second-harmonic generation with spatially non-uniform nonlinear coefficients. *Optics Letters*, **27**(12), P. 1058–1060 (2000).

[13] Buffa R. and Cavalieri S. Optimal control of type I second-harmonic generation with ultrashort laser pulses. *J. Opt. Soc. Am. B*, **17**(11), P. 1901–1905 (2000).

[14] Conforti M., Baronio F. and Angelis C. De. From femtosecond infrared to picosecond visible pulses: temporal shaping with high efficiency conversion. *Optics Letters*, **32**(13), P. 1779–1789 (2007).

[15] Reid D.T. Engineered quasi-phase-matching for second-harmonic generation. *J. Opt. A: Pure Appl. Opt.*, **5**, P. S97–S102 (2003).

[16] Sapaev U.K., Reid D.T. General second-harmonic pulse shaping in grating-engineered quasi-phase-matched nonlinear crystals. *Optics Express*, **13**(9), P. 3264–3276 (2005).

[17] Sapaev U.K. Optimum shaping of a spectral response of second harmonic generation process in the aperiodic quasi-phase matched nonlinear crystal. *Optics Spectroscopy*, **102**(6), P. 1023–1027 (2007).

[18] Sapaev U.K., Assanto G. Femtosecond pulse synthesis by efficient second harmonic generation in engineered quasi phase matching gratings. *Optics Express*, **15**(12), P. 7448–7457 (2007).

[19] Sapaev U.K., Yusupov D. B., Sherniyzov A.A., Uzakov A. A. Theory of backward second-harmonic generation of short laser pulses in periodically and aperiodically poled nonlinear crystals. *Journal of Russian Laser Research*, **33**(2), P. 196–210 (2012).

NANOSYSTEMS: PHYSICS, CHEMISTRY, MATHEMATICS, 2015, 6 (2), P. 249–261

Nanocatalysis: hypothesis on the action mechanism of gold

B. L. Oksengendler[1], B. Askarov[1], I. N. Nurgaliyev[1], S. E. Maksimov[2], V. N. Nikiforov[3]

[1]Institute of chemistry and physics of polymers,Uzbek Academy of Sciences, Tashkent, Uzbekistan

[2]Institute of ion-plasma and laser technologies,Uzbek Academy of Sciences, Tashkent, Uzbekistan

[3]Physics Department, M.V.Lomonosov State University, Moscow, Russia

oksengendlerbl@yandex.ru, dr.asqarov@mail.ru, ilnar82@mail.ru, maksimov_s@yahoo.com, pppnvn@yandex.ru

PACS 75.50.Tt, 81.16.Hc, 87.85.Rs DOI 10.17586/2220-8054-2015-6-2-249-261

In this article, the problem of nanocatalysis is considered when the catalysts are gold nanoparticles. The main experimental facts are presented and basic qualitative dependences are highlighted. The hypothesis considers the role of Tamm states of gold nanoparticles, with the modification of these states to reduce nanoparticle sizes. A semi-quantitative quantum-chemical reaction scheme of oxygen dissociation with gold nanocatalysis is shown. A theoretical answer to the basic experimental test has been obtained.

Keywords: nanocatalysis, d-atoms, Tamm levels.

Received: 2 February 2015

1. Introduction

Although the catalytic properties of Au (hydrogen-deuterium exchange, the reduction of NO_x by using of H_2, isomerization of paraffins, partial oxidation) had been quite widely studied until the end of the 1980's [1-6], it was found that Au is a much less efficient catalyst than the group VIII elements of Mendeleev's table and other transition metals. However, in 1987, it was found by Haruta et al. [7-9] that small size Au particles increased the activity of CO oxidation dramatically, performing the reaction at temperatures below those of such classical catalysts as Pt [7-10]. This circumstance greatly increased the interest in gold as a catalyst [11-18].

The main results of the basic experiment are the following:

1) The growth of the catalytic activity was observed for nanoparticles with size less than R=50 Å, particularly for nanoparticles with R<30 Å [8-10; 19-29].

2) The increased catalytic activity was observed as in small Au particles [23], in complexes of the partially oxidized/metal particles [30,31], in gold atom clusters [32,33] and in the cationic Au particles.

3) The role of the substrate in the catalysis of CO oxidation by Au particles was also important [8-11,30].

4) Most catalytic activity was observed for Au nanoparticles on TiO_2 and Fe_2O_3 substrates [8-11, 24].

5) It was assumed that the activation of O_2 molecule took place at the metal-substrate interface [36, 37], or directly on the substrates [8-11,19,21].

6) Changes in some properties of Au clusters are thought to vary as the function of their sizes; which are assumed to be important in the nanocatalysis problem:

a) the structural phase transition from FCC (bulk material) to the dodecahedral cluster (at R=25 Å) and icosahedral cluster (at R=16Å) [38] is discussed; there are data that the latter transition is observed at a much larger size (not at 100 atoms, but at 550 atoms in the cluster) [39]. Note that the transition to the icosahedron was experimentally observed in Y-zeolites at R=10 Å [41] and in 50-atomic Pt clusters on carbon [40];

b) there was a decrease in the bond lengths of Cr, Fe, Cu, Ag, Pd, Au, Pt metals at the size R<30 Å [42-53]; so, at R=30 Å the length of Au-Au bond is d=2.84 Å, and at R=8 Å it is d=2.72 Å, whereas the bulk material has d=2.88 Å [48,49,51].

c) such shortening of the bond lengths is characteristic for metal dimers (Fe, Mg) [54]; reduction of the Au-Au bond length also occurs in clusters;

d) there was a reduction of the bond lengths in the metal particles on the substrates, like carbon, which are weakly interacting with the metal particles [52,55,56];

e) there are changes in other properties of metal clusters (electronic, magnetic, chemical) at the scale of few nanometers [57, 64]; the most important of which is the modification of the electronic spectrum, namely, the displacement of d-band of Cu in its atomic spectrum with decreasing particle size[60]; the same effect was also observed for Pt and Pd [59].

The appearance of a gap in the spectrum at the Fermi level (E_e=0.45 eV) is observed for Au clusters with R <19 Å on a carbon substrate, so that there is a metal-insulator transition; a similar effect is also observed for two-dimensional particles of Au (200 atoms) on a TiO_2 substrate with E_e=0.2-0.6 eV [23] (Figure 1).

Concerning the theoretical interpretation of the Au nanoparticles' unique catalytic activity, only general considerations have been expressed:

a) about the role of reducing the coordination number of surface atoms;

b) about the general increase of the relative part of the total number of surface atoms;

c) about the existence of the evident correlation between the increased catalytic activity and the existence of metal-insulator transition with decreased cluster size;

d) about the correlation of the increase in nanoparticle catalytic activity and the decrease of the interatomic Au-Au distance in smaller cluster sizes;

e) about the role the substrate plays in increased catalytic activity.

The most important of these five positions are the positions c) and e), i.e. that the high catalytic activity of the gold nanoparticles promotes the formation of a gap in the electronic spectra of nanoparticles. In this regard, it is very important to discuss of the role of Tamm states in the nanoparticle, taking into account their modification with decreased nanoparticle size.

2. Tamm states of nanoparticles

In 1932, on the basis of quantum mechanics, I.E.Tamm for the first time demonstrated that apart from the band states of electrons in a crystal known at that time, electron states of a completely different type can exist on a crystal surface [65]. These surface electron states have a discrete energy spectrum and wavefunctions that exponentially decay with increasing distance from the surface to within or away from the crystal. During more than 80 years since then, the theory of surface states has been considerably developed with regards to computational techniques and the analysis of such states in various crystals [66,67]. Due to the evolution of nanoscience, the problem of surface states has become even more relevant. However, general analysis of the surface states problem shows that basically new factors that were not reflected in the proposed model should be considered when applied

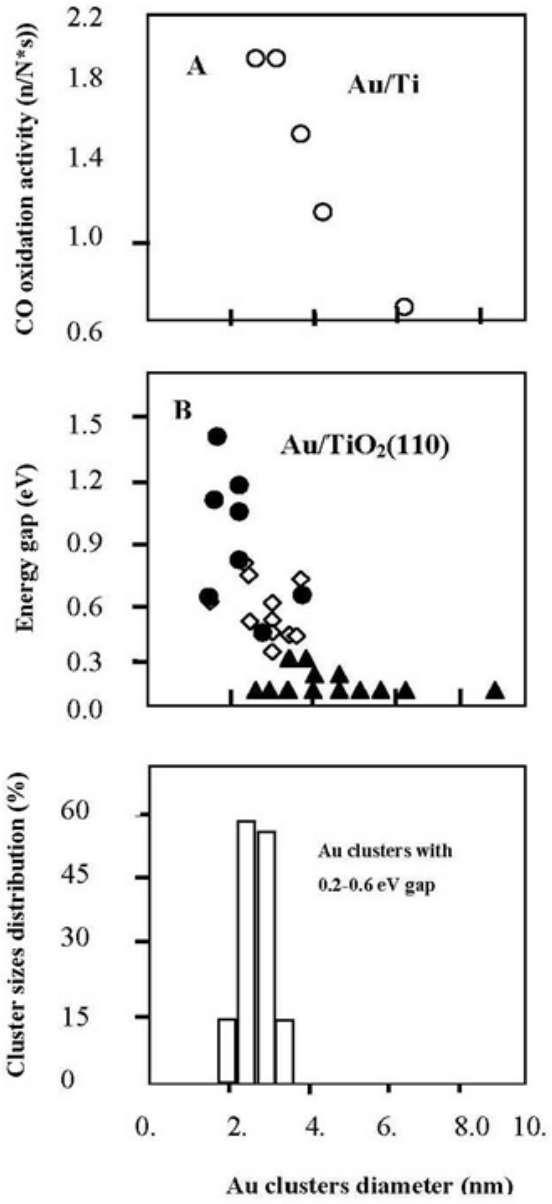

FIG. 1. Dependence of the CO oxidation activity, the energy gap in the electronic spectrum of the gold nanoparticles and their size distribution on Au cluster size

to nanoclusters. Concepts such as the role of the surface curvature (nonplanar surface), the sharpness of the potential barrier simulating the width of the surface region (diffuse nature of the interface), and finiteness of the nanocluster size (in contrast to the case of a semi-infinite crystal) should be introduced into the theory. At the same time, nanoparticles have a characteristic that describes the above properties in an integrated manner; we are speaking of confinement of elementary excitations in a nanoparticle. The most important property determined by the confinement of electrons is the discretization of their electronic spectra, which accompanies the increase in the spectral gap width; the broadening of the gap increases when the characteristic size of a nanoparticle decreases [4]. Therefore, it is reasonable to consider the features introduced into the Tamm surface states of nanoparticles by a fundamental property like the electron confinement.

2.1. Model

Our analysis is based on a combination of three models: the Tamm model of surface states [65], the well-known Kronig–Penney model of a solid [68], and results obtained by Efros on the electron structure of a nanosphere [69]. For this purpose, each model will be slightly developed.

The basic scheme of Tamm's analysis [65] is shown in Fig. 2.

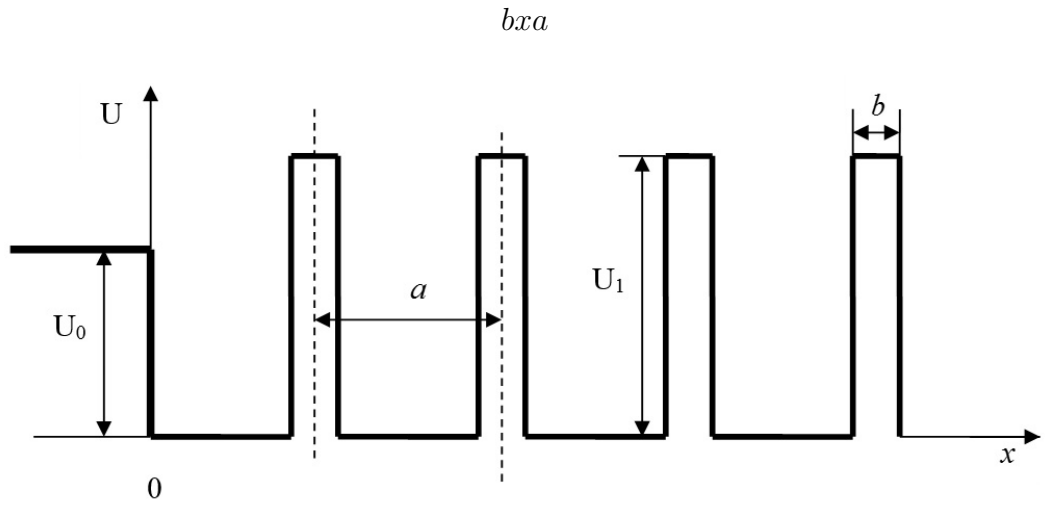

FIG. 2. Potential energy of a crystal with a surface in the Tamm– Kronig–Penney model

Tamm presented the wavefunction of a surface electron state outside the crystal (for x <0) in the form:

$$\Psi = A\exp[\frac{\sqrt{2m(U_0 - E)}}{h^2}x], \tag{1}$$

where E (energy of Tamm's state) satisfies the condition $0 < E < U_0$.

Introducing the parameters (see Fig.2.):

$$\xi = \frac{a}{h}\sqrt{2mE}; \quad q = \frac{a}{h}\sqrt{2mU_0}; \quad p = ab\frac{mU_1}{h^2}, \tag{2}$$

Tamm obtained the following equation for energy E:

$$\xi ctg\xi = \frac{q^2}{2p^2} - q\sqrt{1 - \frac{\xi^2}{q^2}}. \tag{3}$$

Let us simplify this expression for low energies ($\xi << 1$):

$$E(qa^2 - \frac{2m}{h^2}) = q - \frac{q^2}{2p^2} \quad . \tag{4}$$

Thus, we obtain the dependence of energy E on the dimensionless parameter p, appearing in the Kronig–Penney model [69]. This model can also be represented in Fig.2 if we consider the range of $X >> 0$. The equation for allowed energy values in the Kronig–Penney model has the form (in notation used in [69-70]):

$$\left\{ \begin{array}{l} \left|\cos(ka - actg(\frac{\Omega a}{ka}))\right| \leqslant \frac{1}{\sqrt{1+\left(\frac{\Omega a}{ka}\right)^2}} \\ E = \frac{h^2}{2ma^2}(ka)^2 \end{array} \right\}, \tag{5}$$

where Ωa characterizes the dimensionless barrier penetrability. For low energies, ($\Omega a/ka >> 1$), Eq.(5) is transformed to:

$$|\sin(ka)| \leqslant \frac{ka}{\Omega a}. \tag{6}$$

Expanding $\sin(ka)$ (for $ka < 1$), we obtain the first two solutions $E = f(\Omega a)$:

$$E_1 = 0; \quad E_2 = \frac{h^2}{2ma^2} 6(1 - \frac{1}{\Omega a})^2. \tag{7}$$

The graphical form of Eq. (6) is shown in Fig.3.

Combining Fig.3 with Eq. (7), we obtain penetrability parameter Ωa as a function of the first band gap:

$$E^1_{gap} = E_2 - E_1 :$$

$$\frac{1}{\Omega a} = 1 - \sqrt{\frac{E^1_{gap}}{h^2/2ma^2}}/6. \tag{8}$$

Matching the Kronig–Penney model and the Tamm model by the condition $p = \Omega a$, we obtain from expressions (8) and (4):

$$\frac{E}{h^2/2ma^2} = 2\sqrt{\frac{U_0}{h^2/2ma^2}} - \frac{U_0}{h^2/2ma^2} - \left[1 - \frac{1}{6}\sqrt{\frac{E^1_{gap}}{h^2/2ma^2}}\right]^2. \tag{9}$$

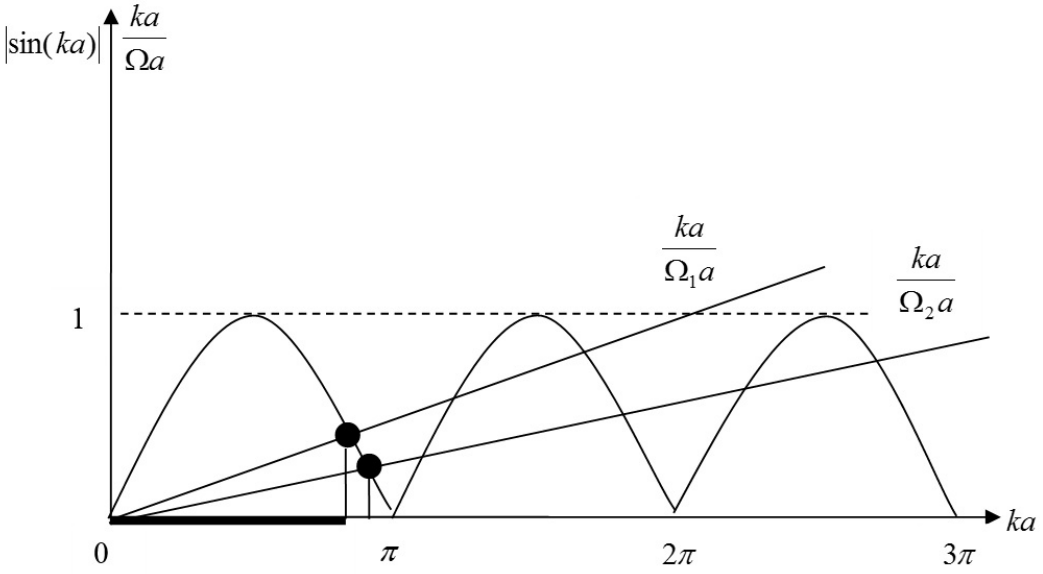

FIG. 3. Plot for determining the boundaries of allowed and forbidden bands (bullets); $\Omega_1 < \Omega_2$

Let us now consider the dependence of gap width E^1_{gap} on radius (R) of a nanosphere [68]:

$$E^1_{gap} = E^0_g + \frac{A}{R^2}, A \equiv h^2\pi^2/2m, \tag{10}$$

where E^0_g is the gap width for the bulk material. Substituting expressions (10) into (9), we obtain the following dependence of the position of the Tamm level on nanoparticle radius R:

$$E = \frac{h^2}{2ma^2}\varphi(R), \tag{11}$$

where:

$$\varphi(R) \equiv \left\{ 2\sqrt{\frac{U_0}{h^2/2ma^2}} - \frac{U_0}{h^2/2ma^2} - \left[1 - \frac{1}{6}\sqrt{\frac{E_g^0 + A/R^2}{h^2/2ma^2}} \right] \right\}. \tag{12}$$

It should be noted that $d\varphi(R)/dR < 0$.

Thus, exponent α in the wavefunction $\psi(x) = A\exp(\alpha x)$; $(x < 0)$ for the Tamm electron has the form:

$$\alpha = \frac{1}{a}\sqrt{\frac{U_0}{h^2/2ma^2} - \varphi(R)}. \tag{13}$$

Analyzing Eq. (13), we can easily see that the value of α decreases with R:

$$\frac{d\alpha}{dR} > 0. \tag{14}$$

Consequently, we obtain two important results (Fig.4):

1) upon a decrease in nanoparticle radius R, the Tamm level increases, approaching U_0 from below;

2) the degree of localization of Tamm wavefunction α decreases upon a decrease in radius R.

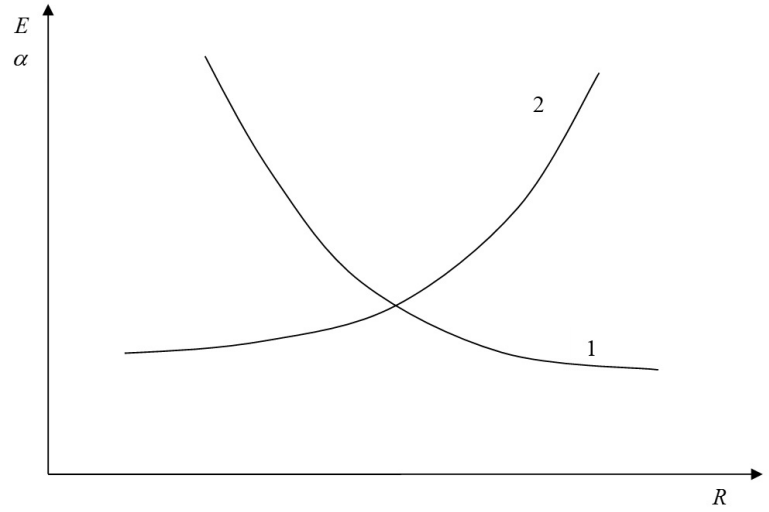

FIG. 4. Schematic qualitative dependence of the energy of Tamm's level (1) and damping factor of the wavefunction of a Tamm electron (2) on the nanoparticle radius

3. Model of nanocatalysis of the oxygen molecule dissociation by Au nanoclusters

The geometric model diagram for the chemical interaction of an oxygen molecule with a nanocatalytic gold cluster is shown in Fig. 5.

It is clear that the Tamm orbital of gold cluster increasingly penetrates into the space between the oxygen atoms as the oxygen molecule approaches the nanocluster; we also note that since the empty state of the oxygen molecule $\sigma^*_{p_z S}$ is antibonding, there is a lack of electron density at the center of the molecule. Furthermore, it can be assumed that the appearance of electron density of the Tamm states in the center of the oxygen molecule will lead to Coulomb repulsion of the two oxygen atoms, so that the interaction of the molecule

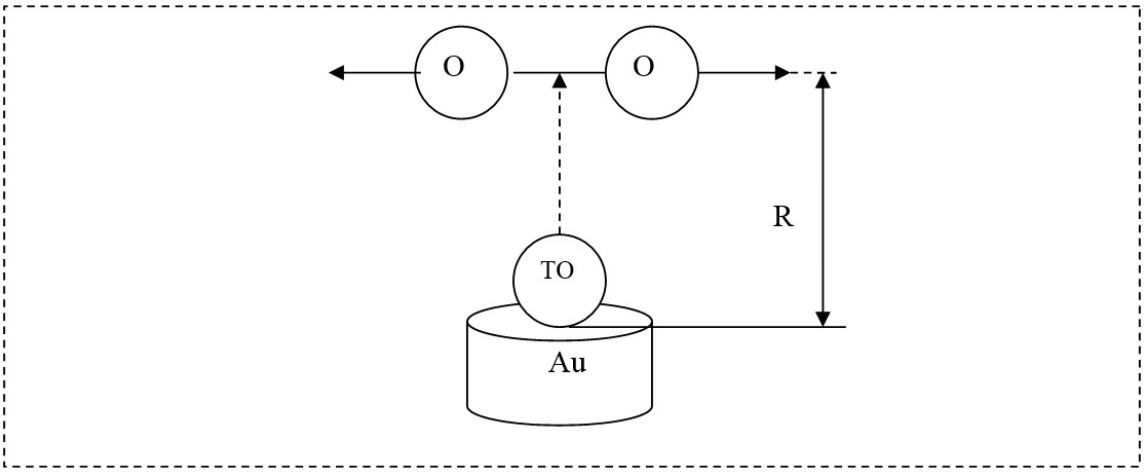

FIG. 5. Geometric scheme for oxygen molecule interaction with Tamm state of gold nanocluster

with the nanocluster occurs through the synchronous reaction: approach of O_2 with the nanocluster is accompanied by an increase in the distance between the oxygen atoms. From another point of view, separation of the oxygen atoms, according to the quantum chemistry laws [71], reduces the splitting of all levels (the drop of the exchange integral), so that the $\sigma^*_{p_zS}$ level is reduced (Figure 6).

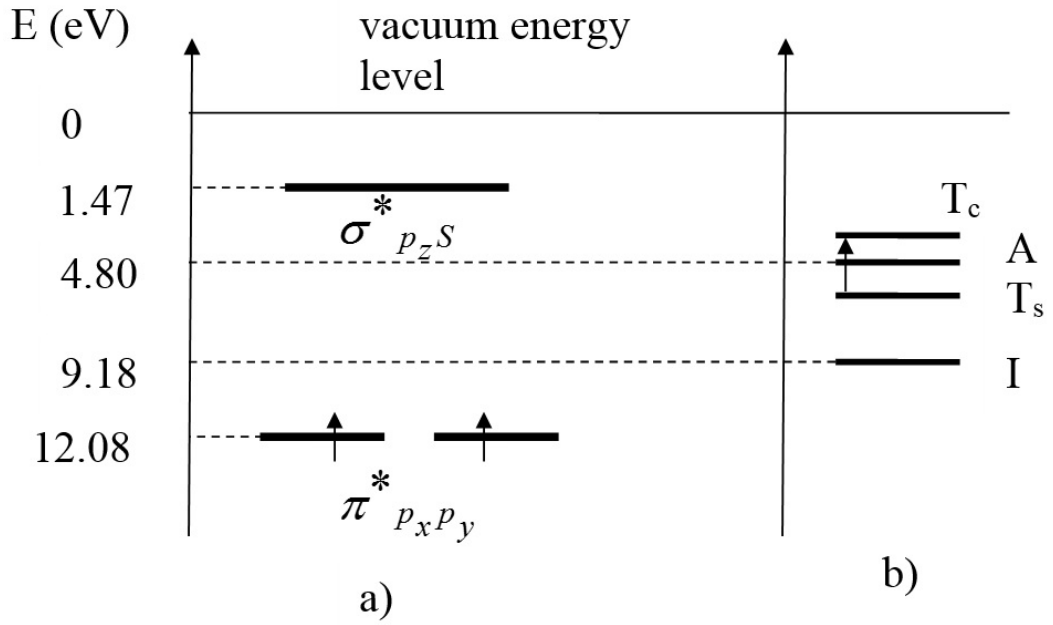

FIG. 6. Quantum-chemical model for the interaction of the electronic states of the oxygen molecule with Tamm states of gold nanoclusters; electronic energy levels of: a) the HOMO and LUMO of O_2; b) I is the ionization potential of Au atom, T_c is the Tamm level of the Au nanocatalysts, T_s is the Tamm level of the semi-infinite Au catalyst, A is the work function of gold

Note further that Figure 6 shows the diagram of the electronic levels of the oxygen molecule and of the gold nanoclusters. We see that the Tamm state lies below the $\sigma^*_{p_zS}$ level,

so lowering the $\sigma^*_{p_zS}$ level and its approach to the Tamm level promotes the superposition of the wave function for the free oxygen molecule and the wavefunction of the Tamm state. The total wavefunction of the "oxygen molecule + gold nanocluster" system has the form:

$$\Psi(R) = C_1(R)\sigma^*_{p_zS} + C_2(R)\varphi_{TO}. \tag{15}$$

In this expression, $C_1(R)$ and $C_2(R)$ are the contributions of the $\sigma^*_{p_zS}$ oxygen states and of the Tamm orbitals φ_{TO} in the total wave function of the combined system. Note that the coincidence of the lowering $\sigma^*_{p_zS}$ energy levels and of the Tamm states' flow of electrons into the oxygen molecule occurs most effectively, since the Franck-Condon factor is maximal in such a resonance [72]. From the point of view of quantum chemistry, the filling of the antibonding state of the oxygen molecule destabilizes it, i.e. reduces the dissociation energy of about 100 kJ/mol [73]. Taking into account that the Tamm level may be filled by two electrons initially and they (couple) can overflow to the $\sigma^*_{p_zS}$ level, then energy reduction to zero takes place, so that the oxygen molecule dissociates spontaneously.

In this scheme, the question about the role of the size of the gold nanoclusters is of great interest. As was shown in the previous section, the nanocluster size affects both the length of the Tamm states' wave function and the depth of its position (Eqs. (11), (13)), so for smaller nanocluster, first, the Tamm wave function penetrates into the interoxygen space with the approach of the reagents earlier, and, second, the resonance of $\sigma^*_{p_zS}$ and φ_{TO} also occurs earlier than in case of large clusters. Therefore, the effectiveness of the nanocluster catalyst in our model increases with decreasing gold nanocluster size, which is in full agreement with experimental results (see Fig. 1).

4. Test of the model correctness

It is desirable for the qualitative description of the gold nanoparticle catalysis model to be supported by quantitative confirmation. The criterion for the correctness of this theory can be the test of the dependence "catalysis efficiency" $\sim$" $1/d^3$", where the d is the size of the gold nanoparticles (Figs. 1, 7) [14,74].

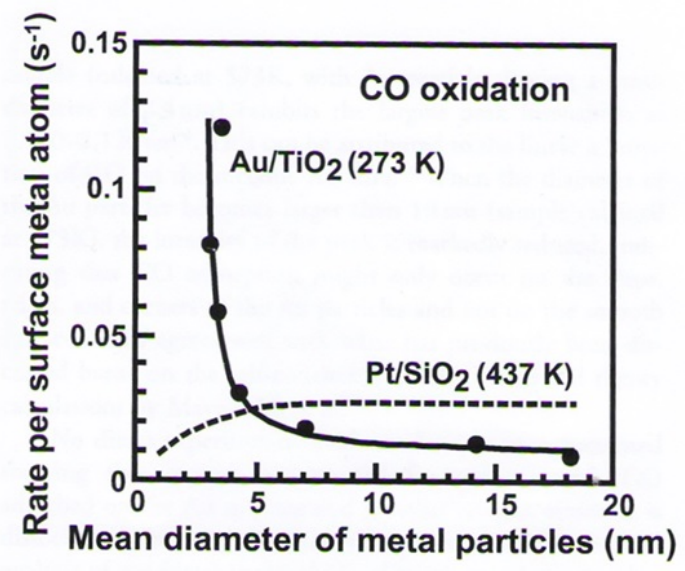

FIG. 7. Turnover frequency (TOF) for CO oxidation over Au/TiO_2 as a function of the mean diameter of Au particles [14,74]

Note that the law "$1/d^3$" is confirmed in a very broad class of experiments for both different substrates and types of contacts for Au nanoparticles with the substrates [74,75].

We consider such an approach of an O_2 molecule to a Au nanoparticle, when the Tamm electron is already located between two oxygen atoms (Fig. 8).

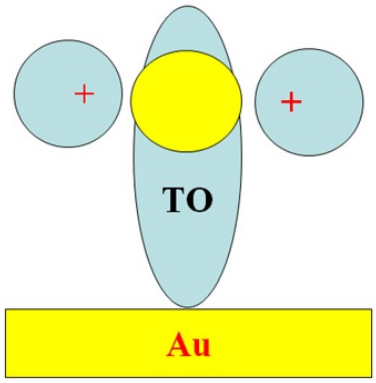

FIG. 8. Hellmann-Feynman scheme for the change of the dissociation energy of oxygen molecule at the penetration of Tamm orbital into the center of the molecule

According to the Hellmann-Feynman theorem [70], the resulting system can be considered electrostatically, so that the activation energy Q_0 of dissociation process of the oxygen molecule decreases by ΔQ, which is proportional to the part of the Tamm state electron density located between the two oxygen atoms (shaded part of orbital in Fig.8), i.e.:

$$\Delta Q = \beta \frac{1}{\alpha} \left(\frac{C_2}{C_1} \right)^2, \tag{16}$$

where β is the proportionality coefficient, $\frac{1}{\alpha}$ is the "size" of Tamm wave function (see (15)), $\left(\frac{C_2}{C_1}\right)^2$ is the proportion of Tamm state penetrated into the space between the oxygen atoms.

According to the two-center chemical bond theory [70], we have:

$$\left(\frac{C_2}{C_1} \right)^2 = \frac{1}{4} \left(l - \sqrt{l^2 + 4} \right)^2, \tag{17}$$

where $l = \frac{H_{11} - (H_{22} - E)}{H_{12}}$, H_{12} is the exchange integral of the states of $\left(\sigma^*_{P_Z S}\right)$ antibonding of the oxygen molecule and of the Tamm state (see. (15)); $-H_{11} = J_1$ is the ionization potential of $\sigma^*_{P_Z S}$ antibonding; $-H^0_{22} = J_2$ is the ionization energy of the Tamm state of semi-infinite Au crystal, E is the energy of the Tamm state of Au nanoparticles.

It is essential that the value $\frac{1}{\alpha}\left(\frac{C_2}{C_1}\right)^2$ depends on the function $\varphi(R)$ (α is based on Eq.(13), $\left(\frac{C_2}{C_1}\right)^2$ is based through E on Eq. (11)), and therefore from the fact that $\varphi(R)$ has a small value, it is easy to obtain:

$$\frac{1}{\alpha} \left(\frac{C_2}{C_1} \right)^2 = \frac{a}{\sqrt{M - \varphi(R)}} \frac{L}{2} \left[\tilde{L} + \varphi(R) \right], \tag{18}$$

where the dimensionless quantities L, $\tilde{L}$ and $M$are the functions of $\hbar^2/2ma^2, U_0, E^0_g, H_{11}$ and H_{12}.

Further, freed from the radicals in the $\varphi(R)$ function, we easily obtain:

$$\frac{1}{\alpha}\left(\frac{C_2}{C_1}\right)^2 \approx B + C\frac{1}{R^2} + D\frac{1}{R^4} \tag{19}$$

Now, we can write the expression for the probability of oxygen molecule dissociation on the surface of a Au nanoparticle:

$$e^{-\frac{Q_0-\Delta Q}{kT}} \geqslant e^{-Q_0/kT} + e^{-Q_0/kT}\frac{Q_0}{kT}\beta\frac{1}{\alpha}\left(\frac{C_2}{C_1}\right)^2. \tag{20}$$

Using (19), we obtain:

$$e^{-\frac{Q_0-\Delta Q}{kT}} \geqslant e^{-Q_0/kT} + e^{-Q_0/kT}\beta\left[B + \frac{C}{R^2} + \frac{D}{R^4}\right]\frac{Q_0}{kT}, \tag{21}$$

where B, C, D are the constants.

It is obvious that the bracketed expression is very close to the function $Const/R^3$; in our view, this indicates reasonable agreement between the model and experiment (Fig. 7), which has not been obtained in other approaches [74, 75].

5. Conclusion

On the basis of the analysis of existing experimental data, it is found with a high degree of reliability that the catalytic activity of Au nanoparticles depends on a combination of three factors:

-size of the gold nanoparticles;

- type of substrate upon which the Au nanoparticle is placed;

- type of the contact of Au nanoparticles with the substrate.

The most important of these three factors is the first one, and it was found that a gap appears in the electronic spectrum of Au nanoparticles when the size of those nanoparticles is of 50 Å or less, and that from this point, their catalytic properties sharply increase.

We have assumed that the catalytic activity of Au nanoparticles is related to features of the surface Tamm states formed in the gap of Au nanoparticle electronic spectra.

The above model of Tamm states in the nanoparticle showed that the properties of these states are modified with the decreasing nanoparticle size: Tamm orbitals "stretch" radially from the surface, and the energy levels of these states are raised. Using the quantum-chemical model for O_2 molecule dissociation on the surface of a Au nanoparticle showed that the catalytic activity of Au nanoparticles increase as their radii decrease as $\frac{Const_1}{R^2} + \frac{Const_2}{R^4}$, which is very close to the experimentally observed dependence "$1/R^3$" and can thus serve as a "litmus test" for the model, confirming its reliability.

References

[1] Bond G.C. The catalytic properties of gold. *Gold Bull.*, **5**(1), P. 11–13 (1972).
[2] Schwank J. Catalytic gold. *Gold Bull.*, **16**(4), P. 103–110 (1983).
[3] Hutchings G.J. Catalysis. A golden future. *Gold Bull.*, **29**(4), P. 123–130 (1996).
[4] Somorjai G.A., Park J.Y. Evolution of the surface science of catalysis from single crystals to metal nanoparticles under pressure. *J. Chem. Phys.*, **128**(18), P. 182504 (2008).
[5] Thompson D. New advances in gold catalysis. Part I. *Gold Bull*, **31**(4), P. 111–118 (1998).
[6] Bond G.C., Thompson D.T. Catalysis by gold. *Catal. Rev.Sci. Eng.*, **41**(3-4), P. 319–388 (1999).
[7] Haruta M., Kobayashi T., Sano H., Yamada N. Novel Gold Catalysts for the Oxidation of Carbon Monoxide at a Temperature far Below 0°. *Chem. Lett.*, **2**, P. 405–408 (1987).
[8] Haruta M. Size and support dependency in the catalysis of gold. *Catal. Today*, **36**, P. 153–166 (1997).
[9] Haruta M. Novel catalysis of gold deposited on metal oxides. *Catal. Surv. Asia.*, **1**, P. 61–73 (1997).

[10] Haruta M. Gold as a low temperature catalyst: factors controlling activity and selectivity. In book: 3-World Congress on Oxidation Catalysis. Elsevier Science, Amsterdam, P. 123–134 (1997).
[11] Haruta M., Daté M. Advances in the catalysis of Au nanoparticles. *Appl. Catal.*, **A 222**, P. 427–437 (2001).
[12] Grisel R.J.H., Weststrate K.-J., Gluhoi A., Nieuwenhuys B.E. Catalysis by Gold Nanoparticles. *Gold Bull.*, **35**(2), P. 39–45 (2002).
[13] Santra A.K., Goodman D.W.Oxide-supported metal clusters: models for heterogeneous catalysts. *J. Phys.: Condens. Matter*, **14**, P. R31–R62 (2002).
[14] Hutchings G.J. Gold catalysis in chemical processing. *Catal. Today*, **72**, P. 11–17 (2002).
[15] Haruta M. When Gold Is Not Noble: Catalysis by Nanoparticle. *Chem. Record.*, **3**(2), P. 75–87 (2003).
[16] Haruta M. Nanoparticulate Gold Catalysts for Low-Temperature CO Oxidation. *J. New Mater. Electrochem. Syst.*, **7**, P. 163–172 (2004).
[17] Meyer R., Lemire C., Shaikhutdinov S.K., Freund H.J. Surface chemistry of catalysis by gold. *Gold Bull.*, **37**, P. 72–124 (2004).
[18] Hutchings G.J. Catalysis by gold. *Catal. Today*, **100**, P. 55–61 (2005).
[19] Haruta M., Tsubota S., Kobayashi T., Kageyama H., Genet M.J., Delmon B. Low-temperature oxidation of CO over gold supported on TiO_2, alpha-Fe_2O_3 and Co_3O_4. *J. Catal.*, **144**, P. 175–192 (1993).
[20] Tsubota S., Cunningham D.A.H., Bando Y., Haruta M. Prep. Catal. VI, Scientific Basis for the Preparation of Heterogeneous Catalysts. Elsevier, Amsterdam, 277 p. (1995).
[21] Boccuzzi F., Chiorino A., Tsubota S., Hurata M. FTIR Study of Carbon Monoxide Oxidation and Scrambling at Room Temperature over Gold Supported on ZnO and TiO_2. *J. Phys. Chem.*, **100**(9), P. 3625–3631 (1996).
[22] Bamwenda G.R., Tsubota S., Nakamura T., Haruta M. The influence of the preparation methods on the catalytic activity of platinum and gold supported on TiO_2 for CO oxidation. *Catal. Lett.*, **44**(1-2), P. 83–87 (1997).
[23] Valden M., Lai X., Goodman D.W. Onset of catalytic activity of gold clusters on titania with the appearance of nonmetallic properties. *Science*, **281**, P. 1647–1650 (1998).
[24] Kozlov A.I., Kozlova A.P., Asakura K., Matsui Y., Kogure T., Shido T., Iwasawa Y. Supported gold catalysts prepared from a gold phosphine precursor and As-precipitated metal-hydroxide precursors: Effect of preparation conditions onthe catalytic performance. *J. Catal.*, **196**, P. 56–65 (2000).
[25] Claus P., Bruckner A., Mohr C., Hofmeister H. Supported gold nanoparticles from quantum dot to mesoscopic size scale: Effect of electronic and structural properties on catalytic hydrogenation of conjugated functional groups. *J. Am. Chem. Soc.*, **122**, P. 11430–11439 (2000).
[26] Schumacher B., Plzak V., Kinne K., Behm R.J. Highly active Au/TiO_2 catalysts for low-temperature CO oxidation: Preparation, conditioning and stability. *Catal. Lett.*, **89**(1-2), P. 109–114 (2003).
[27] Zanella R., Giorgio S., Shin C.-H., Henry C.R., Louis C. Characterization and reactivity in CO oxidation of gold nanoparticles supported on TiO_2 prepared by deposition-precipitation with NaOH and urea. *J. Catal.*, **222**, P. 357–367 (2004).
[28] Schwartz V., Mullins D.R., Yan W., Chen B., Dai S., Overbury S.H. XAS study of Au supported on TiO_2: Influence of oxidation state and particle size on catalytic activity. *J. Phys. Chem. B.*, **108**(40), P. 15782–15790 (2004).
[29] Remediakis I.N., Lopez N., Nørskov J.K. CO oxidation on rutile-supported Au nanoparticles. *Angew. Chem. Int. Ed.*, **44**(12), P. 1824–1826 (2005).
[30] Bond C.G., Thompson D.T. Gold-catalysed oxidation of carbon monoxide. *Gold Bull.*, **33**, P. 41–50 (2000).
[31] Costello C.K., Yang J.H., Law H.Y., Wang Y., Lin J.N., Marks L.D., Kung M.D., Kung H.H. On the potential role of hydroxyl groups in CO oxidation over Au/Al_2O_3. *Appl. Catal. A*, **243**, P. 15–24 (2003).
[32] Sanchez A., Abbet S., Heiz U., Schneider W.D., Häkkinen H., Barnett R.N., Landman U. When gold is not noble: nanoscale gold catalysts. *J. Phys. Chem.A*, **103**, P. 9573–9578 (1999).
[33] Yoon B., Häkkinen H., Landman U., Wörz A.S., Antonietti J.-M., Abbet S.,Judai K., Heiz U. Charging effects on bonding and catalyzed oxidation of CO on Au8 clusters on MgO. *Science*, **307**, P. 403–407 (2005).
[34] Fu Q., Saltsburg H., Flytzani-Stephanopoulos M. Active Nonmetallic Au and Pt Species on ceria-based water-gas shift catalysts. *Science*, **301**, P. 935–938 (2003).

[35] Guzman J., Gates B.C. Structure and Reactivity of a Mononuclear Gold-Complex Catalyst Supported on Magnesium Oxide. *Angew. Chem. Int. Ed.*, **42**, P. 690–693 (2003).
[36] Molina L.M., Hammer B. Active role of oxide support during CO oxidation at Au/MgO. *Phys. Rev. Lett.*, **90**, P. 206102 (2003).
[37] Liu Z.-P., Gong X.-Q., Kohanoff J., Sanchez C., Hu P. Catalytic role of metal oxides in gold-based catalysts: a first principles study of CO oxidation on TiO_2 supported Au. *Phys. Rev. Lett.*, **91**, P. 266102 (2003).
[38] Cleveland C.L., Landman U., Schaaff T.G., Shafigullin M.N., Stephens P.W., Whetten R.L. Structural evolution of smaller gold nanocrystals: The truncated decahedral motif. *Phys. Rev. Lett.*, **79**, P. 1873–1876 (1997).
[39] Uppenbrink J., Wales D.J. Structure and Energetics of Model Metal Clusters. *J. Chem. Phys.*, **96**, P. 8520–8534 (1992).
[40] Yacaman M.J., Fuentes S., Dominguez J.M. The effect of shape and crystal structure of small particles on their catalytic activity. *Surf. Sci.*, **106**, P. 472–477 (1981).
[41] Moraweck B., Renouprez A.J. EXAFS determination of the structure of small platinum particles. *Surf. Sci.*, **106**, P. 35–44 (1981).
[42] Berry C.R. Electron diffraction from small crystals. *Phys. Rev.*, **88**(3), P. 596–599 (1952).
[43] Wasserman H.J., Vermaak J.S. On the determination of a lattice contraction in very small silver particles. *Surf. Sci.*, **22**, P. 164–172 (1970).
[44] Purdum H., Montano P.A., Shenoy G.K., Morrison T.I. Extended-x-ray-absorption-fine-structure study of small Fe molecules isolated in solid neon. *Phys. Rev.B*, **25**(7), P. 4412–4417 (1982).
[45] Montano P.A., Schulze W., Tesche B., Shenoy G.K., Morrison T.I. Extended x-ray-absorption fine-structure study of Ag particles isolated in solid argon. *Phys. Rev.B*, **30**, P. 672–677 (1984).
[46] Montano P.A., Purdum H., Shenoy G.K., Morrison T.I. X-ray absorption fine structure study of small metal clusters isolated in rare-gas solids. *Surf. Sci.*, **156**, P. 228–233 (1985).
[47] Heinemann K., Poppa H. In-situ TEM evidence of lattice expansion of very small supported palladium particles. *Surf. Sci.*, **156**, P. 265–274 (1985).
[48] Balerna A., Bernieri E., Picozzi P., Reale A., Santucci S., Burattini E.,Mobilio S. A structural investigation on small gold clusters by EXAFS. *Surf. Sci.*, **156**, P. 206–213 (1985).
[49] Balerna A., Bernieri E., Picozzi P., Reale A., Santucci S., Burattini E., Mobilio S., Extended x-ray-absorption fine-structure and near-edge-structure studies on evaporated small clusters of Au. *Phys. Rev.B*, **31**(8), P. 5058–5065 (1985).
[50] Montano P.A., Shenoy G.K., Alp E.E., Schulze W., Urban J. Structure of copper microclusters isolated in solid argon. *Phys. Rev.Lett.B.*, **56**, P. 2076–2079 (1986).
[51] Pinto A., Pennisi A.R., Faraci G., D'Agostino G., Mobilio S., Boscherini F. Evidence for truncated octahedral structures in supported gold clusters. *Phys. Rev.B*, **51**(8), P. 5315–5321 (1995).
[52] Klimenkov M., Nepijko S., Kuhlenbeck H., Bäumer M., Schlögl R., Freund H.-J. The structure of Pt-aggregates on a supported thin aluminum oxide film in comparison with unsupported alumina: a transmission electron microscopy study. *Surf. Sci.*, **391**, P. 27–36 (1997).
[53] Oudenhuijzen M.K., Bitter J.H., Koningsberger D.C. The Nature of the Pt–H bonding for strongly and weakly bonded hydrogen on platinum. A XAFS spectroscopy study of the Pt–H antibonding shaperesonance and Pt–H EXAFS. *J. Phys. Chem.B.*, **105**(20), P. 4616–4622 (2001).
[54] Montano P.A., Zhao J., Ramanathan M., Shenoy G.K., Chulze W. EXAFS study of Ag, Fe and Ge microclusters. *Physica B*, 158, 1989(1-3), P. 242–242.
[55] Apai G., Hamilton J.F., Stöhr J., Thompson A. Extended X-ray-absorption fine structure of small Cu and Ni clusters: binding-energy and bond-length changes with cluster size. *Phys. Rev. Lett.*, **43**(2), P. 165–169 (1979).
[56] Crescenzi M., Picozzi P., Santucci S., Battistoni C., Mattogno G. Cluster growth of Cu on graphite: XPS, Auger and electron energy loss studies. *Solid State Commun.*, **51**(10), P. 811–815 (1984).
[57] Dupree R., Forwood C.T., Smith M.J.A. Conduction electron spin resonance in small particles of gold. *Phys. Status Solidi*, **24**, P. 525–530 (1967).
[58] Monot R., Câtelain A., Borel J.P. Conduction electron spin resonance in small particles of pure gold. *Phys. Lett. A.*, **34**, P. 57–58 (1971).
[59] Mason M.G., Gerenser L.J., Lee S.T. Electronic structure of catalytic metal clusters studied by X-Ray photoemission spectroscopy. *Phys. Rev. Lett.*, **39**(5), P. 288–291 (1977).

[60] Schmeisser D., Jocobi K., Kolb D.M. Photoemission study of matrix isolated Cu atoms and clusters. *J. Chem. Phys.*, **75**(11), P. 5300–5004 (1981).
[61] Lee S.-T., Apai G., Mason M.G., Benbow R., Hurych Z. Evolution of band structure in gold clusters as studied by photoemission. *Phys. Rev. B.*, **23**(2), P. 505–508 (1981).
[62] Kreibig U., Genzel L. Optical absorption of small metallic particles. *Surf. Sci.*, **156**, P. 678–700 (1985).
[63] Schmid G. Large clusters and colloids: Metals in the embryonic state. *Chem. Rev.*, **92**, P. 1709–1727 (1992).
[64] Binns C. Nanoclusters deposited on surfaces. *Surf. Sci. Rep.*, **44**, P. 1-49 (2001).
[65] Tamm I.E. *Collection of scientific works.* (In Russian). Nauka, Moscow, V. 1, 440 p. (1975).
[66] Morrison S.R. *The Chemical Physics of Surfaces.* Plenum Press, New York-London, 415 p. (1977).
[67] Davison S.G., Levine J.D. *Surface States.* Academic press, New York, 149 p. (1970).
[68] Flugge. S. *Practical Quantum Mechanics.* Springer, Berlin, Part I. 628 p. (1971).
[69] Efros Al.L., Efros A.L. Interband absorption of light in a semiconductor ball. *Fizika i tekhnika poluprovodnikov*, **16**(7), P. 1209–1214 (1982). (In Russian).
[70] Kronig R.L, Penney W.G. Quantum mechanics of electrons in crystal lattices. *Proc. Roy. Soc.*, **130**, P. 499–513 (1931).
[71] Eyring H., Walter J., Kimball G.E. *Quantum Chemistry.* Wiley, New York, 345 p. (1944).
[72] Eyring H., Lin S.H., Lin S.M. *Basic Chemical Kinetics.* Wiley, New York, 493 p. (1980).
[73] W.Haberditzl. *Structure of Matter and Chemical Bonding.* Mir, oscow, 296 p. (1974). (in Russian).
[74] Moshfegh A.Z. Nanoparticle catalysts. *J.Phys. D:Appl.Phys.*, **42**(23), P. 233001 (2009).
[75] Miller J.T., Krops A.J., Zha Y., Regalluto J.R., L.Delannoy, C.Louis, Bus E., Bokhoven J.A. The effect of gold particle size on Au-Au bond length and toward oxygen in supported catalysts. *J.Catal.*, **240**, P. 222–234 (2006).

NANOSYSTEMS: PHYSICS, CHEMISTRY, MATHEMATICS, 2015, 6 (2), P. 262–267

Particle dynamics in corrugated rectangular billiard

T. Akhmadjanov, E. Rakhimov and D. Otajanov

National University of Uzbekistan, Faculty of Physics,
Department of Optics and laser physics, Tashkent, Uzbekistan

t_akhmadjanov@rambler.ru

PACS 05.20, 05.45 **DOI 10.17586/2220-8054-2015-6-2-262-267**

The particle dynamics in one side corrugated rectangular billiard system is investigated with the help of numerical analysis. The dependence of chaotic behavior in particle dynamics on the corrugation height h is shown. The focusing mechanism of the corrugated billiard is investigated by analyzing the dependence of the total path on particle incident angle.

Keywords: optical fiber, chaos, ray dynamics, corrugated waveguide, Fermi acceleration, billiards.

Received: 2 February 2015

1. Introduction

Particle dynamics in waveguides has attracted much attention during past few decades. Such interest is caused by the potential application of waveguides in different topics of contemporary physics, such as optics, cold atom physics and different systems of nanoscale physics. In most of the cases, particle and wave dynamics in waveguides can be modeled by billiards. The latter are the domains confined by hard or soft walls. Dynamics of waves and particles in such a domain strongly depend on the geometry of its walls. In particular, classical equations of motion can be integrable or non-integrable, depending on the geometrical shape of the billiard boundary. Earlier, billiards were the topic of extensive study in the context of nonlinear dynamics and quantum chaos theory [1–5]. It was found that, depending on the shape of the billiard walls, particle dynamics can be chaotic, regular or mixed. A pioneering study of classical particle dynamics in billiards dates back to Birkhoff, who presented a strict formulation for classical mechanics in confined domains [1]. Later, more strict mathematical analysis of Hamiltonian systems in billiards was provided be Sinai [2]. Currently, billiards has become one of the main paradigms in the theory of deterministic chaos. One of the most convenient realistic systems where billiards can be experimentally realized is microwave resonators [4].

Recently, billiards were successfully applied to describe charge transport in nanoscale quantum dots [6]. Besides static billiards, so-called time-dependent billiards has become subject for extensive research during the past decade [7–10]. Such billiards can be realized in atom optics and provide powerful testing ground for classical and Fermi acceleration [11].

Comprehensive and systematic studies of time-dependent billiards were done by several authors in the Refs. [11–15]. Unlimited growth of the particle velocity was not found to be possible for regular (integrable) billiards, while for some types of chaotic billiards, one can observe such an acceleration [16]. The answer for the question whether the energy of the particle can grow to infinity is far from trivial. It depends on the perturbation type on the boundary and the boundary geometry. It was shown by Loskutov, Ryabov and Akinshin in [17] that Fermi acceleration (FA) will be observed in time-dependent billiards if these billiards possess chaotic properties in the autonomous case. Later, this assumption was confirmed for stadium [18] and annular [15] billiards by the same authors. An elliptical billiard was shown to have regular

dynamics in the case when the billiard has static boundaries, exhibits FA in case when the billiard has time-dependence boundaries. More strict analysis of particle dynamics in time-dependent billiards was provided recently by Robnik and co-authors [16], who derived criteria for the shape and time-dependence of the walls from the viewpoint of Fermi acceleration.

Besides Fermi acceleration, time-dependent billiards have generated a certain interest in fiber optics and waveguides. An important and interesting characteristic of the radiation pulses propagating in the optical fiber is the propagation time of rays through the waveguide. Ray dynamics in the corrugated waveguides are becoming more interesting because of the nature of media where the wave can be propagated are more curved by the external fluctuations. This properties help such systems to create some kind of channel for the waves propagating in it, where the signals can be transmitted effectively with minimal loss of information. A similar problem was also considered and the different fractal properties of ray propagation were shown using an underwater acoustic model. They have shown the mechanism of signal cooling when the width of spatial spectra dispersion is significantly reduced. The open stadium billiard model was investigated in [10] using phase space methods. There, they derived the expression for the long time survival probability function for the stadium billiard with a hole [10]. One of example of time-dependent focusing billiards – a stadium-like billiard with periodically perturbed boundary was studied, explained the origin of the increase and decrease of the particle velocity [11].

In this paper, we study particle dynamics in rectangular billiard with a corrugated wall. The phase space portraits for the two dimensional billiard system are obtained for both flat and corrugated billiards. In the next section, we will present the analytical and numerical analyses in detail. The dependence of the particle trajectory and path on the initial incident angle will also be analyzed.

2. Corrugated rectangular billiard

The system we want to study is the rectangular billiard (side lengths are a and b) with a corrugated wall presented in Fig. 1. The main characteristic to be studied is the coordinate of the particle after N collisions with the billiard walls. We analyze phase space trajectory corresponding to such coordinates.

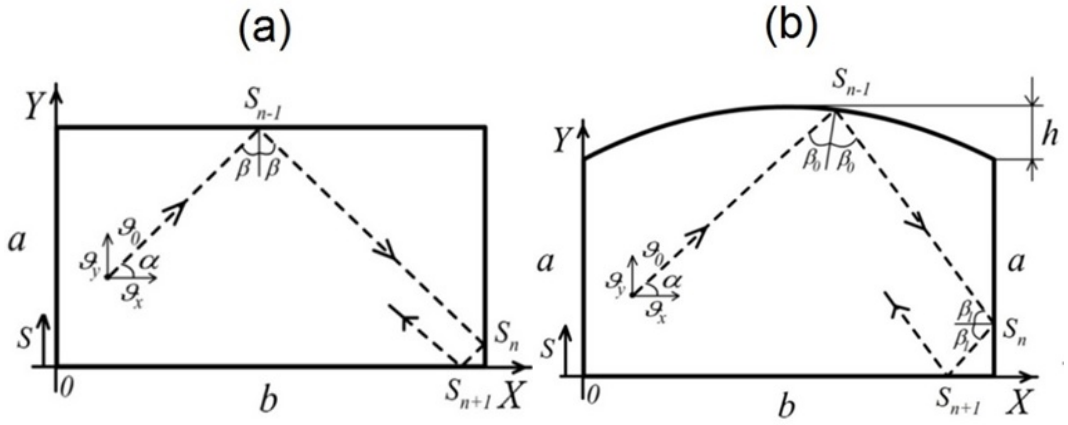

FIG. 1. Billiard model in the form of rectangle with the sides a and b (a) and the same model with corrugated at one side (b)

First, we consider the simple case, a rectangular billiard without corrugation i.e. flat at sides (Fig. 1a), with the sides sizes a and b.

In this case, the boundaries of the billiard will be expressed in XOY plane as follows:

$$\begin{aligned} y(x) &= \begin{cases} a, & \text{if} \quad 0 \le x \le b; \\ 0, \end{cases} \\ x(y) &= \begin{cases} b, & \text{if} \quad 0 \le y \le a. \\ 0, \end{cases} \end{aligned} \tag{1}$$

Here a and b are lengths of the billiard sides.

Let the particle starts its motion at the point of $(x_{0,}y_0) \in XOY$ with the initial velocity v_0:

$$\begin{aligned} v_x &= v_0 \cdot \cos\alpha, \\ v_y &= v_0 \cdot \sin\alpha, \end{aligned}$$

where α is the angle between v_0 and v_x vectors.

Then, one can define the coordinate of the particle after n collision as follows:

$$\begin{aligned} \tau_1 &= \begin{cases} \dfrac{(a-y_n)}{v_y}, & \text{if} \quad v_y \ge 0; \\ \dfrac{y_n}{v_y}, & \text{if} \quad v_y < 0; \end{cases} \\ \tau_2 &= \begin{cases} \dfrac{(b-x_n)}{v_x}, & \text{if} \quad v_x \ge 0; \\ \dfrac{x_n}{v_x}, & \text{if} \quad v_x < 0; \end{cases} \\ t_n &= \min\left(\tau_1, \tau_2\right), \\ x_{n+1} &= x_n + v_x \cdot t_n, \\ y_{n+1} &= y_n + v_y \cdot t_n. \end{aligned} \tag{2}$$

Phase space portraits are given on the plane of the momentum of particle in the direction of billiard walls, $p = v_0 \cdot \sin\beta$ and the path of particle, S.

Using this map (2), phase-space trajectories can be plotted as in Fig. 2 and 3.

Now, we proceed to the case of corrugated billiard presented in Fig. 1b. The corrugation function is given as follows:

$$f(\xi) = 4 \cdot h \cdot \xi \cdot (1-\xi), \tag{3}$$

where $\xi = x/b$, a, b are the rectangular billiard sides and h is the corrugation height.

The boundaries of such a billiard system can be written:

$$\begin{aligned} y(x) &= \begin{cases} a + f(\xi), & \text{if} \quad 0 \le x \le b; \\ 0, \end{cases} \\ x(y) &= \begin{cases} b, & \text{if} \quad 0 \le y \le a + f(\xi). \\ 0, \end{cases} \end{aligned} \tag{4}$$

Trajectories of the particle in such billiard can be given in terms of the following map:

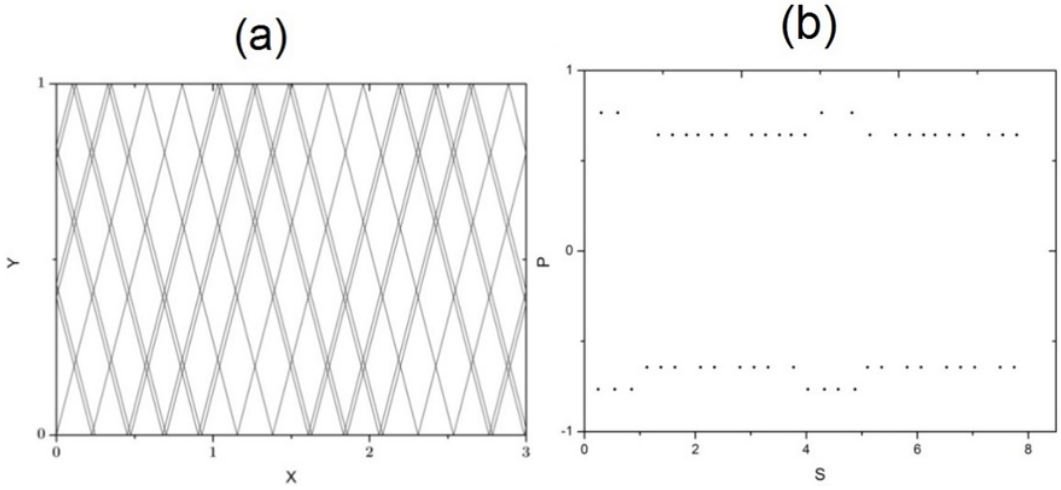

FIG. 2. Trajectory (a) and phase portrait (b) of a particle motion in rectangular billiard for the following billiard parameter values: $a = 1$; $b = 3$; and initial values for the particle: $x_0 = 0$; $y_0 = 0$; $\alpha = 60^\circ$

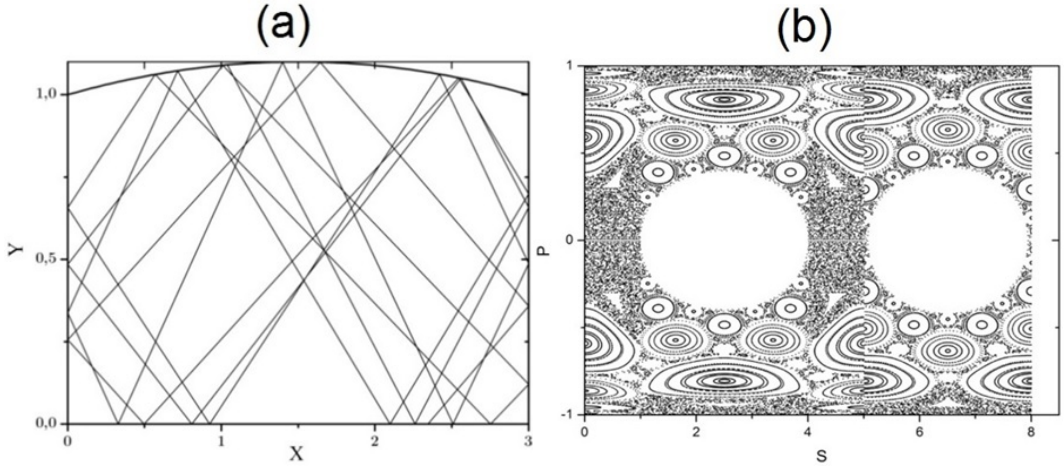

FIG. 3. Particle trajectory (a) and its corresponding phase space portrait (b) for the corrugated rectangular billiard parameters: $a = 1$; $b = 3$; $h = 0.1$

$$\begin{aligned} x_{n+1} &= x_n + v_x \cdot t_n, \\ y_{n+1} &= y_n + v_y \cdot t_n, \\ t_n &= \frac{1}{2A}\left(-B + \sqrt{B^2 - 4AC}\right). \end{aligned} \tag{5}$$

Where the values for the parameters are given as:

$$\begin{aligned} A &= v_x^2, \\ B &= \frac{v_y b^2}{4h} + v_x(2x_n - b), \\ C &= x_n(x_n - b) + \frac{y_n - a}{4h} b^2. \end{aligned}$$

Using this map given in (2), also taking into account the expression (5), we obtain the particle trajectory (Fig. 3a) and its corresponding phase space portrait (Fig. 3b).

One can observe from the Fig. 3 that particle motion is chaotic in this regime, and 'more chaos' can be seen by increasing of h.

If we consider the path of particles after N collision, with the initial values of particle coordinate as $x_0 = 0$, $y_0 = 0$, and for the incident angles range, $0 < \alpha < \pi/2$, we obtain an interesting result for the particle total path, depending on the particle incident angles (Fig. 4).

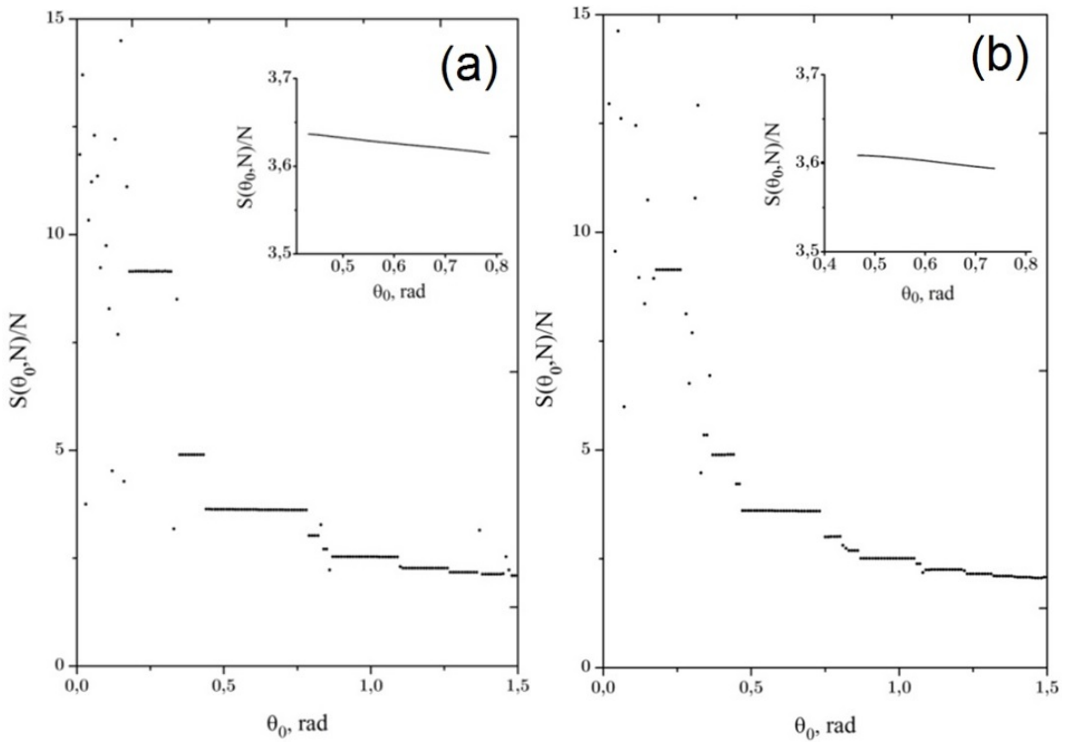

FIG. 4. The dependence of the total path on the incident angle for the parameters $b/a = 3$ and $\Delta\theta_0 = 0.01$ of different values of height of corrugation: $h/a = 0.03$ (a); $h/a = 0.05$ (b). Scaled region is calculated with the resolution of $\Delta\theta_0 = 0.001$

As can be seen from Fig. 4, 'horizontal lines' in the distributions means that particles will have equal paths after N collisions for different particle incident angles. This gives us the potential to focus the particles in needed directions, thus minimizing signal modes in an optical fiber. Moreover, this allows us to say that chaotic behavior will be increased, according to the increase of the corrugation height relative to the billiard side, h/a.

3. Conclusions

Thus, we derived two dimensional map presented by Eq. (5) for the rectangular billiard system with a corrugated wall. Using the numerical calculations, we showed the possibility of focusing particle transport by tuning the corrugation paramaters.

The obtained results can be helpful for the problem of transport and chaos control in different waveguides and acoustic systems.

References

[1] Birkhoff G.D. *Dynamical Systems*. Amer. Math. Soc. Colloquium Publ. 9. Providence: American Mathematical Society, 1927.

[2] Sinai Y.G. Dynamical Systems with Elastic Reflections. Ergodic Properties of Dispersing Billiards. *Russ. Math. Surveys*, **25**, P. 137 (1970).

[3] Abdullaev S.S. and Zaslavskii G.M. Classical nonlinear dynamics and chaos of rays in problems of wave propagation in inhomogeneous media. *Sov. Phys. Usp.*, **34** (8), P. 645 (1991).

[4] G.M. Zaslavsky and S. S. Abdullaev. Chaotic transmission of waves and 'cooling' of signals. *CHAOS*, **7** (1) (1997).

[5] Stoeckmann H.J. *Quantum Chaos – An Introduction*. University Press, Cambridge, UK, 1999, 384 p.

[6] Nakamura K. and Harayama T. *Quantum chaos and quantum dots*. Oxford University Press, Oxford, UK. 2004, 216 p.

[7] Loskutov A.Yu., Ryabov A.B. and Akinshin L.G. Properties of some chaotic billiards with time-dependent boundaries. *J. Phys. A.*, **33**, P. 7973 (2000).

[8] Loskutov A.Yu. and Ryabov A.B. Particle dynamics in time-dependent stadium-like billiards. *J. Stat. Phys.*, **108** (5–6), P. 995 (2002).

[9] Loskutov A.Yu. Dynamical chaos: systems of classical mechanics. *Phys. Usp.*, **50** (9), P. 939 (2007).

[10] Ryabov A.B. and Loskutov A.Yu. Time-dependent focusing billiards and macroscopic realization of Maxwell's Demon. *J. Phys. A.*, **43**, P. 125104 (2010).

[11] Loskutov A.Yu., Ryabov A. and Leonel E.D. Separation of particles in time-dependent focusing billiards. *Physica A*, **389** (23), P. 5408 (2010).

[12] Loskutov A.Yu., et al. Billiards with time-dependent boundaries and some their properties. *Nonlinear dynamics*, **6** (3), P. 573 (2010).

[13] Livorati A.L.P., Loskutov A.Yu. and Leonel E.D. A peculiar Maxwell's Demon observed in a time-dependent stadium-like billiard. *J. Phys. A*, **391** (20), P. 4756 (2012).

[14] Carvalho R.E., de Souza F.C., and Leonel E.D. Fermi acceleration on the annular billiard: a simplified version. *J. Phys. A*, **39** (14), P. 3561 (2006).

[15] Batistić B. and Robnik M. Fermi acceleration in time-dependent billiards: theory of the velocity diffusion in conformally breathing fully chaotic billiards. *J. Phys. A*, **44**, P. 365101 (2011).

[16] Oliveira D.F.M. and Robnik M. Scaling invariance in a time dependent elliptical billiard. *Int. J. of Bifurcation and Chaos*, **22**, P. 1250207 (2012).

[17] Oliveira D.F.M. and Pöschel T. Competition between unlimited and limited energy growth in a two-dimensional time-dependent billiard. *Phys. Lett. A*, **337**, P. 2052 (2013).

[18] Batistić B. Fermi acceleration in chaotic shape-preserving billiards. *Phys. Rev. E*, **89**, P. 022912 (2014).

NANOSYSTEMS: PHYSICS, CHEMISTRY, MATHEMATICS, 2015, 6 (2), P. 268–273

Inverse problem for the identification of a memory kernel from Maxwell's system integro – differential equations for a homogeneous anisotropic media

D. K. Durdiev

Bukhara State University,
Bukhara, Uzbekistan
durdiev65@mail.ru

PACS 02.30.Zz **DOI 10.17586/2220-8054-2015-6-2-268-273**

We consider the problem of reconstructing the time-dependent history of electromagnetic fields from Maxwell's system of equations for an homogeneous anisotropic medium. As additional information, the Fourier image of electric and magnetic field intensity vectors for values $\nu = 0$ of transformation parameter are given. It is shown that if the given functions satisfy some conditions of agreement and smoothness, the solution of the posed problem is uniquely defined in a class of continuously differentiable functions.

Keywords: inverse problem, integro-differential equation, delta function, Fourier transformation, agreement condition.

Received: 12 January 2015

Revised: 16 January 2015

1. Setting up the problem and main result

The unique dependence of D and B (the electric displacement and the magnetic induction, respectively) on E and H (the intensities of the respective fields) at the same instance of time is violated in rapidly varying electromagnetic fields whose frequencies are not small compared with the electric and magnetic polarization onset frequencies typical for the medium. The values of D and B at a given time have been proven to not only depend on E and H, but also on the entire time history of these fields (such a medium is called *a medium with aftereffect*) [1]:

$$\begin{gathered} D(x,t) = \hat{\epsilon}E + \int\limits_0^t \varphi(t-\tau)E(x,t)d\tau, \\ B(x,t) = \hat{\mu}H + \int\limits_0^t \psi(t-\tau)H(x,t)d\tau, \\ E = (E_1, E_2, E_3),\ H = (H_1, H_2, H_3),\ D = (D_1, D_2, D_3), \\ B = (B_1, B_1, B_3),\ x = (x_1, x_2, x_3), \end{gathered} \tag{1}$$

where $\hat{\epsilon} = (\hat{\epsilon}_{ij})_{3\times 3}$ and $\hat{\mu} = (\hat{\mu}_{ij})_{3\times 3}$ are the permittivity and permeability matrices, respectively; $\varphi(t) = \operatorname{diag}(\varphi_1, \varphi_2, \varphi_3)$ and $\psi(t) = \operatorname{diag}(\psi_1, \psi_2, \psi_3)$ are diagonal matrices representing the memory.

Many technically important materials and crystals which have become popular in new technologies are anisotropic. The physical properties of homogeneous isotropic crystals do not depend on the direction and the position inside the medium. At the same time, physical properties of anisotropic crystals essentially depend on orientation and position. An anisotropic crystal is called homogeneous when its physical properties depend on orientation and do not depend on position.

Suppose that, according to (1), the vectors E and H form a solution of the Cauchy problem for the system of Maxwell's equations for homogeneous anisotropic crystals with zero initial data:

$$\nabla \times H = \frac{\partial D(x,t)}{\partial t} + j, \quad \nabla \times E = -\frac{\partial B(x,t)}{\partial t}, \quad (x,t) \in \mathbb{R}^4, \\ E|_{t\le 0} = 0, \quad H|_{t\le 0} = 0. \tag{2}$$

where $j = (j_1, j_2, j_3)$ is the density of the electric current with components $j_i = j_i(x,t)$. The matrices $\hat{\epsilon}$ and $\hat{\mu}$ in equations (1) are assumed to be known constant matrices. Moreover, $\hat{\epsilon}$ – is a symmetric positive definite matrix. We will solve problems (1) and (2) for the case in which the function $j(x,t)$ has the form:

$$j(x,t) = \vec{e}\delta(x)\delta(t), \tag{3}$$

where $\vec{e} = (1,0,0)$ is unit vector; $\delta(x) = \delta(x_1)\delta(x_2)\delta(x_3)$ is the Dirac delta function of the space variable concentrated at $x_1 = 0$, $x_2 = 0$, $x_3 = 0$; $\delta(t)$ is the Dirac delta function of the time variable concentrated at $t = 0$.

The problem in which the vectors $E(x,t)$, $H(x,t)$ should be determined from (1) – (3) for a given matrix functions $\varphi(t)$, $\psi(t)$ will be called the *direct problem*.

Let $\tilde{E} = \left(\tilde{E}_1, \tilde{E}_2, \tilde{E}_3\right)(\nu,t)$, $\tilde{H} = \left(\tilde{H}_1, \tilde{H}_2, \tilde{H}_3\right)(\nu,t)$ be the Fourier image of $E(x,t)$, $H(x,t)$ with respect to $x = (x_1, x_2, x_3) \in \mathbb{R}^3$, respectively, i.e.:

$$\tilde{E}_j(\nu,t) = \int\limits_{R^3} E_j(x,t)e^{i(x,\nu)}dx, \quad \tilde{H}_j(\nu,t) = \int\limits_{R^3} H_j(x,t)e^{i(x,\nu)}dx,$$

$$\nu = (\nu_1, \nu_2, \nu_3) \in \mathbb{R}^3, \quad (x,\nu) = \sum_{\lambda=1}^{3} x_\lambda \nu_\lambda, \quad j = 1,2,3.$$

We pose the following inverse problem: find the functions $\varphi(t) = \mathrm{diag}(\varphi_1, \varphi_2, \varphi_3)$, $\psi(t) = \mathrm{diag}(\psi_1, \psi_2, \psi_3)$ occurring in the integral in equations (1) from the information on the Fourier image $\tilde{E}$, $\tilde{H}$ of the electric and magnetic fields at an arbitrary time $t \ge 0$ for the values $\nu = 0$ of the Fourier transformation:

$$\left(\tilde{E}_1, \tilde{E}_2, \tilde{E}_3,\ \tilde{H}_1, \tilde{H}_2, \tilde{H}_3\right)(0,t) = g(t), \quad g(t) = (g_1, g_2, ..., g_6). \tag{4}$$

Definition. *Solutions of the inverse problem are matrix functions $\varphi(t)$ and $\psi(t)$, such that the corresponding solution of problem (1) –(3) satisfies condition (4).*

Among the problems devoted to determining a sub-integral function, belonging to hyperbolic equations, we note works [2,3]. In work [2], the problem of determining the memory, belonging to a three-dimensional wave equation with delta function at the right side is investigated. Furthermore, in work [3], this problem is generalized in the case of hyperbolic equation of the second order with constant main part and variable coefficients at minor derivatives. Similar problems with distributed sources of disturbance are seen in

works [4,5]. In article [6], the problem of reconstructing the time history of an electric field from the electrodynamic equation is investigated. Also, we recall that papers [7,8,9,10] are concerned with the determination of memory kernel from integro-differential equations with an integral of convolution type. In the present paper, we consider the problem of reconstructing the time-dependent history of the electromagnetic fields from Maxwell's system of equations for an anisotropic medium. It is shown that if the vector function $g(t)$ satisfies some conditions of agreement and smoothness, the solution to the inverse problem is uniquely defined in a class of continuously differentiable functions on the intercept $[0,T]$, where T is any positive fixed number.

The main result of the present paper is the following theorem.

Theorem. *Suppose that* $g(t) \in C^2[0,T]$, $g(0) \neq 0$ *and the agreement conditions:*

$$\sum_{k=1}^{3} \hat{\epsilon}_{1k} g_k(0) = -1, \quad \sum_{k=1}^{3} \hat{\epsilon}_{ik} g_k(0) = 0, \quad i = 2,3; \quad \sum_{k=1}^{3} \hat{\mu}_{jk} g_{3+k}(0) = 0, \quad j = 1,2,3$$

hold. Then, the inverse problem (1) –(4) has a unique solution $(\varphi(t), \psi(t)) \in \mathbb{C}^1[0,T]$ *for any fixed* $T > 0$.

2. Maxwell's equations as a first order symmetric hyperbolic system

Equations (1) –(3) can be written as the following first order symmetric hyperbolic system:

$$A_0 \frac{\partial V}{\partial t} + \sum_{i=0}^{3} A_i \frac{\partial V}{\partial x_i} + \Phi_0 V + \int_0^t \Phi'(t-\tau) V(x,\tau) d\tau = F(x,t), \tag{5}$$

with the initial condition:

$$V|_{t \leq 0} = 0, \tag{6}$$

where:

$$A_0 := \begin{pmatrix} \hat{\epsilon} & 0 \\ 0 & \hat{\mu} \end{pmatrix}_{6\times 6}, \quad A_j := \begin{pmatrix} 0 & A_j^1 \\ (A_j^1)^* & 0 \end{pmatrix}_{6\times 6}, \quad A_1^1 := \begin{pmatrix} 0 & 0 & 0 \\ 0 & 0 & 1 \\ 0 & -1 & 0 \end{pmatrix},$$

$$A_2^1 := \begin{pmatrix} 0 & 0 & -1 \\ 0 & 0 & 0 \\ 1 & 0 & 0 \end{pmatrix}, \quad A_3^1 := \begin{pmatrix} 0 & 1 & 0 \\ -1 & 0 & 1 \\ 0 & 0 & 0 \end{pmatrix}, \quad \Phi_0 := \begin{pmatrix} \varphi(0) & 0 \\ 0 & \psi(0) \end{pmatrix}_{6\times 6},$$

$$\Phi'(t) := \begin{pmatrix} \varphi'(t) & 0 \\ 0 & \psi'(t) \end{pmatrix}_{6\times 6}, \quad V := (E,H)^*, \quad F := (-j,\ 0_{1\times 3})^*;$$

* is the symbol of transposition; $0_{1\times 3}$ denote the vector line with elements $0,0,0$; $\Phi'(t) := (\partial/\partial t)\Phi(t)$.

We apply to both parts of (5) and (6) the Fourier transformation. The Fourier transform of the vector function $V(x,t)$ exists at any finite t, since the vector function $V(x,t)$ as the solution of the direct problem (5) and (6) is a sum of a certain singular generalized vector function and a regular vector function, the support of the vector function $V(x,t)$ being finite [11, chapter 4]. For any fixed ν, the vector function $\tilde{V}(\nu,t)$ ($\tilde{V}(\nu,t)$ – the Fourier transformation of $V(x,t)$ with respect to x) satisfies differential equation:

$$A_0\frac{\partial\tilde{V}}{\partial t} - iB\tilde{V} + \int\limits_0^t \Phi'(t-\tau)\tilde{V}(\nu,\tau)d\tau = \tilde{F}(t), \tag{7}$$

the initial, and as follows from (4), the supplementary conditions, respectively:

$$\tilde{V}|_{t\leq 0} = 0, \tag{8}$$

$$\tilde{V}|_{\nu=0} = g(t), \quad g(t) = (g_1, g_2, ..., g_6), \quad t \geq 0. \tag{9}$$

In equation (7), we denoted $B := \sum_{j=1}^{3}\nu_j A_j + \Phi_0$, $\tilde{F}(t) = -\vec{e_0}\delta(t)$, $\vec{e_0} := (1,0,0,0,0,0)^*$.

We compute A_0^{-1}, which is the inverse to A_0. If we denote by $\epsilon = (\epsilon_{ij})$, $\mu = (\mu_{ij})$ the matrices which are the inverse to $\hat{\epsilon}$, $\hat{\mu}$, respectively, then:

$$A_0^{-1} = \begin{pmatrix} \epsilon & 0 \\ 0 & \mu \end{pmatrix}_{6\times 6}.$$

When we multiply the left-hand side of (7) by A_0^{-1}, we get:

$$I\frac{\partial\tilde{V}}{\partial t} - iC\tilde{V} + \int\limits_0^t \Psi(t-\tau)\tilde{V}(\nu,\tau)d\tau = F_0, \tag{10}$$

where I is the identity matrix,

$$C := \begin{pmatrix} \epsilon\varphi(0) & \epsilon\Sigma_{i=0}^{3}\nu_i A_i^1 \\ \mu\Sigma_{i=0}^{3}\nu_i \left(A_i^1\right)^* & \mu\psi(0) \end{pmatrix}_{6\times 6},$$

$\Psi(t) := A_0^{-1}\Phi'(t)$, $F_0 := A_0^{-1}\tilde{F} = -A_0^{-1}\vec{e_0}\delta(t)$.

Thus, inverse problems (1) – (4) are reduced to the problem of determining the kernel $\Psi(t)$ of the integral part in equation (10) on the bases of equalities (8) – (10).

3. Proof of the main result

We integrate the differential equation (10). Using the initial condition (8), one gets:

$$\tilde{V}(\lambda,t) = -A_0^{-1}\vec{e_0} + iC\int\limits_0^t \tilde{V}(\lambda,\tau)d\tau - \int\limits_0^t\int\limits_0^\tau \Psi(\alpha)\tilde{V}(\lambda,\tau-\alpha)d\alpha d\tau. \tag{11}$$

Taking into account (9), from the equality (11) we obtain:

$$g(t) = -A_0^{-1}\vec{e_0} + iC_0\int\limits_0^t g(\tau)d\tau + \int\limits_0^t \Psi(\alpha)\int\limits_\alpha^t g(\tau-\alpha)d\tau d\alpha, \quad t > 0, \tag{12}$$

where $C_0 := A_0^{-1}\Phi_0$. By differentiating the equation (12), we derive:

$$\int\limits_0^t \Psi(\tau)g(t-\tau)d\tau = g'(t) - iC_0 g(t). \tag{13}$$

In the equality, assuming $t = 0$ and taking into account $C_0 = A_0^{-1}\Phi_0$, we get:

$$g' = iA_0^{-1}\Phi_0 g(0).$$

It follows from the last equation that the elements of the matrix Φ_0 are expressed by the known numbers:

$$\varphi_i(0) = -\frac{i}{g_i(0)} \sum_{k=1}^{3} \hat{\epsilon}_{ik} g'_k(0); \quad \psi_i(0) = -\frac{i}{g_{3+i}(0)} \sum_{k=1}^{3} \hat{\mu}_{ik} g'_{3+k}(0), \quad i = 1, 2, 3.$$

Furthermore, constants $\varphi_i(0)$, $\psi_i(0)$, $i = 1, 2, 3$ will be assumed as knowns.

From (13), by differentiating, we obtain:

$$\Psi(t)g(0) + \int_0^t \Psi(\tau) g'(t-\tau) d\tau = g''(t) - iA_0^{-1} g'(t).$$

When we multiply the left-hand part of the last equality by A_0, we find:

$$\Phi'(t)g(0) + \int_0^t \Phi'(\tau) g'(t-\tau) d\tau = A_0 g''(t) - i\Phi_0 g'(t).$$

The last equality is the linear integral second-order equation of Volterra type with respect to the matrix function $\Phi'(t)$. It can be written relative to the components of matrix $\Phi'(t)$. They are as follows:

$$\varphi'_j(t) + \int_0^t \varphi'_j(\tau) \frac{g'_j(t-\tau)}{g_j(0)} d\tau = \frac{1}{g_j(0)} \left\{ \sum_{k=1}^{3} \hat{\epsilon_{jk}} g''_k - i\varphi_j(0) g'_k(t) \right\}, \quad j = 1, 2, 3; \tag{14}$$

$$\psi'_j(t) + \int_0^t \psi'_j(\tau) \frac{g'_{3+j}(t-\tau)}{g_{3+j}(0)} d\tau = \frac{1}{g_{3+j}(0)} \left\{ \sum_{k=1}^{3} \hat{\mu_{jk}} g''_{3+k}(t) - i\psi_j(0) g'_{3+k}(t) \right\}, \quad j = 1, 2, 3. \tag{15}$$

To integral equations (14) and (15), we combine the following obvious relations:

$$\varphi_j(t) - \int_0^t \varphi'_j(\tau) d\tau = \varphi_j(0), \quad \psi_j(t) - \int_0^t \psi'_j(\tau) d\tau = \psi_j(0), \quad j = 1, 2, 3. \tag{16}$$

Equations (14) – (16) are the linear integral second-order equations of the Volterra type with respect to unknown functions φ'_i, φ_i, ψ'_i, ψ_i, $i = 1, 2, 3$. As known, these equations have unique solutions.

References

[1] Landau L. D. and Lifshits E. M. Continuum Electrodynamics. Nauka, Moscow, 1959. (in Russian)

[2] Durdiev D. K. An inverse problem for a three-dimensional wave equation in the medium with memory. *Math. Anal. and Disc. Math.*, Novosibirsk, NGU, P. 19–26 (1989). (in Russian)

[3] Durdiev D. K. To the question of correctness of one inverse problem for hyperbolic integro-differential equation. *Sib. Math. Journ.*, **33** (3), P. 69–77 (1992). (in Russian)

[4] Lorensi A. An identification problem related to a nonlinear hyperbolic integro-differential equation. *Nonlinear Analysis: Theory, Methods and Applications*, **22**, P. 297–321 (1994).

[5] Janno J. and Von Welfersdorf L. Inverse problems for identification of memory kernels in viscoelasticity. *Math. Methods in Appl. Sciences*, **20** (4), P. 291–314 (1997).

[6] Durdiev D. K. Global solvability of an inverse problem for an integro-differential equation of electrodynamics. *Differential Equations*, (44) (7), P. 893–899 (2008).
[7] Jaan J. and Von Wolfersdorf L. An inverse problem for identification of a time- and space-dependent memory kernel in viscoelasticity. *Inverse Problems*, **17**, P. 13–24 (2001).
[8] Colombo F. and Guidetti D. A global in time existence and uniqueness result for a semilinear integrodifferential parabolic inverse problem in Sobolev spaces. *Math. Methods in Appl. Sciences*, **17**, P. 1–29 (2007).
[9] Colombo F. and Guidetti D. Some results on the Identification of memory kernels. *Oper. Theory: Adv. Appl.*, **216**, P. 121–138 (2011).
[10] Favaron A. Identification of Memory Kernels Depending on Time and on an Angular Variable. *Zeitschrift fur Analysis und ihre Anwendungen*, **24**, (4), P. 735–762 (2005).
[11] Romanov V. G. *Inverse problems of mathematical physics*. Nauka, Moscow, 1984. (in Russian)

NANOSYSTEMS: PHYSICS, CHEMISTRY, MATHEMATICS, 2015, 6 (2), P. 274–279

Renyi entropy for the doped graphene at low temperatures

N. N. Konobeeva[1], A. A. Polunina[1], M. B. Belonenko[1,2]

[1]Volgograd State University, Volgograd, Russia

[2]Volgograd Institute of Business, Volgograd, Russia

yana_nn@inbox.ru, polunina_a@mail.ru, mbelonenko@yandex.ru

PACS 72.80.Vp, 73.22.Pr **DOI 10.17586/2220-8054-2015-6-2-274-279**

The distribution function for the perimeter of a simply connected cluster containing undoped lattice sites is based on percolation theory and the hypothesis of scale invariance. The Renyi entropy for doped graphene at low temperatures was calculated on the basis of this distribution function.

Keywords: nanostructure, graphene, Renyi entropy.

Received: 24 November 2014

Revised: 2 December 2014

Final revision: 16 December 2014

1. Introduction

Renyi entropy plays an important role in various fields of human activity: in ecology and statistics as the diversity index, in quantum information – as a measure of complexity, in statistical mechanics – to describe quantum dissipative systems [1, 2]. The most important areas for the application of entropy are quantum-mechanical and relativistic objects. The applications of entropy are of great interest in quantum physics and astrophysics. It is just enough to merely mention one of the most important results of black hole thermodynamics: the entropy of a black hole is equal to one quarter of its surface area (the area of the event horizon) (Hawking, 1978) [3].The broad appeal of the formulas of the type $s \sim k \sum p \log(p)$ in different areas may be linked to the special role of power laws in nature [4]. For such cases, the expression $p \log(p)$ is a convenient additive measure. Many scientific papers concerning Renyi entropy and entanglement have been published recently [5] – the phenomenon in which quantum state objects are interdependent even passing between them through space. The spectral complexity and entropy concept is becoming a powerful tool to gain access to such universal values as Central charge, which is associated with the conformal field theory and used to describe the main conditions and their degeneration. This effect can also be useful for quantum computing or quantum cryptography.

It should be noted that graphene electrons near the Fermi level are described with the conformal field theory (in this case the Dirac equations reduce to the Laplace equation). Additionally, technology development allows one to form a graphene field with different boundaries (including limited boundaries) [6-8], which makes possible experimental verification of the consequences of the conformal theories and of the applications to quantum information theory.

2. The statement of the problem

The main result of the use of conformal field theory states that the Renyi entropy can be found from the formula [9]:

$$s_n = \frac{n+1}{6n} \ln\left(\frac{L}{a}\right), \tag{1}$$

here, a is the lattice constant, L is the perimeter of the closed path (in units of a), n is the order of entropy. Higher values of n, directing to infinity, give the Renyi entropy, which is greatly determined by considering only the highest probability events. Lower values of n, tending to zero, give the Renyi entropy, which increasingly considers all possible events more uniformly, regardless their probabilities.

After averaging according to the size of the cluster, formula (1), under the assumption of the power distribution function, gives:

$$s_n = \frac{n+1}{6n} \int_a^\infty \ln\left(\frac{L}{a}\right)\left(\frac{L}{a}\right)^\beta dL. \tag{2}$$

This integral converges when $\beta \leqslant -2$.

Here, it is necessary to make a major retreat. It is possible to describe the behavior of the main variables by a power law (it is well-known fact from the theory of phase transitions in the critical region near the phase transition point where the fluctuations are particularly large). The corresponding indicators are called critical exponents. Such behavior has been obtained in the framework of scaling theory, and other approaches. Actually, the existence of scaling [10] means that in the system (in the area near-critical), there is no allocated length scale and fluctuations can have an arbitrarily large amount of spatial correlation. So, it is reasonable to assume that the dependence of the distribution function upon the perimeter will be of power-law form, with the index, which will be defined below.

It should be noted that the power distribution function follows from scale invariance theory. The scale invariance theory is based on a power dependence of some properties, and the exponent depends on the dimension of space and the symmetry of the system [11].Thus, the calculation of the Renyi entropy is reduced to the problem of determining the index β. This has been solved by modeling methods.

The principle of modeling distribution of admixtures on the surface of a hexagonal lattice of a graphene was used in this case (Fig. 1). It was assumed that the electron cannot access the area (nodes, node) occupied by the admixture. In areas which are not occupied by admixtures, electron motion is described by the well-known Dirac equation for graphene [12]:

$$H\psi = i\hbar\frac{d\psi}{dt}, H = -i\hbar\upsilon_f\bar{\sigma}\cdot\bar{\nabla}. \tag{3}$$

At the Fermi level, this equation is reduced to the conformal theory with the central charge c = 1.

3. The simulation of the confined areas

Electrons in graphene have a band structure and move on the lattice sites freely [13]. However, with the appearance in the graphene lattice sites of impurity atoms forming carbon bond, the site becomes unavailable for an electron, which is located in the conduction band. I.e. there is a border, and in the case of the first approximation value of the potential barrier for electrons can be considered as infinity, because of the site unavailability. In the wave approximation, the modeling problem of electron motion was solved in paper [14]. It is

worth noting that electron motion at the lattice sites does not distort the bond lengths or local charge density, since the electron is already in the conduction band (i.e., electron is delocalized).

It should also be noted that the units engaged with impurity atoms are unavailable for electrons. This leads to distortion of the band structure. For example, when an electron moves in a limited area, which is described by equation (3), there are discrete energy levels and not all values of the electron momentum are allowed. The remaining electron in the conduction band, because of the reflection of the "walls" formed by impurity atoms and further interference, can have only certain values of momentum and energy. The closest analogue is a classic resonator which carves out a certain frequency range. Since the impurities are randomly distributed and the border region has a complex shape, in the general case, the spectrum is continuous but there are features in the density of states described by Anderson [15].

The points of intersection of the lines are called nodes, the lines will be called links or edges. The confined areas, made up of relations – clusters, otherwise are called the corrals.

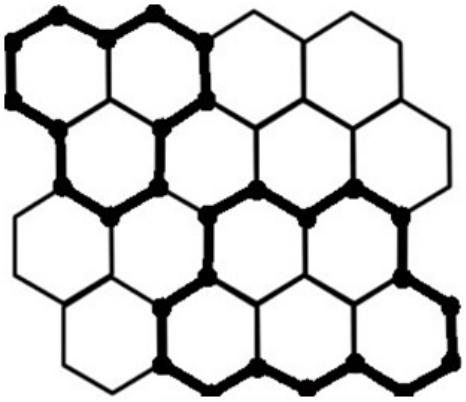

Fig. 1. Confined clusters

To find the clusters, we will solve the problem of relations, that is, we will need to store information about the edges, but not about the actual nodes.

The first stage of simulation is to place admixtures in the nodes of a hexagonal lattice. Since the percolation threshold for a hexagonal lattice is - 0.67, then the total number of nodes occupied by the electrons should be equal to 67% or even higher.

The algorithm for finding the corrals is based on Lee's algorithm (breadth-first search).

Figure 2 shows the initial distribution of admixtures and the found endless paths after performing the algorithm.

At the next stage, the connection between the number of closed paths and the length of the closed path was shown. After approximation, it has the form (Figure 3).

This dependence is approximated by the formula:

$$y \sim x^{-2.97}, \tag{4}$$

and gives $\beta \simeq -3$.

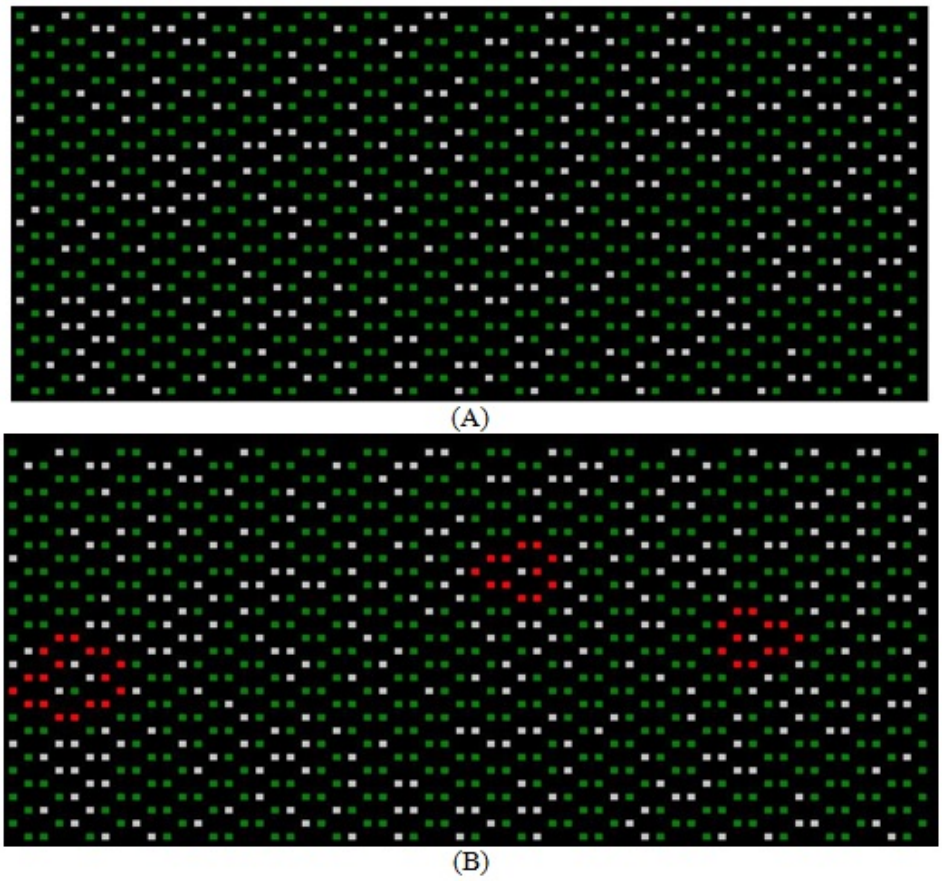

FIG. 2. The distribution of electrons on a hexagonal lattice: (A) before performing the algorithm; (B) after performing the algorithm

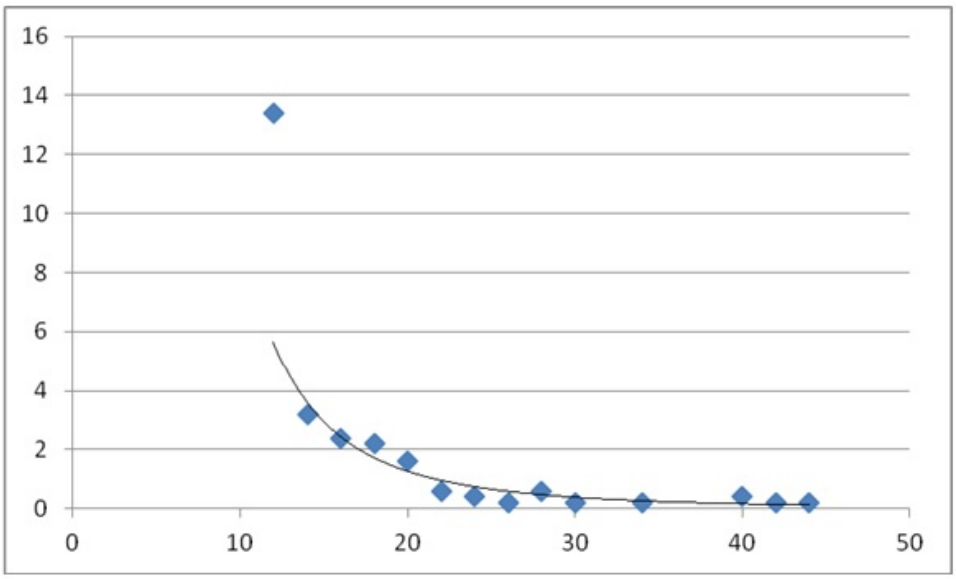

FIG. 3. A plot of the number of closed paths of the length of the closed path

4. The summary and conclusions

In our case, if $\beta \simeq -3$, we obtain the following expression for Renyi entropy:

$$s_n = \frac{n+1}{24n}. \tag{5}$$

The dependence of the Renyi entropy of its order is shown in Figure 4.

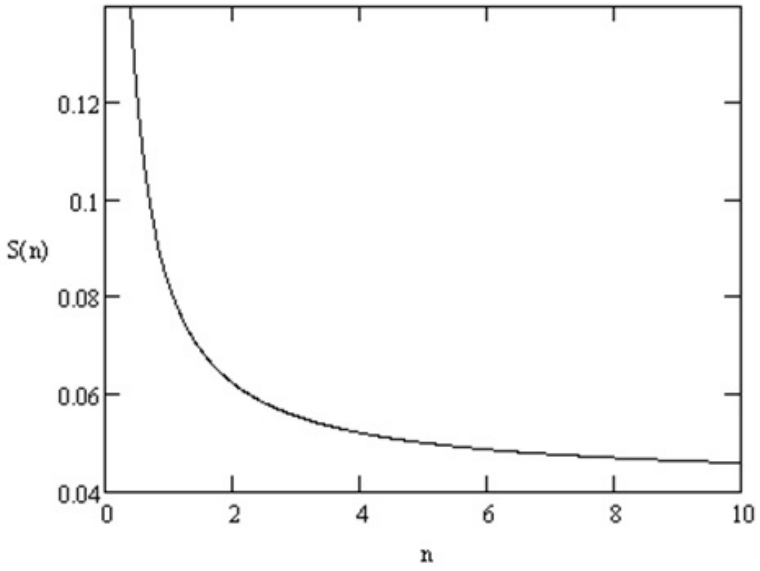

FIG. 4. The dependence of the Renyi entropy upon its order

In conclusion, we will now formulate the main outcomes of this work.

(1) Based on the algorithm of Lee, an algorithm was developed for finding the closed paths containing the electrons of the admixture;
(2) A dependence was constructed for the number of closed paths from their length near the percolation threshold.
(3) The form of the power function was determined, which allowed calculation of the Renyi entropy for doped graphene.
(4) The obtained results can be used to determine the thermodynamic characteristics of doped graphene.

Acknowledgments

This work was supported by the Russian Foundation for Basic Research under project No. 12-02-31654.

References

[1] Kirchanov V.S. Using the Renyi entropy to describe quantum dissipative systems in statistical mechanics. *Theoretical and Mathematical Physics*, **156**(3), P. 444–453 (2008).
[2] Chumak O.V. *Entropy and fractals in data analysis*. Moscow, Izhevsk: SRC "Regular and Chaotic Dynamics", Institute of Computer Science, 164 p. (2011).
[3] Hawking S.W. *Black hole and thermodynamics collection of articles "Black hole". News of fundamental physics*. Issue 9. P. 204–221 (1978).
[4] Schroeder M. *Fractals, Chaos, Power Laws*. Moscow, Izhevsk: R&C Dynamics, 527 p. (2001).
[5] Assaad F.F., Lang T.C., Parisen Toldin F. Entanglement Spectra of Interacting Fermions in Quantum Monte Carlo Simulations (2013). (http://arxiv.org/pdf/1311.5851.pdf).

[6] Xiong H., Wu B. Atomic Quantum Corrals for Bose-Einstein Condensates. *Phys. Rev. A.*, **82**, P. 053634 (2010).
[7] Rossi E., Morr D.K. Spatially dependent Kondo effect in Quantum Corrals. *Phys. Rev. Lett.*, **97**, P. 236602 (2006).
[8] Novoselov K.S., Geim A.K., Morozov S.V., Jiang D., Katsnelson M.I., Grigorieva I.V., Firsov A.A. Two-dimensional gas of massless Dirac fermions in graphene. *Nature*, **438**, P. 197 (2005).
[9] Datta S., David J.R. Renyi entropies of free bosons on the torus and holography (2013). (http://arxiv.org/pdf/1311.1218.pdf).
[10] Patashinskii A.Z., Pokrovskii V.L. *Fluctuation theory of phase transitions.* Moscow: Nauka, 381 p. (1982).
[11] Müller H. Scaling as a fundamental property of natural vibrations of matter and the fractal structure of space-time. *Foundations of physics and geometry.* P. 189–209 (2008).
[12] Gusynin V. P., Shaparov S.G., Carbotte J.P. AC conductivity of graphene: from tight-binding model to 2+1-dimensional quantum electrodynamics. *Int. J. Mod. Phys. B.*, **21**, P. 4611–4658 (2007).
[13] Castro Neto A.H., Guinea F., Peres N.M.R., Novoselov K.S., Geim A.K. The electronic properties of graphene. *Rev. Mod. Phys.*, **81**, P. 109 (2009).
[14] Logemann R., Reijnders K.J.A., Tudorovskiy T., Katsnelson M.I., Yuan S. Modeling Klein Tunneling and Caustics of Electron Waves in Graphene (2014). (http://arxiv.org/pdf/1409.1277v1.pdf).
[15] Gantmaher V.F. *Electrons in disordered media.* Moscow: Fizmatlit, 288 p. (2013).

NANOSYSTEMS: PHYSICS, CHEMISTRY, MATHEMATICS, 2015, 6 (2), P. 280–293

Universality of the discrete spectrum asymptotics of the three-particle Schrödinger operator on a lattice

Mukhiddin I. Muminov[1], Tulkin H. Rasulov[2]

[1]Faculty of Scince, Universiti Teknologi Malaysia (UTM)
81310 Skudai, Johor Bahru, Malaysia
[2]Faculty of Physics and Mathematics, Bukhara State University
M. Ikbol str. 11, 200100 Bukhara, Uzbekistan
mmuminov@mail.ru, rth@mail.ru

PACS 02.30.Tb **DOI 10.17586/2220-8054-2015-6-2-280-293**

In the present paper, we consider the Hamiltonian $H(K)$, $K \in \mathbb{T}^3 := (-\pi;\pi]^3$ of a system of three arbitrary quantum mechanical particles moving on the three-dimensional lattice and interacting via zero range potentials. We find a finite set $\Lambda \subset \mathbb{T}^3$ such that for all values of the total quasi-momentum $K \in \Lambda$ the operator $H(K)$ has infinitely many negative eigenvalues accumulating at zero. It is found that for every $K \in \Lambda$, the number $N(K;z)$ of eigenvalues of $H(K)$ lying on the left of z, $z < 0$, satisfies the asymptotic relation $\lim\limits_{z\to-0} N(K;z)|\log|z||^{-1} = \mathcal{U}_0$ with $0 < \mathcal{U}_0 < \infty$, independently on the cardinality of Λ.

Keywords: Three-particle Schrödinger operator, zero-range pair attractive potentials, Birman-Schwinger principle, the Efimov effect, discrete spectrum asymptotics.

Received: 18 January 2015

1. Introduction

We are going to discuss the following remarkable phenomenon of the spectral theory of the three-particle Schrödinger operators, known as the *Efimov effect*: if a system of three particles interacting through pair short-range potentials is such that none of the three two-particle subsystems has bound states with negative energy, but at least two of them have a zero energy resonance, then this three-particle system has an infinite number of three-particle bound states with negative energy accumulating at zero.

The Efimov effect was discussed in [1] for the first time. Since then, this problem has been studied on a physical level of rigor in [2, 3]. A rigorous mathematical proof for the existence of Efimov's effect was originally carried out in [4], and subsequently, many works have been devoted to this subject, see for example [5–9]. The main result obtained by Sobolev [7] (see also [9]) is an asymptotics of the form $\mathcal{U}_0|\log|z||$ for the number $N(z)$ of eigenvalues on the left of z, $z < 0$, where the coefficient $\mathcal{U}_0$ does not depend on the two-particle potentials v_α and is a positive function of the ratios m_1/m_2 and m_2/m_3 of the masses of the three particles.

In models of solid state physics [10–12] and also in lattice quantum field theory [13], one considers discrete Schrödinger operators, which are lattice analogs of the three-particle Schrödinger operator in continuous space. The presence of Efimov's effect for these operators was demonstrated at the physical level of rigor without a mathematical proof for a system of three identical quantum particles in [10, 11].

In the continuous case [14] (see also [12, 15]), the energy of the center-of-mass motion can be separated out from the total Hamiltonian, that is, the energy operator can be split into the sum of the center-of-mass motion and the relative kinetic energy so that the

three-particle bound states are eigenvectors of the relative kinetic energy operator. Therefore, Efimov's effect either exists or does not exist for all values of the total momentum simultaneously.

In lattice terms, the center-of-mass corresponds to a realization of the Hamiltonians as fibered operators, that is, as the direct integral of a family of operators $H(K)$ depending on the values of the total quasi-momentum $K \in \mathbb{T}^3 := (-\pi;\pi]^3$ (see [12]). In this case, a bound state is an eigenvector of the operator $H(K)$ for some $K \in \mathbb{T}^3$. Typically, this eigenvector depends continuously on K. Therefore, Efimov's effect may exist only for some values of $K \in \mathbb{T}^3$.

The presence of the Efimov effect for three-particle discrete Schrödinger operators was proved in [16–18] and asymptotic formulas for the number of eigenvalues were obtained in [16, 17], which are analogous to the results of [7, 9].

In the present paper, we consider a system of three arbitrary quantum particles on the three-dimensional lattice interacting via zero-range potentials with the dispersion function of the form $\varepsilon(p) = \sum\limits_{i=1}^{3}(1-\cos(np^{(i)}))$ with $n > 1$. We denote by Λ the set of points of $\mathbb{T}^3$ where the function $\varepsilon(\cdot)$ takes its (global) minimum. If at least two of the two-particle operators have a zero energy resonance and third one is non-negative, then we prove that for all $K \in \Lambda$, the three-particle discrete Schrödinger operator $H(K)$ has infinitely many negative eigenvalues accumulating at zero. Moreover, for any $K \in \Lambda$, we establish the asymptotic formula

$$\lim_{z\to-0} N(K;z)|\log|z||^{-1} = \mathcal{U}_0 \quad (0 < \mathcal{U}_0 < \infty),$$

where $N(K;z)$ is the number of eigenvalues of $H(K)$ lying on the left of z, $z < 0$.

It is surprising that the asymptotics for $N(K;z)$ is the same for all $K \in \Lambda$ and is stable with respect to the number n. Recall that in all papers devoted to Efimov's effect for lattice systems, the existence of this effect has been proved only for the zero value of the quasi-momentum ($K = 0$) and for the case $n = 1$. In [19], for all non-trivial values of total quasi-momentum ($K \neq 0$), the finiteness of the discrete spectrum of a system of three bosons on a lattice was proven when the corresponding two-particle operator has a zero energy resonance.

The plan of this paper is as follows: Section 1 is an introduction to the whole work. In Section 2, the Hamiltonians of two- and three-particle systems are described as bounded self-adjoint operators in the corresponding Hilbert spaces and the main result of the paper is formulated. In Section 3, we discuss some results concerning threshold analysis of the two-particle operator $h_\alpha(k)$. In Section 4, we give a modification of the Birman-Schwinger principle for $H(K)$, $K \in \mathbb{T}^3$. In Section 5, we obtain an asymptotic formula for the number of negative eigenvalues of $H(K)$, $K \in \Lambda$.

Throughout the present paper, we adopt the following conventions: For each $\delta > 0$, the notation $U_\delta(p_0) := \{p \in \mathbb{T}^3 : |p - p_0| < \delta\}$ stands for a δ-neighborhood of the point $p_0 \in \mathbb{T}^3$. The subscripts α, β, γ are pair-wisely different and takes values from $\{1, 2, 3\}$.

2. Description of the three-particle operator

Let $\mathbb{Z}^3$ be the three-dimensional lattice and $l_2((\mathbb{Z}^3)^m)$ be the Hilbert space of square-summable functions on $(\mathbb{Z}^3)^m$, $m = 2, 3$. The free Hamiltonian $\widehat{H}_0$ of a system of three arbitrary quantum mechanical particles on $\mathbb{Z}^3$ in the coordinate representation is usually

associated with the following bounded self-adjoint operator on the Hilbert space $l_2((\mathbb{Z}^3)^3)$:

$$(\widehat{H}_0\widehat{\psi})(x_1,x_2,x_3)=\sum_{s\in\mathbb{Z}^3}[\widehat{\varepsilon}_1(s)\widehat{\psi}(x_1+s,x_2,x_3)+\widehat{\varepsilon}_2(s)\widehat{\psi}(x_1,x_2+s,x_3)+\widehat{\varepsilon}_3(s)\widehat{\psi}(x_1,x_2,x_3+s)],$$

where $\widehat{\varepsilon}_\alpha(\cdot)$, $\alpha=1,2,3$ are dispersion functions describing the particle transition from a site to a neighboring site defined by:

$$\widehat{\varepsilon}_\alpha(s):=\begin{cases}\dfrac{3}{m_\alpha} & \text{as} \quad s=0;\\ -\dfrac{1}{2m_\alpha} & \text{as} \quad s=\pm ne_i,\ i=1,2,3;\\ 0 & \text{otherwise.}\end{cases}$$

Here, $m_\alpha>0$ are different numbers, having the meaning of a mass of the particle α, $\alpha=1,2,3$, the elements e_i, $i=1,2,3$ are unit orts on $\mathbb{Z}^3$ and n is a fixed positive integer with $n>1$.

It is easily seen that the function $\widehat{\varepsilon}_\alpha(\cdot)$ is even on $\mathbb{Z}^3$.

The three-particle Hamiltonian $\widehat{H}$ of the quantum-mechanical three particle systems with two-particle interactions $\widehat{v}_{\beta\gamma}$, $\beta,\gamma=1,2,3$ in the coordinate representation is a bounded perturbation of the free Hamiltonian $\widehat{H}_0$:

$$\widehat{H}=\widehat{H}_0-\widehat{V}_1-\widehat{V}_2-\widehat{V}_3,$$

where $\widehat{V}_\alpha$, $\alpha=1,2,3$ are multiplication operators on the Hilbert space $l_2((\mathbb{Z}^3)^3)$

$$(\widehat{V}_\alpha\widehat{\psi})(x_1,x_2,x_3)=\widehat{v}_{\beta\gamma}(x_\beta-x_\gamma)\widehat{\psi}(x_1,x_2,x_3)=\mu_\alpha\delta_{x_\beta x_\gamma}\widehat{\psi}(x_1,x_2,x_3),\quad \widehat{\psi}\in l_2\left((\mathbb{Z}^3)^3\right).$$

Here, $\mu_\alpha>0$ is the interaction energy of the particles β and γ, $\delta_{x_\beta x_\gamma}$ is the Kronecker delta.

It is clear that the three-particle Hamiltonian $\widehat{H}$ is a bounded self-adjoint operator on the Hilbert space $l_2((\mathbb{Z}^3)^3)$.

Similarly, as we introduced $\widehat{H}$, we introduce the corresponding two-particle Hamiltonians $\widehat{h}_\alpha$, $\alpha=1,2,3$ as bounded self-adjoint operators on the Hilbert space $l_2\left((\mathbb{Z}^3)^2\right)$:

$$\widehat{h}_\alpha=\widehat{h}^0_\alpha-\widehat{v}_\alpha,$$

where

$$\left(\widehat{h}^0_\alpha\widehat{\varphi}\right)(x_\beta,x_\gamma)=\sum_{s\in\mathbb{Z}^3}\left[\widehat{\varepsilon}_\beta(s)\widehat{\varphi}(x_\beta+s,x_\gamma)+\widehat{\varepsilon}_\gamma(s)\widehat{\varphi}(x_\beta,x_\gamma+s)\right],$$

$$\left(\widehat{v}_\alpha\widehat{\varphi}\right)(x_\beta,x_\gamma)=\mu_\alpha\delta_{x_\beta x_\gamma}\widehat{\varphi}(x_\beta,x_\gamma),\quad \widehat{\varphi}\in l_2((\mathbb{Z}^3)^2).$$

Let us rewrite our operators in the momentum representation. We denote by $\mathbb{T}^3$ the three-dimensional torus, the cube $(-\pi,\pi]^3$ with appropriately identified sides and $L_2\left((\mathbb{T}^3)^m\right)$ be the Hilbert space of square integrable (complex) functions defined on $(\mathbb{T}^3)^m$, $m=1,2,3$.

Let $\mathcal{F}_m: L_2\left((\mathbb{T}^3)^m\right)\to l_2((\mathbb{Z}^3)^m)$, $m=2,3$ be the discrete Fourier transform. The three-particle Hamiltonian in the momentum representation is given by the bounded self-adjoint operator on the Hilbert space $L_2\left((\mathbb{T}^3)^3\right)$ as follows $\widetilde{H}=\mathcal{F}_3^{-1}\widehat{H}\mathcal{F}_3$. Introducing the total quasi-momentum $K\in\mathbb{T}^3$ the operator $\widetilde{H}$ can be decomposed into von Neumann direct integrals of the family of bounded self-adjoint operators $\widetilde{H}(K)$, $K\in\mathbb{T}^3$. The operator $\widetilde{H}(K)$, $K\in\mathbb{T}^3$ is called the three-particle discrete Schrödinger operator, which is unitarily

equivalent (see [16–18]) to the family of bounded self-adjoint operators $H(K)$, $K \in \mathbb{T}^3$, acting on the Hilbert space $L_2\left((\mathbb{T}^3)^2\right)$ according to the formula:

$$H(K) = H_0(K) - V_1 - V_2 - V_3,$$

where $H_0(K)$ is the multiplication operator by the function:

$$\mathcal{E}_K(p,q) := \varepsilon_1(p) + \varepsilon_2(q) + \varepsilon_3(K-p-q),$$

where

$$\varepsilon_\alpha(p) := \frac{1}{m_\alpha}\varepsilon(p), \quad \varepsilon(p) := \sum_{i=1}^{3}\left(1-\cos(np^{(i)})\right),$$

and

$$(V_1 f)(p,q) = \frac{\mu_1}{(2\pi)^3}\int\limits_{\mathbb{T}^3} f(p,s)ds, \quad (V_2 f)(p,q) = \frac{\mu_2}{(2\pi)^3}\int\limits_{\mathbb{T}^3} f(s,q)ds,$$

$$(V_3 f)(p,q) = \frac{\mu_3}{(2\pi)^3}\int\limits_{\mathbb{T}^3} f(s,p+q-s)ds.$$

Similarly, the study of the spectral properties of the $\widetilde{h}_\alpha = \mathcal{F}_2^{-1}\widehat{h}_\alpha\mathcal{F}_2$ can be reduced to the study of the spectral properties of the family of bounded self-adjoint operators $h_\alpha(k)$, $k \in \mathbb{T}^3$, corresponding to the two-particle lattice Hamiltonians on the Hilbert space $L_2(\mathbb{T}^3)$:

$$h_\alpha(k) = h_\alpha^0(k) - v_\alpha.$$

The non-perturbed operator $h_\alpha^0(k)$ is the multiplication operator on $L_2(\mathbb{T}^3)$ by the function:

$$E_k^{(\alpha)}(p) := \varepsilon_\beta(p) + \varepsilon_\gamma(k-p), \quad \beta<\gamma, \quad \alpha,\beta,\gamma = 1,2,3.$$

The perturbation v_α is an integral operator of rank one on $L_2(\mathbb{T}^3)$:

$$(v_\alpha f)(p) = \frac{\mu_\alpha}{(2\pi)^3}\int\limits_{\mathbb{T}^3} f(s)ds.$$

Therefore, by the Weyl theorem, the continuous spectrum $\sigma_{\rm cont}(h_\alpha(k))$ of the operator $h_\alpha(k)$ coincides with the spectrum of $\sigma(h_\alpha^0(k))$ of $h_\alpha^0(k)$. More specifically:

$$\sigma_{\rm cont}(h_\alpha(k)) = \left[E_{\min}^{(\alpha)}(k); E_{\max}^{(\alpha)}(k)\right],$$

where

$$E_{\min}^{(\alpha)}(k) := \min_{p\in\mathbb{T}^3} E_k^{(\alpha)}(p) \quad \text{and} \quad E_{\max}^{(\alpha)}(k) := \max_{p\in\mathbb{T}^3} E_k^{(\alpha)}(p).$$

3. Formulation of the main results

We denote by $\sigma_{\rm ess}(\cdot)$ and $\sigma_{\rm disc}(\cdot)$ the essential spectrum and the discrete spectrum of a bounded self-adjoint operator, respectively.

The following theorem, [17, 18], describes the location of the essential spectrum of the operator $H(K)$.

Theorem 3.1. *For the essential spectrum of $H(K)$, the following equality holds:*

$$\sigma_{\rm ess}(H(K)) = \bigcup_{\alpha=1}^{3}\bigcup_{p\in\mathbb{T}^3}\left\{\sigma_{\rm disc}(h_\alpha(K-p)) + \varepsilon_\alpha(p)\right\} \cup \left[\mathcal{E}_{\min}(K); \mathcal{E}_{\max}(K)\right], \tag{3.1}$$

where

$$\mathcal{E}_{\min}(K) := \min_{p,q\in\mathbb{T}^3} \mathcal{E}_K(p,q) \quad \textit{and} \quad \mathcal{E}_{\max}(K) := \max_{p,q\in\mathbb{T}^3} \mathcal{E}_K(p,q).$$

Let us consider the following subset of $\mathbb{T}^3$:

$$\Lambda := \left\{ (p^{(1)}, p^{(2)}, p^{(3)}) : p^{(i)} \in \left\{ 0, \pm\frac{2}{n}\pi; \pm\frac{4}{n}\pi; \ldots; \pm\frac{n'}{n}\pi \right\} \cup \Pi_n,\ i = 1,2,3 \right\},$$

where

$$n' := \begin{cases} n-2, \text{ if } n \text{ is even;} \\ n-1, \text{ if } n \text{ is odd,} \end{cases} \quad \text{and} \quad \Pi_n := \begin{cases} \{\pi\}, \text{ if } n \text{ is even;} \\ \emptyset, \quad \text{if } n \text{ is odd.} \end{cases}$$

Direct calculation shows that the cardinality of Λ is equal to n^3. It is easy to verify that for any $K \in \Lambda$, the function $\mathcal{E}_K(\cdot,\cdot)$ has non-degenerate zero minima at the points of $\Lambda \times \Lambda$, that is, $\mathcal{E}_{\min}(K) = 0$ for $K \in \Lambda$.

Since $\mathbf{0} = (0,0,0) \in \Lambda$, the definition of the functions $E_k^{(\alpha)}(\cdot)$ and $\mathcal{E}_K(\cdot,\cdot)$ imply the identities $h_\alpha(\mathbf{0}) \equiv h_\alpha(k)$ and $H(\mathbf{0}) \equiv H(K)$ for all $k, K \in \Lambda$.

Let $C(\mathbb{T}^3)$ and $L_1(\mathbb{T}^3)$ be the Banach spaces of continuous and integrable functions on $\mathbb{T}^3$, respectively. Let G_α be the integral operator on $C(\mathbb{T}^3)$ with the kernel:

$$G_\alpha(p,s) = \frac{\mu_\alpha}{(2\pi)^3} \frac{m_\beta m_\gamma}{m_\beta + m_\gamma} \frac{1}{\varepsilon(s)}.$$

Definition 3.2. *The operator $h_\alpha(\mathbf{0})$ is said to have a zero energy resonance if the number 1 is an eigenvalue of the operator G_α. If the number 1 isn't an eigenvalue of the operator G_α, then we say that $z = 0$ is a regular-type point for the operator $h_\alpha(\mathbf{0})$.*

We note that in Definition 3.2 the requirement of the existence of the eigenfunction $\varphi_\alpha \in C(\mathbb{T}^3)$ corresponding to the eigenvalue 1 of G_α corresponds to the existence of a solution of $h_\alpha(\mathbf{0}) f_\alpha = 0$, and this solution does not belong to $L_2(\mathbb{T}^3)$. More precisely, if the operator $h_\alpha(\mathbf{0})$ has a zero energy resonance, then the function:

$$f_\alpha(p) = \varphi_\alpha(p)(\varepsilon(p))^{-1},$$

is a solution (up to a constant factor) of the Schrödinger equation $h_\alpha(\mathbf{0}) f_\alpha = 0$ and $f_\alpha \in L_1(\mathbb{T}^3) \setminus L_2(\mathbb{T}^3)$ (see Lemma 4.4).

We set:

$$\mu_\alpha^0 := 8\pi^3 \frac{m_\beta + m_\gamma}{m_\beta m_\gamma} \left(\int\limits_{\mathbb{T}^3} \frac{ds}{\varepsilon(s)} \right)^{-1}, \quad \alpha = 1,2,3.$$

Simple calculation shows that the operator $h_\alpha(\mathbf{0})$ has a zero energy resonance if and only if $\mu_\alpha = \mu_\alpha^0$ (see Lemma 4.2).

For $K \in \mathbb{T}^3$, let us denote by $\tau_{\text{ess}}(K)$ the bottom of the essential spectrum of $H(K)$ and by $N(K;z)$ the number of eigenvalues of $H(K)$ lying on the left of z, $z < \tau_{\text{ess}}(K)$. It is clear that $N(\mathbf{0};z) = N(K;z)$ for any $K \in \Lambda$.

Since the operator $h_\alpha(\mathbf{0})$ has no negative eigenvalues for all $\mu_\alpha \le \mu_\alpha^0$ (see Lemma 4.3), the operator $h_\alpha(\mathbf{0})$ is non-negative for all $\mu_\alpha \le \mu_\alpha^0$. Then, by Theorem 1 of [21], the operator $h_\alpha(k)$ is non-negative for all $\mu_\alpha \le \mu_\alpha^0$ and $k \in \mathbb{T}^3$. Hence, the assertion $\mathcal{E}_{\min}(K) = 0$, $K \in \Lambda$ implies $\tau_{\text{ess}}(K) = 0$ for $K \in \Lambda$ and $\mu_\alpha \le \mu_\alpha^0$.

The main result of the present paper is given in the following theorem.

Theorem 3.3. *Assume $\mu_\alpha = \mu_\alpha^0$, $\mu_\beta = \mu_\beta^0$ and $\mu_\gamma \le \mu_\gamma^0$. Then the operator $H(\mathbf{0})$ has infinitely many negative eigenvalues accumulating at zero and the function $N(\mathbf{0};\cdot)$ obeys the relation:*

$$\lim_{z\to-0} \frac{N(\mathbf{0};z)}{|\log|z||} = \mathcal{U}_0, \quad 0<\mathcal{U}_0<\infty. \tag{3.2}$$

Remark 3.4. *The constant $\mathcal{U}_0$ does not depend on the interaction energies μ_α, $\alpha=1,2,3$; it is positive and depends only on the ratios m_β/m_α, $\alpha\neq\beta$, $\alpha,\beta=1,2,3$ between the masses.*

Remark 3.5. *Clearly, by equality* (3.2)*, the infinite cardinality of the negative discrete spectrum of $H(\mathbf{0})$ follows automatically from the positivity of $\mathcal{U}_0$.*

Remark 3.6. *It is surprising that the asymptotics* (3.2) *don't depend on the cardinality of Λ, that is, these asymptotics are the same for all $n\in\mathbb{N}$. Since $\Lambda|_{n=1}=\{\mathbf{0}\}$ in fact, Theorem* 3.3 *was proved in* [17] *for $n=1$.*

4. Threshold analysis of the two-particle operator $h_\alpha(k)$

In this section, we study the spectral properties of the two-particle discrete Schrödinger operator $h_\alpha(k)$.

For any $\mu_\alpha>0$, $k\in\mathbb{T}^3$ and $z\in\mathbb{C}\setminus\sigma_{\rm cont}(h_\alpha(k))$ we define the function (the Fredholm determinant associated with the operator $h_\alpha(k)$):

$$\Delta_\alpha(k\,;z) := 1-\frac{\mu_\alpha}{(2\pi)^3}\int\limits_{\mathbb{T}^3}\frac{ds}{E_k^{(\alpha)}(s)-z}.$$

Note that the function $\Delta_\alpha(\cdot\,;\cdot)$ is analytic in $\mathbb{T}^3\times(\mathbb{C}\setminus\sigma_{\rm cont}(h_\alpha(k)))$.

The following lemma is a simple consequence of the Birman-Schwinger principle and the Fredholm theorem.

Lemma 4.1. *The number $z\in\mathbb{C}\setminus\sigma_{\rm cont}(h_\alpha(k))$ is an eigenvalue of the operator $h_\alpha(k)$, $k\in\mathbb{T}^3$ if and only if $\Delta_\alpha(k\,;z)=0$.*

We remark that from the definition of $E_k^{(\alpha)}(\cdot)$, it follows that $\Delta_\alpha(\mathbf{0}\,;0)=\Delta_\alpha(k\,;0)$ for $k\in\Lambda$.

Lemma 4.2. *The following statements are equivalent:*
(i) *the operator $h_\alpha(\mathbf{0})$ has a zero energy resonance;*
(ii) $\Delta_\alpha(\mathbf{0}\,;0)=0$;
(iii) $\mu_\alpha=\mu_\alpha^0$.

For the proof of Lemma 4.2, see Lemma 5.3 of [17].

Lemma 4.3. *The operator $h_\alpha(\mathbf{0})$ has no negative eigenvalues for all $\mu_\alpha\le\mu_\alpha^0$.*

Proof. Since the function $\Delta_\alpha(\mathbf{0}\,;\cdot)$ is decreasing on $(-\infty;0)$, we have

$$\Delta_\alpha(\mathbf{0}\,;z)>\Delta_\alpha(\mathbf{0}\,;0) \tag{4.1}$$

for all $z<0$. Definition of μ_α^0 implies $\Delta_\alpha(\mathbf{0}\,;0)\ge0$ for all $\mu_\alpha\le\mu_\alpha^0$. Hence by inequality (4.1) we have $\Delta_\alpha(\mathbf{0}\,;z)>0$ for any $\mu_\alpha\le\mu_\alpha^0$ and $z<0$. By Lemma 4.1, it means that the operator $h_\alpha(\mathbf{0})$ has no negative eigenvalues for all $\mu_\alpha\le\mu_\alpha^0$. □

In the sequel, we denote by C_1, C_2, C_3 different positive numbers and for $\delta > 0$ we set:

$$\mathbb{T}_\delta := \mathbb{T}^3 \setminus \bigcup_{p' \in \Lambda} U_\delta(p').$$

Lemma 4.4. *If $h_\alpha(\mathbf{0})$ has a zero energy resonance, then the function $f_\alpha(p) = \varphi_\alpha(p)(\varepsilon(p))^{-1}$ obeys the equation $h_\alpha(\mathbf{0})f_\alpha = 0$ and $f_\alpha \in L_1(\mathbb{T}^3) \setminus L_2(\mathbb{T}^3)$, where the function $\varphi_\alpha \in C(\mathbb{T}^3)$ is a unique (up to a constant factor) solution of $G_\alpha\varphi_\alpha = \varphi_\alpha$ satisfying the condition $\varphi_\alpha(\mathbf{0}) \neq 0$.*

Proof. Let the operator $h_\alpha(\mathbf{0})$ have a zero energy resonance. One can see that the function f_α defined in Lemma 4.4 satisfies $h_\alpha(\mathbf{0})f_\alpha = 0$. Let us show that $f_\alpha \in L_1(\mathbb{T}^3) \setminus L_2(\mathbb{T}^3)$. First we recall that the solution of $G_\alpha\varphi_\alpha = \varphi_\alpha$ is equal to $\varphi_\alpha(p) \equiv 1$ (up to constant factor). The definition of the function $\varepsilon(\cdot)$ implies the existence of positive constants C_1, C_2, C_3 and δ such that:

$$C_1|q - p'|^2 \leq \varepsilon(q) \leq C_2|q - p'|^2, \quad q \in U_\delta(p'), \quad p' \in \Lambda; \tag{4.2}$$

$$\varepsilon(q) \geq C_3, \quad q \in \mathbb{T}_\delta. \tag{4.3}$$

Using the estimates (4.2) and (4.3) we have:

$$\int_{\mathbb{T}^3} |f_\alpha(s)|^2 ds \geq \int_{U_\delta(\mathbf{0})} \frac{ds}{\varepsilon^2(s)} \geq C_2 \int_{U_\delta(\mathbf{0})} \frac{ds}{|s|^4} = \infty;$$

$$\int_{\mathbb{T}^3} |f_\alpha(s)| ds = \sum_{p' \in \Lambda} \int_{U_\delta(p')} \frac{ds}{\varepsilon(s)} + \int_{\mathbb{T}_\delta} \frac{ds}{\varepsilon(s)} \leq C_1 \sum_{p' \in \Lambda} \int_{U_\delta(p')} \frac{ds}{|s - p'|^2} + C_3 < \infty.$$

Therefore, $f_\alpha \in L_1(\mathbb{T}^3) \setminus L_2(\mathbb{T}^3)$. □

We denote:

$$m_{\beta\gamma} := \frac{m_\beta + m_\gamma}{m_\beta m_\gamma}, \quad n_\alpha := \frac{m_1 + m_2 + m_3}{m_\alpha(m_\beta + m_\gamma)}.$$

Now, we formulate a lemma (zero energy expansion for the Fredholm determinant, leading to behaviors of the zero energy resonance), which is important in the proof of Theorem 3.3, that is, the asymptotics (3.2).

Lemma 4.5. *Let $\mu_\alpha = \mu_\alpha^0$ and $K, p' \in \Lambda$. Then, the following decomposition:*

$$\Delta_\alpha(K - p\,; z - \varepsilon_\alpha(p)) = \frac{n\mu_\alpha^0 m_{\beta\gamma}^{3/2}}{2\pi} \sqrt{n_\alpha|p - p'|^2 - \frac{2z}{n^2}} + O(|p - p'|^2) + O(|z|)$$

holds for $|p - p'| \to 0$ and $z \to -0$.

Proof. Let us sketch the main idea of the proof. Take a sufficiently small $\delta > 0$ such that $U_\delta(p') \cap U_\delta(q') = \emptyset$ for all $q' \in \Lambda$ with $q' \neq p'$. Let $\mu_\alpha = \mu_\alpha^0$ and $K, p' \in \Lambda$. Using the additivity of the integral, we rewrite the function $\Delta_\alpha(K - p\,; z - \varepsilon_\alpha(p))$ as:

$$\Delta_\alpha(K - p\,; z - \varepsilon_\alpha(p)) =$$

$$1 - \frac{\mu_\alpha^0}{(2\pi)^3} \left(\sum_{q' \in \Lambda} \int_{U_\delta(q')} \frac{ds}{E_p^{(\alpha)}(s) + \varepsilon_\alpha(p) - z} + \int_{\mathbb{T}_\delta} \frac{ds}{E_p^{(\alpha)}(s) + \varepsilon_\alpha(p) - z} \right). \tag{4.4}$$

Since the function $\mathcal{E}_K(\cdot,\cdot)$ has non-degenerate zero minima at the points (p',q'), $p',q' \in \Lambda$, analysis similar to [17] shows that:

$$\int\limits_{U_\delta(q')} \frac{ds}{E_p^{(\alpha)}(-s)+\varepsilon_\alpha(p)-z} = \int\limits_{U_\delta(q')} \frac{ds}{E_{p'}^{(\alpha)}(-s)+\varepsilon_\alpha(p')} - \frac{4\pi^2 m_{\beta\gamma}^{3/2}}{n^2}\sqrt{n_\alpha|p-p'|^2-\frac{2z}{n^2}} + O(|p-p'|^2)+O(|z|);$$

$$\int\limits_{\mathbb{T}_\delta} \frac{ds}{E_p^{(\alpha)}(s)+\varepsilon_\alpha(p)-z} = \int\limits_{\mathbb{T}_\delta} \frac{ds}{E_{p'}^{(\alpha)}(s)+\varepsilon_\alpha(p')} + O(|p-p'|^2)+O(|z|)$$

as $|p-p'| \to 0$ and $z \to -0$. Substituting the last two expressions into (4.4), we obtain:

$$\Delta_\alpha(K-p\,;z-\varepsilon_\alpha(p)) = \Delta_\alpha(K-p'\,;0) + \frac{n\mu_\alpha^0 m_{\beta\gamma}^{3/2}}{2\pi}\sqrt{n_\alpha|p-p'|^2-\frac{2z}{n^2}} + O(|p-p'|^2)+O(|z|)$$

as $|p-p'| \to 0$ and $z \to -0$. Now, the equality $\mu_\alpha = \mu_\alpha^0$, that is, $\Delta_\alpha(K-p'\,;0)=0$ completes the proof of Lemma 4.5. □

Corollary 4.6. *Let $\mu_\alpha = \mu_\alpha^0$ and $K \in \Lambda$. For some $C_1, C_2, C_3 > 0$ and $\delta > 0$ the following inequalities hold:*
(i) $C_1|p-p'| \le \Delta_\alpha(K-p\,;-\varepsilon_\alpha(p)) \le C_2|p-p'|$, $p \in U_\delta(p')$, $p' \in \Lambda$;
(ii) $\Delta_\alpha(K-p\,;-\varepsilon_\alpha(p)) \ge C_3$, $p \in \mathbb{T}_\delta$.

Proof. Lemma 4.5 yields the assertion (i) for some positive numbers C_1, C_2. The positivity and continuity of the function $\Delta_\alpha(\cdot\,;-\varepsilon_\alpha(\cdot))$ on the compact set $\mathbb{T}_\delta$ imply the assertion (ii). □

5. The Birman-Schwinger principle

For a bounded self-adjoint operator A acting in the Hilbert space $\mathcal{R}$, we define the number $n(\gamma, A)$ as follows:

$$n(\gamma,A) = \sup\{\dim F : (Au,u) > \gamma,\ u \in F \subset \mathcal{R},\ ||u|| = 1\}.$$

The number $n(\gamma, A)$ is equal to infinity if $\gamma < \max\sigma_{\text{ess}}(A)$; if $n(\gamma, A)$ is finite, then it is equal to the number of the eigenvalues of A larger than γ.

By the definition of $N(K;z)$, we have:

$$N(K;z) = n(-z,-H(K)),\ -z > -\tau_{\text{ess}}(K).$$

Let $\mu_\alpha > 0$ and $K \in \mathbb{T}^3$. Then we have $\Delta_\alpha(K-p\,;z-\varepsilon_\alpha(p)) > 0$ for any $p \in \mathbb{T}^3$ and $z < \tau_{\text{ess}}(K)$.

In what follows, we deal with the operators in various spaces of vector-valued functions. They will be denoted by bold letters and will be written in matrix form.

Let $\Omega \subset \mathbb{R}^3$ be the measurable set and $L_2^{(m)}(\Omega)$ be the Hilbert space of m-component vector functions $w = (w_1, \dots, w_m)$, $w_i \in L_2(\Omega)$, $i = 1, \dots, m$.

In our analysis of the discrete spectrum of $H(K)$, the crucial role is played by the 3×3 self-adjoint block operator matrix $\widehat{\mathbf{T}}(K;z)$, $z < \tau_{\text{ess}}(K)$ acting on $L_2^{(3)}(\mathbb{T}^3)$ with the

entries $\widehat{T}_{\alpha\beta}(K;z)$, where $\widehat{T}_{\alpha\beta}(K;z)$, $\alpha \le \beta$ is the integral operator on $L_2(\mathbb{T}^3)$ with kernel $\widehat{T}_{\alpha\alpha}(K;z;\cdot,\cdot)$:

$$\widehat{T}_{\alpha\alpha}(K;z;p,q)=0;$$
$$\widehat{T}_{12}(K;z;p,q)=\frac{\sqrt{\mu_1\mu_2}}{\sqrt{\Delta_1(K-p\,;z-\varepsilon_1(p))}}\frac{(\mathcal{E}_K(p,q)-z)^{-1}}{\sqrt{\Delta_2(K-q\,;z-\varepsilon_2(q))}},$$
$$\widehat{T}_{13}(K;z;p,q)=\frac{\sqrt{\mu_1\mu_3}}{\sqrt{\Delta_1(K-p\,;z-\varepsilon_1(p))}}\frac{(\mathcal{E}_K(p,q-p)-z)^{-1}}{\sqrt{\Delta_3(q\,;z-\varepsilon_3(K-q))}},$$
$$\widehat{T}_{23}(K;z;p,q)=\frac{\sqrt{\mu_2\mu_3}}{\sqrt{\Delta_2(K-p\,;z-\varepsilon_2(p))}}\frac{(\mathcal{E}_K(q-p,p)-z)^{-1}}{\sqrt{\Delta_3(q\,;z-\varepsilon_3(K-q))}},$$

and for $\alpha>\beta$ the operator $\widehat{T}_{\alpha\beta}(K;z)$ is the adjoint operator to $\widehat{T}_{\beta\alpha}(K;z)$.

The following lemma is a realization of the well-known Birman-Schwinger principle for three-particle Schrödinger operators on a lattice (see [7, 16, 17]).

Lemma 5.1. *For $z<\tau_{\rm ess}(K)$ the operator $\widehat{\mathbf{T}}(K;z)$ is compact and continuous in z and*

$$N(K;z)=n(1,\widehat{\mathbf{T}}(K;z)).$$

For the proof of the lemma, we refer to [17].

6. Asymptotics for the number of negative eigenvalues of $H(\mathbf{0})$

In this section, we derive the asymptotic relation (3.2) for the number of negative eigenvalues of $H(\mathbf{0})$.

First, we recall that $\widehat{\mathbf{T}}(\mathbf{0};z)\equiv\widehat{\mathbf{T}}(K;z)$ for all $K\in\Lambda$. Let $\mathbb{S}^2$ be the unit sphere in $\mathbb{R}^3$ and $\sigma=L_2(\mathbb{S}^2)$. As we shall see, the discrete spectrum asymptotics of the operator $\widehat{\mathbf{T}}(\mathbf{0};z)$ as $z\to-0$ is determined by the integral operator $\mathbf{S_r}$, $\mathbf{r}=1/2|\log|z||$ in $L_2((0,\mathbf{r}),\sigma^{(3)})$ with the kernel $S_{\alpha\beta}(y,t)$, $y=x-x'$, $x,x'\in(0,\mathbf{r})$, $t=\langle\xi,\eta\rangle$, $\xi,\eta\in\mathbb{S}^2$, where:

$$S_{\alpha\alpha}(y,t)=0;\quad S_{\alpha\beta}(y,t)=\frac{1}{4\pi^2}\frac{u_{\alpha\beta}}{\cosh(y+r_{\alpha\beta})+s_{\alpha\beta}t};$$
$$u_{\alpha\beta}=k_{\alpha\beta}\left(\frac{m_{\beta\gamma}^{-1}m_{\alpha\gamma}^{-1}}{n_\alpha n_\beta}\right)^{1/4},\quad r_{\alpha\beta}=\frac{1}{2}\log\frac{m_{\beta\gamma}}{m_{\alpha\gamma}},\quad s_{\alpha\beta}=\frac{(m_{\alpha\gamma}m_{\beta\gamma})^{1/2}}{m_\gamma},$$

$k_{\alpha\beta}$ being such that $k_{\alpha\beta}=1$ if both subsystems α and β have zero energy resonances, otherwise, $k_{\alpha\beta}=0$. The eigenvalue asymptotics for the operator $\mathbf{S_r}$ have been studied in detail by Sobolev [7], by employing an argument used in the calculation of the canonical distribution of Toeplitz operators.

Let us recall some results of [7] which are important in our work.

The coefficient in asymptotics (3.2) of $N(\mathbf{0};z)$ will be expressed by means of the self-adjoint integral operator $\widehat{\mathbf{S}}(\theta)$, $\theta\in\mathbb{R}$, in the space $\sigma^{(3)}$, whose kernel is of the form:

$$\widehat{S}_{\alpha\alpha}(\theta,t)=0;\quad \widehat{S}_{\alpha\beta}(\theta,t)=\frac{1}{4\pi^2}u_{\alpha\beta}e^{ir_{\alpha\beta}\theta}\frac{\sinh[\theta\arccos s_{\alpha\beta}t]}{\sqrt{1-s_{\alpha\beta}^2t}\sinh(\pi\theta)},$$

and depends on the inner product $t = \langle \xi, \eta \rangle$ of the arguments $\xi, \eta \in \mathbb{S}^2$. For $\gamma > 0$, we define:

$$U(\gamma) := \frac{1}{4\pi} \int\limits_{-\infty}^{+\infty} n(\gamma, \widehat{\mathbf{S}}(\theta)) d\theta.$$

This function was studied in detail in [7]; it is used in the existence proof for the Efimov effect. In particular, the function $U(\cdot)$ is continuous in $\gamma > 0$, and the limit:

$$\lim_{\mathbf{r} \to 0} \frac{1}{2} \mathbf{r}^{-1} n(\gamma, \mathbf{S}_{\mathbf{r}}) = U(\gamma), \tag{6.1}$$

exists such that $U(1) > 0$.

Theorem 3.3 can be derived by using a perturbation argument based on the following lemma.

Lemma 6.1. *Let $A(z) = A_0(z) + A_1(z)$, where $A_0(z)$ $(A_1(z))$ is compact and continuous for $z < 0$ (for $z \leq 0$). Assume that the limit $\lim\limits_{z \to -0} f(z)\, n(\gamma, A_0(z)) = l(\gamma)$ exists and $l(\cdot)$ is continuous in $(0; +\infty)$ for some function $f(\cdot)$, where $f(z) \to 0$ as $z \to -0$. Then, the same limit exists for $A(z)$ and $\lim\limits_{z \to -0} f(z)\, n(\gamma, A(z)) = l(\gamma)$.*

For the proof of Lemma 6.1, see Lemma 4.9 in [7].

Remark 6.2. *Since the function $U(\cdot)$ is continuous with respect to γ, it follows from Lemma* 6.1 *that any perturbation of $A_0(z)$ treated in Lemma* 6.1 *(which is compact and continuous up to $z = 0$) does not contribute to the asymptotic relation* (3.2).

Now, we are going to reduce the study of the asymptotics for the operator $\widehat{\mathbf{T}}(\mathbf{0}; z)$ to that of the asymptotics $\mathbf{S}_{\mathbf{r}}$.

Let $\mathbf{T}(\delta; |z|)$ be the 3×3 block operator matrix in $L_2^{(3)}(\mathbb{T}^3)$ whose entries $T_{\alpha\beta}(\delta; |z|)$ are integral operators with the kernel $T_{\alpha\beta}(\delta; |z|; \cdot, \cdot)$:

$$T_{\alpha\alpha}(\delta; |z|; p, q) = 0;$$

$$T_{\alpha\beta}(\delta; |z|; p, q) =$$

$$D_{\alpha\beta} \sum_{p', q' \in \Lambda} \frac{\chi_\delta(p - p') \chi_\delta(q - q') \left(n_\alpha |p - p'|^2 + 2|z|/(n^2)\right)^{-\frac{1}{4}} \left(n_\beta |q - q'|^2 + 2|z|/(n^2)\right)^{-\frac{1}{4}}}{m_{\alpha\gamma}^{-1} |p - p'|^2 + 2 m_\gamma^{-1} (p - p', q - q') + m_{\beta\gamma}^{-1} |q - q'|^2 + 2|z|/(n^2)},$$

where

$$D_{\alpha\beta} = \frac{m_{\alpha\gamma}^{-3/4} m_{\beta\gamma}^{-3/4}}{2n^3 \pi^2}, \quad \alpha, \beta, \gamma = 1, 2, 3, \quad \alpha \neq \beta \neq \gamma,$$

and $\chi_\delta(\cdot)$ is the characteristic function of the domain $U_\delta(\mathbf{0})$.

Lemma 6.3. *Let $\mu_\alpha = \mu_\alpha^0$, $\mu_\beta = \mu_\beta^0$, $\mu_\gamma \leq \mu_\gamma^0$. For any $z \leq 0$ and sufficiently small $\delta > 0$, the difference $\widehat{\mathbf{T}}(\mathbf{0}; z) - \mathbf{T}(\delta; |z|)$ belongs to the Hilbert-Schmidt class, and is continuous with respect to $z \leq 0$.*

Proof. We prove the lemma in the case $\mu_\alpha = \mu_\alpha^0$, $\alpha = 1, 2, 3$. The case $\mu_\alpha = \mu_\alpha^0$, $\mu_\beta = \mu_\beta^0$, $\mu_\gamma < \mu_\gamma^0$ can be proven similarly.

By the definition of $\varepsilon_\alpha(\cdot)$, we have:

$$\varepsilon_\alpha(p) = \frac{n^2}{2m_\alpha} |p - p'|^2 + O(|p - p'|^4),$$

as $|p-p_i|\to 0$ for $p'\in\Lambda$, which implies the expansion:

$$E^{(\alpha)}_{K-p}(q)+\varepsilon_\alpha(p)=n^2\left[\frac{|p-p'|^2}{2m_{\alpha\gamma}}+\frac{(p-p',q-q')}{m_\gamma}+\frac{|q-q'|^2}{2m_{\beta\gamma}}\right]+O(|p-p'|^4)+O(|q-q'|^4),$$

as $|p-p'|$, $|q-q'|\to 0$ for $K,p',q'\in\Lambda$. Then, there exist $C_1,C_2>0$ and $\delta>0$ such that:

$$\begin{aligned}&C_1(|p-p'|^2+|q-q'|^2)\le E^{(\alpha)}_{K-p}(q)+\varepsilon_\alpha(p)\le C_2(|p-p'|^2+|q-q'|^2),\\&(p,q)\in U_\delta(p')\times U_\delta(q')\quad\text{for}\quad K,p',q'\in\Lambda;\\&E^{(\alpha)}_{K-p}(q)+\varepsilon_\alpha(p)\ge C_1,\quad (p,q)\in\mathbb{T}^2_\delta,\quad K\in\mathbb{T}^3.\end{aligned}$$

Applying last estimates and Corollary 4.6, we obtain that there exists $C_1>0$ such that the kernel of the operator $\widehat{T}_{\alpha\beta}(\mathbf{0};z)-T_{\alpha\beta}(\delta;|z|)$ can be estimated by the square-integrable function:

$$C_1\sum_{p',q'\in\Lambda}\left[\frac{1}{|p-p'|^2+|q-q'|^2}+\frac{|p-p'|^{-1/2}}{|p-p'|^2+|q-q'|^2}+\frac{|q-q'|^{-1/2}}{|p-p'|^2+|q-q'|^2}+1\right].$$

Hence, the operator $\widehat{T}_{\alpha\beta}(\mathbf{0};z)-T_{\alpha\beta}(\delta;|z|)$ belongs to the Hilbert-Schmidt class for all $z\le 0$. In combination with the continuity of the kernel of the operator with respect to $z<0$, this implies the continuity of $\widehat{T}_{\alpha\beta}(\mathbf{0};z)-T_{\alpha\beta}(\delta;|z|)$ with respect to $z\le 0$. The lemma is proved. □

The following theorem is fundamental for the proof of the asymptotic relation (3.2).

Theorem 6.4. *The following relation holds*

$$\lim_{|z|\to 0}\frac{n(\gamma,\mathbf{T}(\delta;|z|))}{|\log|z||}=U(\gamma),\quad \gamma>0. \tag{6.2}$$

Proof. First we prove Theorem 6.4 under the condition that all two-particle operators have zero energy resonances, that is, in the case where $\mu_\alpha=\mu^0_\alpha$, $\alpha=1,2,3$. The case where only two operators $h_\alpha(\mathbf{0})$ and $h_\beta(\mathbf{0})$ have zero energy resonance can be proven similarly.

The subspace of vector functions $w=(w_1,w_2,w_3)$ with components having support in $\bigcup\limits_{p'\in\Lambda}U_\delta(p')$ is an invariant subspace for the operator $\mathbf{T}(\delta;|z|)$.

Let $\mathbf{T}_0(\delta;|z|)$ be the restriction of the operator $\mathbf{T}(\delta;|z|)$ to the subspace $L^{(3)}_2(\bigcup\limits_{p'\in\Lambda}U_\delta(p'))$, that is, a 3×3 block operator matrix in $L^{(3)}_2(\bigcup\limits_{p'\in\Lambda}U_\delta(p'))$ whose entries $T^{(0)}_{\alpha\beta}(\delta;|z|)$ are the integral operators with the kernel $T^{(0)}_{\alpha\beta}(\delta;|z|;\cdot,\cdot)$, where $T^{(0)}_{\alpha\alpha}(\delta;|z|;p,q)=0$ and the function $T^{(0)}_{\alpha\beta}(\delta;|z|;\cdot,\cdot)$ is defined on $\bigcup\limits_{p'\in\Lambda}U_\delta(p')\times\bigcup\limits_{q'\in\Lambda}U_\delta(q')$ as:

$$T^{(0)}_{\alpha\beta}(\delta;|z|;p,q)=D_{\alpha\beta}\frac{(n_\alpha|p-p'|^2+2|z|/(n^2))^{-\frac14}\,(n_\beta|q-q'|^2+2|z|/(n^2))^{-\frac14}}{m^{-1}_{\alpha\gamma}|p-p'|^2+2m^{-1}_\gamma(p-p',q-q')+m^{-1}_{\beta\gamma}|q-q'|^2+2|z|/(n^2)},$$

$(p,q)\in U_\delta(p')\times U_\delta(q')$ for $p',q'\in\Lambda$.

In the remainder of the proof, for convenience, we numerate the points of Λ as $p_1,\dots,p_{n^3}$ and set $\overline{1,n}=1,\dots,n$.

Since $L_2(\bigcup_{i=1}^{n^3} U_\delta(p_i)) \cong \bigoplus_{i=1}^{n^3} L_2(U_\delta(p_i))$, we can express the integral operator $T^{(0)}_{\alpha\beta}(\delta;|z|)$ as the following $n^3 \times n^3$ block operator matrix $\mathbf{T}^{(0)}_{\alpha\beta}(\delta;|z|)$ acting on $\bigoplus_{i=1}^{n^3} L_2(U_\delta(p_i))$ as:

$$\mathbf{T}^{(0)}_{\alpha\beta}(\delta;|z|) = \begin{pmatrix} T^{(1,1)}_{\alpha\beta}(\delta;|z|) & \dots & T^{(1,n^3)}_{\alpha\beta}(\delta;|z|) \\ \vdots & \ddots & \vdots \\ T^{(n^3,1)}_{\alpha\beta}(\delta;|z|) & \dots & T^{(n^3,n^3)}_{\alpha\beta}(\delta;|z|) \end{pmatrix},$$

where $T^{(i,j)}_{\alpha\beta}(\delta;|z|) : L_2(U_\delta(p_j)) \to L_2(U_\delta(p_i))$ is an integral operator with the kernel $T^{(0)}_{\alpha\beta}(\delta;|z|;p,q)$, $(p,q) \in U_\delta(p_i) \times U_\delta(p_j)$ for $i,j = \overline{1,n^3}$.

It is easy to show that $\mathbf{T}_0(\delta;|z|)$ is unitarily equivalent to the 3×3 block operator matrix $\mathbf{T}(r)$, $r = |z|^{-\frac{1}{2}}$, acting on $L_2^{(n^3)}(U_r(\mathbf{0})) \oplus L_2^{(n^3)}(U_r(\mathbf{0})) \oplus L_2^{(n^3)}(U_r(\mathbf{0}))$ with the entries $\mathbf{T}_{\alpha\beta}(r) : L_2^{(n^3)}(U_r(\mathbf{0})) \to L_2^{(n^3)}(U_r(\mathbf{0}))$:

$$\mathbf{T}_{\alpha\alpha}(r) = 0; \quad \mathbf{T}_{\alpha\beta}(r) = \begin{pmatrix} T_{\alpha\beta}(r) & \dots & T_{\alpha\beta}(r) \\ \vdots & \ddots & \vdots \\ T_{\alpha\beta}(r) & \dots & T_{\alpha\beta}(r) \end{pmatrix},$$

where $T_{\alpha\beta}(r)$ is the integral operator on $L_2(U_r(\mathbf{0}))$ with the kernel:

$$D_{\alpha\beta} \frac{(n_\alpha|p|^2 + 2/(n^2))^{-\frac{1}{4}} (n_\beta|q|^2 + 2/(n^2))^{-\frac{1}{4}}}{m^{-1}_{\alpha\gamma}|p|^2 + 2m^{-1}_{\gamma}(p,q) + m^{-1}_{\beta\gamma}|q|^2 + 2/(n^2)}.$$

The equivalence is realized by the unitary dilation ($3n^3 \times 3n^3$ diagonal matrix):

$$\mathbf{B}_r : \bigoplus_{i=1}^{3n^3} L_2(U_\delta(p_i)) \to L_2^{(3n^3)}(U_r(\mathbf{0})),$$
$$\mathbf{B}_r = \operatorname{diag}\{B_r^{(1)}, \dots, B_r^{(n^3)}, B_r^{(1)}, \dots, B_r^{(n^3)}, B_r^{(1)}, \dots, B_r^{(n^3)}\}.$$

Here, the operator $B_r^{(i)} : L_2(U_\delta(p_i)) \to L_2(U_r(\mathbf{0}))$, $i = \overline{1,n^3}$ acts as:

$$(B_r^{(i)} f)(p) = \left(\frac{r}{\delta}\right)^{-\frac{3}{2}} f\left(\frac{\delta}{r}p + p_i\right).$$

Let us introduce the $3n^3 \times 1$ and $1 \times 3n^3$ block operator matrices:

$$\mathbf{E} : L_2^{(3n^3)}(U_r(\mathbf{0})) \to L_2^{(3)}(U_r(\mathbf{0})), \quad \mathbf{A}_r : L_2^{(3)}(U_r(\mathbf{0})) \to L_2^{(3n^3)}(U_r(\mathbf{0}))$$

of the form

$$\mathbf{A}_r = \begin{pmatrix} 0 & \mathbf{A}_{12}(r) & \mathbf{A}_{13}(r) \\ \mathbf{A}_{21}(r) & 0 & \mathbf{A}_{23}(r) \\ \mathbf{A}_{31}(r) & \mathbf{A}_{32}(r) & 0 \end{pmatrix}, \quad \mathbf{E} = \operatorname{diag}\{\mathbf{I}, \mathbf{I}, \mathbf{I}\},$$

where $\mathbf{A}_{\alpha\beta}(r)$ and $\mathbf{I}$ are the $n^3 \times 1$ and $1 \times n^3$ matrices of the form:

$$\mathbf{A}_{\alpha\beta}(r) = \begin{pmatrix} T^{(1)}_{\alpha\beta}(r) \\ \vdots \\ T^{(1)}_{\alpha\beta}(r) \end{pmatrix}, \quad \mathbf{I} = (I \dots I),$$

respectively, here I is the identity operator on $L_2(U_r(\mathbf{0}))$.

It is well known that if B_1, B_2 are bounded operators and $\gamma \neq 0$ is an eigenvalue of B_1B_2, then γ is an eigenvalue for B_2B_1 as well of the same algebraic and geometric multiplicities (see *e.g.* [20]). Therefore, $n(\gamma, \mathbf{A}_r\mathbf{E}) = n(\gamma, \mathbf{E}\mathbf{A}_r)$, $\gamma > 0$. Note that $\mathbf{T}_{\alpha\beta}(r) = \mathbf{A}_{\alpha\beta}(r)\mathbf{I}$ and: $n^3 T_{\alpha\beta}(r) = \mathbf{I}\mathbf{A}_{\alpha\beta}(r)$. Hence, direct calculation shows that $\mathbf{T}(r) = \mathbf{A}_r\mathbf{E}$ and

$$\mathbf{E}\mathbf{A}_r : L_2^{(3)}(U_r(\mathbf{0})) \to L_2^{(3)}(U_r(\mathbf{0})), \quad \mathbf{E}\mathbf{A}_r = n^3 \begin{pmatrix} 0 & T_{12}^{(1)}(r) & T_{13}^{(1)}(r) \\ T_{21}^{(1)}(r) & 0 & T_{13}^{(1)}(r) \\ T_{31}^{(1)}(r) & T_{32}^{(1)}(r) & 0 \end{pmatrix}.$$

So, $n(\gamma, \mathbf{T}_1(r)) = n(\gamma, \mathbf{E}\mathbf{A}_r)$, $\gamma > 0$.

Furthermore, we can replace:

$$\left(n_\alpha|p|^2 + \frac{2}{n^2}\right)^{\frac{1}{4}}, \ \left(n_\beta|q|^2 + \frac{2}{n^2}\right)^{\frac{1}{4}} \text{ and } \frac{|p|^2}{m_{\alpha\gamma}} + \frac{2(p,q)}{m_\gamma} + \frac{|q|^2}{m_{\beta\gamma}} + \frac{2}{n^2}$$

by the expressions:

$$\left(n_\alpha|p|^2\right)^{\frac{1}{4}}(1-\chi_1(p))^{-1}, \ \left(n_\beta|q|^2\right)^{\frac{1}{4}}(1-\chi_1(q))^{-1} \text{ and } \frac{|p|^2}{m_{\alpha\gamma}} + \frac{2(p,q)}{m_\gamma} + \frac{|q|^2}{m_{\beta\gamma}},$$

respectively, because the corresponding difference is a Hilbert-Schmidt operator and continuous up to $z = 0$. In this case, we obtain the block operator matrix $\mathbf{S}(r)$ on $L_2^{(3)}(U_r(\mathbf{0}) \setminus U_1(\mathbf{0}))$ whose entries $S_{\alpha\beta}(r)$ are the integral operators with the kernel $S_{\alpha\beta}(r;\cdot,\cdot)$:

$$S_{\alpha\alpha}(r;p,q) = 0; \quad S_{\alpha\beta}(r;p,q) = \frac{n^3 D_{\alpha\beta}}{(n_1n_2)^{1/4}} \frac{|p|^{-1/2}|q|^{-1/2}}{m_{\alpha\gamma}^{-1}|p|^2 + 2m_\gamma^{-1}(p,q) + m_{\beta\gamma}|q|^2}.$$

Using the dilation:

$$\mathbf{M} = \operatorname{diag}\{M, M, M\} : L_2^{(3)}(U_r(\mathbf{0}) \setminus U_1(\mathbf{0})) \to L_2((0,\mathbf{r}), \sigma^{(3)}), \quad (Mf)(x,w) = e^{3x/2} f(e^x w),$$

where $\mathbf{r} = \frac{1}{2}|\log|z||$, $x \in (0,\mathbf{r})$, $w \in \mathbb{S}^2$, one can see that the operator $\mathbf{S}(r)$ is unitarily equivalent to the integral operator $\mathbf{S}_\mathbf{r}$.

Since the difference of the operators $\mathbf{S}_\mathbf{r}$ and $\mathbf{T}(\delta;|z|)$ is compact (up to unitary equivalence) and $\mathbf{r} = 1/2|\log|z||$, we obtain the equality:

$$\lim_{|z|\to 0} \frac{n(\gamma, \mathbf{T}(\delta;|z|))}{|\log|z||} = \lim_{\mathbf{r}\to 0} \frac{1}{2}\mathbf{r}^{-1} n(\gamma, \mathbf{S}_\mathbf{r}), \quad \gamma > 0.$$

Now Lemma 6.1 and the equality (6.1) completes the proof of Theorem 6.4. □

Proof of Theorem 3.3. Let $\mu_\alpha = \mu_\alpha^0$, $\alpha = 1, 2, 3$. Using Lemmas 6.1, 6.3 and Theorem 6.4 we have:

$$\lim_{|z|\to 0} \frac{n(1, \widehat{\mathbf{T}}(z))}{|\log|z||} = U(1).$$

Taking into account the last equality and Lemma 5.1, and setting $\mathcal{U}_0 = U(1)$, we complete the proof of Theorem 3.3. □

Acknowledgements

The authors would like to thank Prof. A. Teta for helpful discussions about the results of the paper. This work was supported by the TOSCA Erasmus Mundus grant. T. H. Rasulov wishes to thank the University of L'Aquila for the invitation and hospitality.

References

[1] V. Efimov. Energy levels arising from resonant two-body forces in a three-body system. *Phys. Lett. B*, **33** (8), P. 563–564 (1970).

[2] S. Albeverio, R. Höegh-Krohn, T.T. Wu. A class of exactly solvable three-body quantum mechanical problems and the universal low energy behavior. *Phys. Lett. A*, **83** (3), P. 105–109 (1981).

[3] R.D. Amado, J.V. Noble. On Efimov's effect: a new pathology of three-particle systems. *Phys. Lett. B*, **35**, P. 25–27 (1971); II. *Phys. Lett. D*, **5** (3), P. 1992–2002 (1972).

[4] D.R. Yafaev. On the theory of the discrete spectrum of the three-particle Schrödinger operator. *Math. USSR-Sb.*, **23**, P. 535–559 (1974).

[5] G.F. Dell'Antonio, R. Figari, A. Teta. Hamiltonians for systems of N particles interacting through point interactions. *Ann. Inst. Henri Poincaré, Phys. Theor.*, **60** (3), P. 253–290 (1994).

[6] Yu.N. Ovchinnikov, I.M. Sigal. Number of bound states of three-body systems and Efimov's effect. *Ann. Phys.*, **123** (2), P. 274–295 (1979).

[7] A.V. Sobolev. The Efimov effect. Discrete spectrum asymptotics. *Commun. Math. Phys.*, **156** (1), P. 101–126 (1993).

[8] H. Tamura. The Efimov effect of three-body Schrödinger operators. *J. Func. Anal.*, **95** (2), P. 433–459 (1991).

[9] H. Tamura. The Efimov effect of three-body Schrödinger operators: asymptotics for the number of negative eigenvalues. *Nagoya Math. J.*, **130**, P. 55–83 (1993).

[10] D. Mattis. The few-body problem on a lattice. *Rev. Modern Phys.*, **58** (2), P. 361–379 (1986).

[11] A.I. Mogilner. Hamiltonians in solid state physics as multiparticle discrete Schrödinger operators: problems and results. *Advances in Sov. Math.*, **5**, P. 139–194 (1991).

[12] M. Reed, B. Simon. *Methods of Modern Mathematical Physics. III: Scattering theory*. Academic Press, New York, 1979.

[13] V.A. Malishev, R.A. Minlos. *Linear infinite-particle operators*. Translations of Mathematical Monographs. 143, AMS, Providence, RI, 1995.

[14] L.D. Faddeev. *Mathematical aspects of the three-body problem in quantum mechanics*. Israel Program for Scientific Translations, Jerusalem, 1965.

[15] L.D. Faddeev, S.P. Merkuriev. *Quantum scattering theory for several particle systems*. Kluwer Academic Publishers, 1993.

[16] Zh.I. Abdullaev, S.N. Lakaev. Asymptotics of the discrete spectrum of the three-particle Schrödinger difference operator on a lattice. *Theor. Math. Phys.*, **136** (2), P. 1096–1109 (2003).

[17] S. Albeverio, S.N. Lakaev, Z.I. Muminov. Schrödinger operators on lattices. The Efimov effect and discrete spectrum asymptotics. *Ann. Henri Poincaré*, **5**, P. 743–772 (2004).

[18] S.N. Lakaev, M.É. Muminov. Essential and discrete spectra of the three-particle Schrödinger operator on a lattices. *Theor. Math. Phys.*, **135** (3), P. 849–871 (2003).

[19] Zh.I. Abdullaev. Finiteness of the discrete spectrum for non-trivial of the full quasi-momentum in the system of three bosons on a lattice. *Russian Math. Surveys*, **62** (1), P. 175–201 (2007).

[20] P.R. Halmos. *A Hilbert space problem book*. Springer-Verlag New York Inc., second edition, 1982.

[21] M.I. Muminov. Positivity of the two-particle Hamiltonian on a lattice. *Theoret. Math. Phys.*, **153** (3), P. 1671–1676 (2007).

NANOSYSTEMS: PHYSICS, CHEMISTRY, MATHEMATICS, 2015, 6 (2), P. 294–298

Dependence of the dimension of the associates of water-soluble tris-malonate of light fullerene – $C_{60}[=C(COOH)_2]_3$ in water solutions at 25 °C

K. N. Semenov[1], N. A. Charykov[2,3], A. S. Kritchenkov[1], I. A. Cherepkova[2], O. S. Manyakina[2], D. P. Tyurin[2], A. A. Shestopalova[2], V. A. Keskinov[2], K. V. Ivanova[2], N. M. Ivanova[1], D. G. Letenko[4], V. A. Nikitin[5], E. L. Fokina[1], M. S. Gutenev[5]

[1]St. Petersburg State University, Saint-Petersburg, Russia
[2]St. Petersburg State Technological Institute (Technical University), Saint-Petersburg, Russia
[3]St. Petersburg State Electro-Technical University (LETI), Saint-Petersburg, Russia
[4]St. Petersburg State University of Architecture and Civil Engineering, Saint-Petersburg, Russia
[5]Peter the Great St. Petersburg Polytechnic University, Saint-Petersburg, Russia

keskinov@mail.ru

PACS 61.48.+c **DOI 10.17586/2220-8054-2015-6-2-294-298**

Investigation of the concentration dependence of the size and type $C_{60}[=C(COOH)_2]_3$ aggregation in aqueous solutions at 25 °C was accomplished with the help of a dynamic light scattering method. It was determined that three types of aggregates are realized in the solutions. The average number of $C_{60}[=C(COOH)_2]_3$ molecules in smaller aggregates and all types of aggregates were calculated. One can see that over the whole concentration range, from 0.01 to 10 g/dm^3, aqueous solutions of $C_{60}[=C(COOH)_2]_3$ are characterized by sub-micro-heterogeneous behavior (because second-type aggregates with the linear dimensions – hundreds of nm are formed in all solutions). Additionally, the most concentrated solution ($C = 10$ g/dm^3) is characterized by micro-heterogeneous or colloid behavior (because third-type aggregates with the linear dimensions on the order of μm – are formed). In order to describe or explain such behavior, a stepwise aggregation model was invoked.

Keywords: tris-malonate of light fullerene, method of the dynamic light scattering.

Received: 10 August 2014

1. Introduction

This article further develops investigations which were initiated previously [1–4]. These studies were devoted to the synthesis and identification of tris-malonate $C_{60}[=C(COOH)_2]_3$ [1] (the original synthesis of this water soluble derivative was described earlier in [5]), the investigation of volume and refraction properties of its aqueous solutions at 25 °C [2], poly-thermal solubility and complex thermal analysis [3], concentration dependence of electric conductivity and hydrogen ion concentration for aqueous solutions [4]. This study was undertaken to investigate the concentration dependence of $C_{60}[=C(COOH)_2]_3$ aggregate sizes in aqueous solutions at 25 °C, and as in the earlier article [3], these studies to investigate the state of $C_{60}[=C(COOH)_2]_3$ and its aggregation processes were performed in aqueous solutions over a wide concentration range – 0.1 ÷ 10 g/dm^3.

TABLE 1. Linear dimensions of C_{60}[=C(COOH)$_2$]$_3$ aggregates in aqueous solutions at 25 °C

Concentration of C_{60} tris-malonate C (g/l)	Diameter of monomer $\bar{d}_0 \approx 1.8$ nm (nm)	Diameter of first type associates d_1-interval ($\bar{d}_1$) (nm)	Diameter of second type associates d_2-interval ($\bar{d}_2$) (nm)	Diameter of third type associates d_3-interval ($\bar{d}_3$) (nm)
0.01	No effect	30–70 (50)	200–400 (300)	No effect
0.1	No effect	40–80 (60)	300–500 (400)	No effect
1.0	No effect	40–80 (60)	300–500 (400)	No effect
5.0	No effect	40–80 (60)	300–500 (400)	No effect
10.0	No effect	40–80 (60)	500–1000 (750)	4000–6000 (5000)
Concentration of C_{60} tris-malonate C (g/l)	Average number of monomer molecular of C_{60} tris-malonate in clusters of the first order $N_{0\to1}$ (units)	Average number of clusters of the first order in clusters of the second order $N_{1\to2}$ (units)	Average number of clusters of the second order in clusters of the third order $N_{2\to3}$ (units)	
0.01	$1.1 \cdot 10^4$	$1.1 \cdot 10^2$	No effect	
0.1	$1.9 \cdot 10^4$	$1.6 \cdot 10^2$	No effect	
1.0	$1.9 \cdot 10^4$	$1.6 \cdot 10^2$	No effect	
5.0	$1.9 \cdot 10^4$	$1.6 \cdot 10^2$	No effect	
10.0	$1.9 \cdot 10^4$	$1.0 \cdot 10^3$	$1.6 \cdot 10^2$	

2. Dimension of the associates of C_{60}[=C(COOH)$_2$]$_3$ in water solutions at 25 °C

To investigate the concentration dependence of C_{60}[=C(COOH)$_2$]$_3$ aggregate size in aqueous solutions at 25 °C, we utilized a dynamic light scattering method in the visible wavelength region. The Malvern Zeta Nanosizer device was used. Data are represented in Table 1 and Fig. 1 and 2 (as the examples).

To estimate the linear size of the C_{60}[=C(COOH)$_2$]$_3$ monomer, $d_0(monomer)$ was obtained from the refraction data [2]. Molar refraction of C_{60} tris-malonate $R_{tris-malonate} \approx 201$ cm^3/mole, so: $R_{tris-malonate} \approx 2.01 \cdot 10^{-4}/6.02 \cdot 10^{23} \approx 3.0 \cdot 10^{-27}$ m^3/molecule, so: in the spherical approximation, the linear dimension: $d_0(monomer) \approx [18/\pi \cdot 10^{-27}]^{1/3} \approx 1.8 \cdot 10^{-9}$ m $= 1.8$ nm.

3. Number of i-th type associates packed into $(i+1)$-th type associates

The number of i-th type aggregates packed into $(i+1)$-th type aggregates – $N_{i\to i+1}$ was estimated by the following equation:

$$N_{i\to i+1} = (d_{i+1}/d_i)^3 \cdot K_{pack}, \tag{1}$$

where: $K_{pack} \approx 0.52$ – is formal pack coefficients for the case of 'little spheres', packed in the 'larger sphere' ($1 - K_{pack} \approx 0.48$ – volume fraction, which is empty of is fulfilled by a molecular of H_2O).

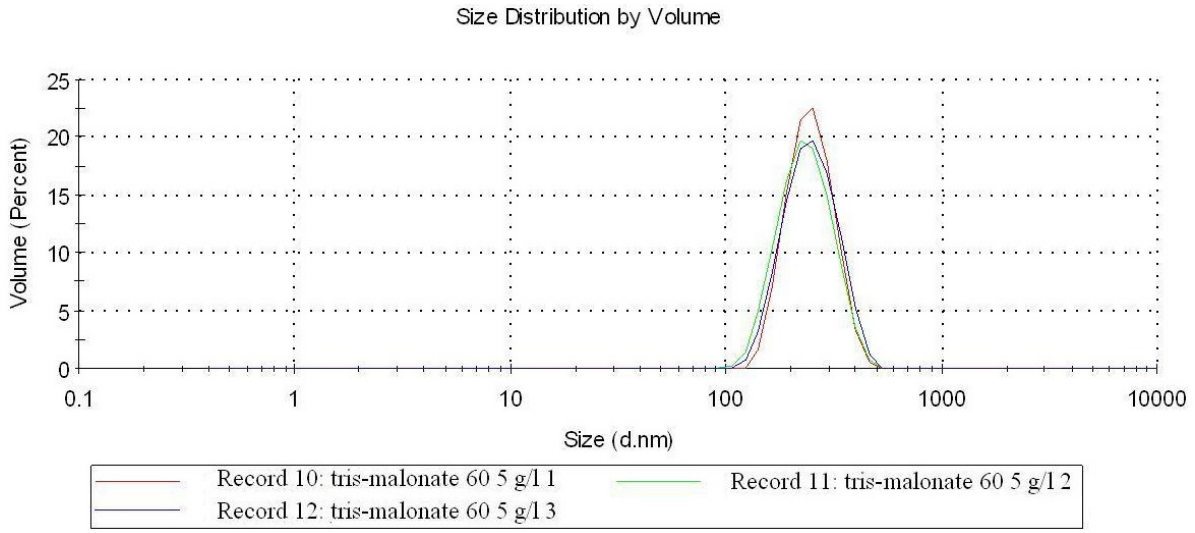

FIG. 1. Distribution according to linear dimension of C_{60} tris-malonate aggregates in aqueous solution at concentration of C_{60} tris-malonate $C = 5$ g/dm^3 (example) – 3 signals correspond to the different times of signal sum

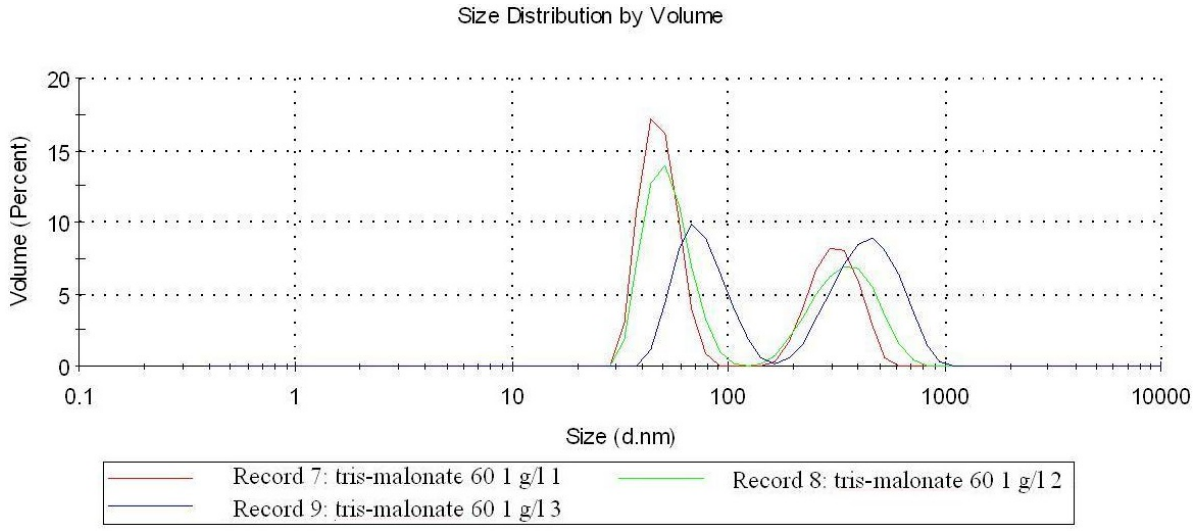

FIG. 2. Distribution according to linear dimension of C_{60} tris-malonate aggregates in aqueous solution at concentration of C_{60} tris-malonate $C = 1$ g/dm^3 (example) – 3 signals correspond to the different times of signal sum

Calculated, concerning $N_{i\to i+1}$-values data are also represented in Table 1.

From obtained data one can see the following:

1. No monomer molecular (with linear dimension-diameter $\bar{d}_0 \approx 1.8$ nm) are seen in all investigated solutions, even in the dilute solution ($C = 0.1$ g/dm^3).
2. The diameter of first type aggregates (first order clusters of percolation) have the similar linear dimension-diameter $\bar{d}_1 \approx 60 \pm 20$ nm over the whole concentration range (a slight decrease is seen only for the most dilute solution ($C = 0.01$ g/dm^3) – $\bar{d}_1 \approx 50 \pm 20$ nm).
3. The diameter of second type aggregates (second order clusters of percolation) also have a similar linear dimension-diameter $\bar{d}_2 \approx 400 \pm 100$ nm in the concentration range $0.1 \div 5$ g/dm^3 (again, a slight change is seen only for the most dilute solution at

$C = 0.01$ g/dm^3 – $\bar{d}_2 \approx 300 \pm 100$ nm and for the most concentrated solution at $C = 10$ g/dm^3 – $\bar{d}_2 \approx 750 \pm 250$ nm – solution 'is preparing to become heterogeneous').

4. Third type associates (third order clusters of percolation) have not been seen at any concentrations except the most concentrated solution at $C = 10$ g/dm^3, where clusters with extremely huge linear dimension-diameter $\bar{d}_3 \approx 5000 \pm 1000$ nm (5 ± 1 μm) are observed – the solution 'becomes very heterogeneous' but stable as a colloid system).
5. So, to describe such facts in the aggregation process, a stepwise model of particle growth was invoked. We consider that monomer spherical molecules form the first type spherical aggregates, then, the first type spherical associates form second type spherical associates. Next, the second type spherical associates form third type spherical associates (the last ones correspond to the colloidal heterogeneous system). A similar stepwise aggregation model was used by us earlier for the description of particle growth in water-fullerenol-d systems (see, for example [6]).

To prove the formation of the micro-heterogeneity (with the linear dimensions on the order of μm) in the most concentrated solution ($C = 10$ g/dm^3), we obtained a photo of the film this solution. An optical polarizing microscope Labo-Pol (variant 2) was used. Samples were prepared by the crystallization of C_{60} tris-malonate crystals from aqueous solutions under quick isothermal evaporation of water from the solution (a drop of the solution was put on the surface of silicate glass). A typical photo is represented in the Fig. 3. One can see typical spherical formations (centers of crystallization) with enough characteristic linear dimensions which were observed earlier in the dynamic light scattering investigations as third type aggregates (see Table 1). Crystal formations, proceeding from these spheres, gave the crystal-like film in the quick evaporation-crystallization process.

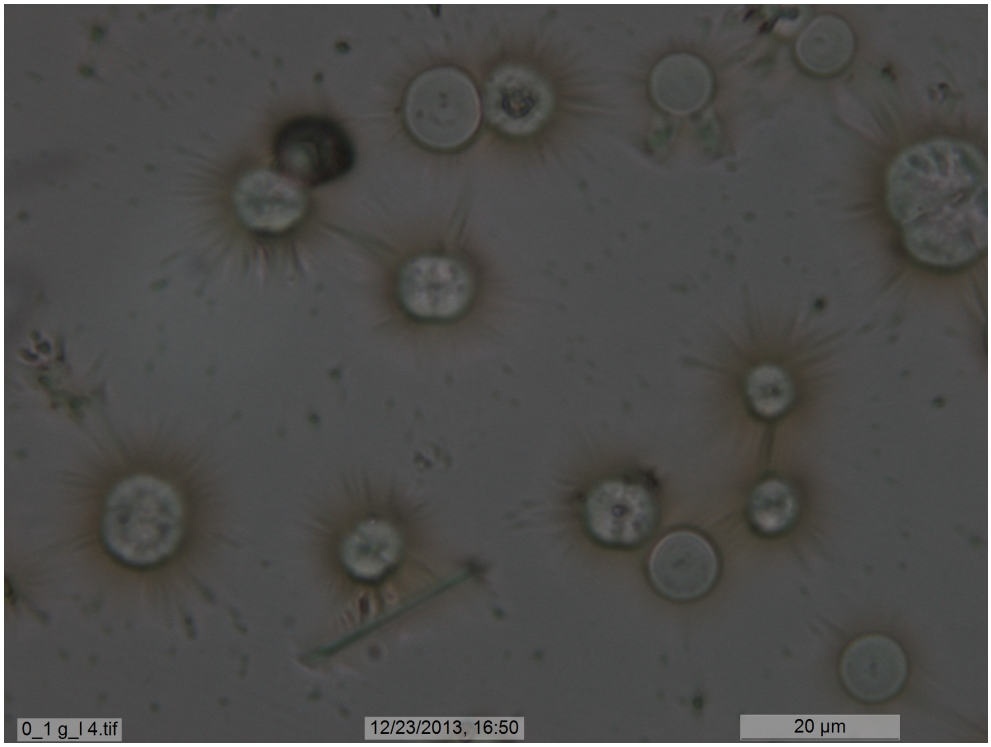

FIG. 3. Here is an optical polarizing microscope photo of C_{60} tris-malonate crystals (scale $\times 1000$). The initial (before evaporation) solution had a concentration C of 10 g C_{60} tris-malonate of per dm^3 H_2O

Acknowledgments

Investigations were supported by Russian Foundation for Basic Research – RFBR (Project No. 15-08-08438).

References

[1] K.N.Semenov, N.A.Charykov, A.S.Kritchenkov et al. Synthesis and identification water-soluble tris-malonate of light fullerene – $C_{60}[=C(COOH)_2]_3$. *Nanosystems: Physics, Chemistry, Mathematics*, **5** (2), P. 315–319 (2014).

[2] K.N.Semenov, N.A.Charykov, A.S.Kritchenkov et al. Volume properties of water solutions and refraction at 25 °C water soluble tris-malonate of light fullerene – $C_{60}[=C(COOH)_2]_3$. *Nanosystems: Physics, Chemistry, Mathematics*, **5** (3), P. 427–434 (2014).

[3] K.N.Semenov, N.A.Charykov, A.S.Kritchenkov et al. Poly-thermal solubility and complex thermal analysis of water soluble tris-malonate of light fullerene – $C_{60}[=C(COOH)_2]_3$. *Nanosystems: Physics, Chemistry, Mathematics*. **5** (3), P. 435–440 (2014).

[4] K.N. Semenov, N.A. Charykov, A.S. Kritchenkov et al. Concentration dependence of electric conductivity and hydrogen indicator for water solutions of water soluble tris-malonate of light fullerene –$C_{60}[=C(COOH)_2]_3$. *Nanosystems: Physics, Chemistry, Mathematics*. **5** (5), P. 709–717 (2014).

[5] I. Lamparth, A. Hirsch. Water-soluble malonic acid derivatives of C_{60} with a defined three-dimensional structure. *J. Chem. Soc Chem. Commun.*, **14**, P. 1727–1728 (1994).

[6] K.N. Semenov, N.A. Charykov, V.A. Keskinov. Synthesis and Identification. Properties of Fullerenol Water Solutions. *J. Chem. Eng. Data*, **56**, P. 230–239 (2011).

Mathematical Challenge of Quantum Transport in Nanosystems
ITMO University, Saint Petersburg, Russia (September 9-11, 2015)

September 9-11, 2015 *Young Researchers Symposium (YRS)*
September 9-11, 2015 *Pierre Duclos Workshop*

Invited Speakers (confirmed)

- Jussi Behrndt (Graz, Austria)
- Boris Pavlov (Auckland, New Zealand)
- Hagen Neidhardt (Berlin, Germany)
- Johannes Brasche (Clausthal, Germany)
- Pavel Stovicek (Prague, Czech Republic)
- Andrea Posilicano (Lombardia, Italy)
- Silvestro Fassari (Locarno, Switzerland)
- Claudio Cacciapuoti (Como, Italy)
- Andrea Mantile (Reims, France)

The main topics of the conference:

- Spectral theory
- Scattering
- Quantum transport
- Quantum communications and computations

Conference language: English.

Location: The workshop will take place in the Saint Petersburg National Research University of Informational Technologies, Mechanics, and Optics: Kronverkskiy, 49, 197101 Saint Petersburg, Russia.

Registration fee: (paid the equivalent sum in rubles on arrival) For Pierre Duclos Workshop: 100 euro (book of abstracts, conference bag, coffee breaks, conference dinner). For YRS: 20 euro (book of abstracts, conference bag, coffee breaks). Students and postgraduate students who attend YRS can attend "Pierre Duclos Workshop" sessions as well.

The **Proceedings** will be published in the journal "Nanosystems: Physics, Chemistry, Mathematics".

Deadlines: Visa Application and Registration (for Shengen zone residents who need a Russian visa): July 1, 2015. Visa Application and Registration (for other countries residents who need a Russian visa): June 15, 2015. Registration (for participants who do not need a Russian visa): September 3, 2015.

Contact: Prof. Igor Yu. Popov, ITMO University, Kronverkskiy, 49, 197101 Saint Petersburg, Russia.
tel: +7-812-232-67-65, **fax:** +7-812-232-67-65, **e-mail:** popov1955@gmail.com
Conference site: http://mathdep.ifmo.ru/mcqtn2015/

1st Announcement

KSR Group of Institutions
TIRUCHENGODE

INTERNATIONAL CONFERENCE ON NANOMATERIALS AND NANOTECHNOLOGY

NANO 2015

DEC 7-10

- **Plenary Talks**
  - Nobel Laureates
    - **Prof.Robert Huber** (Chemistry 1998), Germany
    - **Prof.Kurt Wuthrich** (Chemistry 2002), USA
  - **Prof.S.Banerjee** Mumbai, India
  - **Prof.Baldev Raj** Bangalore, India
  - **Prof.G.Sundararajan** Hyderabad, India
- **12 Key Note Address**
- **45 Invited Talks**

REGISTRATION

• Conference Participation • Academic Partnership • Exhibition

SPONSORSHIP

PLATINUM | GOLD | SILVER | CO-SPONSORSHIPS | CONFERENCE REGISTRATION | CONFERENCE LUNCH/DINNER | CONFERENCE SOUVENIR

IMPORTANT DATES

May 05,2015 : Last Date of Receipt of Abstract (500 Words Max.)
May 15,2015 : Notification of Abstract Acceptance
Jun 15,2015 : Full Paper Submission
Aug 22,2015 : Notification of Full Paper Acceptance
Sep 05,2015 : Final Camera Ready Accepted Paper Submission

PUBLICATIONS

• Proceedings Hard/Soft copy • More than 6 peer reviewed international journals

ADDRESS FOR COMMUNICATION

Dr. V.Rajendran
Organising Chair, Nano-2015
Director, Research and Development
Centre for Nanoscience and technology
K S R Group of Institutions
K S R Kalvi Nagar, Tiruchengode - 637 215
Namakkal (Dt), Tamil Nadu, India
Phone : 91-4288-274880 (Direct), 274741-4
Fax : 91-4288-274880(Direct), 274860
Mob : 91-99941 30303
Email : directorrd@ksrct.ac.in | nano15@ksrct.ac.in

Prof. Dr. Kurt. E. Geckeler
Organising Co-Chair,NANO 2015
Department of Nanobio Materials and Electronics
World Class University (WCU)
Gwangju Institute of Science and Technology (GIST)
Republic of Korea
Email : nano15@ksrct.ac.in

www.nano15.ksrct.ac.in

RUSH YOUR REGISTRATION

Venue
NANO 2015
KSR Campus
Tamil Nadu, India

KSRCT NANOCONFERENCE

NANO Ф&Х&М

NANOSYSTEMS:

PHYSICS, CHEMISTRY, MATHEMATICS

INFORMATION FOR AUTHORS

The journal publishes research articles and reviews, and also short scientific papers (letters) which are unpublished and have not been accepted for publication in other magazines. Articles should be submitted in English. All articles are reviewed, then if necessary come back to the author to completion.

The journal is indexed in Chemical Abstract Service of the American Chemical Society and in Russian Scientific Citation Index.

Author should submit the following materials:

1. Article file in English, containing article title, the initials and the surname of the authors, Institute (University), postal address, the electronic address, the summary, keywords, MSC or PACS index, article text, the list of references.
2. Files with illustrations, files with tables.
3. The covering letter in English containing the article information (article name, MSC or PACS index, keywords, the summary, the literature) and about all authors (the surname, names, the full name of places of work, the mailing address with the postal code, contact phone number with a city code, the electronic address).
4. The expert judgement on possibility of publication of the article in open press (for authors from Russia).

Authors can submit a paper and the corresponding files to the following addresses: nanojournal.ifmo@gmail.com, popov1955@gmail.com.

Text requirements

Articles should be prepared with using of text editors MS Word or LaTEX (preferable). It is necessary to submit a pdf copy. In the name of files the English alphabet is used. The recommended size of short communications (letters) is 4-6 pages, research articles – 6-15 pages, reviews – 30 pages.

Recommendations for text in MS Word:

Formulas should be written using Math Type. Figures and tables with captions should be inserted in the text. Additionally, authors present separate files for all figures and Word files of tables.

Recommendations for text in LaTex:

Please, use standard LaTex without macros and additional style files. The list of references should be included in the main LaTex file. Single LaTex file of the paper with the corresponding pdf file should be submitted.

References in the article text are given in square brackets. The list of references should be prepared in accordance with the following samples:

[1] N. Surname. *Book Title*. Nauka Publishing House, Saint Petersburg, 281 pp. (2000).
[2] N. Surname, N. Surname. Paper title. *Journal Name*, **1**(5), P. 17-23 (2000).
[3] N. Surname, N. Surname. Lecture title. In: Abstracts/Proceedings of the Conference, Place and Date, P. 17-23 (2000).
[4] N. Surname, N. Surname. Paper title (2010). URL: http://books.ifmo.ru/ntv.
[5] N. Surname, N. Surname. Patent Name. Patent No. 11111, Bul. No. 33, 5 pp. (2010).
[6] N. Surname, N. Surname. Thesis Title. Thesis for full doctor degree in math. and physics, Saint Petersburg, 105 pp. (2000).

Requirements to illustrations

Illustrations should be submitted as separate black-and-white files. Formats of files – jpeg, eps, tiff.

N A N O
Ф&Х&М

NANOSYSTEMS:

PHYSICS, CHEMISTRY, MATHEMATICS

Журнал зарегистрирован
Федеральной службой по надзору в сфере связи, информационных технологий и массовых коммуникаций
(свидетельство ПИ № ФС 77 - 49048 от 22.03.2012 г.)
ISSN 2220-8054

Учредитель: федеральное государственное автономное образовательное учреждение высшего образования
«Санкт-Петербургский национальный исследовательский университет информационных технологий, механики и оптики»

Издатель: федеральное государственное автономное образовательное учреждение высшего образования
«Санкт-Петербургский национальный исследовательский университет информационных технологий, механики и оптики»

Отпечатано в Учреждении «Университетские телекоммуникации»
Адрес: 197101, Санкт-Петербург, Кронверкский пр., 49

Подписка на журнал НФХМ
На второе полугодие 2015 года подписка осуществляется через
ОАО Агентство «Роспечать»
Подписной индекс 57385 в каталоге «Издания органов научно-технической информации»